Dissertation Advisor: Dr. Arlene Sharpe Peter The Sage

Mechanisms of CD4 T cell antigen recognition and effector cell differentiation and function

Abstract

The ability for CD4 T cells to efficiently search for and subsequently respond to microbial pathogens is essential for protective immunity, but mechanisms controlling these responses are not completely understood. In this thesis I study the regulation of CD4 T cell responses at two different stages during an immune response. First, I analyze one of the most basic mechanisms by which T cells search for and become activated by an antigenic stimulus during the initial events in an adaptive immune response. Using human memory CD4 T cells *in vitro* I have identified a novel role for actin-rich invadapodia-like protrusions (ILPs) in overcoming the energy barrier required for the T cell receptor (TCR) to send signals into T cells when interacting with peptide-loaded MHC II. My studies show that ILPs, which are used during migration, are also essential for surveying the surface of other cells during cellular communication. Secondly, I explore the costimulatory requirements and function of T follicular regulatory (TFR) cells, a newly identified

subset of regulatory T (TREG) cells. Using mouse models, I have discovered that the costimulatory receptor PD-1 inhibits the differentiation and function of TFR cells *in vivo*. My work also has revealed that TFR cells can circulate within the blood and that blood TFR cells can potently inhibit B cell mediated antibody production *in vivo*. Taken together, the studies presented here not only provide insights into the very initial events leading to adaptive immunity, but also demonstrate how adaptive immunity is controlled during the effector phase of an immune reaction.

If through science I can seize phenomena and enumerate them, I cannot, for all that, apprehend the world.

Albert Camus, *The Myth of Sisyphus*

Acknowledgements

Over the course of my graduate studies I have been fortunate to have met and been helped by so many people. I would like to specially thank the following:

To my thesis advisor, Dr. Arlene Sharpe, for taking a chance on me as an inexperienced graduate student, and taking the time to guide me into the scientist I am today. I am forever grateful for the commitment, attention to detail and motherly advice that came with each and every conversation (of which there were many). I am a much better scientist, as well as a much better person because of all your help along the way. Thank you so much for your trust in my scientific work and never doubting me. I wouldn't have had the confidence to succeed without it.

To my co-mentor, Dr. Chris Carman, for helping me along as a scientist long before I even started my graduate career, and particularly during graduate school where I learned the most. Only because of the unlimited patience and consistent help over the years during many experiments have I been able to be where I am. I am also forever grateful for the endless professional guidance you have given me that has led me to pursue my PhD. I would not have made it without you. Chris also helped perform many of the experiments contained in Chapter 1.

To all the lab members of the Sharpe Lab for their years of support and friendship. A special thank you to Dr. Loise Franscisco for years of scientific help and guidance. Thanks goes out to Robert Ortega, Caroline Armet, Flor Gonzalez, Dr. Dan Brown and Dr. Sun Lee for outstanding technical help. More thanks goes to Sarah Hillman for ordering and scheduling help.

To all the Carman lab members for their years of friendship and instruction during many a dark nights in the microscope room. A special thank you to Laya Varghese, who provided technical help and performed some of the experiments in Chapter 1.

To my thesis committee, Dr. Kai Wucherpfennig, Dr. Thorsten Mempel and Dr. Shannon Turley. Your comments have been instrumental in guiding my projects.

To John Sullivan in the flow cytometry core for all the help on sorting and analyzing samples.

To Jennifer Lee for being there for me every step of the way and helping me stay sane during this process.

To all of the coauthors and collaborators on the projects presented here who have been instrumental in helping the projects progress.

Last but not least, to my parents and family. Only through many years of unwavering love and support am I able to be where I am today. And especially to Dr. J.D. Sage, my grandfather, who set me on the path to scientific discovery.

Table of Contents

Chapter 1. Mechanisms of Antigen Recognition by Memory/Effector T Cells

Note: The contents of this project have been published previously[1].

Introduction

Adaptive immunity relies on the ability of T cell receptors (TCRs) expressed on lymphocytes to efficiently recognize peptide antigen (Ag) bound to major histocompatibility complex (MHC) molecules [3]. During the priming phase, naïve lymphocytes constitutively scan professional Ag presenting cells (APCs) such as dendritic cells and B cells within lymph nodes in order to find and respond to cognate antigen. Through identifying cognate antigen T cells can be activated, differentiate into effector cells, and perform their functions. During the effector phase, memory/effector T cells need to effectively survey an extremely wide range of APCs and potential target cells with a broad range of phenotypic and morphological characteristics both within secondary lymphoid organs as well as in peripheral tissues in order to become reactivated. Only after reactivation can the memory/effector T cell then fufill its function by producing cytokines and/or lysing infected cells to protect the host from infection. Fundamental cellular mechanisms for such immune surveillance for memory T cell reactivation remain incompletely understood.

At the heart of immune surveillance is the requirement for T cells to form extremely intimate (~14 nm, the total height of the TCR-MHC complex[5]) contacts with neighboring cells. This allows the TCR to directly sample the peptide antigen bound within the binding groove of MHC proteins and is required for detecting cognate antigen and triggering T cell responses. The surfaces of all cells are modified by a relatively thick (50-500 nm) gel-like polysaccharide coat termed the glycocalyx[6], which provides a formidable energy barrier (via steric and electrostatic repulsion) to close membrane-membrane proximity, and therefore limits interaction of immune receptor-ligand pairs such as TCR-MHC[7, 8].

The glycocalyx is composed of sulfated proteoglycans, hyaluronan, glycoproteins and plasma proteins that come together to form a complex and dense network. Some proteins, such as chemokines, can be "trapped" in this dense network. Therefore, the glycocalyx can also convey information extracellularly to cells interacting with it. Glycosaminoglycans with primarily acidic side chains cause the glycocalyx to have a net negative charge. Therefore, not only are immune receptors buried within the dense glycocalyx, cells coming into close contact will be repelled from each other based on the negative charges of both glycocalyces. In this way, immune receptors, such as TCR-MHC, are effectively shielded and immune recognition is strongly opposed [8-13]. Thus, a fundamental question is how do T cells overcome this energy barrier to engage immune receptors?

It has long been appreciated that as a consequence of antigen recognition, specialized cell-cell interfaces form that involve membrane alignment, cytoskeletal remodeling, clustering/segregation of immune receptors/adhesion molecules and glycocalyx components [8, 14-18]. These 'immunological synapses' (ISs) form within minutes of Ag recognition and are thought to amplify and sustain signaling, as well as facilitate exchange of cytokine and/or cytotoxic materials [8, 14-18]. Although the mechanisms of TCR triggering has not been completely elucidated, it has been shown that the length of the TCR-MHC complex is essential in TCR signaling, and truncating or elongating the distance of MHC from the plasma membrane of the APC leads to suboptimal T cell activation[19]. This has lead to proposal of the kinetic-segregation model, where stable ISs form because TCR-MHC molecules "squeeze" out inhibitory molecules such as CD45. Therefore, ISs are able to transmit signals because of the highly ordered orientation of stimulatory and inhibitory proteins contained within it.

Although many studies have focused on the orientation of ISs, the detailed mechanisms facilitating initial Ag sampling between T cells and APCs, and how these lead to early IS formation, are not completely understood [20, 21]. It has been shown previously using preformed T cell contacts with bio-engineered substrates coated with MHC and a photoactivable antigen (i.e., which becomes unmasked

through photoconversion) that the offset time, or the time from when the antigen is 'un-masked', until T cell activation is about 6.5 seconds[22]. Thus, responses are acutely coupled to detection of antigen. However, precisely how and when antigen becomes initially detected in settings of cell:cell interactions remains poorly characterized. This stems from technical challenges associated with irregular topologies of APC surfaces and poorly controlled orientation of the cell-cell interaction planes, issues that profoundly limit the requisite imaging approaches [20, 21, 23].

Investigators have partially circumvented these restrictions by developing planar substrate models (i.e., lipid bilayers and antibody-coated surfaces) that provide optimal spatiotemporal resolution for monitoring Ag response dynamics [24-28]. These models have afforded invaluable insights, such as the discovery of TCR micro-clusters as the critical mediators of effective signaling and not the ISs as a whole [24-28]. However, these systems lack key features of cellular APC surfaces, such as the glycocalyx, topological deformability and molecular complexity. Therefore, it remains uncertain how to translate such findings to physiologic cell-cell immune surveillance.

Here we employed vascular endothelial cells (ECs) as a planar antigen presentation cell model to interrogate the details of initial Ag recognition dynamics on a

physiologic cellular substrate. ECs represent the interface between the blood circulation and tissue and play critical roles in barrier function including regulating immune cell trafficking [3, 29, 30]. The discovery that ECs express MHC-I, MHC-II and a large number of costimulatory molecules (e.g., CD40, LFA3, ICOSL, 4-1BB, OX40L, TL1A, PD-L1; but not CD80 and CD86) has lead to the controversial hypothesis that endothelium can also function as a type of APC [31-33]. Indeed, several studies have demonstrated that endothelium can effectively re-stimulate CD4 and CD8 memory/effector, but not naïve, T cells [34-38]. Critically, when grown *in vitro,* ECs form virtually planar cell surfaces that are ideal for high spatiotemporal resolution imaging of topological dynamics [39]. Primary ECs can also be easily transfected with fluorescent constructs, something that has been extremely difficult in primary immune cell APCs. Importantly, vascular endothelial cells have perhaps the most studied glycocalyx in biology. Indeed, the endothelial glycocalyx has been shown to have essential roles as a modulator of permability, as a mechanotransducer of shear stress and as an inhibitor to cellular migration[6]. For instance, when expression of a key glycocalyx component, heparin sulfate, was conditionally deleted from endothelial cells, there was increased rolling of lymphocytes, which was attributed to the lack of charge repulsion of the T cell glycocalyx [40].

Taking all of the above into account, this study provides, one of the first detailed investigation of the initial events in CD4 and CD8 T cell scanning for and

recognition of Ag in the context of a physiologic APC. It had been previously discovered that lymphocytes actively probe the surface of the endothelium by dynamic insertion and retraction of sub-micron-scale, actin-rich cylindrical protrusions related to invadosomes [41] termed invadosome/podosome-like protrusions (i.e., 'ILPs') [39]. These were demonstrated to function in supporting migratory pathfinding [39, 42] (Fig. 1.1). ILPs in general are formed by a wide variety of cells including cancer cells, monocytes, lymphocytes, smooth muscle cells and osteoclasts[41]. These structures are defined morphology and by their molecular composition through, yet some ambiguity still exists in their regulation and function. ILPs have actin cores and are enchriched in actin-associated molecules such as Arp2/3 and cortactin. They also are enriched in focal adhesion proteins such as talin, vinculin and paxillin. ILPs represent foci for signaling and are hot spots for tyrosine phosphorylation[43]. Typically ILPs (as few as one or more than 100 per cell, depending on context) form to support adherence to extracellular matrices and can be visualized as individual actin puncta localized between cells or between a cell and its substrate. The persistence of these structures can vary widely, ranging anywhere from tens of seconds to an hour.

Transendothelial migration is an energetically unfavorable process that results in T cells passing through endothelial monolayers. T cells can pass either paracellularly (through junctions between endothelial cells) or transcellularly (through the

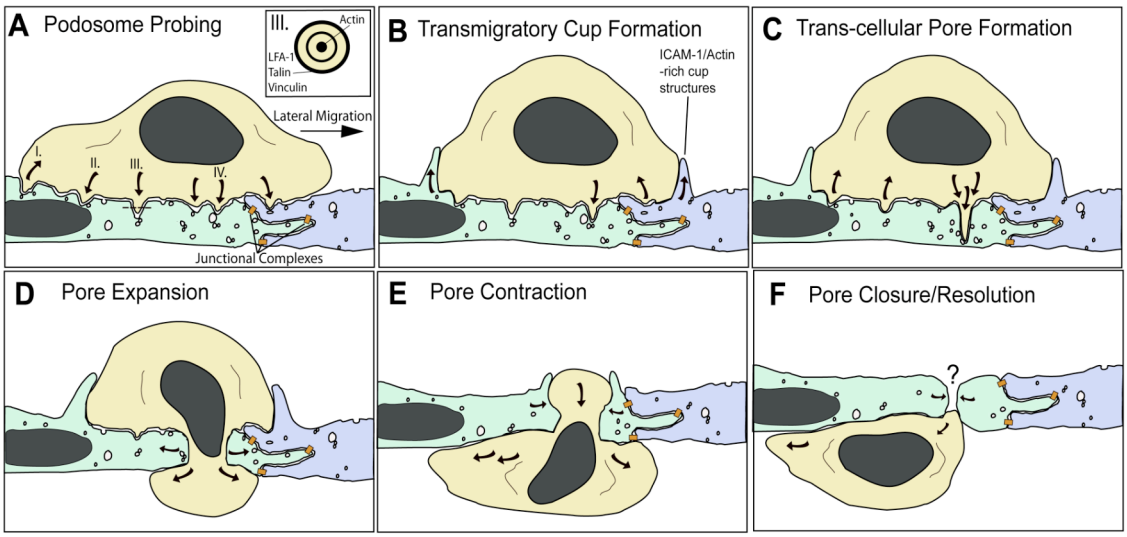

Figure 1.1 Mechanisms for trans-cellular diapedesis. The schematic summarizing basic morphologic features broadly observed *in vivo* and *in vitro* as a leukocyte (tan) progressively migrates across the endothelium through a trans-cellular pore. A small segment of endothelium is depicted in which two individual endothelial cells are distinguished by green and blue coloring. Locations where specific junctional adhesion complexes (i.e., tight, adherens and gap junctions) form are indicated (orange). (**A**). Podosome Probing. The schematic depicts a 'snapshot' of a lymphocyte laterally migrating toward an intact inter-endothelial junction. During migration dozens of actin-dependent podosome-like protrusions dynamically form (downward pointing arrows) and retract (upward pointing arrows), concomitantly forcing endothelial invaginations termed 'podo-prints'. This dynamic protrusion behavior is thought serve in migratory pathfinding as a means of 'probing' the endothelial surface for sites permissive to trans-cellular diapedesis. I. Shows a trailing edge podosome retracting. II. Shows a podosome protruding into, and being frustrated by, the rigid nuclear lamina. III. Shows a podosome and its cross-section (inset), highlighting the peripheral LFA-1 integrin/talin/vinculin zone and the actin-rich core. IV. Highlights a specific podosome that progressively extends to become an 'invasive podosome' and facilitate trans-cellular pore formation in panels B and C. Endothelial vesicles, VVO and caveolae ('vesicles') are seen enriched near or directly fused to podo-prints. (**B**). Transmigratory Cup Formation. Overlapping temporally with podosome probing (A), endothelial cells proactively protrude actin-dependent, ICAM-1/VCAM-1-enriched protrusions (*) that embrace adherent leukocytes, forming 'transmigratory cups' that are thought to facilitate transition from lateral to trans-endothelial migration. Note many podosomes-like protrusions have or are retracting while one continues to protrude. (**C**). Trans-cellular pore formation. At permissive sites a podosome-like protrusions progressively extend, transitioning to 'invasive podosomes', which forces the endothelial apical and basal plasma membrane into close opposition thereby facilitating initial trans-cellular pore formation for diapedesis. Active SNARE complex-dependent fusion of endothelial vesicle at the site of protrusion may facilitate this process. (**D**). Pore expansion. The leukocyte progressively pushes across the trans-cellular pore causing expansion of its diameter to as much as 5 microns. (**E**). Pore contraction. As the leukocyte completes diapedesis the pore contracts, maintaining close endothelial cell-leukocyte contacts. (**F**). Pore closure/resolution. The leukocyte finally, exits the pore completely. Substantial *in vitro* and *in vivo* data support the existence of rapid resealing of the vacated pore. However, no details currently exist on the mechanisms of this important process. **Taken from**[4]**.**

endothelial cell itself). Although paracellular transmigration has been thought to be the predominant mechanism by which T cells enter the tissues, there is evidence supporting an equal if not predominant role of transcellular diapedesis[4]. The first step of diapedesis is T cell probing the endothelium looking for sites permissive for transmigration. The T cell uses ILPs to interrogate the surface mechanically, breaking first through the glycocalyx and then indenting the plasma membrane and cell cortex (which is ~10-fold stiffer than the glycocalyx) (Fig. 1.1).

Since the endothelium has a dense glycocalyx, which is disrupted by T cell ILPs during transmigration, and ILPs and ISs share some similar molecular features such as dependence on actin assembly, we hypothesized that ILPs may be responsible for initiating TCR signaling. By using endothelial cells as a model with ideal topology for high spatio-temporal resolution imaging, we discovered that dynamic ILP probing by CD4 and CD8 memory/effector lymphocytes enforces close T cell-EC apposition, which facilitates Ag recognition and TCR signaling. Moreover, T cell activation is sustained through a novel IS architecture dominated by dense arrays of calcium-stabilized ILPs (each enriched in signaling molecules) that we term a 'podo-synapse'. Complementary studies with model substrates and professional APCs (B and dendritic cells) suggest that rather than being a *unique feature* of T cell-EC ISs, ILPs are *uniquely revealed* in this setting. Together our results indicate that

memory/effector T cells use ILPs to facilitate efficient search for Ag and to help sustain the resulting signaling responses.

MATERIALS AND METHODS

Cells

Natural human T memory cells (nT_{mem}) ($CD4^+CD45RO^+CD45RA^-$) were isolated via negative selection from peripheral blood of healthy donors using a CD4 T cell isolation kit, followed by $CD45RA^+$ cell depletion (Miltenyi Biotec) to >95% purity and used within hours of isolation. Induced/expanded human T memory cells iT_{mem} ($CD4^+CD45RO^+$) were made by culturing peripheral blood buffy coats for 72 hrs in 1 mg/ml of bacterial superantigens staphylococcal enterotoxin B (SEB) and toxic shock syndrome toxin 1 (TSST) (Toxin Technology) in RPMI complete media. CD4 memory cells were enriched by using a CD4 T cell memory negative isolation kit (Miltenyi Biotec). Cells were cultured 3-10 days in 20 ng/ml IL-15 (R&D Systems) in RPMI complete media to maintain memory phenotype.

Mouse CD4 or CD8 T cells were isolated by magnetic separation from either $OTII^+TCRa^{-/-}CD45.1^{+/+}$ (crossed from OTII mice from Taconic Farms) or $OTI^+Thy1.1^{+/+}$ (crossed from OTI mice from Taconic Farms) mice and activated with irradiated splenocytes in the presence of 30 μg/ml OVA 323-339 (OTII) or 500ng/ml OVA-SIINFEKL (OTI) supplemented with IL-2 for 3 days. T cells were reselected with CD4 magnetic beads and rested in culture in the presence of IL-2 for a further 3 days. Human Lung Microvascular ECs (HLMVEC), Human Dermal Microvascular ECs (HDMVEC) and Human Umbilical Vein ECs (HUVEC) were from Lonza and cultured

on fibronectin (10 mg/ml; Invitrogen) in EBM-2 MV media (Lonza). Mouse Heart ECs were isolated from C57Bl/6 mice by collagenaze digestion of heart tissue of 9-15 day old mice with 500U/ml collagenase for 30 min. followed by positive selection with anti-CD31(MEC13.3) coated beads (Dynal). ECs were cultured for 7 days in media with EC Growth Supplement (Biomedical Technologies) followed by reselection with beads coupled to anti-CD102. ECs were >95% purity based on expression of $CD105^{+}CD102^{+}$. ECs were transfected by Amaxa electroporation according to manufacturers instructions (Lonza). Palmitoylated YFP ("Mem-YFP") and soluble monomeric DsRed (sDsRed) constructs were from Clontech. Palmitoylated DsRed (Mem-DsRed) and ICAM-1-GFP were generated as described [39]. ECs were activated for 48 hr with 100 ng/ml IFN-γ (R&D Systems) and 12 hr with 50 ng/ml TNF-α (R&D Systems). The Priess B cell line was a kind gift from Dr. Kai Wucherpfennig. Chinese Hamster Ovary (CHO)-K1 epithelial cells were from ATCC and were transfected by Amaxa electroporation. Murine bone marrow-derived dendritic cells (BMDCs) were prepared from bone marrow cells isolated from femurs and tibias of C57Bl/6 or *Ciita*$^{-/-}$ mice (Jackson Labs) and cultured in 30 ng/ml GM-CSF (Peprotech) for 6 days. Cells were transfected with constructs by Amaxa electroporation.

Transendothelial Migration

Lymphocyte transendothelial migration assays were conducted in both static and shear conditions as described [39]. In general, endothelial cells were plated to 90 percent confluency on fibronectin-coated coverslips and cultured for 72 hours with 100ng/ml

IFN-γ and overnight with 50ng/ml TNF-α in EBM-2 media (Lonza). ECs were washed twice and T cells were added in imaging buffer (HBSS with 1% human serum albumin, 1mM HEPES, 1mM Ca^{2+} and 1mM Mg^{2+}). In some cases T cells were added to 8 mm pore transwell inserts that were pre-seeded with ECs and then collected from the bottom chamber 6 hr later and analyzed by flow cytometry.

Live-cell Imaging and Analysis

Live cell imaging was performed on an Axiovert S200 microscope with a 40x oil objective and analyzed with Axiovision software (Zeiss). For calcium imaging, T cells were pre-incubated with 1 μg/ml Fura-2-AM or Fluo-4-AM (Invitrogen) for 30 min. For Fura-2, standard Fura-2 filters were used according to manufacturers instructions (Chroma) and ratiometric calcium flux was calculated (340_{nm}EX-510_{nm}EM-background/380_{nm}EX-510_{nm}EM-background) for each cell using Axiovision. For Fluo-4, green fluorescence filters were used and basal fluorescence signal was established by imaging cells on uncoated chambers. T cell polarity was calculated from bright field images as the ratio of the greatest edge-to-edge dimension in the x-y plane (i.e., the long axis) divided by the perpendicular axis. Migration velocity was measured for cells using the Axiovision Cell Tracking Module. Podo-print/ILP lifetimes were assessed using podo-print appearance and disappearance on mem-dsRed- or mem-YFP-transfected ECs as a readout for the presence of ILPs [39]. Podo-print/ILP lifetimes were calculated as: the last time point when an individual podo-print/ILP was visible – the time point when that podo-print/ILP first appeared. Podo-print/ILP lateral translocation was assessed by

determining the distance between the T cell centroid and the first and last positions of an individual podo-print/ILP during its lifetime. Podo-print/ILP index, a measure of the total number of ILPs per cell, was calculated at 5 min post addition of T cells. 'Offset Time' was used to describe relative time between first podo-print/ILP formation and calcium flux rise above background. Temporal resolution was limited to 10 seconds, the maximal achievable acquisition frame rate of this analysis. Data was then sorted into 10 second interval bins.

For selected studies, lymphocyte were pre-incubated, or lymphocyte and APCs co-incubated, with select pharmaceutical agents, incuding latrunculin-A (1 μg/ml, Sigma), PP2 (10 μM, Calbiochem), BAPTA-AM (40 μM, Sigma), BTP2 (20 μM, Calbiochem), thapsigargin (1μM Sigma), CAMKII inhibitor CK59 (50μM, EMD Biosciences) as indicated. For calcium blockade conditions, T cell were pretreated with BAPTA-AM and BTP2 in imaging buffer containing high (45 mM) potassium. T cells were added to ECs and imaged with additional BTP2 for the duration of imaging.

Fixed-cell Imaging

Fixed cell samples were imaged on a LSM 510 confocal microscope (Zeiss) with a 63x dipping objective. Samples were fixed and stained for αL integrin (TS2/4), ICAM-1 (IC1/11), F-actin (phalloidin), MHC II (WR18, Abcam), PKC-θ, talin (rabbit anti-talin, a gift from Dr. Keith Burridge), CD3 (OKT3, ebioscience), CD43 (L60, BD Biosciences), CD45 (HI30 or UCHL1, ebioscience), HS1 (clone 9, BD Biosciences or

rabbit anti-HS1, Cell Signaling), ZAP-70 (Santa Cruz), P-Y (4G10 platinum, Millipore) or NFAT (BD Biosciences). Transmigration was analyzed by confocal microscopy as described [44]. Z-stack images were taken at 0.5μm intervals through endothelial monolayers with T cells. Position of transmigration was quantified by scrolling through z-stack images and identifying LFA-1/Actin positive T cells. T cells that were adherent to endothelial monolayers with no transcellular pores were identified as adherent. T cells that had transcellular pores (LFA-1/Actin rich structures protruding into and through the endothelial monolayer which displaces endothelial ICAM-1) were identified as transmigrating. T cells that were completely underneath the endothelium without any transcellular pores present were identified as transmigrated. Areas of non-continuous endothelial monolayers were omitted.

CTL Killing Assay

For specific killing assay, murine ECs were labeled with either 0.6μM or 0.02μM CFSE ($CFSE^{hi}$ and $CFSE^{low}$, respectively). The $CFSE^{hi}$ population was pulsed with 1μg/ml SIINFEKL for 20 minutes and washed extensively. Both $CFSE^{hi}$ and $CFSE^{low}$ populations were plated together in a 1:1 ratio overnight. Activated OTI CD8 T cells were rested for 5 hours and added to monolayers in a 3:1 T cell:target cell ratio. Cultures were trypsinized, and were stained for CD105 to differentiate the ECs from T cells, and analyzed by flow cytometry. Specific lysis was calculated by the following equation $(1-((CFSE^{hi} /(CFSE^{hi} + CFSE^{low}))/(\text{control } CFSE^{hi}/CFSE^{low}))*100)$.

Planar Coated-Glass APC Model

Coated glass immune synapse (IS) models were prepared as described [25, 45]. Briefly, imaging chambers were coated with ICAM-1-Fc (10 μg/ml; R&D Systems) alone, or together with anti-CD3, anti-CD43, anti-CD45 or control IgG antibody (10 μg/ml). Fluo-4-labelled lymphocytes were added and imaged by fluorescence and interference reflection (IRM) microscopy.

Coated-Cell APC Model

CHO-K1 cells were transfected with ICAM-1-GFP and soluble dsRed via electroporation using the Amaxa electroporation system. Cells were then coated with antibodies via a biotin/steptavidin (SA)-based approach [46]. For this, cells were subjected to primary amine-targeted cell surface biotinylation for 15 min with biotin-NHS-ester (Thermo Electron) (0.5 μg/ml). Cells were washed and then incubated with unlabeled streptavidin, at 10 μg/ml for 15 min. Cells were then washed and incubated with biotinylated anti-CD3, -CD43 or -CD45 (eBiosciences) at 10 μg/ml for 15 min. Surface coupling was determined by using a fluorescent anti-mouse antibody and visualized on the microscope.

T cell Activation by CD3 Cross-linking

Fluo-4- labeled T cells were settled onto uncoated glass chambers and 10μg/ml anti-CD3 and CD28 were added to the imaging chambers and calcium was monitored.

Transmission Electron Microscopy

Transmission electron microscopy of T cell-APC complexes was performed as described [39]. EC monlayers were fixed with 2.5% glutaraldehyde and 2% paraformaldehyde in 1.0M sodium cacodylate buffer (pH 7.4) for 2 hours, post-fixed in 1.5% sym-collidine-buffered OsO_4 for 1 hour, stained en bloc with uranyl acetate, dehydrated with sequential washes in increasing alcohol concentrations and embedded in Eponate. Samples were lifted with a short exposure to liquid nitrogen and reembedded so that the EC monolayers were perpendicular to the face of the block. 90nm sections were cut with and imaged with a Phillips CM-10 electron microscope at 80kV. 50 randomly selected micrographs were analyzed by enumerating zones of membrane apposition (<20 nm) and correlating them with respect to ILP location. The electron microscopy was carried out in collaboration with Dr. Ann Dvorak and Tracey Scuito.

Statistical Analysis

Error bars represent standard error or standard deviation as indicated. P values were calculated via unpaired Student's T tests in Graphpad Prism. Statistical significance is indicated with p values as follows: *** = $p<0.0005$, ** = $p<0.005$, * = $p<0.05$.

Results

Endothelial-Presented Ag Promotes Activation of CD4 Memory T cells

We wanted to elucidate the mechanisms by which memory/effector T cells initially probe for and recognize Ag utilizing endothelial cells as model APCs. Although T cell lines such as Jurkat T cells have been used extensively to study IS architecture, we had found that they do not effectively interact with vascular endothelial cells *in vitro*. Therefore, we isolated natural CD4 memory-like lymphocytes (nT_{mem}) and generated induced/expanded CD4 memory-like lymphocytes (iT_{mem}), from human peripheral blood. Since nT_{mem} are used directly after isolation from human subjects, they are the most physiological responder T cell that we can use. We cultured iT_{mem} so that we could expand out this population in order to perform experiments that require larger numbers of cells. The isolated nT_{mem} were CD4+, CD45RO+ and contained both central-memory (T_{CM})- and effector-memory (T_{EM}) T cells (~78% and ~22%, respectively) based on CD62L staining (Fig. 1.2). The iT_{mem} were slightly more polarized toward the T_{EM} subtype (~69% vs. ~31%) (Fig. 1.2). Monolayers of HLMVECs (Lung ECs), HDMVECs (Skin ECs) and HUVECs (Umbillical ECs) were used as models for the vasculature. *In vivo* endothelial MHC-II expression is dependent on IFN-γ [31]. This was recapitulated *in vitro* by culturing ECs with exogenous IFN-γ (Fig. 1.2). Endothelium was additionally activated with TNF-α to promote an inflamed phenotype by upregulation of ICAM-1.

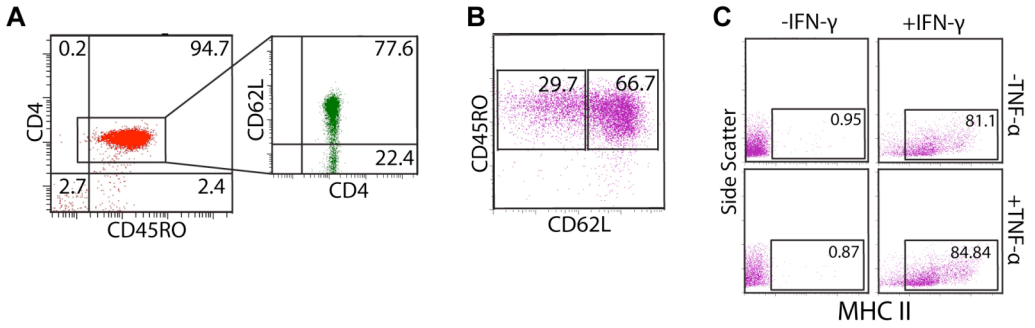

Fig. 1.2. Phenotype of Memory-like CD4 T cells and Endothelium (**A**) CD4 nT_{mem} cells were sorted from human blood according to *Materials and Methods*, stained for indicated surface markers and analyzed by flow cytometry. (**B**) Surface phenotype of cultured induced T memory cells (iT_{mem}). CD4 T cells were isolated, activated and cultured according to *Experimental Procedures*, stained for indicated surface markers and analyzed by flow cytometry. Plots are only CD4 positive gate. (**C**). HLMVEC were incubated with or without IFN-γ for 48 hours and with or without TNF-α for 18 hours, trypsinized, stained for MHC II, and analyzed by flow cytometry.

Next, we set up live cell analysis to concomitantly monitor T cell activation (i.e., calcium flux) and migration on endothelium pulsed with Ag (i.e., bacterial super-antigen, a widely used model Ag [45, 47, 48]). Superantigens bind the TCR and MHC II outside of the TCR-MHC binding pocket to elicit activation. In this way, we could circumvent the need for MHC matching of endothelial donors, which can be cumbersome and costly. In the absence of Ag, nT_{mem} and iT_{mem} fluxed little calcium (Fig. 1.3A.), remained polarized (Fig. 1.3B), and underwent continuous lateral (Fig. 1.3C) and transendothelial migration (i.e., 'diapedesis') consistent with their designation as memory cells (Fig. 1.3D). On HLMVECs pulsed with Ag (1 μg/ml SEB and TSST), T cells rapidly fluxed calcium, lost polarity and arrested migration (Fig. 1.3A-C). Similar results were found with alternate Ag (e.g., SEE (staphylococcal enterotoxin E) and MAM (mycoplasma arthridic antigen) presented by HDMVECs or HUVECs (data not shown). Additionally, in the absence of Ag, the majority of iT_{mem} transmigrated within 30 min, whereas in the presence of Ag, diapedesis was delayed by ~30-60 minutes (Fig. 1.3D). Thus, the migratory stop signal was transient. IT_{mem} also exhibited Ag-dependent transient migration arrest under laminar fluid shear flow conditions similar to those found in microvasculature *in vivo* (2 dyne/cm^2; Fig. 1.3E-G).

During T cell activation the transcription factor NFAT is dephosphorylated by calcineurin and translocates from the cytoplasm to the nucleus, where it stimulates transcription[49]. Incubation of nT_{mem} on Ag-pulsed ECs promoted robust nuclear

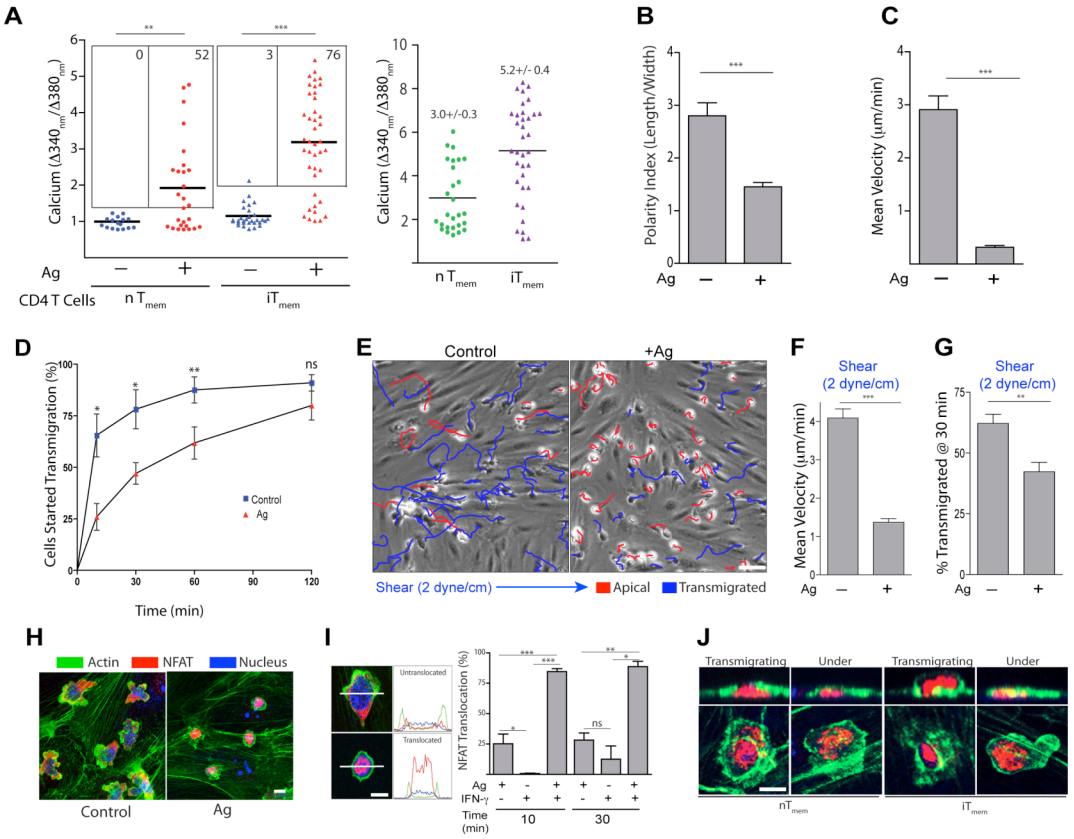

Fig. 1.3 Human Microvascular ECs are Capable of Ag-specific Stimulation of CD4 Memory-like T Cells. (**A**) Human CD4 nT_{mem} (circles) or iT_{mem} (triangles) were loaded with Fura-2 and incubated on Ag-pulsed HLMVECs. Calcium flux at 5 min (left) or at maximal value over a 30 min duration (right) were plotted. (**B** and **C**) iT_{mem} were incubated on HLMVEC pulsed with Ag and T cell polarity (length/width ratio) at 5 min and velocity was calculated over a 30 min duration. (**D**) iT_{mem} transendothelial migration was scored on Ag pulsed ECs as described in *Materials and Methods*. (**E**) iT_{mem} were infused over Ag pulsed HLMVEC at 2 dyne/cm^2 and imaged. Depicted is an end-point image with migration tracks of apical (blue) and transmigrated (red) lymphocytes. (**F** and **G**) Lateral migration velocities for T cells from (E) during both pre- and post-diapedesis phases of migration over 30 min (F) and percent of iTmem transmigrated were measured (G). (**H**) Representative images of nT_{mem} incubated on Ag-pulsed HLMVEC and staining for actin (green), NFAT (red) and nucleus (blue). (**I**) nT_{mem} were incubated on activated HLMVEC. Nuclear NFAT translocation was scored according to line scan profiles (left). (**J**) Samples were acquired as in (H) and representative transmigrating or transmigrated ('Under') lymphocytes are shown. Scale bar = 5 μm. Data represent mean ± SD (B, C) or SEM (D, F, G, I). *p<0.05, **p<.005, ***p<0.0005. *Copyright 2012 The American Association of Immunologist, Inc.*

translocation of NFAT (Fig. 1.3H, I). Significantly, transmigrating nT_{mem} and iT_{mem} cells retained nuclear NFAT demonstrating that these cells remained activated even after transmigration (Fig. 1.3J). NT_{mem} on endothelium that was pulsed with Ag, but not pretreated with IFN-γ (and therefore lacked strong MHC-II expression) exhibited little NFAT translocation (Fig. 1.3I) confirming that the responses to Ag-pulsed endothelium were MHC-II-dependent. Additionally, cells that transmigrated through vascular endothelium that was pulsed with sAg secreted IFNγ, and therefore were fully activated (data not shown). Collectively these results demonstrate that endothelium is able to present model Ag in an MHC-II-dependent manner to primary CD4 memory/effector lymphocytes, which induces a transient delay in diapedesis and full T cell activation.

ILP Arrays Dominate the T Cell-Endothelial Cell Interface During Activation

Next we investigated the cellular and molecular basis for T cell activation in our endothelial APC model. Previously, we transfected fluorescent membrane markers ('mem-YFP' or 'mem-DsRed') expressed in the ECs to detect topological changes in the plasma membrane [39]. In this way, we demonstrated that ~0.5 mm fluorescent rings that formed dynamically on the endothelium under migrating T cells corresponded to cylinder-shaped cell surface invaginations (i.e., 'podo-prints') induced by lymphocyte Invadosome/Podosome-Like Protrusions (ILPs). Thus, podo-prints formed on the EC surface served as an indirect, but extremely sensitive, read-out for T cell ILPs [39]. Direct readout of T cell ILPs by transfection of T cells was not possible because primary T

cells are difficult to transfect and large local volumes of the T cell membrane lead to oversaturation of fluorophores at the endothelial interface, and therefore, suboptimal imaging.

In the current study, we similarly observed in control settings that podo-prints formed and disappeared continuously (with lifetimes of tens of seconds) under the leading edge lamellipodia of migrating iT_{mem} (Fig. 1.4A, C). Strikingly, when ECs were pulsed with Ag, iT_{mem} rapidly formed dense arrays of podo-prints largely localized at the periphery of the T cell-EC interface under symmetrical lamellipodia (Fig. 1.4, Ex1). A minority (~20-30%) of the iT_{mem} cells formed rosette type podo-print arrays that lacked bias for the cell periphery (Fig. 1.4B, Ex2). In both cases, podo-prints/ILPs were significantly stabilized (lifetimes of ~18 min; Fig. 1.4C). Podo-prints/ILPs exhibited limited lateral translocation, a process that is currently visualized during formation of traditional ISs (0.31 ± 1.5 mm; Fig. 1.4D-F). After ~30 min of contact, ILPs began to disappear and T cells initiated transmigration.

As confirmation that the above observations reflected three-dimensional podo-prints in response to T cell ILPs probing the surface and not retraction of membrane away from the T cell, we co-transfected endothelium with mem-DsRed along with soluble GFP (sGFP) as a marker for cytoplasmic volume [39]. This showed individual fluorescent membrane rings of each podo-print, in fact, represented cytosol-displacing invaginations into the EC surface. This demonstrates that the podo-prints form because

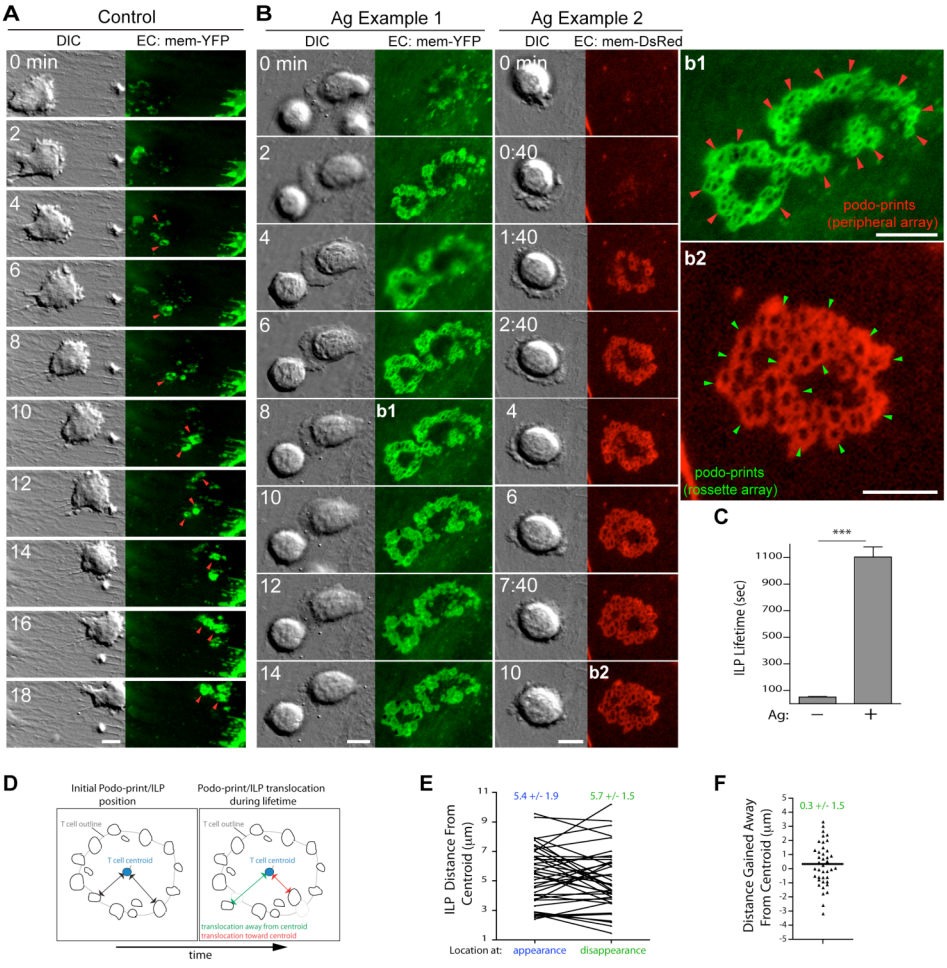

Fig. 1.4 CD4 Memory-like T cells form Stabilized Arrays of ILPs on Ag-Presenting Endothelium. (**A** and **B**) HLMVECs were transfected with mem-YFP or mem-DsRed, activated and pulsed without (A) or with (B) Ag (TSST/SEB). iT_{mem} were imaged live upon addition to ECs. Individual frames at selected time intervals are shown. Arrows indicate fluorescent rings formed on endothelium under adherent lymphocytes. (**C**) Podo-print/ILP lifetimes from imaging studies as in (A and B). Data represents mean ± SEM of at least 80 ILPs formed by at least 25 cells from three or more separate experiments. (**D**) Schematic representation of podo-print/ILP lateral translocation analysis. Grey 'T cell outline' represents a T cell-EC contact area with the 'T cell centroid' indicated as a blue circle and individual podo-prints indicated as black rings. The linear distance between the centroid and podo-print was measured at both the first and last appearance of an individual podo-print/ILP during its lifetime. (**E** and **F**) Podo-print/ILP distances were measured as in (D). Distances from the cell centroid at time of formation and disappearance were plotted for individual podo-prints (E). Data from (E) were further processed to report change in distance (F). Scale bars= 5 µm. *Copyright 2012 The American Association of Immunologist, Inc.*

of ILP pushing into the surface of the endothelium (Fig. 1.5A). Furthermore, confocal imaging showed that podo-prints were ICAM-1-enriched cylindrical EC invaginations into which T cell ILPs extended (Fig. 1.5B). ILPs were enriched in the integrin LFA-1 (Fig. 1.5B), F-actin (Fig. 1.5C) and talin (Fig. 1.5D), similarly to podosomes/invadosomes [41, 42]. Analogous structures formed under physiologic shear flow, with diverse ECs (including HLMVECs (Fig. 1.5A, C and D), HUVECs (Fig. 1.5B), HDMVECs (not shown)), with nT_{mem} (data not shown) and with alternate Ag (Fig. 1.5B)). Similar structures also formed when previously activated murine OT-II CD4+ T cells were incubated on heart microvascular ECs pulsed with OVA 323-339 peptide Ag (data not shown). Thus, memory T cell usage of ILPs to probe for antigen and ILP stabilization due to T cell activation is not only relevant for human memory CD4 T cells, but also occurs in primary murine models.

To assess the T cell-EC interaction in greater detail, we utilized transmission electron microscopy in collaboration with Dr. Ann Dvorak. In the absence of Ag, ILPs averaged 430 $\pm$ 34 nm in depth and 348 $\pm$ 33 nm in width (Fig. 1.5E, F). In the presence of Ag, ILPs were similar in morphology and size (depth = 437 nm, width = 277 nm), but tended to form in denser clusters (Fig. 1.5E-G). An important feature of the ILPs, whether in the absence or presence of Ag, was the existence of zones of extremely close T cell-EC apposition, typically at the tips of the ILPs as if driven by ILP extension (Fig. 1.5F, G, arrows). Though not exclusive to these locations, quantitative analysis revealed that intercellular contacts of <20 nm were 9-fold greater at ILP tips compared to other

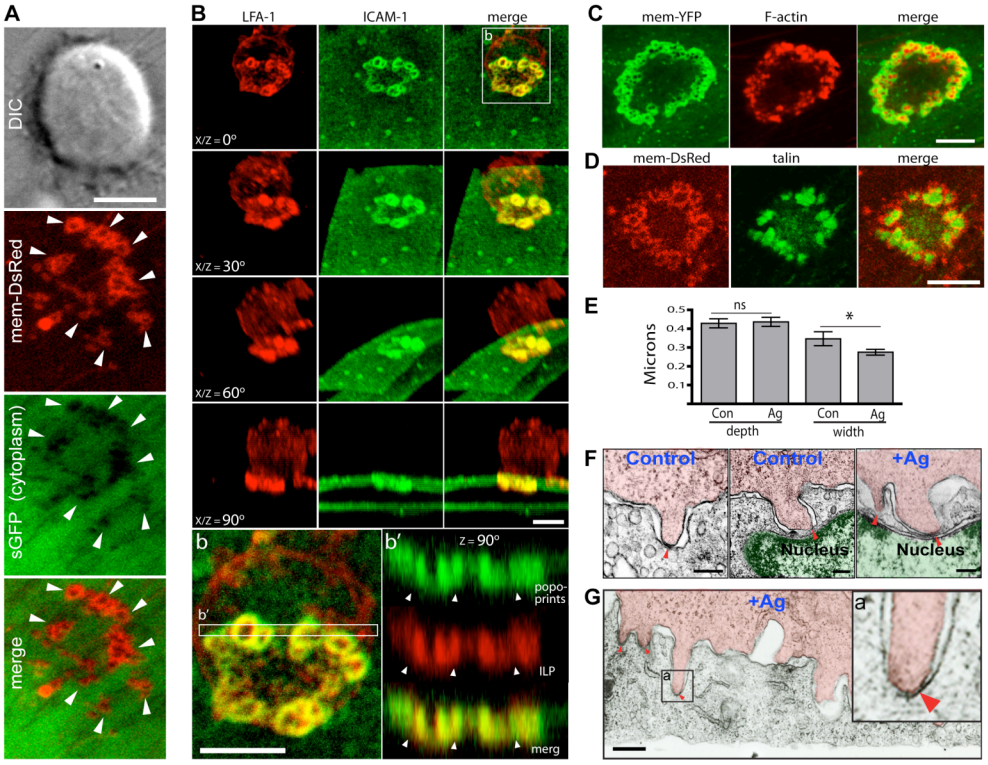

Fig. 1.5 Ag-Stabilized ILPs Exhibit a Discrete 3D Architecture. (**A**) Ag-stabilized T cell ILPs protude into the EC surface. Imaging was conducted as in (Fig. 1.4B) on HLMVECs co-expressing soluble, cytoplasmic GFP (green) and mem-DsRed (red). (**B**) 3D reconstruction from confocal imaging of podo-prints and ILPs. iT_{mem} were incubated for 20 min on activated Ag-pulsed (SEE) HUVEC and then fixed, stained for ICAM-1 (green) and LFA-1(red) and imaged by confocal microscopy. Sections were digitally reconstructed and projected as 3D renderings. Inset (b) provides a magnified view of the ILP arrays. Inset (b') provides an orthogonal cross-section. (**C** and **D**) Ag-stabilized ILPs are enriched in actin and talin. Mem-YFP(C; green)- or mem-DsRed (D; red)-transfected HLMVEC were pulsed with Ag (TSST/SEB) and incubated with iT_{mem} for 5 min and stained for F-actin (C; red) or talin (D; green). (**E**) Quantitation of ultrastructural depth and width of T cell ILPs. Samples as in (C) were imaged by electron microscopy and ILPs were measured. Data represent mean $\pm$ SEM from at least 100 ILPs from at least 20 representative micrographs per condition. (**F** and **G**) ILPs enforce close T cell-EC membrane apposition in the absence and presence of Ag. T cell and endothelial nuclei are indicated with red and green overlays, respectively. Arrows and inset (a) highlight regions of extremely close lymphocyte-EC membrane apposition enforced at the ILP tips. Scale bars in A-D represent 5 μm and in F-G represent 500 nm. Ns = not significant, *p<0.05. *Copyright 2012 The American Association of Immunologist, Inc.*

regions. The idea that ILPs can exert significant force is supported by their ability to both drive trans-cellular diapedesis [39] and to displace/deform organelles such as the nucleus (Fig. 1.5F). It is at these locations at the tips of the ILPs, where it seems like the most force is generated. Therefore, we believe that the very tips of the ILPs are the locations where initial TCR signals are triggered.

Ag-Stabilized ILPs Share Features of Traditional TCR Signaling Micro-clusters

To address how these ILP-dominated cell-cell interfaces relate to TCR signaling and if the ILP tips were spots for TCR signaling we stained for traditional IS markers [18, 25, 26]. Confocal microscopy revealed that podo-prints formed on the surface of the endothelium were modestly, but consistently, enriched in MHC-II compared to MHC-I or mem-YFP (Fig.1.6A, B). T cell ILPs were enriched in CD3 which is the dominant signaling component of the CD3/TCR complex (Fig.1.6C). In some instances the CD3 was enriched precisely at the tip of the ILP (Fig. 1.6C inset b1) and in other cases enriched at the outer edge of the ILP (Fig. 1.6C inset b2). Interestingly, both examples can be found on the same cell, and may reflect ILPs that are in different stages of formation. Comparable CD3 enrichment formed under physiologic shear flow (Fig.1.6I, J). In <5% of T cells CD3 was distributed into a cSMAC-like cluster rather than in peripheral ILPs (Fig. 1.7).

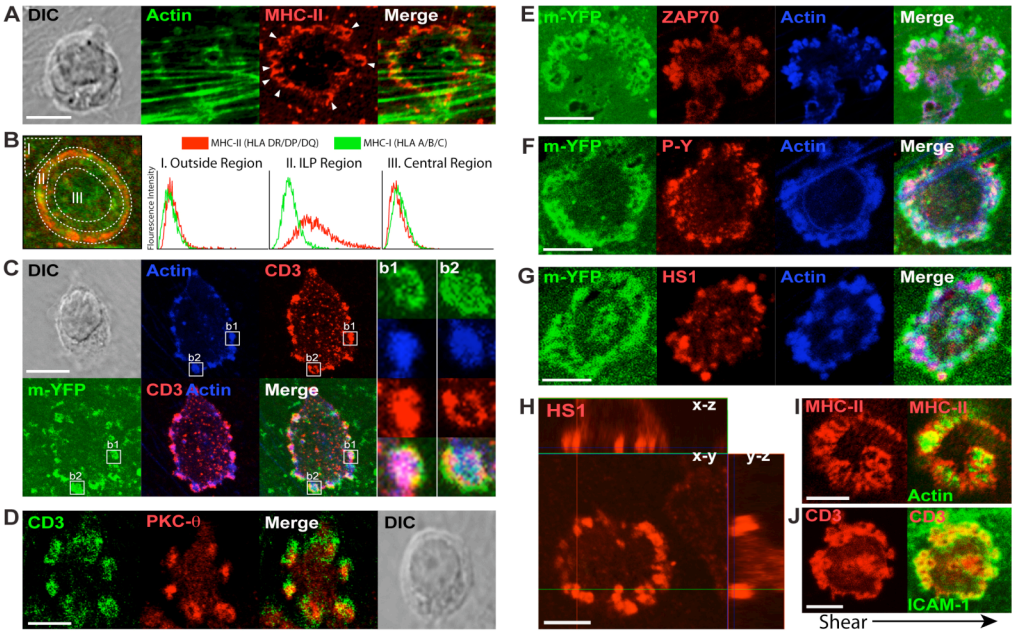

Fig. 1.6 Ag-Stabilized ILPs are Foci for Immune Signaling. IT_{mem} cells were incubated with activated, Ag-pulsed (TSST/SEB) HLMVEC for 5 min, fixed, and stained as indicated and imaged by confocal microscopy. (**A**) Ag stabilized ILPs (F-actin, green) protrude into MHC-II (red)-enriched podo-prints. Arrows indicate MHC-II-enriched podo-prints. (**B**) Samples as in (A) were stained for MHC-II (HLA DR/DP/DQ; red) and MHC-I (HLA A/B/C; green). Schematic of gated regions of interest is shown on the left, and included a region outside of the IS (I), the ILP-rich region of the IS (II) and the central region of the IS (III). Right panels show pixel fluorescence intensity histograms for regions I-III. (**C**) ILPs (F-actin, blue) protruding into podo-prints (mem-YFP, green) are enriched in CD3 (red). Within individual ILPs CD3 is predominantly focused at the tip (insets b1) and to a lesser extent the edge (inset b2). (**D**) PKC-θ(red) is enriched with CD3 (green) in ILPs. (**E-G**) ILPs (F-actin, blue) colocalize with ZAP-70 (E; red), phospho-tyrosine (F; red) and HS1 (G; red). (**H**) HS1 (red) is highly enriched in ILPs. Cross-sectional views from serial-section confocal microscopy are shown of a lymphocyte adherent to the endothelium presenting Ag. (**I** and **J**) ILP arrays were allowed to form as above with the additional presence of physiologic laminar fluid shear flow (2.0 dyne/cm^2, arrow indicates direction). (I) MHC class II (red) and f-actin (green) are shown. (J) CD3 (red) and ICAM-1 (green) are shown. Scale bars = 5μm. *Copyright 2012 The American Association of Immunologist, Inc.*

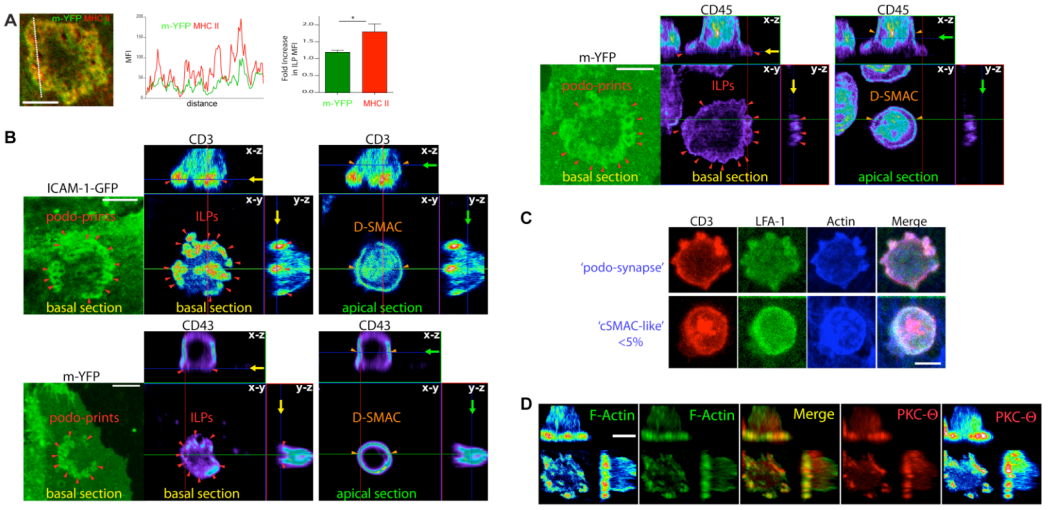

Fig. 1.7 Distribution of Immune Signaling Molecules in the T cell-EC IS. IT_{mem} cells were incubated with activated, Ag-pulsed (TSST/SEB) (and ICAM-1-GFP or mem-YFP-transfected, where indicated) HLMVEC for 5 (A, B, D) or 30 min (C), fixed, and stained as indicated and imaged by confocal microscopy. (**A**) Samples on mem-YFP (green)-transfected ECs were stained for MHC-II (red). Representative micrograph is shown on the left. Middle panel indicates fluorescent values of each channel from line scan (dashed line on left). Right indicates quantitation of fluorescence intensities along the dashed line comparing podo-prints from nearby regions of endothelium outside of the T cell contact zone. (**B**) Samples were prepared as in (A) on ICAM-1-GFP or mem-YFP-expressing HLMVECs and stained for CD3, CD43 or CD45 and LFA-1 as indicated. *En face* (x-y) and orthogonal cross-sectional (x-z, y-z) views are depicted. CD3, CD43 and CD45 are pseudo-colored using a rainbow intensity indicator (blue = low, red = high). Left panels show a relatively basal section (see yellow arrows) at the T cell-EC interface where the podo-print- and ILP arrays are evident (red arrows). Right panel shows a section that is relatively more apical (i.e., distal from the IS, see orange arrows). Note that CD3 has highest intensity within the ILPs compared to parallel oriented segments at the edge of the cell in regions outside of the IS (i.e., the D-SMAC). By contrast, CD43 and CD45 intensity is highest outside of the IS (i.e., in the D-SMAC), shows modest levels within the peripheral ILP region and is lowest in the center if the IS. (**C**) Samples were stained for F-actin (blue), LFA-1 (green) and CD3 (red). Whereas, on the majority of T cells CD3 was either enriched into ILPs after 30 min (upper panels), only a very small fraction (<5%) of cells displayed enriched into cSMAC-like central clusters. A similar fraction showed relatively more diffuse distributions (data not shown). (**D**) Samples were stained for F-actin (green and rainbow intensity pseudo-color) and PKC-θ (red and rainbow intensity pseudo-color), subjected to confocal microscopy and presented as *en face* and orthogonal projections. Scale bars represent 5 μm. *Copyright 2012 The American Association of Immunologist, Inc.*

Molecules implicated in TCR signaling, including PKC-θ (Fig. 1.6D), ZAP-70 (Fig. 1.6E) and phosphotyrosine (P-Y; Fig. 1.6F) were also enriched in ILP cores, suggesting active signaling of immune receptors at these sites. Importantly, the phosphorylated tyrosine that is enriched here is also a general feature of podosomes. The cortactin homolog hematopoietic lineage cell-specific protein 1 (HS1), a known regulator of both podosomes and ISs [45, 50-52] showed particularly strong enrichment within the ILPs (Fig. 1.6G, H). Alternatively, the inhibitory molecules CD43 and CD45 localized primarily to the region outside of the T cell-EC interface consistent with the kinetic segregation model for ISs present in ILPs (Fig. 1.7B). These observations suggest that ILPs may serve as discrete loci for TCR signaling with general features similar to TCR signaling micro-clusters and 'multi-focal' synapses that have been previously reported [18, 26, 27, 53-55].

Collectively, these experiments show that CD4 iT_{mem} activation due to EC MHC-II/Ag is coupled to cell-cell interfaces dominated by arrays of ILPs that are stabilized and subsequently enriched in TCR signaling molecules and podosome proteins. We term this previously undescribed architecture, which shares features of both podosome belts/rosettes and multi-focal ISs, a 'podo-synapse'.

ILPs Support Efficient Ag Recognition and Sustained Signaling

To determine the functional relationship between ILP formation and T cell activation, we concomitantly monitored calcium flux and ILP dynamics. In the presence of Ag, a small amount of calcium flux was evident shortly after the first appearance of ILPs. These initial ILPs tended to form within seconds and at the center of the cellular interface between the T cell and endothelial cell and had a high turnover. After an initial low calcium flux signal which occurred after the first ILPs, calcium flux then peaked several minutes later and gradually decayed over the following 5-60 min (Fig. 1.8A-B). Calcium flux always occurred subsequent to (or in the same 10 sec interval as) the appearance of at least one ILP, with an average offset time of ~25 seconds (Fig. 1.8C). In turn, stabilized ILP arrays became evident in the ~30-60 seconds following the rise in calcium (Fig. 1.8A, B). Interestingly, during ILP stabilization, calcium flux continued to increase and then peaked seconds after the ILP array formed completely. After this time few new ILPs were detected, and calcium flux was maintained at the maximum level.

These observations suggested that the close intercellular contacts driven by ILPs may promote initial Ag recognition and TCR triggering. Testing this hypothesis is challenging as both ILPs and TCR signaling are fundamentally dependent on F-actin assembly and many of the same actin regulatory pathways [39, 41, 56]. Thus, we simply compared effects of F-actin inhibition (via latrunculin-A) on T cell activation by an Ag-pulsed APC *versus* direct TCR cross-linking. When stimulated by Ag-pulsed ECs, iT_{mem} pretreatment with latrunculin-A caused 100% blockade of both ILP formation and

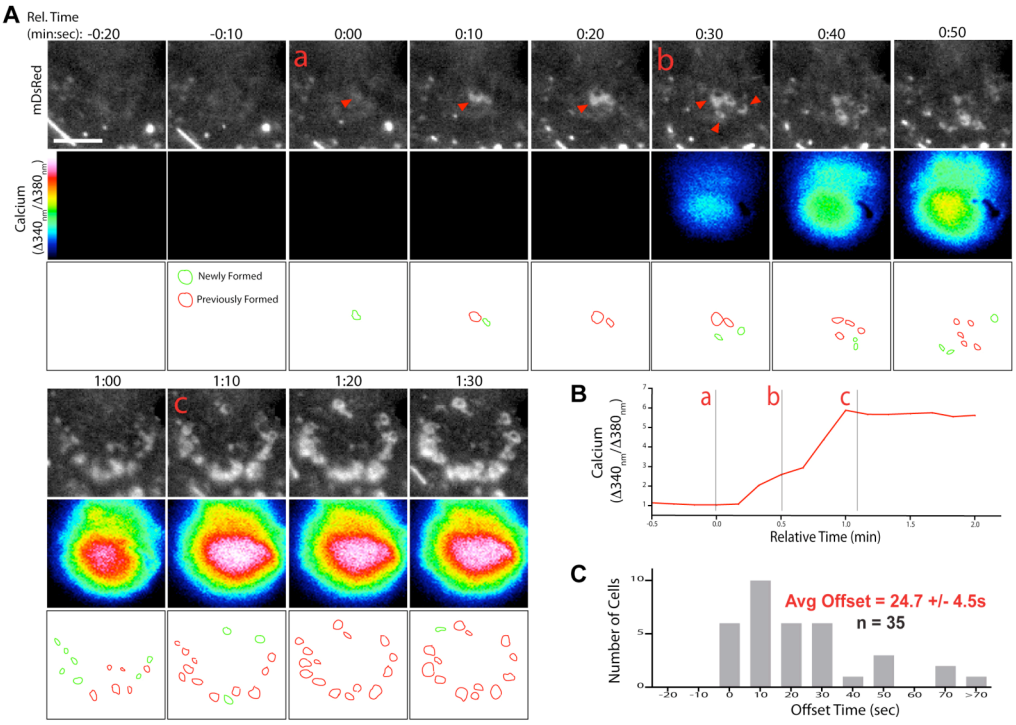

Fig. 1.8. T Cell ILP Formation Precedes Ag Recognition. (**A**) IT_{mem} were labeled with Fura-2 and imaged live (at a maximal temporal resolution of 10 seconds) during migration on mem-DsRed-transfected, Ag-pulsed HLMVECs. Upper panels show mem-DsRed. Arrows indicate initial ILP formation. Middle panels indicate calcium flux values on a rainbow scale. Lower panels provide a schematic representation of newly formed (green) and previously formed (in relation to previous field; red) podo-prints. 'a' is the frame of initial ILP/podoprint. 'b' is the frame when calcium flux rises above background. 'c' is the frame when the peripheral ILP array is stabilized. Note this correlates with peak calcium flux. (**B**) Graphical representation of calcium flux with frames a-c noted. (**C**) Quantitation of ILP-calcium flux offset time. Live-cell imaging was as in (A) and offset time (time from when first ILP forms until calcium flux rises above background) was calculated. Data was binned into 10 second intervals and average +/- SEM is shown for 35 individual T cells from three separate experiments. Scale bars represent 5μm.

calcium flux during the first 5 minutes of co-incubation (Fig. 1.9A, B). By contrast, when TCRs were stimulated directly by anti-CD3/CD28 cross-linking, significant (though attenuated by ~60%), immediate calcium flux was elicited in the presence of latrunculin-A (Fig. 1.9 C,D), as shown previously [57]. From this we conclude that the total latrunculin-A-induced blockade of early response of T cells to Ag-pulsed ECs reflects a defect in ILP formation (Fig. 1.9 C,D). We speculate that the moderate attenuation of calcium signals seen with latrunculin-A treatment on CD3 crosslinking may still be due to blockade of ILP formation, as the mechanism of CD3 crosslinking to achieve TCR signaling may still partially involve force-based triggering elicited by structures such as ILPs.

Calcium Flux is Necessary and Sufficient for Ag-Mediated ILP Stabilization

Next we investigated the transition from dynamic ILP probing to formation of stable ILP arrays. Given the correlation between rise in calcium and appearance of ILP arrays we hypothesized that calcium may be key for stabilizing ILPs. To test this we sought to prevent calcium flux downstream of TCR signaling to determine if we can block ILP stabilization. Initially, pretreating T cells with the widely used calcium chelator BAPTA resulted in normal levels of calcium flux when used alone. We hypothesize that primary human memory cells are sensitized to releasing calcium stores and therefore used a much stronger blockade of calcium signaling. Specifically, we developed a protocol (Ca block) in which we pretreated T cells with the calcium

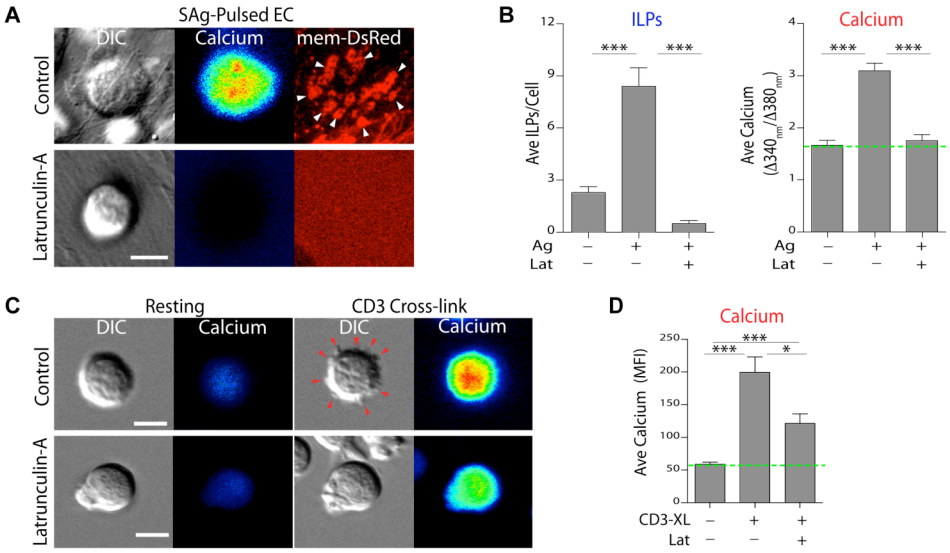

Fig. 1.9. T Cell ILP Formation is Necessary for Ag Recognition. (**A**) Imaging was performed as in (Fig. 1.8.A) with additional pretreatment of T cells with latrunculin-A before addition to Ag-pulsed EC monolayers. (**B**) Podo-print/ILP index (average number of podo-prints/ILPs per cell) and average calcium flux at 5 min were calculated. Both analyses are pooled mean ± SEM from from 3 separate experiments. (**C**) IT_{mem} were labeled with Fluo-4 and imaged live with anti-CD3/CD28 cross-linking with or without latrunculin-A pretreatment. Left panels show resting T cells. Right panels show activated T cells imaged 60 seconds after addition of cross-linking antibodies. Arrows indicate *de novo* formation of micron-scale T cell protrusions. (**D**) Average calcium flux was calculated from three separate experiments as in (B). Scale bars represent 5μm. Data represent mean ± SEM. ***p<0.0005. *Copyright 2012 The American Association of Immunologist, Inc.*

chelator BAPTA as well as the CRAC channel inhibitor BTP2, and furthermore used imaging buffer with a high (45mM) potassium concentration. On Ag-pulsed ECs, this greatly inhibited, but did not completely abolish, calcium flux in iT_{mem} cells, validating its use in these experiments. When we used this calcium blockade on T cells, there was a strong reduction in the number of stabilized ILPs demonstrating that calcium flux is necessary for ILPs (Fig. 1.10A-C). To determine whether calcium flux was sufficient to stabilize ILPs, iT_{mem} were incubated on ECs in the absence of Ag, followed by application of the calcium ionophore thapsigargin to directly elevate intracellular calcium without any direct TCR signaling present. Addition of thapsigargin resulted in robust calcium flux with in seconds. Moreover, artificially fluxing calcium caused iT_{mem} cells already engaged in dynamic ILP probing to arrest ILP turnover and stabilize ILP clusters demonstrating that calcium flux is sufficient for ILP stabilization (Fig. 1.10D-G). Moreover, there was an increase in the number of newly formed ILPs within the 120 seconds after addition of thapsigargin. Thus, whereas dynamic ILP probing of ECs by iT_{mem} seems to facilitate initial Ag recognition, the resulting rise in calcium is both necessary and sufficient to drive formation as well as stabilization of ILPs into podo-synapses.

The above findings point to a putative positive feedback loop for sustaining TCR signaling. In this loop, the ILPs that facilitate initial TCR signaling and are also stabilized by calcium flux downstream of TCR signaling. To break this loop, we sought to block proximal signaling downstream of intracellular calcium flux, specifically

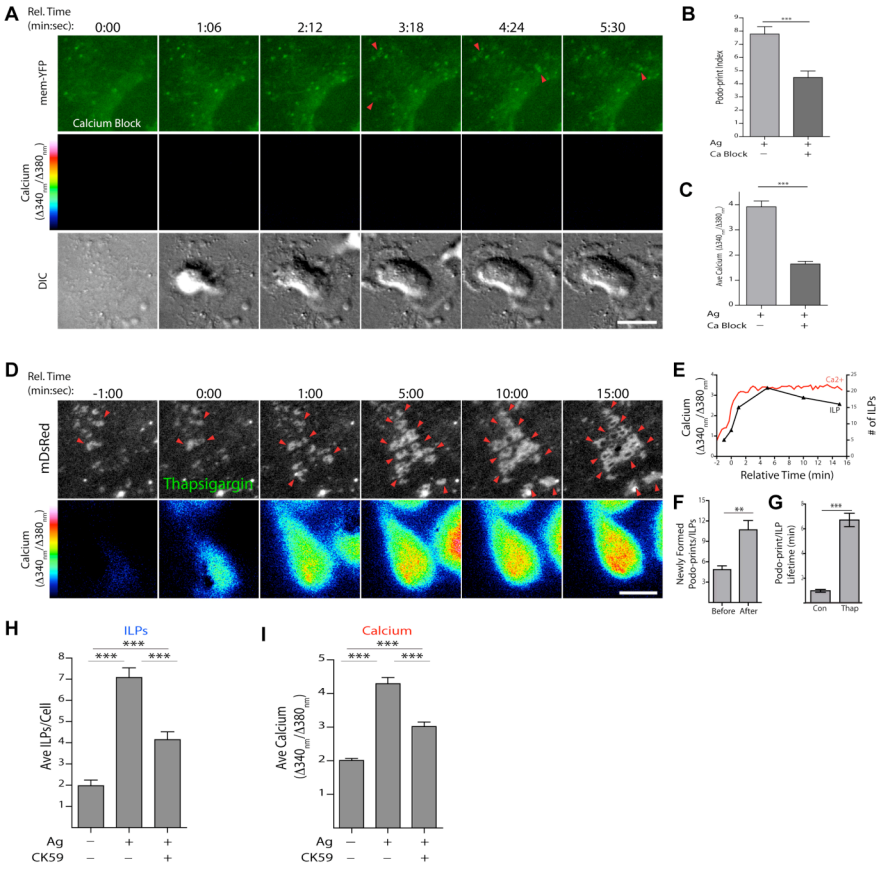

Fig. 1.10. Calcium Flux is Necessary and Sufficient for ILP Stabilization. (**A**) IT_{mem} were Fura-2 labeled, pretreated with the calcium chelator BAPTA and the CRAC channel inhibitor BTP-2 and imaged live on Ag pulsed ECs. Arrows indicate a few sporadically formed podo-prints. (**B** and **C**) Podo-print/ILP index (B) and average calcium flux (C) were calculated at 5 min for experiments as in (A). (**D**) Live cell imaging was conducted in the absence of Ag before and after addition of the calcium ionophore thapsigargin (at time = '0:00'). Arrows indicate ILPs/podo-prints. (**E**) Correlation of calcium flux with ILP number after addition of thapsigargin. (**F**) Quantitation of the number of newly formed ILPs in the 2 minutes before and after addition of thapsigargin. (**G**) Quantitation of the lifetime of ILPs with or without addition of thapsigargin. (**H** and **I**) Imaging and analysis was performed as in A-C except T cells were pretreated with the CAMKII inhbitor CK59. Data represent mean ± SEM. **p<0.005. ***p<0.0005. Scale bars represent 5μm.

targeting calcium-calmodulin dependent kinase II (CAMKII) via the inhibitor CK59 [58]. Blocking CAMKII prevents signaling caused by calcium flux, but does not directly block calcium flux itself nor proximal TCR signaling. Treatment with CK59 attenuated Ag-mediated ILP stabilization by ~50% (Fig. 1.10H). This block in ILP stabilization was coupled to a proportional decrease calcium flux (Fig. 1.10I). Since CAMKII does not block calcium flux directly, the drop in calcium flux in this can possibly be attributed to the prevention of ILP formation and as a consequence, inability to find additional antigen to sustain signaling. Collectively, these results strongly support the interdependence between ILPs and calcium flux.

CD8 Cytotoxic T Lymphocytes (CTLs) use ILPs to Probe for Ag

The endothelium has been shown to initiate MHC-I/Ag-dependent activation of CD8 CTL leading to direct killing of endothelial cells [36, 37]. To investigate the role of ILPs in these responses, previously activated murine OT-I CD8 T cells were incubated on murine heart microvascular ECs pulsed with SIINFEKL peptide Ag. Ag-pulsed ECs initiated a rapid calcium flux (Fig. 1.11A) that was coupled to progressive specific lysis of ECs over a 4 hr duration (~50% lysis ~2 hr; Fig 1.11B). Thus, murine CD8 CTLs can respond to antigen presented by murine endothelium. Live-cell imaging showed that in the absence of Ag, CTLs avidly probed the endothelium with dynamic ILPs while migrating without any visible calcium flux (Fig. 1.11C). This is the first observation in murine studies showing dynamic probing of the endothelium by ILPs looking for sites

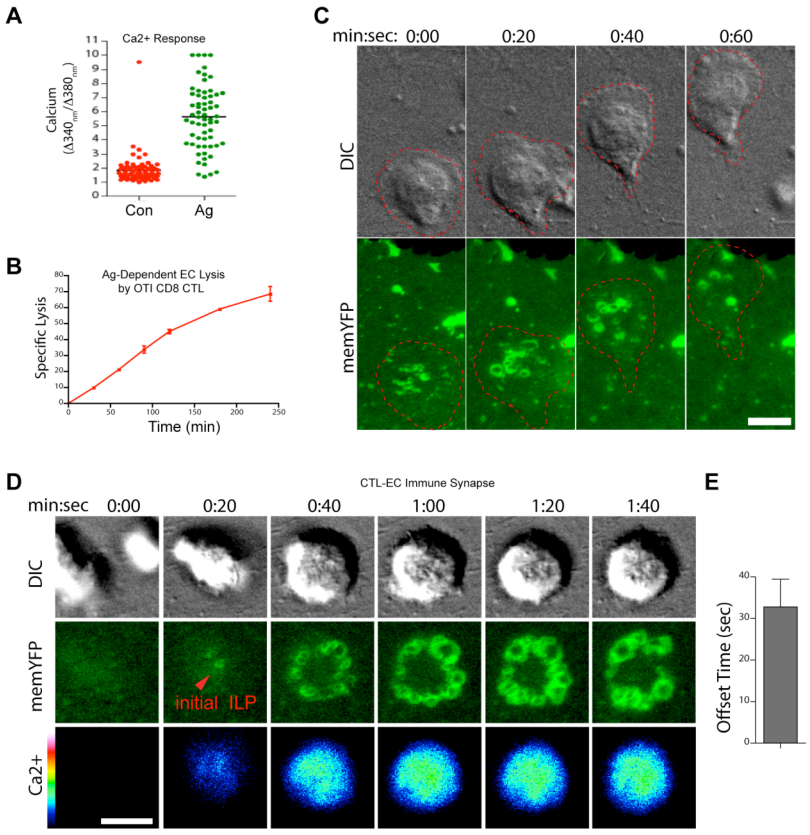

Fig. 1.11. Murine CD8 CTLs Use ILPs to Sense Ag Bound MHC-I on Endothelium. (**A**) Previously activated murine OTI CD8 T cells (CTLs) were imaged on mem-YFP-tranfected, mouse heart MVECs pulsed with SIINFEKL. Individual ratiometric calcium flux values at 5 min were plotted for -/+ Ag conditions. (**B**) CTLs were added to mixed cultures of Ag-pulsed/unpulsed ECs and percentage of specific lysis is plotted at indicated time points. (**C**) CTLs were imaged during EC probing in the absence of Ag. DIC and mem-YFP are shown in the upper and lower panels, respectively. Dashed line represents the outline of the migrating CTL under which transient ILPs are continuously formed. (**D**) Imaging was conducted as in (C) on ECs pulsed with SIINFEKL. Red arrow indicates initial ILP formation preceding calcium flux. (**E**) Average offset time for calcium flux relative to initial ILP formation. Data represent mean $\pm$ SEM. Scale bars 5μm. *Copyright 2012 The American Association of Immunologist, Inc.*

permissive for transmigration, which mirrors what has been published for human T cells. In the presence of Ag, initial ILPs were rapidly followed by calcium flux (offset time = 32.8 +/- 6.6 sec), which then lead to migrational arrest and formation of peripheral ILP arrays similar to those formed by CD4 effector T cells (Fig. 1.11D, E). Thus, T cell ILPs seem to be a general feature of Ag sensing on ECs and not specific only to human CD4 T cell models or to superantigen models.

A Planar Coated Cell Model for Ag Recognition

We next considered whether ILPs either represent unique features of T cell-endothelial Ag recognition or may be more broadly relevant and uniquely *revealed* by endothelium. Observations with CD4 and CD8 T cells in human and mouse models lead us to believe that ILPs may be broadly relevant. However, we speculated that the rigidity of coated substrate models may frustrate/mask ILP formation and orientation/resolution issues might obscure detection of ILPs with traditional cellular APCs [20 21 24], which may help to explain why ILP probing as a mechanism of TCR triggering has not been formally demonstrated previously.

First we simply asked whether evidence for structures consistent with ILPs could be detected in a coated glass model (Fig. 1.12A). Internal Reflection Microscopy (IRM) which detects events close in proximity to the imaging plane revealed that initial 'micro-contacts' (~0.2-1 μm dots consistent with T cell ILPs and/or microvilli)

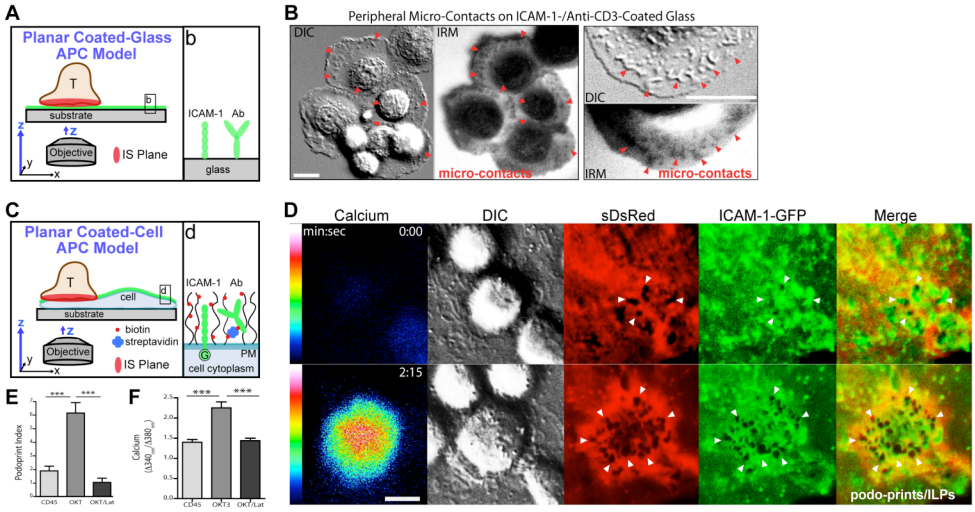

Fig. 1.12. ILPs Facilitate Ag Recognition on Deformable Cell Lines. (**A**) Schematic of the 'Coated-Glass Model' using ICAM-1- and Ab-coated glass. Inset 'b' is a magnified view of the interaction surface. (**B**) iT_{mem} were added to a ICAM-1-Fc- and anti-CD3-coated glass chamber and imaged by DIC and IRM. Arrows indicate IRM-detected 'micro-contacts'. (**C**) Schematic of the 'Planar Coated-Cell APC Model'. CHO-K1 cells expressing ICAM-1-GFP and soluble DsRed were surface 'coated' with Abs against CD3, CD43 or CD45 using a biotin/streptavidin capture approach. Inset 'd' is a magnified view of the interaction surface. (**D**) Cells prepared as in (C) coated with anti-CD3 antibody were imaged live upon addition of Fura-2-labeled iT_{mem}. Panels demonstrate relatively early and later phases of interaction as indicated. Arrows indicate podo-prints/ILPs. (**E** and **F**) Imaging experiments were conducted as in (D) but T cells were pretreated with latrunculin-A. Podo-print/ILP index (E) and calcium flux (F) were calculated. Data represent mean $\pm$ SEM. Scale bars = 5μm. *Copyright 2012 The American Association of Immunologist, Inc.*

preceded calcium flux and new micro-contacts also continued to form after T cell spreading (Fig. 1.12B). We hypothesized that these micro-contacts may at least partly reflect ILP activity that was mechanically frustrated by the rigid substrate. To test this we designed a 'Coated-Cell APC' model whereby the above antibody-coated-glass substrate was recapitulated on the surface of a deformable Chinese hamster ovary (Cho-K1) cell that possesses at least a partial glycocalyx (Fig. 1.12C). In this model, we transfected Cho-K1 cells with soluble dsRed and human ICAM-1 conjugated to GFP and then coated the surface of the Cho-K1 cells with anti-CD3 using a primary amine and biotin-streptavidin approach. In this way, we could detect T cell ILPs by topological changes in the surface of the Cho-K1 cells by displacement. Additionally, enforced localization (placement of) of anti-CD3 on the surface of the Cho-K1 cell allows us to detect T cell activation as a result of ILP probing of the cell surface. In this setting clear 3-dimensional ILP arrays were readily detected that were coupled to calcium flux (Fig. 1.12D). As with iT_{mem} on ECs, initial ILPs always preceded calcium flux (Fig. 1.12D; offset time ~56 sec). These ILPs also functionally support calcium flux because perturbation of ILP formation using latrunculin-A also completely blocked calcium flux (Fig. 1.12E, F). These findings suggest a general tendency of memory/effector T cells to employ ILPs to probe diverse substrates for recognition and response to Ag.

ILPs are Involved in Recognition of Ag Presented by Professional APCs

Next we reexamined Ag recognition with professional APCs. We considered that, although ILP-mediated TCR triggering had not been described before, it may be possible that experimental setups were not optimized to visualize ILPs in previous studies. Thus, iT_{mem} were incubated with Preiss B cells pulsed with Ag and imaged by confocal microscopy. Imaging ILPs in this manner was difficult because of z plane resolution limitations. However imaging of putative ILPs could be seen in occasional examples where the T-cells settle on top of B cells such that the IS aligns with the optimal imaging plane [23] (Fig. 1.13A). In these rare examples, structures resembling ILPs formed in a ring-shaped arrays around the outside edge between the T cell and B cell. Ultrastructural views, evident in a subset of micrographs, further support the presence of T cell ILPs probing the surface of B cells (Fig. 1.13B). Importantly, the ILPs identified within the micrographs have similar morphology as those formed between the T cell and endothelium.

Finally, we wanted to determine if ILPs were relevant for dendritic cell presentation of specific Ag, which is the most broadly relevant T cell-APC interaction. Therefore, we investigated interaction of murine OTII CD4 T cells incubated with bone marrow derived dendritic cells (DCs) co-expressing mem-YFP and soluble DsRed. In this way we could identify ILPs that were probing into the surface of the DC much like what we had observed on the surface of the endothelium. Because of the less regular surface of

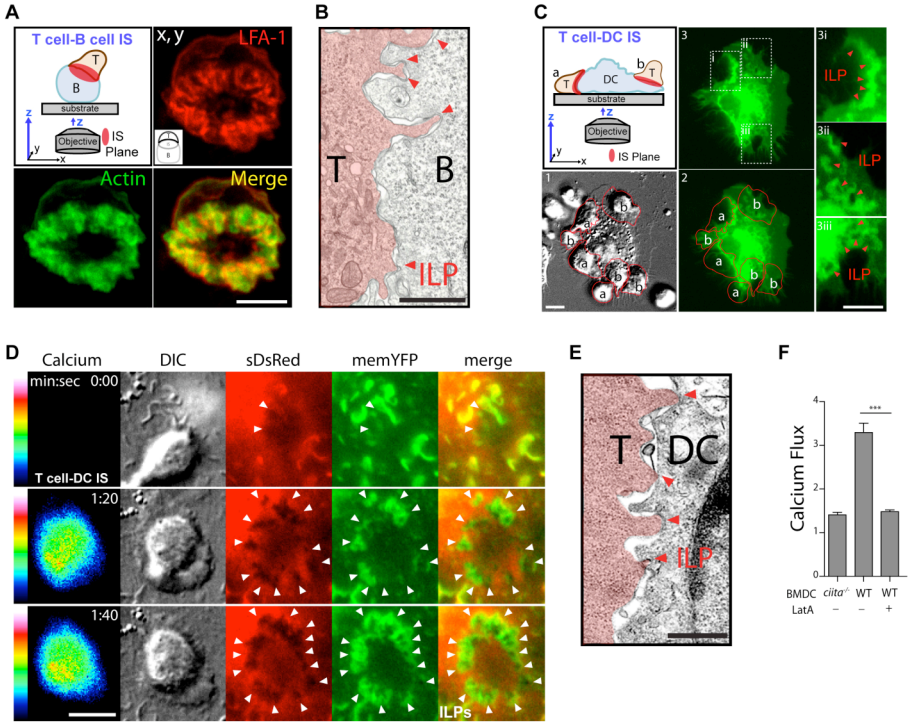

Fig 1.13. ILPs Facilitate Ag Recognition on Professional APCs. (**A**) IT_{mem} were incubated with Ag-pulsed Priess B cells for 5 min and stained for LFA-1 and actin. Image represents a 3-D projection of T cell settled on top of the B cells with the IS forming more nearly parallel to the x-y imaging plane. (**B**) Transmission electron micrograph of T cell-B cell IS as in (**A**). The T cell is identified by a red overlay. Arrows indicate close intercellular contacts formed by T cell ILPs. (**C**) Schematic (upper left panel) shows both lateral (a) and various '*en face*' (b) interfaces typically formed *in vitro* between T cells and the highly irregular surfaces of DCs. Panels 1 and 2 show previously activated murine CD4 OT-II lymphocytes interacting with Ag-pulsed mem-YFP-transfected DCs (green, panel 2). Red outlines depict T cell perimeter based on DIC imaging (panel 1). Panel 3 is identical to panel 2 but shows three boxed regions (i-iii) expanded on the left. 3i shows a lateral interaction in which the T cell has pushed small finger-like invagination into the side of the BMDC putatively formed by ILPs (arrows). 3ii and 3iii show *en face* interactions whereby ILPs seem to be extending normal to the imaging plane giving rise to the typical ring shaped podo-print appearance observed in endothelium (i.e., Fig. 2). (**D**) DCs were transfected with sDsRed and mem-YFP, pulsed with Ag and CD4 OT-II T cells were added. Panels show cytoplasm displacing podo-prints/ILP (arrows) which precede calcium flux and are stabilized after calcium flux. (**E**) Transmission Electron Micrograph of T cell-DC IS as in (D) fixed after 5 min. The T cell is identified by a red overlay. Arrows indicate close intercellular contacts formed by T cell ILPs. (**F**) Calcium flux of previously activated CD4 OTII T cells 8 min after interaction with C57BL/6 (WT) or *Ciita*$^{-/-}$ Ag-pulsed DCs with or without latrunculin-A pretreatment. Data represent mean $\pm$ SEM. Scale bars = 5μm. *Copyright 2012 The American Association of Immunologist, Inc.*

DCs compared to ECs, T cells interacted with DCs both laterally (Fig. 1.13C, 'a' subset) and to a lesser extent through *en face* contacts (Fig. 1.13C 'b' subset). In the former, side views of DC invaginations were readily evident that were similar to podo-prints/ILPs seen on endothelium (Fig. 1.13C, 3i). *En face* interactions also revealed discrete circular podo-prints/ILPs (Fig. 1.13C, 3ii, 3iii), though these were generally less obvious than those formed on endothelium due to the highly active and irregular surface topology of DCs. Dynamic imaging showed that when the DCs were pulsed with antigen (OVA 323-339), ILP probing preceded calcium flux, which in turn was coupled to peripheral ILP array formation similarly to ILP arrays formed on ECs (Fig. 1.13D). Ultrastructural confirmation of ILP formation could also be obtained in a subset of electron micrographs (Fig. 1.13E). Finally, treatment of T cells with latrunculin-A strongly inhibited ILPs (data not shown) and completely blocked initial calcium responses to Ag presented by DCs (Fig. 1.13F). Therefore, T cell probing for antigen by ILPs occurs when they are interacting with surfaces of both professional APCs as well as other diverse cell surfaces, a finding which until now had been difficult to identify due to suboptimal assay conditions.

DISCUSSION

We find that human CD4 T memory cells use ILPs to probe the surface of antigen presenting cells to find cognate antigen. These ILPs not only are responsible for overcoming the steric and electrostatic barriers that prevent TCR-MHC binding, but also are important in the stabilization of signaling. Perturbation of ILPs led to almost complete abolishment of antigen-dependent calcium flux. Moreover, ILP stabilization required calcium flux, forming a positive feedback loop necessary for prolonged signaling. These studies are not only applicable to human CD4 T cells, as studies with murine CD4 and CD8 cells in a number of APC models show strikingly similar phenomenon.

Vascular ECs represent intriguing and understudied APCs/target cells for adaptive immune responses. These MHC-I-, MHC-II- and co-stimulator-expressing cells are strategically positioned at the blood-tissue interface to serve as unique sentinels for the immune system [31]. Previous studies demonstrated that ECs can effectively re-stimulate memory/effector, but not naïve, T cells because they generally lack expression of B7-1 and B7-2 [31 32 33 35 36 59 38]. Thus, ECs have been hypothesized to serve as peripheral ancillary or 'semi-professional' APCs that contribute to the effector phase of adaptive immune responses by activating memory cells. Though overall roles remain controversial, studies suggest that Ag presentation by ECs can

influence T cell activation, differentiation, trafficking and memory [31 32 33 60]. In our current study we demonstrate that CD4 and CD8 memory/effector T cells exhibited a transient arrest in migration coupled, respectively, to activation on ECs presenting MHC/Ag, consistent with previous findings [36 61 62].

We hypothesize that while T cells are probing the surface of the endothelium with ILPs searching for sites permissive for transmigration, they are interacting with immune receptors. Therefore, if antigen is being presented by the endothelium, the T cell would recognize its antigen and become activated. The benefit to this process would be that the T cell would be primed before entering the tissue and would have a quicker and more robust response. For instance, if the endothelium has been exposed to a virus, viral antigens presented on the surface could prime CD8 CTLs undergoing transendothelial migration. Then, the CD8 CTLs would be able to kill the virally infected endothelial cell as well as start producing cytokines so that subsequent killing of virally infected cells in the tissue would be more efficient.

Moreover, since the endothelium can express PD-L1 and other inhibitory molecules, the endothelium may be instrumental in resolving tissue inflammation or preventing autoimmunity. Thus, the endothelium may serve as sentinels of the tissue and can cause functional inactivation of effector cells before they can encounter sensitive tissues. In support of this, it has been shown that *in vitro* blockade of PD-L1

enhances the ability of human CD8 T cells to kill endothelial cells and this blockade further enhances the ability of the CD8 cells to produce IFNγ[63]. Unfortunately, genetic models are lacking to study the role of the vascular endothelium in adaptive immunity *in vivo*, so it is still unclear what role endothelial antigen presentation fills in a physiological setting. The lack of proper *in vivo* models is due largely to "leakiness" of endothelial promoters used to drive Cre recombination for the necessary endothelial-specific conditional knockout strains. For instance, the Tie-2:Cre mouse deletes not only on the endothelium but also on professional APCs such as B cells and DCs [64 65]. This is due to the fact that both endothelial and hematopoietic cells derive from the same developmental precursor termed the hemagioblast[66]. Only through specific conditional deletion of antigen presentation components/costimulatory molecules specifically on the endothelium will the exact role of the endothelium in antigen presentation be clearly delineated.

Importantly, ECs exhibit a virtually planar cell surface *in vitro*, which we previously established to be ideal for high spatiotemporal resolution imaging of topological dynamics [39]. We reasoned that ECs might, therefore, serve as physiologic 'planar APC/target cell' models uniquely suited to fill two key gaps in our understanding of immune surveillance mechanisms: i) how initial MHC/Ag-sampling contacts form between T cells and APCs and ii) how these lead to formation of productive ISs. Whereas planar APC substrates (i.e., lipid bilayers, antibody-coated glass) provide

excellent imaging, which has led to critical insights to these responses [18 24 25 26 27], such models are inherently limiting. Additionally, details of physiologic cell-cell scanning dynamics are profoundly obscured by orientation-related imaging issues [20 21 23]. The imaging afforded with our planar endothelial APC model in the current study revealed unexpected involvement of ILPs in Ag recognition and response activities.

ILPs ('invadosome-like protrusions') are lymphocyte equivalents [42] to podosomes (formed largely by myeloid lineage cells) and invadopodia (formed by transformed cells), collectively termed 'invadosomes' [41]. Invadosomes and ILPs are actin-dependent cylindrical protrusive organelles (~200-1000 nm in diameter and depth) that form on the ventral surface of migratory cells [41]. Distinct from invadosomes, characterized to form on matrix, bone, glass/plastic substrates, T cell ILPs have only been seen on cellular substrates, as shown in a range of *in vitro* [39 67 68] and *in vivo* studies (reviewed in [4]). In such settings, dynamic ILP probing seems to function in migratory pathfinding, apparently serving as biomechanical sensors [39 67 68 69]. The current studies suggest that ILPs may also facilitate biochemical or 'informational' scanning of diverse cell surfaces (Fig. 1.14). This informational scanning may not be limited to scanning for antigen. We hypothesize that this scanning is important for recognition of other immune receptors and also for search for chemokines that are trapped within the glycocalyx.

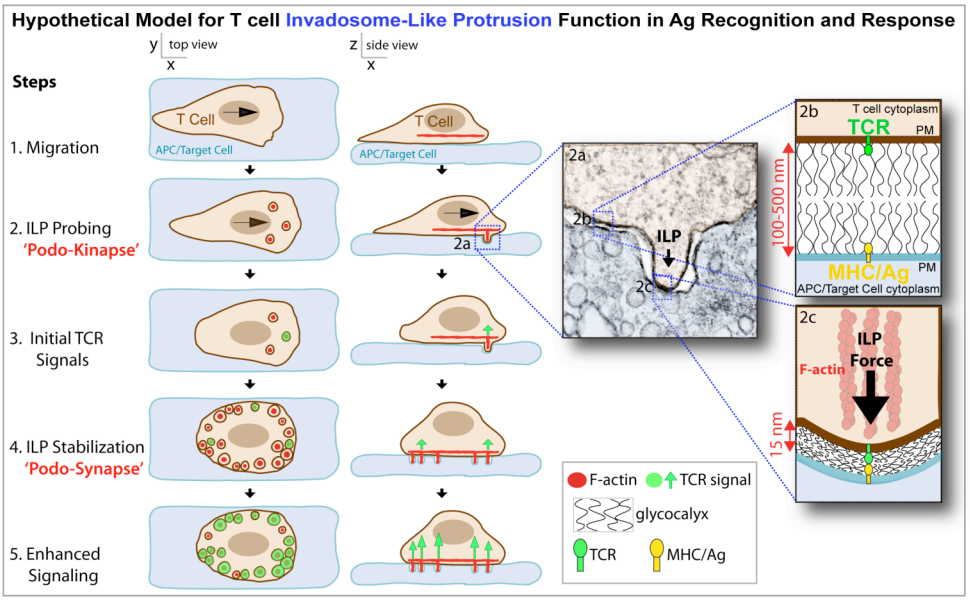

Fig. 1.14. Hypothetical Model for ILP Function in Ag Recognition and Response Schematic depicts top-down and side views of a memory/effector T cell interacting with an APC/target cell. Lymphocytes initiate lateral migration (**Step 1**) and begin to dynamically drive ILPs against the apposing cell (**Step 2, inset 2a**). Close interactions between T and APC/target cells, which are partially opposed by the cell glycocalyces (**inset 2b**), form preferentially (but not exclusively) at ILP tips (**insets 2c**). We hypothesize that TCR/MHC interactions may be facilitated in these zones. Initial calcium released upon Ag recognition (green overlay/arrows; **Step 3**) seems to be coupled to stabilization/accumulation of ILP arrays ('podo-synapses'; **Step 4**), which we hypothesize could in turn help sustain/enhance signaling (**Step 5**). *Copyright 2012 The American Association of Immunologist, Inc.*

We speculated that the ILP scanning seen on ECs was uniquely *revealed* by this setting, rather than a unique *feature* of it. IRM imaging of a rudimentary APC model (anti-CD3-coated glass) showed that T cells form a series of micro-contacts with the substrate that are consistent with either ILP or microvilli interactions. Similar micro-contacts were previously shown to be enriched in F-actin, WASP and TCR and hypothesized to represent frustrated podosomes [25 27]. When we tested this hypothesis by recapitulating the same anti-CD3 activation stimuli on a pliable cell surface we, indeed, found that the micro-contacts transitioned into 3D ILPs and podo-prints. Moreover, our studies using approaches optimized for imaging ILPs on professional APCs (i.e., B cells and DCs) readily detected ILPs probing in these settings. We believe that our specific experimental design uniquely allowed us to detect ILPs that are generally present during immune surveillance though not detected in previous studies. Although dynamics, molecular composition and 3D-architectures were not defined, extensive (largely EM-based) studies previously evidenced similar T cell protrusions extending against diverse APCs and target cell surfaces [26 51 70 71 72 73]. Collectively, this suggests broad relevance for memory/effector T cells probing their cellular environment with ILPs.

The important question of whether naïve T cells similarly employ ILPs remains to be addressed. We were unable to determine if naïve cells interacting on endothelium

were able to form ILP structures because naïve cells lack the requisite levels of LFA-1 or responsiveness to inflammatory chemokines to efficiently interact with activated endothelium. Moreover, when we assessed naïve cells on professional APCs, such as dendritic cells, we found some minor evidence of ILP structures, however there was little calcium flux and ILP stabilization in these settings. We believe that the reason for this is that naïve T cells need to have periods of short interaction with professional APCs in a priming step before full calcium flux can be achieved, which has been demonstrated *in vivo* by intravital microscopy[74]. Because we could not measure significant ILPs being formed by naïve cells, and we did not see meaningful calcium flux, we believe that ILPs may still be responsible for activation of naïve T cells, but that the kinetics are delayed beyond the imaging window of our experiments. However, future experimental setups can be designed to test this directly.

One possible role for ILP probing may be in enhancing the efficiency of Ag recognition. The act of Ag detection requires T cell and APC/target membranes to come within ~14 nm of each other [5 75]. Yet all cell membranes are extensively shielded by ~50-500 nm thick glycocalyxes [6 7 8] that physically oppose close contact and negatively modulate immune recognition [8 9 10 11 12 13] (Fig. 1.14, inset 2b). In the periphery, patrolling effector/memory lymphocytes must effectively scan the surfaces of widely varying cell types (indeed, essentially any host cell could become

a target), each with glycocalyxes of different thicknesses and physico-chemical properties. Forces provided by ILPs (which form independently of Ag during lateral migration [39]) are sufficient to deform nuclear lamina, displace and distort cytoskeleton and intracellular organelles and to promote trans-cellular diapedesis [39]. More than sufficient energy would, therefore, seem to be available at the tips of ILPs (Fig. 1.14, inset 2a) to overcome repulsion provided by the glycocalyx and to provide the force required for TCR triggering (Fig. 1.14, inset 2c).

Previous studies showed that lamellipodia of migrating lymphocytes are zones of heightened Ag recognition efficiency [76 77 78]. In both our previous [39] and current work we show that lamellipodia are also the predominant areas of ILP formation. Moreover, in our experimental system ILPs, but not necessarily lamellipodia, consistently preceded calcium flux. Thus, while migration behaviors are necessary for immune surveillance, ILPs may function more directly in promoting intimate contacts and, thereby ensuring efficient Ag sampling. Our studies with Latrunculin A are consistent with such functional roles. It is also interesting to note that forces and membrane bending associated with ILPs are consistent with the hypothesized force-based mechanism for formal triggering of TCR signaling [27 79]. Here we used CD3 crosslinking as an approximate control for TCR signaling that is not dependent on ILPs. Yet, when we added the actin perturbation agent Latrunculin-A we detected less calcium flux. Although some studies have interpreted this to indicate that

Latrunculin-A blocks TCR signaling independently of its function in blocking actin, we believe that even CD3 crosslinking in this setting is facilitated, at least in some part, by forces generated by ILPs. ILPs are probably not absolutely required for either TCR signaling or forming intimate T cell-APC/target contacts, but rather act to ensure efficiency and fidelity of immune surveillance. It is also probable that the curvature and membrane bending elicited by ILPs may also allow immune receptors to assemble in the correct arrangement of molecules to form a proper immune synapse, which is the at the center of the kinetic segregation model.

Another possible function for ILPs may be to support signal amplification and sustenance. Our studies reveal dense arrays of calcium-stabilized ILPs that dominate the IS following Ag recognition. Individual ILPs showed enrichment in TCR and molecules suggestive of active signaling. This feature is generally not unlike TCR signaling micro-clusters defined using planar APC model substrates, with the key distinction that ILPs have a discrete 3D architecture, do not "treadmill" across the T cell interface, and ultimately do not end up forming a c-SMAC architecture. The well developed concept that micro-clusters may function as 'signalosomes' to amplify and sustain signaling by concentrating important molecules/activities, might then be extended to include limited 'reaction volumes' formed within ILPs [21 80 81 82]. Therefore, the tips of ILPs may, in fact, be types of microclusters that are potent locations for signaling. Additionally, stable peripheral ILP arrays are strikingly

similar to osteoclast 'podosome-belts' [83] [84] that form sealing zones for directed secretion of bone degrading enzymes [85]. Thus, it may be hypothesized that peripheral podo-synapses may function analogously for directed secretion of cytokines or cytotoxic materials. For instance, podosynapses would enable a CD8 CTL that is killing a target cell to specifically lyse the virally infected cell while leaving bystander cells unharmed. Staining of perforin or granzyme within the ILPs would help to delineate this possibility.

Collectively, these studies support the hypothesis that ILPs may serve as newly appreciated sensory organelles that facilitate Ag recognition and responses. By virtue of physical force exertion, ILPs allow T cells to get a deeper understanding of their local cellular environment. Such proactive 'informational scanning' might ensure robust sampling of MHC/Ag on diverse cell types. It is tempting to speculate that stabilized TCR-enriched ILPs resulting from Ag recognition represent a clearer, more physiologic, view of TCR-micro-clusters and 'multi-focal' ISs than what is characterized to date.

Chapter 2. The role of PD-1 in controlling Lymph Node and Blood T Follicular Regulatory Cells

Note: The contents of this project have been published previously [86].

Introduction

Humoral immunity refers to B cells in the body being activated to produce soluble antibodies that protect the host from foreign pathogens. The antibodies produced by the B cell have multiple functions including directly neutralizing toxins, aiding in opsonization, triggering activation through Fc receptors on multiple cell types and coating pathogens that get killed by antigen dependent cell cytotoxicity (ADCC). For many years it has been appreciated that CD4 T cells are essential mediators of humoral immunity. In fact, humoral respones have traditionally been categorized as either T cell dependent or T cell independent. It is clear that the vast majority of humoral responses are CD4 T cell dependent, and CD4 T cells are critical in providing help to B cells in these situations[87]. However, for many years, the CD4 T cells that supply this help to B cells could not be phenotypically or functionally separated from T cells that stay in the T cell zone and perform other functions.

T Follicular helper T cells (TFH) are a recently defined subset of CD4 T cells that are essential for helping cognate B cells form and maintain the germinal center (GC) reaction, and for development of humoral immune responses. Tfh cells were first appreciated 12 years ago when the Forster and Moser labs simultaneously isolated tonsilar human CD4 T cells that express the chemokine receptor CXCR5[88 89]. These cells were shown to have the unique ability to stimulate B cells to produce antibody *in vitro* and were physically located within B cell zones *in vivo*.

TFH cells are universally defined by expression of CXCR5, which is responsible for directing them to the B cell follicles. Within the B cell follicles follicular dendritic (FDCs) cells secrete large amounts of the chemokine CXCL13 which allows B cells and T cell subsets to enter the follicle if there is sufficient CXCR5 expressed on the surface of these cells [90]. Germinal centers, where affinity maturation and class switch recombination take place, are locations where there is a particularly high concentration of CXCL13. B cells constitutively express CXCR5, which places them in the B cell zone in the steady state. When B cells become activated, they can upregulate CCR7 and migrate to the T-B border[91]. In contrast, T cell subsets, such as TFH cells, only express CXCR5 after differentiation and activation. It is thought that dendritic cells prime naïve T cells to become TFH cells, however B cells at the T-B border may also function in this capacity. Moreover, it is generally thought that B cells provide important costimulatory cues through ICOS and SAP that lead to

stabilization of the TFH phenotype [92 93]. Until recently, it was thought that TFH cells are the only CD4 T cell subtype that was able to gain entry into the B cell zone and germinal center to regulate B cell responses.

TFH cells express the transcription factor *Bcl6* (which represses Blimp-1/*Prdm*1) and high levels of the costimulatory receptor ICOS, which are both critical for TFH differentiation and maintenance [90, 94-96]. In this way, Bcl6 is thought to be the master transcription factor for TFH differentiation, much like RORγT is for Th17 differentiation. In addition, TFH cells secrete large amounts of IL-21, which aids in germinal center formation, isotype switching and plasma cell formation [97]. It has been demonstrated previously that mice deficient in IL-21 have severely impaired antibody responses[97]. In humans and mice, functionally similar TFH cells can be found in secondary lymphoid organs. Significantly, $CXCR5^+$ TFH cells are also present in peripheral blood and are seen at elevated levels in individuals with autoantibodies, including systemic lupus erythematosis, myasthenia gravis and juvenile dermatomyositis patients. However, the function of these circulating TFH remains unclear, because most data has relied on *in vitro* models [88, 98-100].

TFH cells also express high levels of programmed death (PD)-1 receptor (CD279). PD-1 was originally cloned from a T cell hybridoma undergoing apoptosis after exposure to PMA and ionomycin[101]. PD-1 is an Ig superfamily member that has one

N-terminal IgV-like domain. The cytoplasmic tail of PD-1 has an immunoreceptor tyrosine-based inhibitory motif (ITIM) as well as an immunoreceptor tyrosine-based switch motif (ITSM) [2]. It is currently believed that recruitment of SHP2 via the ITSM domain[102] during PD-1 signaling attenuates TCR signals and inhibits T cell expansion, cytokine production and cytolytic function (Fig. 2.1). In addition, PD-1 promotes the development of induced regulatory T (iTreg) cells from naïve lymphocytes [103-107].

PD-1 has two ligands, PD-L1 (B7-H1;CD274) [108] and PD-L2 (B7-DC; CD273) [109]. PD-L1 is constituitively expressed on many hematopoietic cells such as B cells, T cells, macrophages, dendritic cells, mast cells and endothelial cells and expression can be induced to even higher levels on these cells as well as wide variety of nonhematopoietic cells including pancreatic islet cells. Thus, PD-L1 is broadly expressed in many tissues. PD-L1 has a 27 amino acid cytoplasmic domain that is highly conserved across species, yet has no known signaling domain. PD-L2 is inducibly expressed by hematopoietic cells such as B cells and dendritic cells and has no significant cytoplasmic tail. Importantly, both PD-L1 and PD-L2 can be expressed on GC B cells and dendritic cells, making both ligands potentially important for humoral immune responses [2].

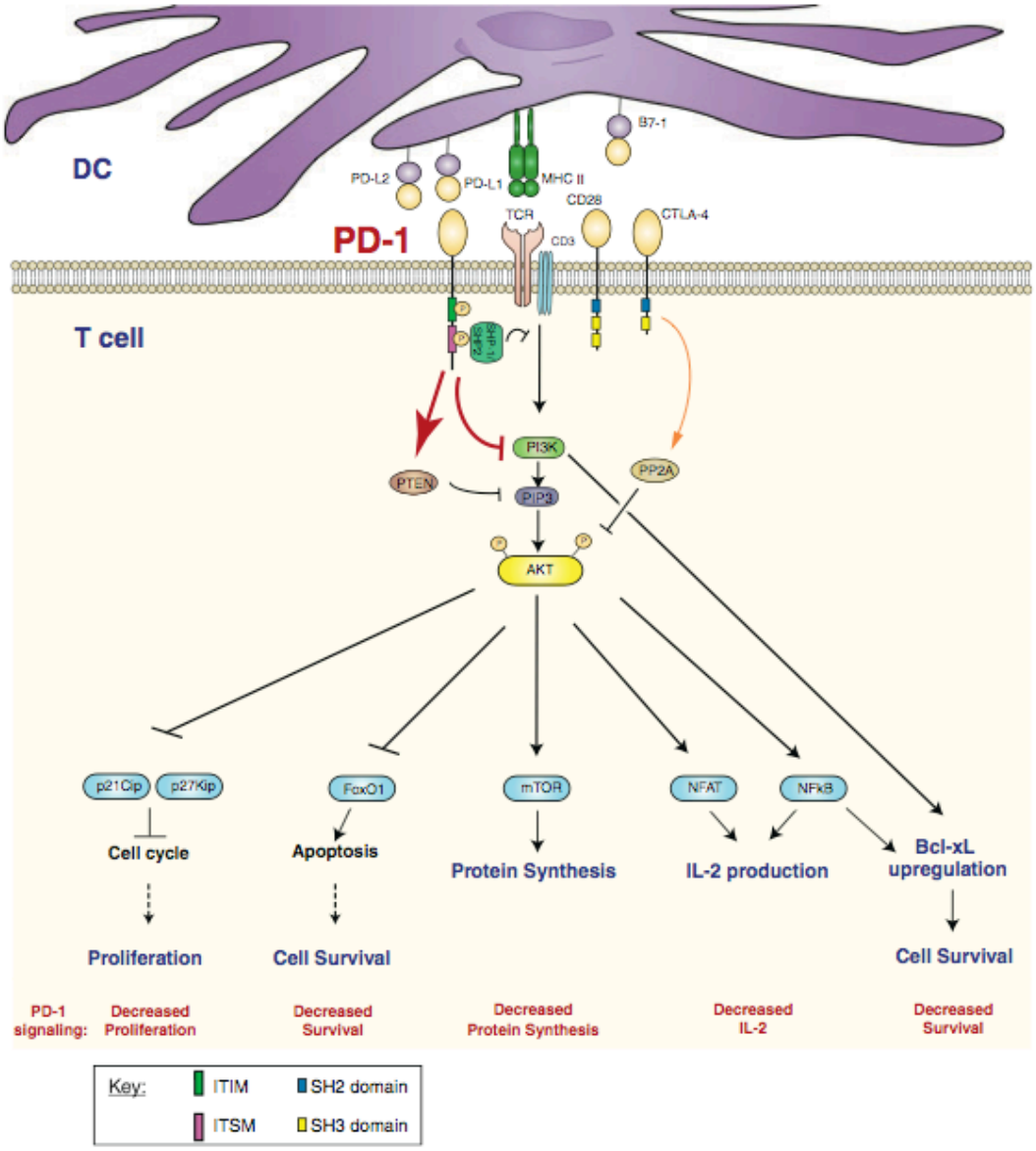

Fig. 2.1. PD-1 Signaling. Studies of PD-1 signaling suggest that binding of the ITSM motif by SHP-2 results in the dephosphorylation of proximal TCR signaling molecules and augmentation of PTEN expression. Together these result in attenuation of the PI3K pathway. Taken from[2].

Perturbation studies suggest critical roles for PD-1 pathway in regulating humoral immune responses. However, there are conflicting reports as to the function of the PD-1 pathway in controlling humoral immunity. Some studies have found that humoral responses are attenuated [110-112], while others have seen that humoral responses are heightened [113, 114] when PD-1:PD-L interactions are prevented. This may be due to the complexity of the signaling in the PD-1 pathway, as multiple cell types express PD-1, PD-L1 and PD-L2. Therefore, it is still uncertain how PD-1 influences humoral immunity and moreover, what cellular interactions are affected by PD-1 to regulate humoral immunity responses.

PD-1 also is found on a newly defined subset of $CD4^+CXCR5^+$ cells called T follicular regulatory (TFR) cells. TFR cells were discovered simultaneously by the Dong and Vinuesa groups in 2011, and since then only one other paper has been published on this cell type. Therefore, we only have a rudimentary understanding of these cells. We know that TFR cells are positive for the transcription factors FoxP3, *Bcl6* and *Prdm1*/Blimp1. Coexpression of Bcl6 and Blimp1 is paradoxical as these transcription factors have been shown to reciprocally modulate eachother in TFH cell differentiation. TFR cells are thought to function in inhibiting the germinal center response [115-117]. However, this hypothesis is based on the observation that these cells have FoxP3 expression, and clear direct evidence of the suppressive nature of the cells is currently lacking. Some genetic models have indirectly demonstrated the

suppressive nature of TFR cells but these models rely on manipulations that do not only alter the function of TFR cells[115 116]. For example, Chung et al. transferred CXCR5 knockout Treg cells into and then immunized recipient mice. The mice that received CXCR5 knockout Treg cells suppressed germinal center B cell development less than wild-type T regulatory cells. However, the regulatory cells that came from the CXCR5 knockout mouse may have been defective from differentiating in an altered lymph node architecture [116]. Additionally, these studies do not separate differentiation from function. Therefore, it is still unclear what the role of TFR cells are in inhibiting humoral immunity. Interestingly, TFR cells originate from natural regulatory T cell (nTreg) cells[115, 116], which makes them one of the only defined effector subsets of nTregs to date[118].

Although they originate from nTregs, TFR cells express similar levels of ICOS, CXCR5 and PD-1 as TFH cells, which prevented these cells from being detected until recently. Thus, TFR cells have been "hiding" in TFH gating strategies all along. Since ICOS, CXCR5 and PD-1 have been widely used to identify and purify 'TFH cells', it seems likely that the inability to define clear functions for PD-1 in GC responses derives from experimental systems containing mixtures of stimulatory TFH cells and inhibitory TFR cells. Separate analyses of the function of PD-1 on TFH and TFR cells are needed to elucidate how PD-1 controls humoral immunity and to gain insight into the individual roles of TFR cells and TFH cells in regulating antibody production.

Here we demonstrate that PD-1:PD-L1 interactions inhibit TFR, but not TFH, cell numbers in lymph nodes. PD-1 deficient mice have increased numbers of lymph node TFR cells compared to wild type mice. PD-1 deficient lymph node TFR cells have enhanced ability to suppress activation of naïve T cells, as well as antibody production *in vitro*. In addition, we show for the first time that TFR cells are present in the peripheral blood of mice, and that these circulating cells can potently regulate humoral immune responses *in vivo*. Using transfer approaches, we demonstrate that blood TFH cells can promote antibody production, while blood TFR cells can strongly inhibit antibody production *in vivo*. We further show that the PD-1 pathway inhibits blood TFR cell function and PD-1 deficient blood TFR cells have enhanced suppressive capacity *in vivo*. Taken together, our studies reveal a new immunoregulatory role for the PD-1:PD-L1 pathway in limiting TFR cell differentiation and function, and further demonstrate the dynamic control of humoral immune responses by migration of TFR cells from the circulation into lymph nodes to control antibody production *in vivo.*

Materials and Methods

Mice. 6-10 week old mice were used for all experiments. WT C57BL/6 and TCRα$^{-/-}$ mice were purchased from The Jackson Laboratory (Bar Harbor, ME). PD-1$^{-/-}$ (*Pdcd1*$^{-/-}$), PD-L1$^{-/-}$ (*Cd274*$^{-/-}$), and PD-L2$^{-/-}$ (*Pdcd1lg2*$^{-/-}$) mice on the C57BL/6 background were generated in our laboratory [119-121]. *Icos*$^{-/-}$ [122] and *Cd28*$^{-/-}$ mice [123] were generated as described. 2D2 TCR Tg mice Foxp3-IRES-GFP knockin mice (Foxp3.GFP; [124] were generated in our laboratory by crossing 2D2 TCR Tg mice [125] with Foxp3.GFP reporter mice. All mice were used according to the Harvard Medical School Standing Committee on Animals and National Institutes of Health animal healthcare guidelines. Animal protocols were approved by the Harvard Medical School Standing Committee on Animals.

Immunizations. For MOG 35-55 immunizations (referred to as "MOG"), mice were injected subcutaneously with 100μg of MOG 35-55 (UCLA Biopolymers Facility) emulsified in a 1:1 emulsion of Mycobacterium tuberculosis H37RA CFA (Sigma) on the mouse flanks. Emulsions were made by mixing MOG in PBS and pulling the mixture into a syringe. A separate syringe was filled with CFA and the two syringes were joined with a 3-way stopcock and mixed until a uniform, thick suspension was generated that did not dissolve in PBS. 100μl of emulsion was injected in two places on the mouse flanks in an optimal location so that the inguinal lymph node is the primary draining lymph node for the immunization. Seven days

after immunization mice were euthanized and the inguinal, and therefore, draining lymph nodes (dLNs) and/or spleen were harvested for flow cytometric analyses. Blood was collected via cardiac puncture with a 1cc syringe and immune cells were isolated by sucrose density centrifugation using Lymphocyte Separation Media (LSM). For NP-OVA immunizations, 100μg NP_{18}-OVA (Biosearch Technologies) was used in a 1:1 H37RA CFA emulsion and injected similarly as MOG/CFA.

ELISA. For *in vitro* quantification of antibody production, supernatants were taken from cultures and incubated on plates that were coated with 1:1000 dilution of pan-IgG capture antibody (Southern Biotech) overnight at 4 degrees. Samples were diluted and added to plates for 1 hour at room temperature. Plates were washed and 1:1000 of alkaline phosphatase conjugated pan-IgG detection antibody (Southern Biotech) was added for 1 hour. A phosphatase substrate (Sigma) was used to quantiate antibody titers.

To assess *in vivo* antibody production, sera were collected from mice at indicated time points by centrifugation in serum separator tubes. NP-specific antibody titers were measured by coating ELISA plates with 100μg/ml NP_{16}-BSA (Biosearch Technologies) in PBS overnight at 4 degrees, and incubating serum for 1hr followed by alkaline phosphatase-conjugated IgG detection antibodies. A standard curve was generated using antibody from an NP-specific IgG1 hybridoma (a kind gift of Dr.

Michael Carroll). This standard curve was used to approximate all IgG subtype antibody levels in the linear range of detection using a Spectramax Elisa plate reader (Molecular Devices).

Flow Cytometry. Cells from lymphoid organs were isolated and resuspended in staining buffer (PBS containing 1% fetal calf serum and 2mM EDTA) and stained with directly labeled antibodies from Biolegend against CD4 (RM4-5), ICOS (15F9), CD19 (6D5), PD-1 (RMP1-30), PD-L1 (10F.9G2), CD69 (H1.2F3), from eBioscience against FoxP3 (FJK-16S), Bcl6 (mGI191E), and from BD bioscience against FAS (Jo2), GL7, Ki67 (B56). For CXCR5 staining, biotinylated anti-CXCR5 (2G8, BD Biosciences) was used followed by streptavidin-brilliant violet 421 (Biolegend). For intracellular staining, the FoxP3 fix/perm kit was used (eBioscience) after surface staining was accomplished. All flow cytometry was analyzed with an LSR II (BD biosciences) using standard filter sets.

Confocal Microscopy. Draining lymph nodes were embedded in OCT which were frozen quickly with liquid nitrogen and 8μm sections were cut on a cryostat, fixed with 4% paraformaldehyde, and stained before imaging on a Zeiss LSM 510 confocal microscope by acquiring z-stacks of 0.5μm with a 40x oil objective. Germinal center quantitation was calculated by drawing outlines around $GL7^{+}IgD^{-}$ areas present within the B cell zone. FoxP3 quantitation was performed by

determining germinal center zones and scrolling through z-stack images to identify large FoxP3 positive spots. Axiovision (Zeiss) software was used to measure distances from germinal center borders. For micrograph panels, single z slices were linearly contrasted and merged images were made in Adobe photoshop. In some cases digital enlargements were made with Adobe photoshop.

Quantitative PCR. RNA was isolated from sorted samples with the RNAqueous micro RNA extraction kit (Ambion) according to manufacturers instructions. Q-PCR was performed using standard FAM or VIC conjugated TaqMAN probes (Applied Biosystems) and an ABI FAST9500 QPCR machine according to the manufacturer's instructions. mRNA levels were normalized to HPRT or β2M, and the $2^{-deltadeltaCT}$ method was used to quantitate mRNA. Each bar graph represents mean values from more than three individual experiments consisting of cells sorted from 10 pooled mice. Samples were normalized to wild-type naïve cells as described in the figure legends.

***In vitro* Suppression Assay.** Cell populations were sorted to 99% purity on an Aria II flow cytometer using a 70 micron nozzle. For TFR suppression assays, sorted cells were counted on an Accuri cytometer (BD biosciences) by gating live cells only. $1x10^5$ $GL7^-$ B cells from dLNs of WT mice immunized with MOG/CFA 7 days previously, $1x10^5$ CFSE labeled $CD4^+CD62L^+FoxP3^-$ T responder cells from

unimmunized WT FoxP3 GFP reporter mice, and $1x10^5$ TFR cells from the draining dLN of 10 pooled mice immunized with MOG/CFA 7 days previously were plated with 2μg/ml soluble anti-CD3 (2C11, BioXcell) and 5μg/ml anti-IgM (Jackson Immunoresearch). After 3 days, cells were harvested and stained for CD4 and CD19. T cell responders were identified as CFSE positive, and percent divided was gated as the percent of cells with CFSE diluted compared to unstimulated T responders. For *in vitro* antibody suppression assay, $GL7^-$ B cells from wild-type MOG-immunized mice were plated with TFH cells and/or TFR cells pooled from MOG-immunized wild-type or *Pdcd1*$^{-/-}$ mice and 2μg/ml soluble anti-CD3 and anti-IgM (as described above). After 6 days, supernatants were collected for antibody analysis by enzyme-linked immunosorbent assay.

Adoptive Transfers. For blood TFH/TFR adoptive transfers, 20 to 30 WT mice were immunized with NP-OVA subcutaneously as described above, and 8 days later blood was collected by cardiac puncture. TFH and TFR cells were sorted as described above. $4x10^4$ blood TFH cells alone or together with $2x10^4$ blood TFR cells in 100μl PBS were adoptively transferred into $CD28^{-/-}$ or $TCR\alpha^{-/-}$ mice by tail vein injection. These recipient mice were immunized with NP-OVA one day later on the flanks as described above. Sera and organs were harvested at indicated times and analyzed by ELISA or flow cytometry.

Statistical Analysis. Unpaired Student's t test was used for all comparisons, data represented as mean +/- SD or SE are shown. P values < 0.05 were considered statistically significant. * $P<0.05$, ** $P<0.005$, *** $P<0.0005$.

Results

PD-1 Controls T Follicular Regulatory Cells

To analyze the role of PD-1 in controlling T follicular regulatory (TFR) cells, we first compared PD-1 expression on CD4 T cell subsets in draining lymph nodes (dLN) of WT C57BL/6 mice subcutaneously immunized with myelin oligodendrocyte glycoprotein (MOG) peptide 35-55 emulsified in CFA (from hereon simply referred to as "MOG/CFA"), an immunization that breaks tolerance and also results in effective TFH cell generation [126]. TFR cells were defined as $CD4^+ICOS^+CXCR5^+FoxP3^+CD19^-$, a gating strategy that separates TFR cells from $CD4^+ICOS^+CXCR5^+FoxP3^-CD19^-$ TFH cells, the cell type that was until recently thought to solely comprise the $CD4^+CXCR5^+$ gate (Fig. 2.2A). TFH cells showed higher expression of PD-1 compared to $ICOS^+CXCR5^-$ effector-like cells and $ICOS^-CXCR5^-$ naïve (referred to as naïve) cells in the draining lymph node on day 7 after immunization. Strikingly, TFR cells had even higher PD-1 expression when compared to the other CD4 T cell subsets examined, including TFH cells (Fig. 2.2B).

To determine the functional significance of PD-1 expression on TFR cells, we immunized WT and *Pdcd1*$^{-/-}$ (PD-1$^{-/-}$) mice and analyzed TFR cells 7 days later. The percentage of TFR cells contained within the $CD4^+FoxP3^+$ gate was about 4 percent in WT lymph nodes and less than 1 percent of all CD4 T cells. In marked contrast,

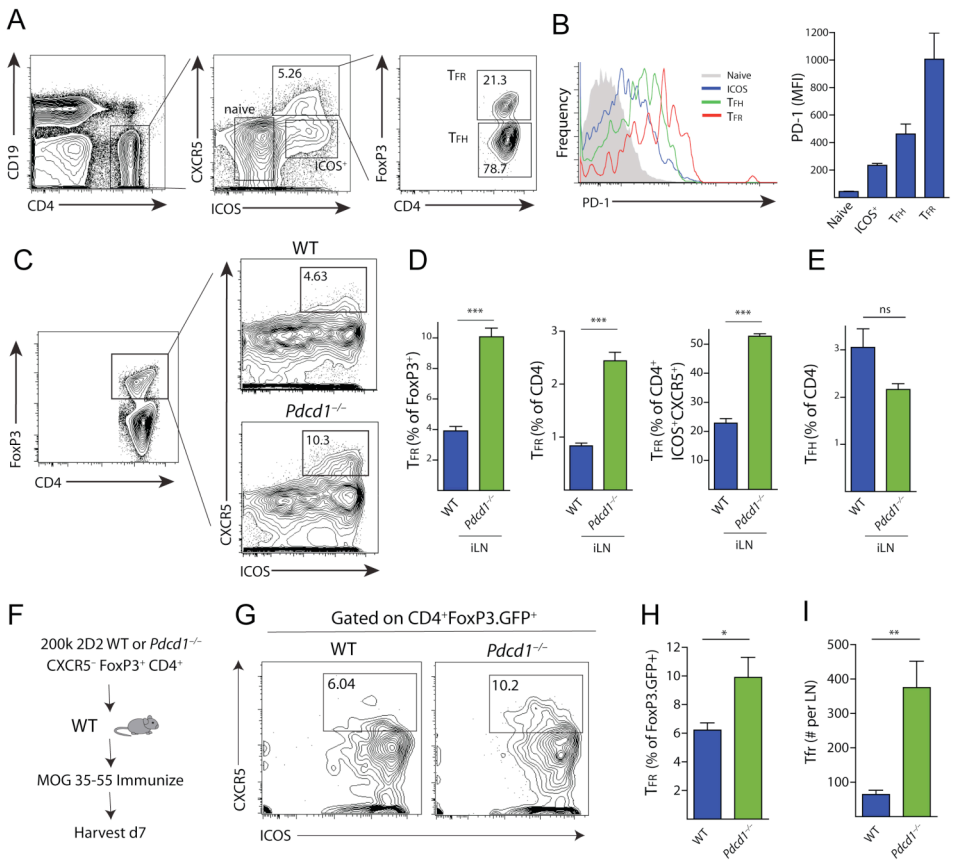

Fig. 2.2. PD-1 Signaling in FoxP3 Tregs Limits the Generation of T Follicular Regulatory Cells. (**A**) Quantitation of TFR cells. WT mice were immunized with MOG/CFA and 7 days later draining lymph nodes were isolated and immediately stained for $CD4^+FoxP3^+ICOS^+CXCR5^+CD19^-$ T follicular regulatory cells (TFR), $CD4^+FoxP3^-ICOS^+CXCR5^+CD19^-$ T follicular helper cells (TFH), $CD4^+ICOS^-CXCR5^-CD19^-$ cells (naive) or $CD4^+ICOS^+CXCR5^-CD19^-$ cells (ICOS+). Numbers indicate percentages of cells located within each gate. (**B**) PD-1 expression by flow cytometry on WT naive, ICOS+, TFR and TFH cells. Populations were gated as in (A). (**C**) Gating of TFR cells from total $FoxP3^+$ cells in WT and PD-$1^{-/-}$ mice immunized with MOG/CFA and analyzed 7 days later and stained as in (**A**). (**D**) Quantitation of WT or PD-$1^{-/-}$ TFR cells gated in (C) and expressed as a percentage of $CD4^+FoxP3^+$ (left), percentage of total CD4 T cells (middle), or percentage of $CD4^+ICOS^+CXCR5^+CD19^-$ gate (right). (**E**) Quantitation of TFH cells as a percentage of total CD4 T cells. Data represent means of 5 mice per group. All error bars indicate standard error. (**F**) PD-1 on $FoxP3^+$ cells has a cell-intrinsic role in inhibiting TFR differentiation *in vivo*. Schematic design of a transfer assay in which 2D2 TCR transgenic $CD4^+FoxP3^+CXCR5^-$ non-TFR Tregs were transferred into WT mice which were subsequently immunized with MOG/CFA. Draining lymph nodes were harvested 7 days later and analyzed for TFR cells. (**G**) Representative gating of TFR cells from transfer experiments described in (F). (**H-I**) Quantitation of TFR cells from transfer experiments expressed as a percentage of FoxP3 GFP^+ cells present on day 7 post immunization (H) or total cell number (**J**) per lymph node. All data are representative of at least two independent experiments with at least 5 mice per group. All error bars indicate standard error. * $P<0.05$, ** $P<0.005$

the percentage of TFR cells in *Pdcd1*$^{-/-}$ mice was about 10 percent of the CD4^{+}FoxP3^{+} gate and greater than 2 percent of all CD4 T cells (Fig. 2.2C-D). Because total numbers of CD4 T cells are typically about two fold higher in the lymph nodes of PD-1 deficient animals, a two-fold increase in TFR cell frequency translates into a ~4-fold increase in absolute numbers of TFR cells (data not shown). When expressed as a percentage of all CD4^{+}ICOS^{+}CXCR5^{+} cells (and therefore the percentage of CD4 T cells that respond to CXCL13 and can migrate to the B cell zone), *Pdcd1*$^{-/-}$ TFR cells comprised half of this population, whereas WT TFR cells comprised only about 20 percent (Fig. 2.2D). The dramatic increase in the percentage of TFR cells in *Pdcd1*$^{-/-}$ mice also was observed when other classical B cell antigens, such as 4-hydroxy-3-nitrophenylacetyl hapten conjugated to ovalbumin (NP-OVA), were used (Fig. 2.3). We did not find a significant difference in the percentage of FoxP3^{-} TFH (from hereon called "TFH") cells when expressed as a percentage of all CD4 T cells in WT and *Pdcd1*$^{-/-}$ mice on day 7 post immunization (Fig. 2.2E).

Since PD-1 can be expressed by a number of hematopoietic cell types including T cells, B cells, macrophages and some dendritic cells [2], we next investigated whether PD-1 regulates TFR cells directly by controlling their generation from FoxP3^{+} T regulatory cells (Treg). To track the fate of FoxP3^{+} cells following transfer into WT mouse recipients, we used antigen-specific FoxP3^{+} T cells from TCR transgenic

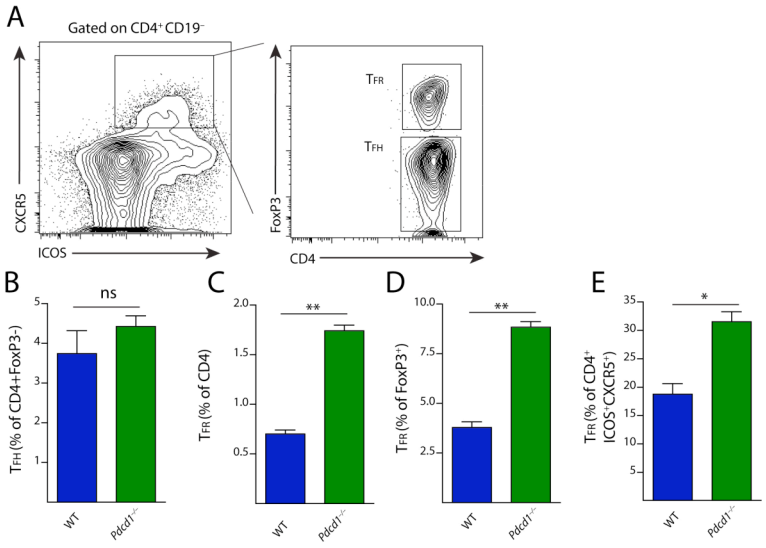

Fig. 2.3. PD-1 Signaling Limits the Generation of T Follicular Regulatory Cells in response to NP-OVA Immunization. (A) Gating of TFH and TFR cells from WT and *Pdcd1*$^{-/-}$ mice immunized with NP-OVA in CFA and analyzed 7 days later. (**B**) Quantification n of WT or PD-1$^{-/-}$ TFH cells and expressed as a percentage of CD4^{+}FoxP3^{-}. **(C)** Quantification of TFR cells expressed as a percentage of total CD4 T cells. **(D)** Quantification of TFR cells expressed as a percentage of FoxP3^{+} CD4 T cells. **(E)** Quantification of TFR cells expressed as a percentage of the CD4^{+}ICOS^{+}CXCR5^{+}CD19^{-} gate. * P<0.05, ** P<0.005

mice for these studies. We chose to use this approach because we could transfer and track Tregs in WT recipients. We wanted to avoid transfer into lymphopenic mice, which would have the potential alter differentiation because of homeostatic proliferation. We sorted FoxP3$^+$ Tregs from WT or *Pdcd1*$^{-/-}$ 2D2 (MOG–specific) TCR transgenic FoxP3 GFP reporter mice and transferred 2x10^5 2D2 WT or *Pdcd1*$^{-/-}$ CD4$^+$CXCR5$^-$FoxP3$^+$ cells into WT recipient mice. We immunized these recipients with MOG/CFA and analyzed cells in the draining lymph node seven days later (Fig. 2.2F). There were a greater percentage (Fig. 2.2G-H) and absolute number (Fig. 2.2I) of 2D2 *Pdcd1*$^{-/-}$ Tregs upregulating CXCR5 and thus differentiating into TFR cells, compared to 2D2 WT Tregs. The increased percentage of PD-1$^{-/-}$ TFR cells in the immunized transfer recipients was similar, but less pronounced, than the increased percentage in TFR cells seen in immunized PD-1 deficient mice (Fig. 2.2D,H). These results demonstrate that PD-1 controls differentiation of FoxP3$^+$ Tregs into TFR cells.

Since CD25 (the alpha chain of the IL-2 receptor) is frequently used as a marker for Tregs and is important in Treg survival, we next compared CD25 expression on WT and *Pdcd1*$^{-/-}$ TFR cells directly *ex vivo* after immunization (Fig. 2.4A). *Pdcd1*$^{-/-}$ TFR cells expressed less CD25 than WT TFR cells (Fig. 2.4B). The attenuated CD25 expression in PD-1 deficient TFR cells is not likely due to decreased activation because the expression of the early activation marker CD69 was virtually identical on WT and *Pdcd1*$^{-/-}$ TFR cells (Fig. 2.4C). To compare the proportion of WT and

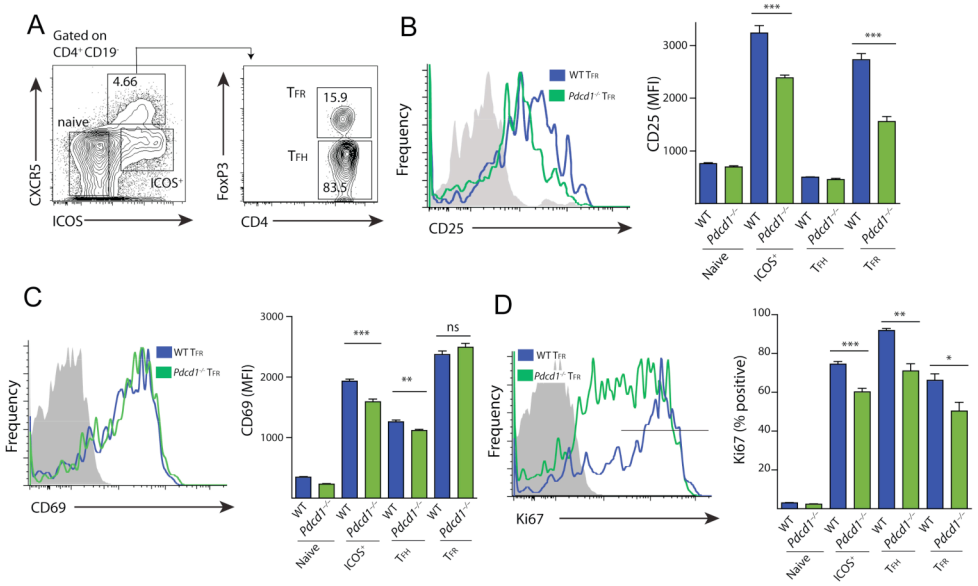

Fig. 2.4. PD-1 Deficient TFR Cells Have Altered Expression of Activation Markers. (**A**) TFR cell gating strategy. WT or PD-1$^{-/-}$ mice were immunized with MOG/CFA and draining lymph nodes were harvested 7 days later. (**B**) CD25 expression on WT and PD-1$^{-/-}$ CD4 subsets gated as in (A). Overlay histograms of WT and PD-1$^{-/-}$ TFR cells (left) and mean fluorescence intensity (MFI) in CD4 subsets gated as in (A) (right). Data represent means of 5 mice per group. (**C**) CD69 expression on WT and PD-1$^{-/-}$ CD4 subsets gated as in (A). Overlay histograms of WT and PD-1$^{-/-}$ TFR cells (left) and MFI (right). Data represent means of 5 mice per group. (**D**) Intracellular staining of cell cycle marker Ki67 in populations as in (A). Overlay histograms of WT and PD-1$^{-/-}$ TFR cells (left) and percent Ki67 high (right) in CD4 subsets gated as in (A). Ki67 high was defined as the highest intensity peak on WT TFR cells and is denoted by a black bar on the histogram. Data represent means of 5 mice per group. All data are representative of at least two independent experiments. All error bars indicate standard error. * P<0.05, ** P<0.005, *** P<0.0005.

Pdcd1$^{-/-}$ TFR cells proliferating at day 7 post immunization, we examined Ki67 expression, a marker widely used to identify cells that are actively dividing [127]. WT ICOS^{+} CXCR5^{-} effectors, TFH and TFR gated cells had high expression of Ki67. In contrast, the WT CXCR5^{-}ICOS^{-} "naïve" cells, lacking CD69 and CD25 expression, had no Ki67 staining consistent with their designation as naïve (Fig. 2.4D). WT TFR cells expressed significantly higher levels of Ki67 compared to PD-1$^{-/-}$ TFR cells, suggesting that the increased numbers of TFR cells in PD-1 deficient animals reflect increased differentiation, and not maintenance, of TFR cells. Ki67 expression was similarly greater in WT ICOS^{+} effectors and TFH cells compared to *Pdcd1*$^{-/-}$ ICOS^{+} CXCR5^{-} effectors and TFH cells. This points to an overall decrease in cell cycling in *Pdcd1*$^{-/-}$ effector cells at 7 days after immunization. Other Treg markers such as CD103 and GITR were not altered on TFR cells in PD-1 deficient mice (Fig. 2.5). Additionally, there was low, but significant expression of PD-L1 on WT and *Pdcd1*$^{-/-}$ TFR cells (Fig. 2.5). Together, these data indicate that PD-1 is important in regulating numbers of TFR cells *in vivo*.

PD-1 Deficient TFR cells are Capable of Homing to Germinal Centers

We next compared the capacity of TFR cells from WT and PD-1 deficient animals to enter the germinal center (GC) in order to inhibit the GC response. First, we evaluated GC formation in lymph node sections harvested 7 days after MOG/CFA

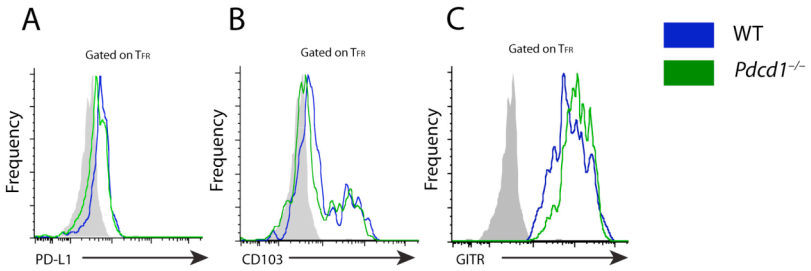

Fig. 2.5. WT and PD-1 Deficient TFR Cells Similarly Express PD-L1, CD103 and GITR. WT or *Pdcd1*$^{-/-}$ mice were immunized with MOG/CFA and 7 days later draining lymph node cells were stained for PD-L1, CD103 and GITR. Histograms show CD4^{+}CD19^{-}ICOS^{+}CXCR5^{+}FoxP3^{+} cells.

immunization. GCs were identified by the presence of PNA/GL7 positively stained and IgD negatively stained B cell zones (Fig. 2.6A). These GCs were determined to be active, based on robust expression of the cell cycle marker Ki67 (Fig. 2.6B). Similar to previous reports [115, 116], $CD4^+FoxP3^+$ TFR cells could be found within GCs of immunized mice (Fig. 2.6C). The FoxP3 protein within the TFR cells was judged to be largely nuclear based on its co-localization with the DAPI staining confirming true FoxP3 staining (Fig. 2.6D).

We then investigated whether the phenotypically distinct TFR cells from PD-1 deficient mice were able to migrate to GCs similarly to WT TFR cells, because PD-1 blockade can prolong the TCR stop signal and decrease T cell migration [128]. We immunized WT and PD-1 deficient mice with MOG/CFA and 7 days later analyzed lymph node sections for IgD, GL7 and FoxP3 expression (Fig. 2.6E). Although the average germinal center area (Fig. 2.6F) and numbers of germinal centers per lymph node (data not shown) were equivalent in WT and *Pdcd1*$^{-/-}$ mice, there were slightly more $FoxP3^+$ cells (and therefore TFR cells) located within the GC borders in PD-$1^{-/-}$ mice as in WT mice (Fig. 2.6G). However, since this increase is proportional to the larger numbers of TFR cells in lymph nodes of PD-1 deficient mice determined by flow cytometry, these data demonstrate that PD-1 deficient TFR cells are not defective in homing to GCs and can enter the GC similarly to WT TFR cells.

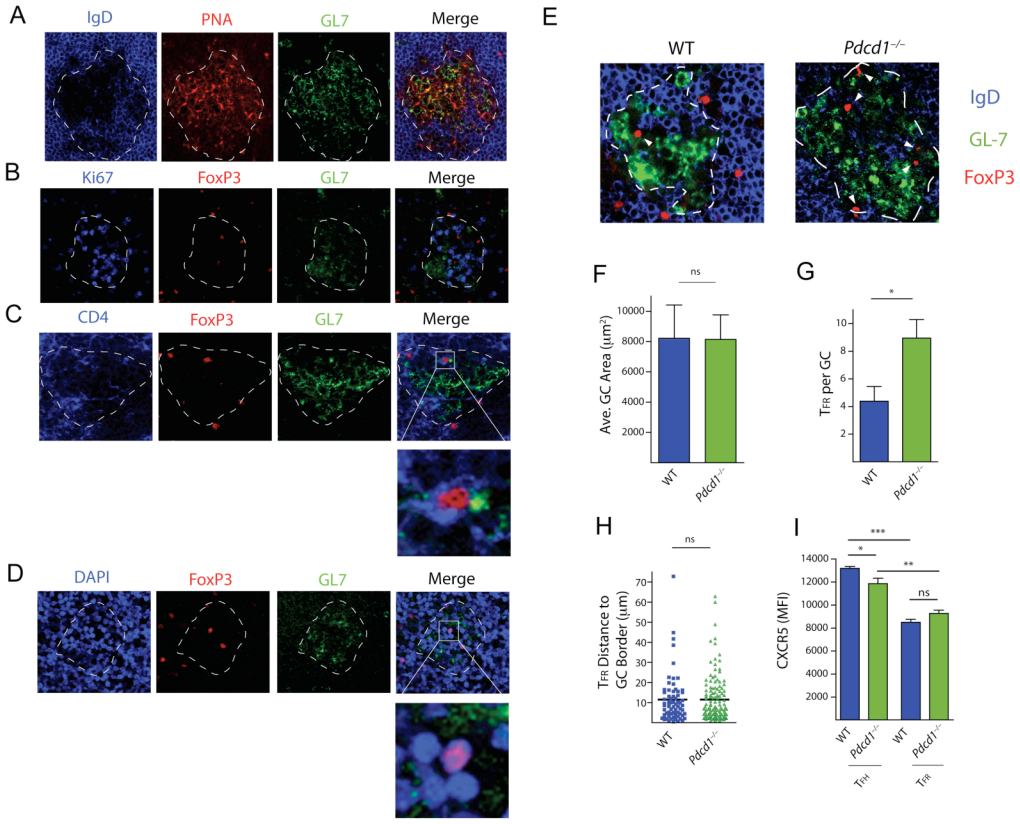

Fig. 2.6. PD-1 Deficient TFR Cells are Capable of Homing to Germinal Centers (GCs). (**A**) Micrographs of draining lymph node sections from WT mice immunized with MOG/CFA and harvested 7 days later. Sections were cut and stained for GL-7 (green), PNA (red) and IgD (blue). GCs were identified by PNA and GL7 positive, but IgD negative, staining. GCs are indicated with a white dotted line. (**B**) Ki67 staining in GCs. Sections were stained for the cell cycle marker Ki67 (blue), FoxP3 (red) and GL7 (green). (**C**) Colocalization of CD4 and FoxP3. Sections were stained for CD4 (blue), FoxP3 (red) and GL7 (green). Box indicates magnification highlighting CD4 positive staining on FoxP3^{+} cells (**D**) Colocalization of FoxP3 in the nucleus. Sections were stained with the nuclear stain DAPI (blue), FoxP3 (red) and GL7 (green). Box indicates magnification highlighting FoxP3 protein within DAPI positive nuclei. (**E**) Comparison of FoxP3^{+} TFR cells in germinal centers of WT and PD-1$^{-/-}$ mice. Representative GC staining in WT and PD-1$^{-/-}$ lymph nodes 7 days after immunization with MOG/CFA. (**F**) Average GC area was determined by calculating the area within the dotted lines according to materials and methods. Data represent mean area per lymph node of 5 individual mice. (**G**) Numbers of FoxP3^{+} cells contained within GCs. Data represent mean per GC from 5 pooled mice. (**H**) Quantitation of the distance of each FoxP3^{+} cell to the GC border. The distance for each FoxP3^{+} cell in (E) from the GC borders (dotted line in (E)) was calculated as described in materials and methods. (**I**) CXCR5 expression was quantified on WT and PD-1$^{-/-}$ CD4^{+}ICOS^{+}CXCR5^{+}FoxP3^{-}CD19^{-} TFH and CD4^{+}ICOS^{+}CXCR5^{+}FoxP3^{+}CD19^{-} TFR cells by flow cytometry 7 days after MOG/CFA immunization. Data represent means of 5 mice per group. * P<0.05, ** P<0.005, *** P<0.0005.

The relative location of FoxP3$^+$ TFR cells within the GC did not differ significantly between WT and PD-1$^{-/-}$ TFR cells (Fig. 2.6H). In both WT and *Pdcd1*$^{-/-}$ mice the FoxP3$^+$ cells tended to reside close to the GC border, with more than half of the FoxP3$^+$ nuclei being positioned within 10μm of the border. Furthermore, when CXCR5 fluorescence was quantified by flow cytometry in TFR cells, there was similar CXCR5 expression on TFR cells in the WT and PD-1$^{-/-}$ mice, indicating similar potential for these cells to respond to chemokine cues to migrate to GCs (Fig. 2.6I). However, TFR cells had lower expression of CXCR5 than TFH cells, which may indicate why TFR cells reside close to GC borders. Taken together, these data indicate that TFR cells are increased in lymph nodes of immunized *Pdcd1*$^{-/-}$ mice, and these PD-1$^{-/-}$ TFR cells are capable of migrating into GCs to regulate B cell responses.

PD-1 deficient TFR cells More Potently Inhibit T Cell Activation

We next compared the function of TFR cells from WT and *Pdcd1*$^{-/-}$ mice. TFR cells express higher levels of GITR on the cell surface than do TFH cells, which allows for separation of the TFH and TFR cells in a similar manner to intracellular staining for FoxP3 (Fig. 2.7A). For functional studies, we sorted TFR cells from immunized mice by taking the lymph node CD4$^+$ICOS$^+$CXCR5$^+$CD19$^-$GITR$^+$ population as TFR cells and the CD4$^+$ICOS$^+$CXCR5$^+$CD19$^-$GITR$^-$ population as TFH cells (Fig. 2.7B).

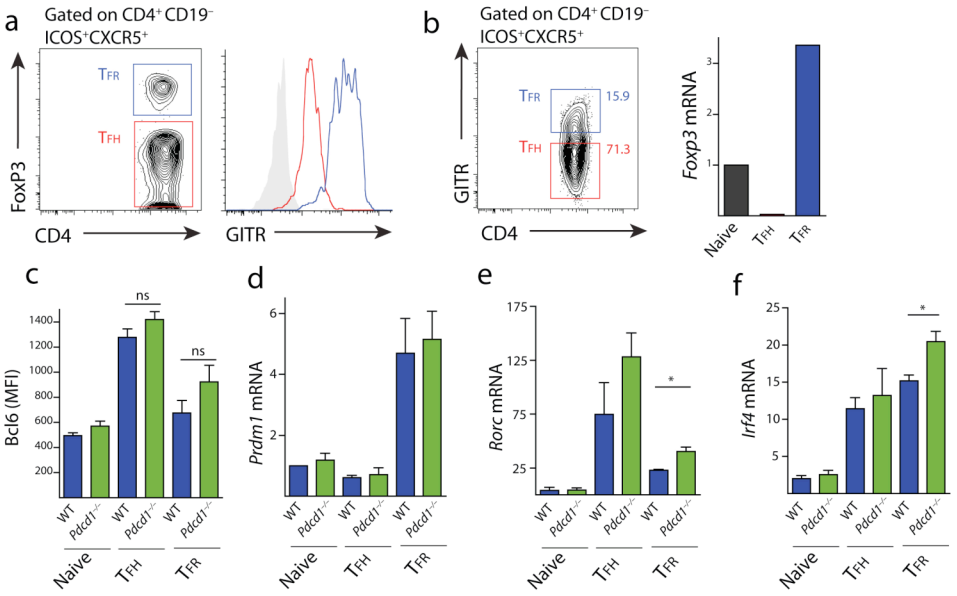

Fig. 2.7. PD-1 Deficient TFR Cells Express More IRF4. (**A**) TFR cells express high levels of GITR. WT mice were immunized with MOG/CFA and 7 days later lymph node cells were isolated and expression of GITR on TFR ($CD4^+FoxP3^+ICOS^+CXCR5^+CD19^-$, blue) and TFH ($CD4^+FoxP3^-ICOS^+CXCR5^+CD19^-$, red) was quantified as shown by histogram overlays. (**B**) Expression of FoxP3 mRNA in sorted TFR ($CD4^+GITR^+ICOS^+CXCR5^+CD19^-$), TFH ($CD4^+GITR^-ICOS^+CXCR5^+CD19^-$) and naive ($CD4^+ICOS^-CXCR5^-CD19^-$) cells. Data represent fold change in mRNA normalized to *Hprt.* (**C**) Bcl6 expression analyzed by intracellular flow cytometry on TFH and TFR cells from WT (blue) and PD-$1^{-/-}$ (green) mice. (**D-F**) mRNA expression of (D) blimp-1/*Prdm1* (E) *Rorc* and (F) *Irf4* from sorted WT (blue) and *Pdcd1*$^{-/-}$ (green) TFR and TFH cells and in CD4-$ICOS^-CXCR5^-$ (naive) cells quantified by qPCR analysis. Data represent means from at least three separate experiments in which cells were sorted from lymph nodes of 10 pooled mice.

Sorting in this fashion shows robust mRNA for FoxP3 in the GITR$^+$ (TFR) population, but essentially no FoxP3 mRNA in the GITR$^-$ (TFH) population, validating the use of this gating strategy to isolate TFR and TFH cells for functional assays. Furthermore, this sorting strategy can be used to compare WT and PD-1 deficient TFR cells since GITR expression is identical on WT and PD-1 deficient TFR cells (Fig. 2.8).

TFR cells express high Blimp1/*Prdm1* and moderate levels of Bcl6 [115]. Bcl6 and Blimp1 reciprocally modulate each other [94]; Bcl6 inhibition of Blimp1 is essential for maintenance of the TFH phenotype, whereas Blimp1 is important in Treg homeostasis in general [129, 130]. Since relative expression of Bcl6 and Blimp1 determines function of TFH subsets, we compared Bcl6 expression in TFR cells from WT and *Pdcd1*$^{-/-}$ mice using flow cytometry to analyze intracellular Bcl6 expression at the protein level. Although TFR cells expressed less Bcl6 at the protein level than TFH cells, WT and PD-1$^{-/-}$ TFR had similar Bcl6 levels (Fig. 2.7C). We next compared the expression of Blimp1 (encoded by *Prdm1*) on TFR cells from WT and *Pdcd1*$^{-/-}$ mice. At the mRNA level, we did not find any consistent differences in Blimp1/*Prdm1* expression between WT and *Pdcd1*$^{-/-}$ TFR cells (Fig. 2.7D). Since FoxP3 can directly interact with and negatively regulate the function of Rorγt [131], at least during iTreg differentiation, we also examined *Rorc* (which encodes Rorγt) in WT and *Pdcd1*$^{-/-}$ TFR cells. *Rorc* mRNA levels were lower in TFR cells compared to

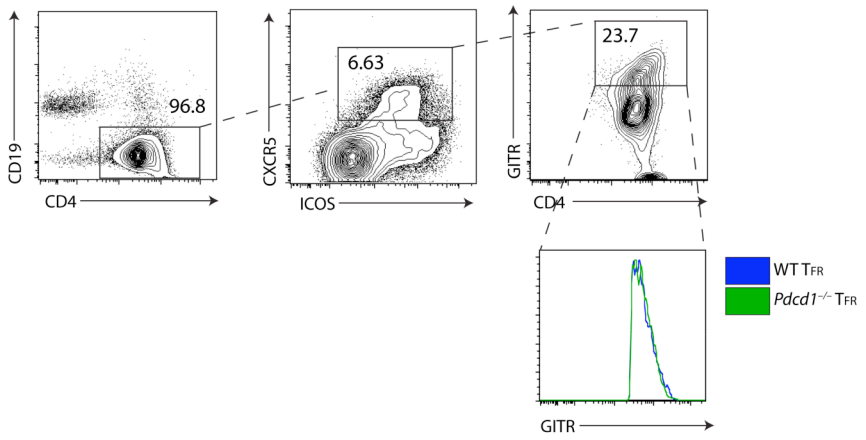

Fig. 2.8. WT and **PD-1 Deficient TFR Cells Similarly Express GITR.** WT or *Pdcd1*–/– mice were immunized with MOG/CFA and 7 days later draining lymph node cells were stained and analyzed on an Aria II flow cytometer.

TFH cells, but *Rorc* expression was increased in *Pdcd1*$^{-/-}$ TFR cells relative to WT TFR cells (Fig. 2.7E). In addition, we compared expression of the transcription factor IRF4 in WT and *Pdcd1*$^{-/-}$ TFR cells, since Blimp1 and IRF4 synergistically control the differentiation and effector functions of regulatory T cells [129]. We found an increase in *IRF4* mRNA in *Pdcd1*$^{-/-}$ TFR cells compared to WT TFR cells (Fig. 2.7F).

IRF4 is essential for the suppressive capacity of regulatory T cells [129]. However, it is unclear which cell types TFR cells can suppress and no *in vitro* suppression assay has been developed to test this. Therefore, we designed suppression assays to be able to directly compare TFR cells *ex vivo* from wild-type or knockout mice. After multiple iterations of comparing number of donor mice, ratios of cells in the well and concentrations of antibodies to stimulate the cells, we were able to develop assays that gave repeatable results. To determine if increased IRF4 mRNA in *Pdcd1*$^{-/-}$ TFR cells translates into an increase in suppression of naïve T cell proliferation, we set up an *in vitro* suppression assay in which we cultured sorted WT GL7^{-} B cells from lymph nodes of mice immunized with MOG/CFA, CFSE labeled WT naïve CD4^{+}CD62L^{+}FoxP3^{-} responder T cells from unimmunized mice, and either WT or *Pdcd1*$^{-/-}$ TFR cells sorted from mice immunized with MOG/CFA together with anti-CD3 and anti-IgM (Fig. 2.9A). The responder T cells highly upregulated CD69 after 3 days of culture with WT B cells. However, when WT TFR cells were added in a 1:1:1 ratio, the CD69 expression on the responder T cells was much lower, consistent

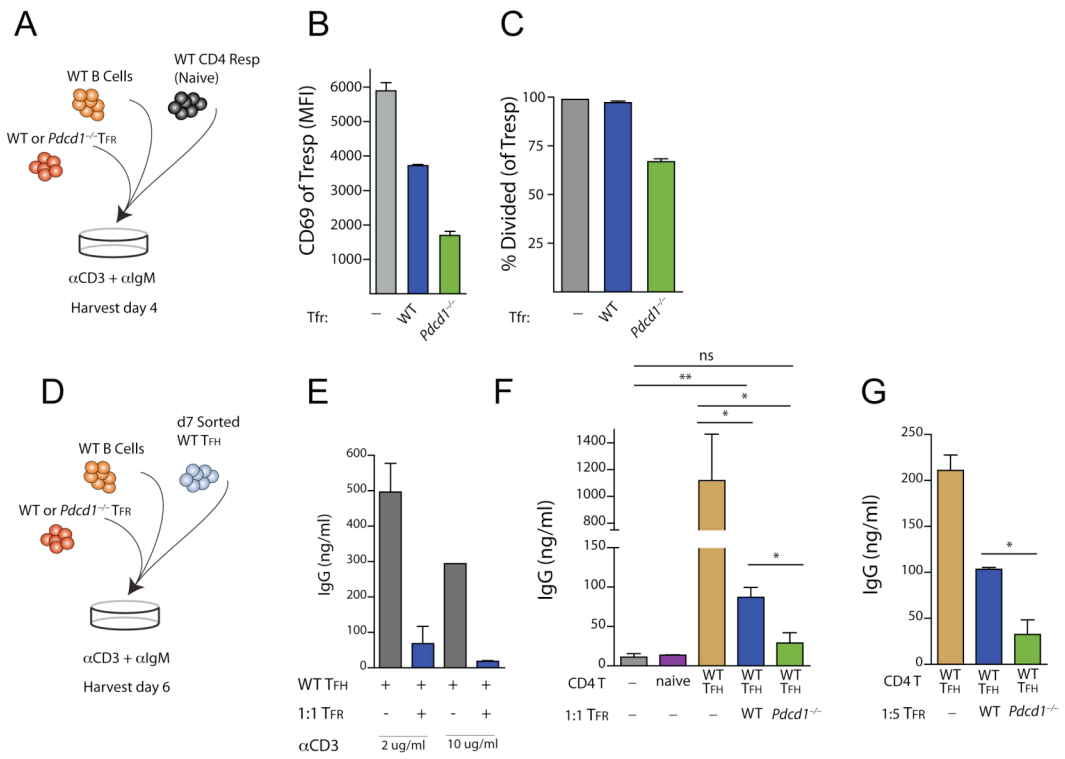

Fig. 2.9. PD-1 Deficient TFR Cells More Potently Suppress Antibody Production. (**A**) Design of assay to analyze capacity of TFR cells to inhibit activation of naïve CD4 T cells. WT and PD-1$^{-/-}$ mice were immunized with MOG/CFA and TFR cells were sorted from draining lymph nodes and plated 1:1:1 with CFSE-labeled CD4 naïve WT (CD4^{+}CD62L^{+}FoxP3^{-}) responder cells and WT GL7^{-}B220^{+} B cells from MOG/CFA immunized mice along with anti-CD3 and anti-IgM for 4 days. 3 days later samples were analyzed by flow cytometry. (**B**) PD-1$^{-/-}$ TFR cells suppress activation of naïve T cells to a greater extent than WT TFR cells. T responders from suppression assays from **(A)** were analyzed for CD69 expression (**B**) and proliferation (**C**) by measuring CFSE dilution. % divided indicates percent of cells that have gone through at least one division. (**D**) *In vitro* IgG suppression assay design. TFR cells sorted as in (**A**) were plated in a 1:1:1 ratio of TFR (CD4^{+}ICOS^{+}CXCR5^{+}GITR^{+}CD19^{-}), TFH (CD4^{+}ICOS^{+}CXCR5^{+}GITR^{-}CD19^{-}), and B (GL-7^{-}B220^{+}) cells from draining lymph nodes of MOG/CFA immunized mice in the presence of anti-CD3 and anti-IgM for 6 days. Total IgG was measured by ELISA from supernatants. (**E**) Suppression assay using two concentrations of anti-CD3. (**F**) PD-1 deficient TFR cells suppress IgG production to a greater extent than WT TFR cells at a 1:1 TFR:TFH ratio. Naive (CD4^{+}ICOS^{-}CXCR5^{-}CD19^{-}) cells from immunized mice were included as controls. (**G**) PD-1 deficient TFR cells suppress IgG production to a greater extent than WT TFR cells at a 1:5 TFR:TFH ratio. Data indicates means +/- standard error of replicate wells and is representative of at least two experiments (B-G). * P<0.05, ** P<0.005, *** P<0.0005.

with the function of TFR cells in suppressing T cell activation (Fig. 2.9B). CD69 upregulation was inhibited to an even greater extent in responder T cells that were cultured with *Pdcd1*$^{-/-}$ TFR cells. Moreover, *Pdcd1*1$^{-/-}$ TFR attenuated the proliferation of responder T cells (Fig. 2.9C), in contrast to WT TFR cells, which did not inhibit the proliferation of responder T cells during the 3 day culture period. Therefore, although TFR cells do not potently suppress naïve T cell activation *per se*, PD-1 deficiency results in slightly better suppression.

Although TFR cells do not potently suppress naïve cells, it may be possible that TFR cells are specialized to inhibit TFH-mediated antibody production. To test this *in vitro*, we designed a separate *in vitro* assay. Originally, we thought by supplying any T cell help to B cells we could stimulate antibody production in the well that we could measure by ELISA. However, this proved uneffective and activating CD4 T cells from lymph nodes with anti-CD3 and supplying anti-IgM to B cells in a well did not result in IgG production. Therefore, although more difficult, we turned to sorting TFH cells as stimulators of the B cells. To assess the capability of TFR cells to suppress B cell antibody production *in vitro*, we cultured WT GL7^{-} B cells from lymph nodes of MOG/CFA immunized mice with WT FoxP3^{-} TFH cells sorted from lymph nodes of MOG/CFA immunized mice for 6 days in the presence or absence of TFR cells sorted from lymph nodes of MOG/CFA immunized mice, anti-IgM and anti-CD3 (Fig. 2.9D). WT B cells produced large amounts of IgG when cultured

with WT FoxP3$^-$ TFH cells plus anti-IgM and anti-CD3 (Fig. 2.9E). No significant IgG was present when CD4$^+$FoxP3$^-$ naïve T cells were used in these experiments (Fig. 2.9F). When TFR cells were added to the wells along with TFH cells, almost no IgG was produced. The TFR-mediated suppression was not due to sequestering of anti-CD3 because there was equally good suppression at the two doses of anti-CD3 tested (Fig. 2.9E), and the anti-CD3 could still be found on the surface of the TFH cells at the end of the suppression assay (Fig. 2.10). *Pdcd1*$^{-/-}$ TFR cells suppressed IgG production more than WT TFR cells at both a 1:1 (Fig. 2.9F) and a 1:5 (Fig. 2.9G) TFR:TFH ratio, with PD-1 deficient TFR cells resulting in a 50% greater reduction in IgG production compared to WT TFR cells. Taken together, these data demonstrate not only that are there increased TFR cells in *Pdcd1*$^{-/-}$ mice, but that these *Pdcd1*$^{-/-}$ TFR cells have increased suppressive capacity.

PD-1 Controls Blood T Follicular Regulatory Cells

One possible explanation for the increase in TFR cells in lymph nodes of immunized PD-1 deficient mice is that *Pdcd1*$^{-/-}$ TFR cells are unable to exit the lymph node. Studies have demonstrated that functional TFH cells can be found in the blood of humans as well as mice [88, 98, 100], but whether TFR cells circulate in the blood of humans or mice is not yet known. Strikingly, we found a significant population of TFH cells, as well as a smaller population of TFR cells, in the blood of WT mice

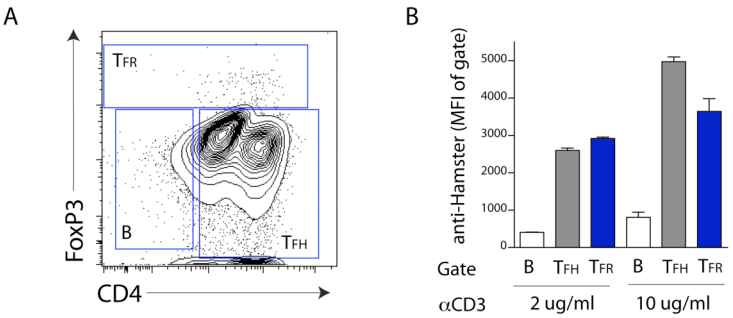

Fig. 2.10. TFR Suppression is Not Due to Anti-CD3 Sequestering. (A) Suppression assays were performed as in Fig. 2.9D and 6 days later cells in the wells were stained for CD4 and FoxP3 to identify TFR, TFH and B cells in the well. (B) Samples were further stained with an anti-hamster secondary antibody and in this way anti-CD3 bound to the surface of the cells was quantified.

immunized with MOG/CFA (Fig. 2.11A-B). When we compared the kinetics of TFH and TFR cell expansion in the lymph node and blood of mice following MOG/CFA immunization, we found that both TFR and TFH cells increase in the draining lymph node of WT immunized mice over a 10 day period.

Importantly, TFH cells, but not TFR cells, increase substantially by percentage in the blood over this time (Fig. 2.11B). Since total T cells increase in the blood during immunization, TFR cells do increase, but this increase is proportional to the increases in cellularity. Without antigenic stimulus, the blood TFR:TFH ratio is fairly high (sometimes greater than 1:1) but upon addition of a stimulus, blood TFH cells expand more than blood TFR cells so that the TFR:TFH ratio is about 1:5. To investigate whether WT blood TFH and TFR cells are quiescent or are actively in cell cycle, we compared Ki67 expression in draining lymph node and blood TFH and TFR cells 7 days after immunization. TFH cells from the draining lymph node had higher Ki67 expression than those found in the blood (Fig. 2.11C). Blood TFH and TFR cells and draining lymph node TFR cells expressed similar levels of Ki67, which was lower than lymph node TFH cells but much higher than naïve T cells. Thus, TFR cells in the blood are equally in cell cycle as the TFR cells that are present in the draining lymph nodes.

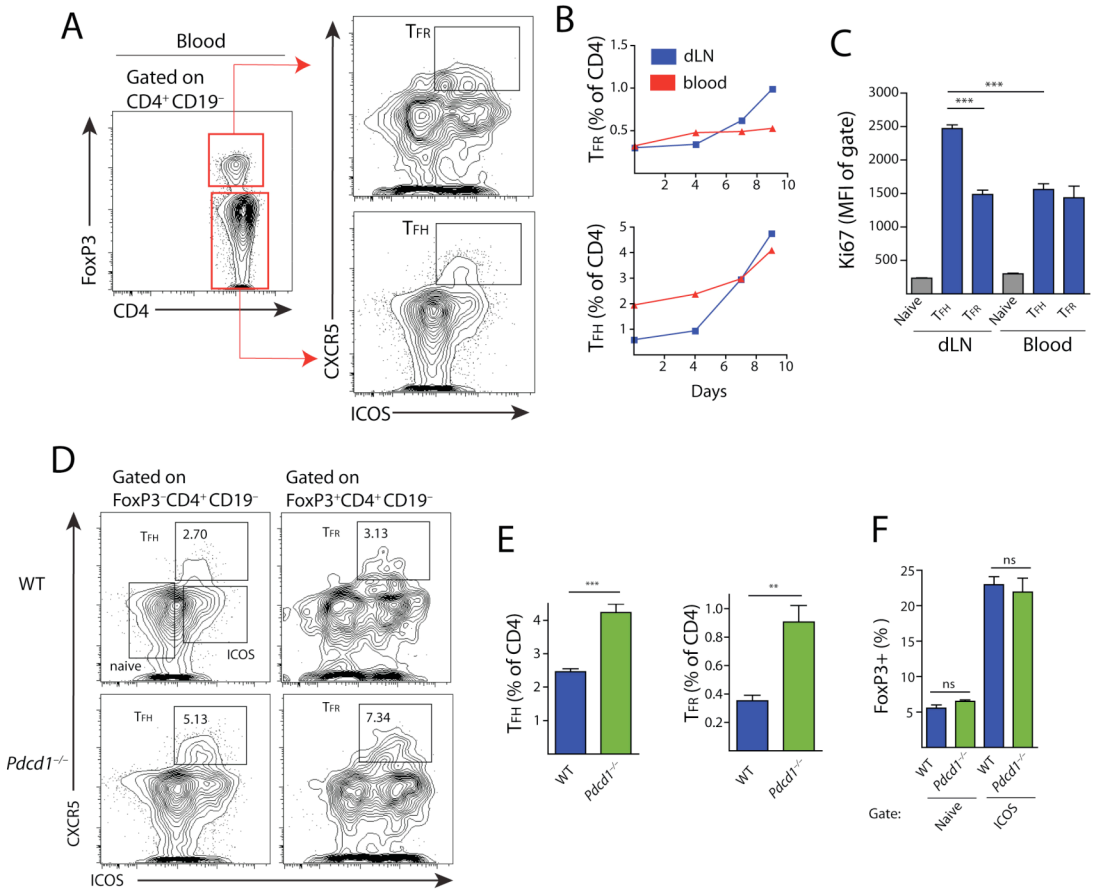

Fig. 2.11. PD-1 controls circulating blood TFR cells. (**A**) Gating strategy to identify circulating TFH and TFR cells from blood. WT mice were immunized with MOG/CFA and blood was collected 7 days later by cardiac puncture. TFH and TFR populations were gated as shown. (**B**) Quantitation of blood TFH and TFR cells following MOG/CFA immunization. Mice were immunized as in (a) and sacrificed on the indicated days. Blood was collected and cells stained and gated as in **(**A**)**. (**C**) Ki67 expression in blood and lymph node TFH, TFR and naïve ($CD4^+ICOS^-CXCR5^-$) cells 7 days after MOG/CFA immunization. (**D-F**) Comparison of blood TFH and TFR cells in WT and PD-$1^{-/-}$ mice immunized as in (A) and harvested 7 days after immunization**.** (**D**) Blood TFH cells are shown gated on $FoxP3^-CD4^+CD19^-$ (left) and TFR cells are shown gated on $FoxP3^+CD4^+CD19^-$ (right). (**E**) Quantitation of blood TFH and TFR cells from immunized WT and PD-$1^{-/-}$ mice gated as in (D) and expressed as a percent of $CD4^+CD19^-$ cells. (**F**) Quantitation of $CXCR5^-$ $FoxP3^+$ cells from immunized WT and PD-$1^{-/-}$ mice, expressed as a percentage of $CXCR5^-$ $CD4^+$ cells. All data indicates means +/- standard error of 5 mice and is representative of at least two independent experiments. * P<0.05, ** P<0.005, *** P<0.0005.

Next we investigated whether TFR cells in the blood were inhibited to the same degree by PD-1 signaling as lymph node TFR cells. We immunized WT and *Pdcd1*$^{-/-}$ mice with MOG/CFA and 7 days later analyzed the blood for TFH and TFR cells. In WT mice ~2-3 percent of CD4^{+}FoxP3^{-}CD19^{-} cells in the blood were TFH cells, but in the *Pdcd1*$^{-/-}$ mice this increased to ~4-5 percent (Fig. 2.11D). This increase in *Pdcd1*$^{-/-}$ TFH cells in blood markedly contrasts with the lymph node, where *Pdcd1*$^{-/-}$ mice have similar, if not less, TFH cells compared to WT mice (Fig. 2.2E). Importantly, TFR cells comprised ~3 percent of all FoxP3 positive cells in the blood of WT mice, but more than 7 percent of FoxP3 positive cells in the blood of PD-1$^{-/-}$ mice (Fig. 2.11D-E). The increase in FoxP3^{+} cells seems to be specific to the blood TFR subset, as the percentage of FoxP3^{+} cells in the ICOS^{+}CXCR5^{-} (ICOS^{+}) and ICOS^{-}CXCR5^{-} naïve cell gates were not increased in *Pdcd1*$^{-/-}$ mice (Fig. 2.11F). Taken together, these data indicate that both TFR and TFH cells are present in the blood of mice, and both subsets are repressed by PD-1 signals.

To investigate whether blood TFH and TFR cells have a central memory phenotype, we analyzed surface expression of CD62L and CD44. CD62L (L-selectin) is essential in mediating migration of naïve and central memory cells to secondary lymphoid organs[132] and CD44 is important for survival, differentiation and homing of CD4 T memory cells[133]. Moreover, high CD44 expression on Treg cells has been shown to have a positive correlation with suppressive function due to increased

expression of IL-10 in CD44^{hi} Treg cells[134]. About 60% of WT and PD-1$^{-/-}$ blood TFR cells had high expression of CD62L (Fig. 2.12A). This contrasts with the greater than 90% of ICOS^{-}CXCR5^{-} naïve cells that had high CD62L expression. Interestingly, *Pdcd1*$^{-/-}$ TFH cells had lower CD62L compared to WT TFH cells, which may indicate a lower potential of *Pdcd1*$^{-/-}$ TFH cells to home to secondary lymphoid organs. CD44 was highly expressed on all WT and *Pdcd1*$^{-/-}$ blood TFR cells, but *Pdcd1*$^{-/-}$ blood TFR cells had slightly lower surface expression (Fig. 2.12B). Furthermore, PD-1 was expressed at lower levels on blood TFR cells than lymph node TFR cells which may indicate that these cells are less activated since PD-1 expression is increased in T cells upon activation (Fig. 2.12C). Taken together, these data indicate that blood TFR cells can have a central memory homing phenotype based on surface expression of central memory surface markers.

The increase in TFR cells in *Pdcd1*$^{-/-}$ mice led us to investigate which PD-1 ligand is critical for controlling lymph node and blood TFR generation. Although many studies have analyzed PD-1 ligand expression on B cells and dendritic cells, these studies did not analyze similar organs and activation stimuli with the conditions that we are using here for TFR stimulation. Therefore, we first compared PD-L1 and PD-L2 expression on B cells and DCs present in dLNs of immunized WT mice because both B cells and dendritic cells (DCs) contribute to proper TFH differentiation and maintenance in the lymph node [90]. It is not yet clear whether B cells, DC or both are

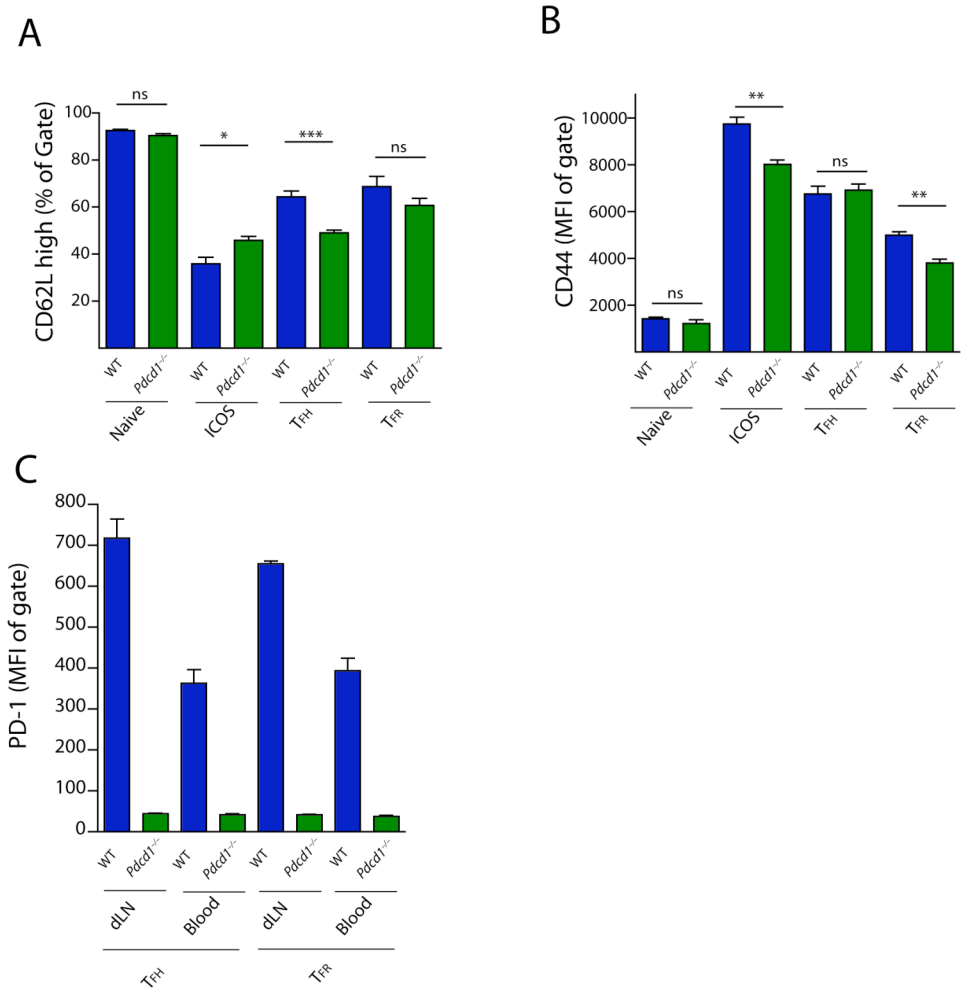

Fig. 2.12. Blood TFH and TFR Cells Express Central Memory Homing Markers. WT and PD-1$^{-/-}$ mice were immunized with MOG/CFA and 7 days later populations from blood were analyzed for CD62L (**A**) and CD44 (**B**) expression. (**C**) PD-1 expression was compared on WT and PD-1 deficient mice from draining lymph node and blood TFH and TFR cells 7 days after NP-OVA immunization.

needed for TFR differentiation and/or maintenance. To study GC B cells, we immunized mice with NP-OVA subcutaneously and 12 days later compared PD-L1 and PD-L2 expression on $FAS^+GL7^+CD19^+$ GC B cells, as well as $CD138^+$ positive plasma cells (PC) from the dLN. We found that all B cell subsets expressed high levels of PD-L1, but only GC B cells expressed high levels of PD-L2 (Fig. 2.13A). To quantify PD-L1 and PD-L2 expression on DCs, we immunized mice with NP-OVA and analyzed DC populations from the draining lymph node 3 days later. Both $CD8\alpha^+$ and $CD8\alpha^-$ DC populations expressed high levels of PD-L1 and moderate levels of PD-L2 (Fig. 2.13B). A subpopulation of $CD8\alpha^-$ DCs expressed high levels of PD-L2.

To determine which ligand is important for TFH and TFR generation, we immunized WT, *Cd274*$^{-/-}$ (PD-L1) and *Pdcd1lg2*$^{-/-}$ (PD-L2) mice with MOG/CFA, and analyzed TFH and TFR cells 7 days post-immunization in the draining lymph node and blood. The percentages of lymph node TFH cells in *Cd274*$^{-/-}$ and *Pdcd1lg2*$^{-/-}$ mice were comparable to WT mice (Fig. 2.13C) and *Pdcd1*$^{-/-}$ mice (Fig. 2.2E). *Cd274*$^{-/-}$, but not *Pdcd1lg2*$^{-/-}$ mice, had greater blood TFH cell numbers, which was similar to *Pdcd1*$^{-/-}$ mice (Fig. 2.13E). TFR cells, however, were increased in the lymph nodes as well as the blood of *Cd274*$^{-/-}$, but not *Pdcd1lg2*$^{-/-}$ mice (Fig. 2.13D). Similar to *Pdcd1*$^{-/-}$ mice, *Cd274*$^{-/-}$ mice did not exhibit any increases in non-TFR $FoxP3^+$ effector cells within

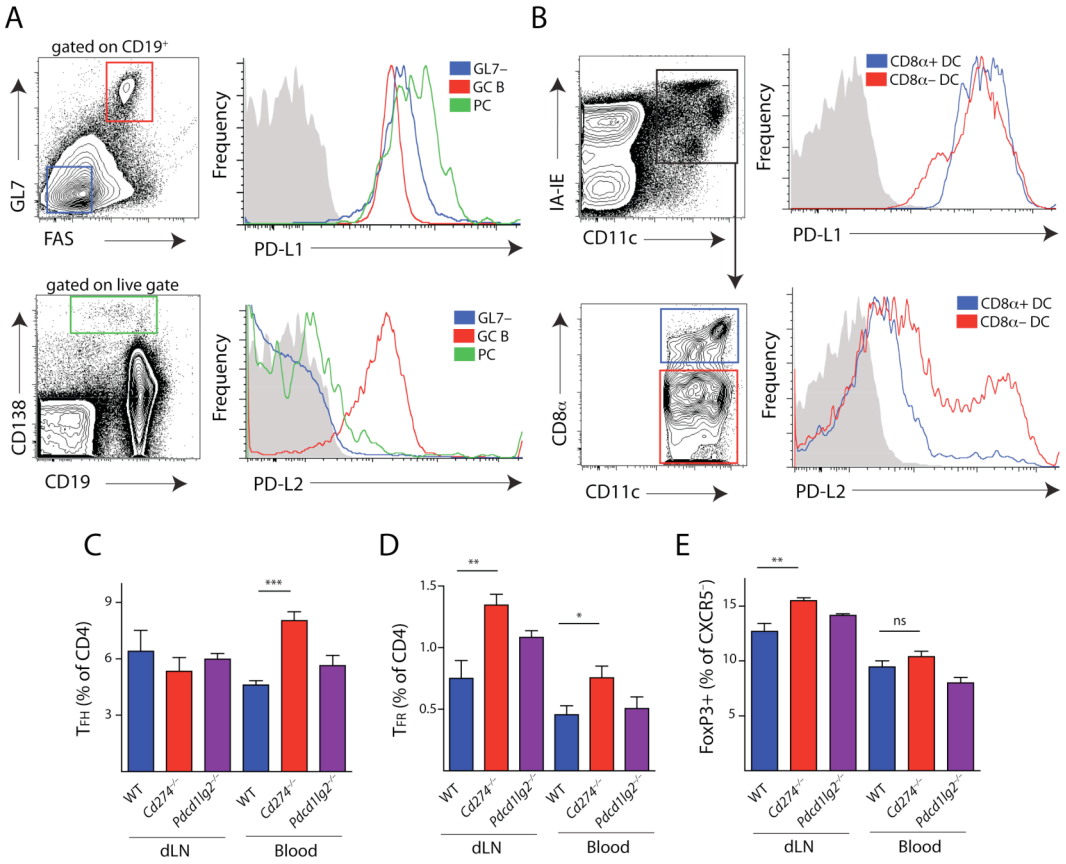

Fig. 2.13. PD-L1 but not PD-L2 Controls Blood TFR Cells. (**A**) PD-L1 and PD-L2 expression on B cell subsets. WT mice were immunized with NP-OVA subcutaneously and 12 days later germinal center B (GC B), GL7^{-}, and plasma cells (PC) from draining lymph nodes were analyzed for PD-L1 (top) and PD-L2 (bottom) expression. (**B**) PD-L1 and PD-L2 expression on dendritic cells (DC). WT mice were immunized with NP-OVA and 3 days later CD8α^{+} DC and CD8α^{-} DC subsets from draining lymph nodes were analyzed for PD-L1 (top) and PD-L2 (bottom) expression. (**C-E**) Lymph node and blood TFH and TFR cells in PD-1 ligand deficient mice. WT, PD-L1$^{-/-}$ and PD-L2$^{-/-}$ mice were immunized with MOG/CFA, and 7 days later draining lymph nodes and blood were harvested and analyzed for TFH (C), TFR (D) and CXCR5^{-} FoxP3^{+} (E) CD4 T cells. Data represent means of 5 mice per group. All data are representative of at least two independent experiments. * P<0.05, ** P<0.005, *** P<0.0005.

the blood (Fig. 2.13E). These studies demonstrate that PD-L1, but not PD-L2, is responsible for controlling lymph node and blood TFR cells.

Blood TFH and TFR cells require CD28 and ICOS Signals

We further investigated the costimulatory requirements for blood TFR cells, focusing on the effects of CD28 and ICOS costimulation on $CD4^+ICOS^+CXCR5^+FoxP3^+CD19^-$ TFR populations in the blood due to the important roles of these costimulatory receptors in controlling lymph node TFH and TFR cells. *Cd28*$^{-/-}$ mice are deficient in lymph node TFH and TFR cells [115]. *Icos*$^{-/-}$ mice are deficient in lymph node TFH cells [126]. We analyzed CD28 and ICOS deficient animals for the presence of TFR cells in the lymph nodes and blood 7 days after immunization with MOG/CFA. In WT mice, there were fewer TFH and TFR cells in the blood compared to the draining lymph node (Fig. 2.14A-B). In order to identify TFR cells in ICOS deficient mice, we could not use ICOS as a surface marker. Therefore we gated $CD4^+CD44^+CXCR5^+FoxP3^+$ cells as TFR cells, essentially replacing ICOS with CD44, which is highly expressed on all TFR cells (Fig. 2.12B). Numbers of TFR (and TFH) cells were greatly attenuated in the blood, as well as lymph nodes, of ICOS deficient mice (Fig. 2.14A-C). CD28 deficient mice had similar severe deficiencies in $CD4^+ICOS^+CXCR5^+FoxP3^+$ TFR and $CD4^+ICOS^+CXCR5^+FoxP3^-$ TFH cell percentages in both lymph nodes and blood

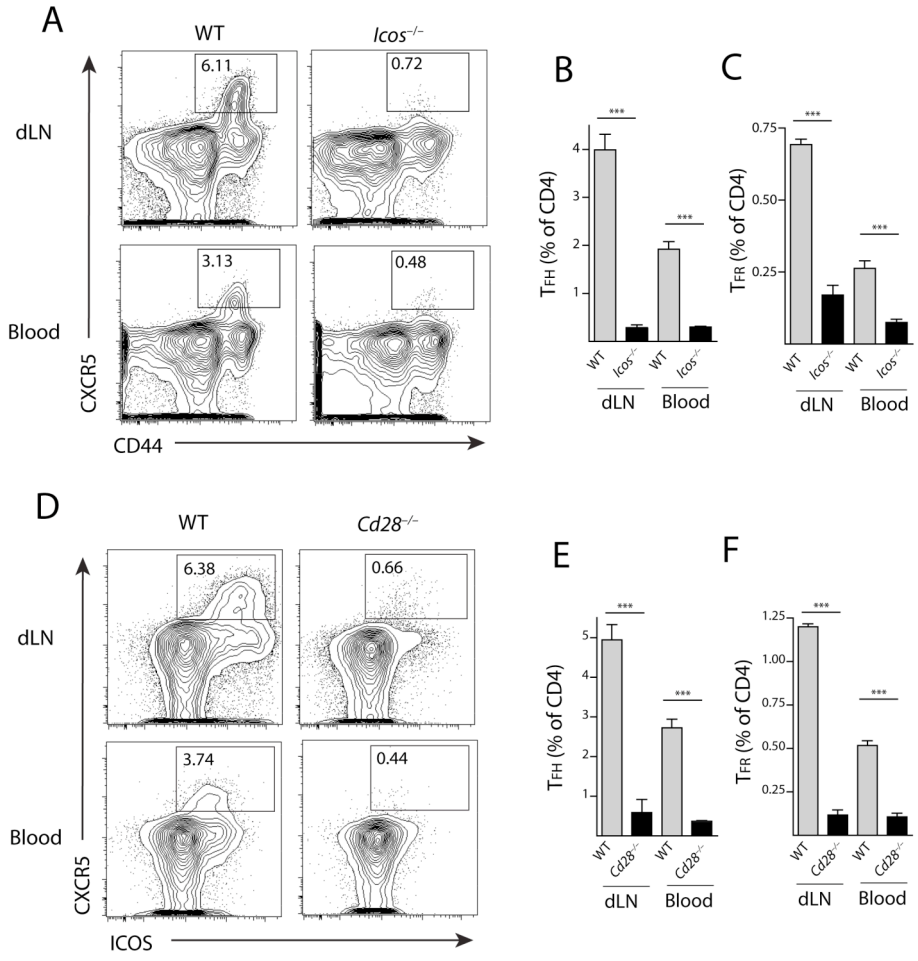

Fig. 2.14. Blood TFR Cells Require ICOS and CD28 Costimulation. (**A**) TFH and TFR gating in WT and ICOS$^{-/-}$ mice. Mice were immunized with MOG/CFA and 7 days later draining lymph nodes (dLN) and blood were harvested. TFH cells were gated as CD4^{+}CD44^{+}CXCR5^{+}FoxP3^{-} CD19^{-}, and TFR cells as CD4^{+}CD44^{+}CXCR5^{+}FoxP3^{+}CD19^{-} cells. TFH (**B**) and TFR (**C**) quantitation in lymph nodes (dLN) and blood of WT and ICOS$^{-/-}$ mice as in (A). (**D**) TFH and TFR gating strategy in WT and CD28$^{-/-}$ mice. Mice were immunized as in (A) and TFH cells were gated as CD4^{+}ICOS^{+}CXCR5^{+}FoxP3^{-}CD19^{-} and TFR cells as CD4^{+}ICOS^{+}CXCR5^{+}FoxP3^{+}CD19^{-}. TFH (**E**) and TFR (**F**) quantitation in lymph nodes and blood of WT and CD28$^{-/-}$ mice gated as in (D). All data are representative of at least two independent experiments. * P<0.05, ** P<0.005, *** P<0.0005.

(Fig. 2.14D-F). Thus, ICOS and CD28 supply essential costimulatory signals for TFR and TFH cells in the blood as well as the lymph nodes and lack of either costimulatory receptor results in almost complete blockade in differentiation of TFH and TFR cells.

PD-1 deficient blood TFR cells more potently regulate antibody production *in vivo.*

We next investigated the function of blood TFR cells in humoral immune responses. Because TFH cells in human blood can function in B cell activation and antibody production *in vitro* [88, 98], we analyzed whether circulating blood TFR cells contribute to suppression of antibody production *in vivo*. Although genetic approaches could be used to block TFR generation, we wanted to distinguish function from differentiation to specifically analyze how TFR cells function. Therefore, we designed transfer experiments in which we immunized >20 WT donor mice with NP-OVA subcutaneously and 8 days later sorted TFR ($CD4^+ICOS^+CXCR5^+GITR^+CD19^-$) and TFH ($CD4^+ICOS^+CXCR5^+GITR^-CD19^-$) cells from the blood (Fig. 2.15A). This approach is technically challenging because of the relatively few blood TFR cells (about 1,000 TFR and 4,000 TFH per mouse) that we can obtain by sorting. We transferred these cells into *Cd28*$^{-/-}$ or *Tcra*$^{-/-}$ mice because they lack both blood and lymph node TFH and TFR cells. This approach enabled us to determine if blood TFR

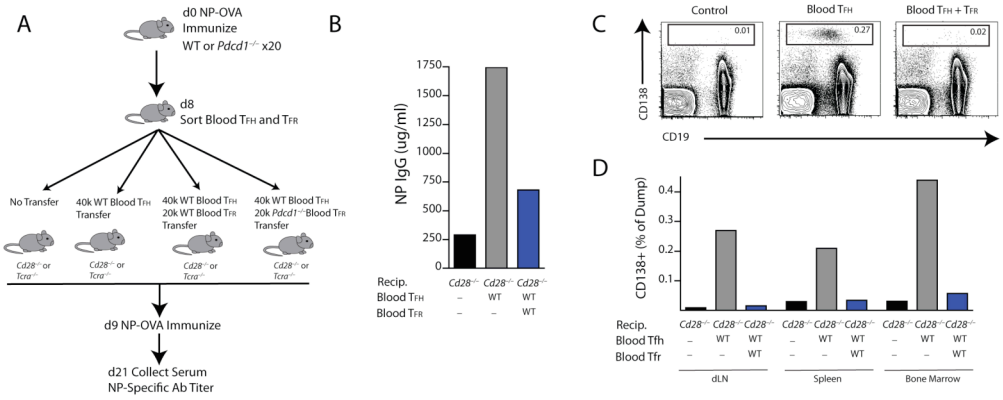

Fig. 2.15. **Blood TFR Cells Regulate Antibody Production *In Vivo.*** (**A**) Experimental strategy to assess blood TFH and TFR cell function by transfer of blood TFH and/or TFR cells into mice that lack both lymph node and blood TFH/TFR cells. Blood TFH and/or TFR cells were isolated from 20 pooled mice immunized with NP-OVA 8 days previously and $CD4^+CXCR5^+GITR^-CD19^-$ TFH and $CD4^+CXCR5^+GITR^+CD19^-$ TFR cells were purified by cell sorting; recipient $CD28^{-/-}$ or $TCR\alpha^{-/-}$ mice received either no cells, $4x10^4$ TFH cells, or $4x10^4$ TFH plus $2x10^4$ TFR cells. One day later recipients were immunized with NP-OVA. 12 days later sera were collected and NP-specific antibody titers quantified by ELISA. (**B**) WT blood TFR cells potently suppress antibody production. NP-specific antibody titers from experiments as in (A) in which WT TFH or WT TFH plus WT TFR cells were transferred into $CD28^{-/-}$ recipients. (**C**) $CD138^+$ plasma cell percentages in draining lymph nodes of $CD28^{-/-}$ recipients following no transfer (Control), Blood TFH transfer (Blood TFH) or Blood TFH plus TFR cell transfer (Blood TFH + TFR) 24 days after immunization. Cells are gated as a percentage of $CD11b^-CD11c^-Ly6c^-$ (dump) cells.

and TFH cells could regulate humoral responses. Since the transferred blood TFH and TFR cells are the only follicular T cells in *Cd28*$^{-/-}$ and *Tcra*$^{-/-}$ recipients, any responses in the draining lymph node would be due to trafficking of the blood TFR and TFH cells. Therefore, not only does this approach allow us to study TFR cell function separately from differentiation, but also allows us to study blood TFR function, without the interference of starting lymph node TFR cells.

Initially, we adoptively transferred $4x10^4$ TFH cells alone or together with $2x10^4$ TFR cells into CD28$^{-/-}$ mice (approximately a two-fold higher ratio of TFR:TFH cells than is found in blood after immunization). We immunized recipients 1 day later with NP-OVA and analyzed NP-specific IgG titers 12 days after immunization (Fig. 2.15B). Without blood TFH or TFR cell transfer, *Cd28*$^{-/-}$ mice were unable to produce significant amounts of NP-specific IgG (Fig. 2.15B). The transfer of blood TFH cells alone resulted in a substantial increase in NP-specific IgG titers. Transfer of blood TFH cells led to substantial production of IgG1, but also smaller increases in other isotypes (data not shown). This IgG1 bias is consistent with immunization of WT mice with NP-OVA. Significantly, transfer of blood TFR cells along with blood TFH cells resulted in robust inhibition of NP-specific antibody production, demonstrating the potent regulatory capacity of blood TFR cells in suppressing antibody production (Fig. 2.15B). To evaluate the impact of TFR cells on plasma cell generation, draining lymph nodes, spleens and bone marrow were harvested 24 days after immunization

and plasma cells were quantified. $CD138^+$ plasma cells were absent from the lymph nodes of immunized *Cd28*$^{-/-}$ mice (Fig. 2.15C-D). Transfer of blood TFH cells resulted in a sizable population of plasma cells in the draining lymph node, spleen and bone marrow (Fig. 2.15C-D). Blood TFR cells almost completely prevented plasma cell formation/survival in all organs analyzed.

Next we transferred blood TFH and/or TFR cells into *Tcra*$^{-/-}$ recipients. Transfer of $4x10^4$ TFH cells resulted in high levels of NP-specific IgG and at a greater titer than an immunized WT mouse in most experiments (Fig. 2.16A). The robust antibody production elicited by blood TFH cells depends on the "follicular program" because transfer of total CD4 T cells from CXCR5$^{-/-}$ mice nor $CD4^+CXCR5^-FoxP3^-$ naïve cells resulted in near background levels of antibody production in these experiments (Fig. 2.16A). When blood TFR cells were transferred together with blood TFH cells, the NP-specific antibody titers were markedly reduced, demonstrating the suppressive capacity of these cells (Fig. 2.16A). The blood TFR cells resulted in both lower plasma cell percentages in the spleen (Fig. 2.16B), as well as lower percentages of TFH cells within the lymph node (Fig. 2.16C). When we compared the functions of blood TFH cells and draining lymph node TFH cells following transfer into *Tcra*$^{-/-}$ recipients, we found that blood TFH cells have an increased capacity to promote NP-specific IgG production (Fig. 2.16D). TFR suppression of TFH cells also depends on the "follicular program" in these cells because neither blood

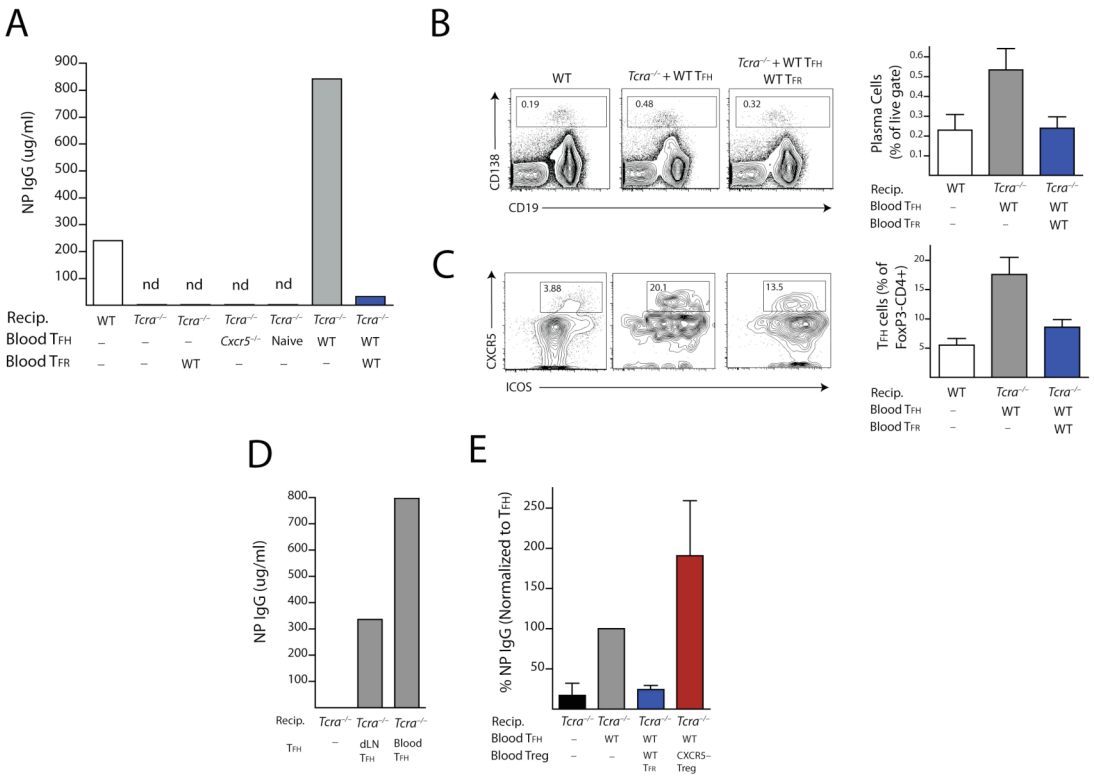

Fig. 2.16. TFR Cell Regulation of Antibody Production Depends on The Follicular Program (**A**) Blood TFH and/or TFR Transfer into TCRα$^{-/-}$ recipients using experimental design as in (Fig. 2.12A). Comparison of NP-specific antibody titers in (1) WT control mice, (2) TCRα$^{-/-}$ recipients given no cells, (3) TCRα$^{-/-}$ recipients given WT blood TFR cells alone, (4) TCRα$^{-/-}$ recipients given total blood CD4 T cells from CXCR5$^{-/-}$ mice immunized with NP-OVA 8 days previously, (5) TCRα$^{-/-}$ recipients given blood CD4^{+}FoxP3^{-} cells from unimmunized FoxP3-GFP mice, (6) TCRα$^{-/-}$ recipients given WT blood TFH cells, and (7) TCRα$^{-/-}$ recipients given WT blood TFH cells plus TFR cells. NP specific IgG levels were determined by ELISA. (**B**) CD138^{+} plasma cells from the spleen (gated as a percent of live cells) and (**C**) CD4^{+}FoxP3^{-} TFH cells from the draining lymph node pre-gated on CD4^{+}FoxP3^{-} were quantified from experiments in (A) 12 days after secondary immunization. Error bars indicate standard error of at least three separate experiments. (**D**) Blood TFH cells can have an enhanced ability to stimulate antigen-specific antibody production compared to lymph node TFH cells. Blood TFH cells and draining lymph node TFH cells were isolated from WT mice immunized with NP-OVA 8 days previously and 4x10^{6} cells were transferred into TCRα$^{-/-}$ mice and immunized as in (A). (**E**) Blood TFR cell suppression is aided by the follicular program. Blood TFH cells were transferred to TCRα$^{-/-}$ mice along with blood CXCR5- FoxP3 GFP^{+} cells from FoxP3 reporter mice or blood TFR cells. Antibody titers were quantified 12 days after NP-OVA immunization and NP IgG levels are expressed as a percent of TFH transfer group. Data indicate standard error of at least three independent experiments.

$CD25^+CD62L^+$ Tregs from *Cxcr5*$^{-/-}$ mice (data not shown) nor blood $CXCR5^-$ FoxP3 GFP^+ Tregs from FoxP3 reporter mice possess the same suppressive capacity as WT blood TFR cells (Fig. 2.16E). Interestingly, although there was a wide range of antibody titers, transfer of $CXCR5^-$ Tregs seemed to lead to an increase in antibody titers. We found that within this range that there was a correlation between lower antibody titers and small amounts of differentiation in TFR cells. Thus, if we had been able to block TFR generation completely in these assays we may have seen even greater antibody titers when non-TFR blood Tregs were transferred along with blood TFH cells.

Finally, we investigated the suppressive capacity of PD-1 deficient blood TFR cells *in vivo* since we have found that PD-1 deficient lymph node TFR cells more potently suppress antibody production *in vitro*. We adoptively transferred $4x10^4$ blood TFH cells alone or together with $1.5 x10^4$ blood TFR cells from WT or PD-1 deficient mice into either *Cd28*$^{-/-}$ or *Tcra*$^{-/-}$ recipients and immunized as in Fig. 2.15A. PD-1 deficient TFR cells inhibited antibody production to a greater extent than WT TFR cells in *Cd28*$^{-/-}$ (Fig. 2.17A) as well as *Tcra*$^{-/-}$ (Fig. 2.17B) recipients, demonstrating that they have increased suppressive capacity. The increased suppression was more evident in *Tcra*$^{-/-}$ than *Cd28*$^{-/-}$ recipients, but PD-1 deficient TFR cell transfers always resulted in less antibody production compared to WT TFR transfers. Together, these

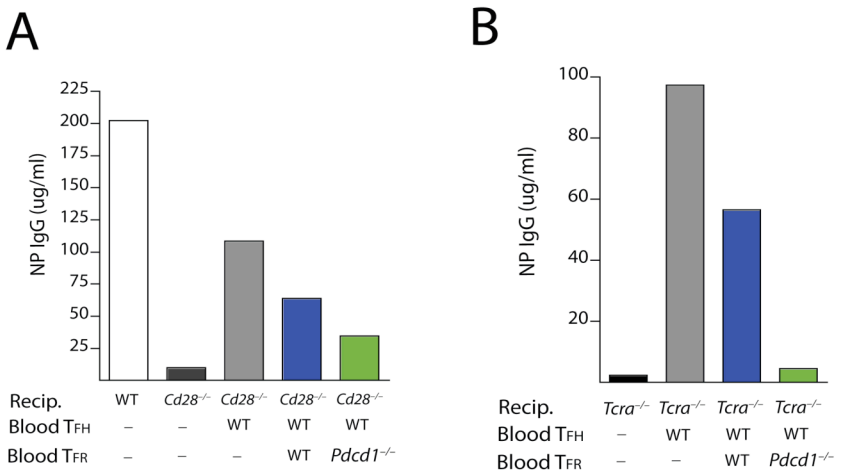

Fig. 2.17. PD-1 Deficient Blood TFR Cells More Potently Regulate Antibody Production *In Vivo*. Experiments were performed as in Fig. 2.12.A. $4x10^4$ WT blood TFH and $1.5x10^4$ WT or PD-1 deficient blood TFR cells from mice immunized with NP-OVA 8 days previously were transferred into $CD28^{-/-}$ mice (**A**) or $TCR\alpha^{-/-}$ mice (**B**). Recipient mice were immunized with NP-OVA, and NP specific antibody titers were measured from serum 12 days later. Data are representative of two independent experiments.

data show that blood TFR cells potently inhibit antibody production *in vivo* and PD-1 deficiency results in enhanced TFR cell suppressive capacity.

Discussion

The immunoregulatory functions of the newly defined T Follicular Regulatory cell subset are only beginning to be elucidated. Relatively little is known about how these cells differentiate and function. A mechanistic understanding of TFR cell differentiation and function is needed to gain insight into how humoral immune responses are regulated by TFH and TFR cells. Although TFR cells originate from different precursors than TFH cells, TFR and TFH cells have nearly identical surface receptors. The shared expression of ICOS, CXCR5 and PD-1 by TFR and TFH cells means that functional studies of TFH cells have, in fact, examined mixtures of stimulatory TFH cells and inhibitory TFR cells. This explains, in part, why TFR cells have only recently been identified, even though TFH cells have been studied for over ten years. The PD-1 pathway regulates many effector arms of the immune response, however biological complexity has lead to inconsistencies regarding the role of this pathway in humoral immune responses [110-114].

In this study, we identify a new mechanism by which PD-1 regulates humoral immunity: PD-1 controls the generation and function of suppressive TFR cells. We found that lack of PD-1, or its ligand PD-L1, resulted in greater numbers of TFR cells in the draining lymph node of immunized mice. These PD-1 deficient lymph node TFR cells expressed more *IRF4* and showed an enhanced ability to suppress antibody

production. We also discovered that TFR cells are present in the blood of mice, and that PD-1 controls the numbers of blood TFR cells, as evidenced by the substantial increases in PD-1 deficient mice. Importantly, we demonstrated a functional role for blood TFH cells in promoting antibody production and blood TFR cells in suppressing antibody production *in vivo*. PD-1 deficient blood TFR cells more potently suppress antibody production compared to WT blood TFR cells. Thus, PD-1 limits the development and function of TFR cells in lymph nodes and in the circulation (Fig. 2.18).

We have found that PD-1 signaling inhibits the numbers of TFR cells, but not TFH cells, in the lymph node, skewing the TFR to TFH ratio. It is possible that the greater suppressive capacity of PD-1 deficient TFR cells, together with the increased ratio of TFR to TFH cells in PD-1 deficient mice, results in inhibition of PD-1 deficient TFH cells. Alternatively, there may be alterations in PD-1 deficient TFH cells that promote their departure from the lymph node and homing to other sites to perform effector functions. These hypotheses are not mutually exclusive. We hypothesize that the TFH cells in PD-1 deficient mice have increased stimulatory capacity on a per cell basis, which partially balances the increased suppressive capacity of the PD-1 deficient TFR cells. Increased numbers of TFH cells in the blood of PD-1 deficient mice supports this idea because within the circulation, there is less TFR contact with TFH cells that may lead to less suppression. Therefore, the phenotype of the PD-1

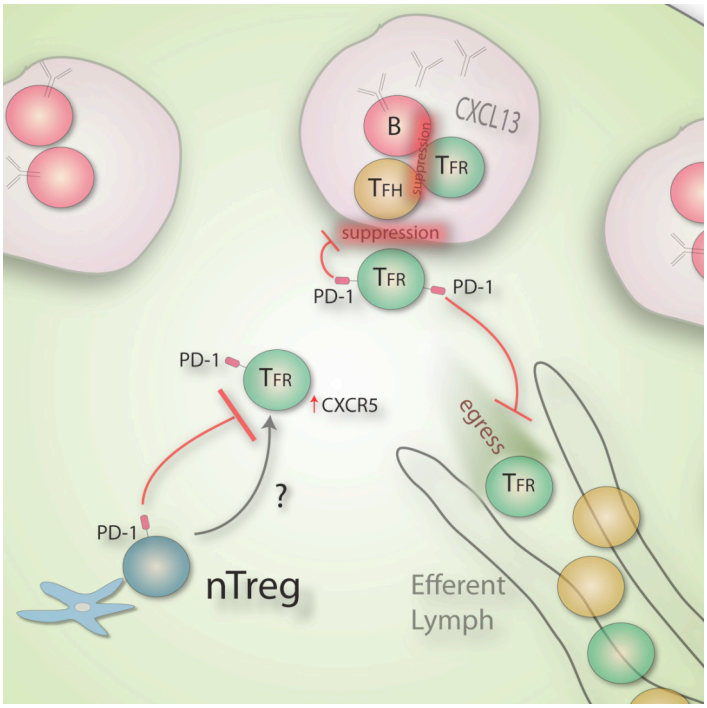

Fig. 2.18. Expanded role of PD-1 in TFR differentiation and function. Data indicate that PD-1 has at least three roles during the differentiation and effector function of TFR cells. First, PD-1 expressed on the natural Treg (nTreg) inhibits differentiation into TFR cells. When PD-1 signaling is lacking, TFR differentiation is increased. Second, PD-1 signaling on the TFR cell inhibits suppressive capacity. Lacking PD-1 results in an increased ability to suppress antibody production. Third, PD-1 signaling inhibits egress out of the lymph node. Lacking PD-1 results in increased numbers of cells in the circulation.

deficient mouse regarding humoral immunity is not straight forward. Indeed, there is much conflicting data as to the role of the PD-1 pathway in humoral immunity. Some studies have described increases in lymph node/spleen TFH cells in PD-1 deficient mice; however the contribution of TFR cells in these studies was not assessed [110, 112, 113]. It is likely that increased TFR cells in PD-1/PD-L1 deficient mice may have contributed to the increases in TFH cells observed in these studies, and may explain, at least in part, conflicting data regarding the role of PD-1 in regulating TFH cells and germinal center reactions. For example, Kawamoto et al. described increased $CD4^{+}CXCR5^{+}$ (TFH) cells in the Peyer's patches of PD-1 deficient mice[112]. However, upon transfer, these cells were non-functional in supporting IgA production. Increases in TFR cells contained within the TFH gate in PD-1 deficient Peyer's patches may explain these data. However, it is still not yet clear if TFR cells play a role in controlling IgA production in the intenstine.

Our TFR cell data would suggest that PD-1 deficient mice would have suppressed humoral responses. In agreement with this, Shlomchik and colleagues showed that PD-1 deficient mice have deficiencies in the number of long-lived plasma cells, resulting in overall lower antibody titers compared to WT mice[110]. Interestingly, this study described a similar phenotype in both PD-1, PD-L1 and PD-L2 deficient mice. Moreover, Finnegan and colleagues also showed that in PD-L1 knockout mice there was less antigen-specific antibody titers in a proteoglycan-induced arthritis model in

PD-L1 deficient mice[111]. Interestingly, although overall proteoglycan antibody titers were attenuated in this study, overall arthritis score was increased. This is probably due to the role of PD-1 in controlling the potency of effector T cells within tissues, and illustrates nicely the biological complexity surrounding the PD-1 pathway because PD-1 can inhibit both pro-inflammatory and anti-inflammatory effector cells. It is possible that different antigenic stimuli and different anatomical locations may lead to opposing phenotypes depending on how these conditions influence TFR cells. For instance a viral infection causing a strong inflammatory response may cause large expansion of TFH cells while not expanding TFR cells. Therefore, it is important to understand the biological cues that are necessary for TFR cell development and maintenance so that it is possible to design experimental approaches to specifically test the function of TFR cells.

TFR cells depend on SAP, CD28 and *Bcl6* for differentiation [115, 116]. However, the pathways that limit TFR cell differentiation are less clear. To date, only the transcription factor Blimp1 has been shown to inhibit TFR cell differentiation [115]. Paradoxically, TFR cells express both Bcl6 and Blimp1, two transcription factors that reciprocally modulate each other. Naïve T cells that overexpress Bcl6 upregulate more CXCR5 and T cells that overexpress Blimp1 are not able to upregulate CXCR5[94]. This phenotype is consistent for TFH cells, which do not express Blimp1. However for TFR cells, this is paradoxical. It is unclear how a transcription factor,

such as Blimp1, that is highly expressed by TFR cells and is also necessary for Treg survival, can inhibit TFR cell differentiation. Blimp1 suppresses TFH development by directly inhibiting Bcl6. Therefore, it is possible that the increased TFR cells in Blimp1 deficient mice is due to a dependence of TFR cell differentiation on help from TFH cells, and not a Treg-intrinsic mechanism. In support of this notion, SAP deficient mice lack both TFH and TFR cells, however, SAP is only expressed by TFH cells, but not TFR cells (Sage, data not shown). Analysis of mice with conditional deficiency of Blimp1 and/or SAP only on T regulatory cells through use of a FoxP3-Cre would be a beneficial approach for studying if TFR cells depend on TFH cells for differentiation.

Data presented here show PD-1 as the first surface receptor that inhibits TFR cell development and function. We also show that PD-1 predominantly interacts with PD-L1, and not PD-L2, to inhibit TFR cell generation. Our adoptive transfer studies demonstrate a cell-intrinsic role for PD-1 in TFR cell differentiation from $FoxP3^+$ Treg cells. Therefore, the increase in TFR cells in PD-1 deficient mice appears to reflect increased differentiation and not the maintenance of these cells. We observed a general trend for a decrease in cell cycling of CD4 $PD\text{-}1^{-/-}$ effector cells, because $ICOS^+CXCR5^+FoxP3^-$ and $ICOS^+CXCR5^-$ effector cells also had diminished Ki67 expression, at least at day 7 after immunization, which may temporally correspond to a maintenance phase. Based on these data, we hypothesize that, rather than simply

inhibiting responses, the PD-1:PD-L pathway can act as a molecular switch that controls cell fate decisions in naïve CD4 T cells. Integration of signals through PD-1, the TCR and cytokine receptors may direct CD4 T cell subset differentiation. Likewise, PD-1 may limit differentiated effector T cell expansion, cytokine production and/or survival depending on how signals through the TCR, PD-1 and cytokine receptors are integrated. Thus, the PD-1 pathway can influence CD4 T cell lineage commitment in distinct ways, depending on molecular cues and the local environment.

For instance, PD-L1 can promote induced Treg (iTreg) differentiation from naïve T cell precursors [103-107, 135]. However, we find that PD-1 inhibits differentiation of TFR cells. TFR cells arise from natural T regulatory cell (nTreg) precursors (shown here and previously [115]). Therefore, our studies suggest that PD-1 may have distinct roles in iTreg and nTreg differentiation. Moreover, TFR cells are one of the only defined effector nTreg subsets. It will be interesting to determine if PD-1 also inhibits other nTreg effector cells, which have roles other than suppressing B cell function. However, it is technically challenging to study the distinct roles of PD-1 on nTreg and iTreg cells since methods for discriminating nTreg and iTreg cells *in vivo* are still being developed. In addition genetic background may contribute to the affects of PD-1 deficiency. These studies were performed with C57Bl/6J mice, without any autoimmune susceptibility mutations. We use a combination of self-antigen (MOG)

and foreign antigen (NP-OVA) for these studies. However, it is possible that autoantibody-prone models, such as mice that have Fas mutations, may limit the effectiveness of TFR cells and result in increased antibodies due to a predominant TFH phenotype. In support of this, it has been shown that PD-L1$^{-/-}$ mice have decreased survival when on the MRL-*Fas*^{lpr} background [136]. MRL-*Fas*^{lpr} mice produce large quantities of autoantibodies, however, the phenotype in the PD-L1 deficient mice on this background may be due to effector T cells and may not be necessarily antibody-mediated. Conditional knockout strategies where PD-1 is deleted only T regulatory cells may help to solve this unresolved question.

Here we find that blocking the PD-1 pathway leads to increased functionality of TFR cells. Increased functionality during PD-1 blockade is also a phenotype for exhausted T cells. It has been previously shown that PD-1 is highly expressed on exhausted T cells during chronic viral infection with LCMV [137]. In the setting of chronic viral infection, PD-1 mediates exhaustion of CD8 effector cells, preventing them from effectively responding to viral antigens. When PD-1 was blocked with a PD-L1 blocking antibody, the CD8 effector cells partially regained their ability to respond to viral antigens and more potently cleared virus. PD-1 also can inhibit CD8 T cell functionality within the tumor microenvironment [138] and it can inhibit CD4 and CD8 T cell functionality in the setting of HIV infection [139]. Therefore, PD-1 suppression of function is relevant on multiple cell types. TFR cells similarly have

increased functionality when the PD-1 pathway is blocked. However, TFR cells do not seem to be exhausted like the CD8 or CD4 T cells in chronic viral infection because TFR cells are actively proliferating within the germinal center, as evidenced by Ki67 expression.

PD-1 and its ligands also have key roles in mediating tolerance [119] [140]. PD-1 is also be expressed on other cell type such as B cells, monocytes and myeloid DCs [2]. Therefore, bidirectional signaling may be possible between T cells, B cells and DCs since all three cells can express PD-1 and PD-L1. Although PD-1 inhibits B cell signaling through the B cell receptor, the role of PD-1 on B cells *in vivo* is still not yet clear [141]. Although we demonstrate a T cell-intrinsic mechanism by which PD-1 acts on nTregs in *in vivo* adoptive transfer models, it is possible that PD-1 deficiency on the B cell may have a role in the phenotype of increased TFR cells in the PD-1 knockout. Determining if PD-1 has a role on B cells during the generation/maintenance of TFR cells could be assessed by enumerating TFR cells in adoptive transfers in which wild-type or PD-1 deficient B cells are transferred along with CD4 T cells into RAG deficient mice.

Because of the recent discovery of TFR cells, there is a lack of fundamental knowledge about TFR cell biology, so we developed novel assays to analyze mechanisms by which PD-1 regulates TFR cell function. TFR cells have the potential

to directly inhibit actition of naïve T cells, TFH cell function, and/or B cell activation. Additionally, TFR cells may regulate TFH or B cell responses either inside the B cell follicle and/or control activation and differentiation of T cells outside the B cell follicle. Here, we present the first specific assays for TFR cell function *in vitro* and show that sorted wild type TFR cells from the lymph node are extremely potent at inhibiting antibody production, but not very effective at suppressing activation of naïve T cells. Therefore, TFR cells seem to be specific for inhibiting humoral responses.

The specificity of TFR cells for inhibiting humoral responses makes them attractive targets for therapy. PD-1 deficient TFR cells inhibit naïve T cell activation and attenuate antibody production *in vitro* to a greater extent than WT TFR cells. However, the mechanism by which TFR cells exert their suppressive functions has not been fully investigated. TFR cells produce large amounts of IL-10, but this does not seem to be the mechanism of suppression, because preliminary experiments blocking IL-10 *in vitro* does not appear to alter the suppressive function of TFR cells (Sage, data not shown). Moreover, blocking IL-10 with a neutralizing antibody does not attenuate TFH cell numbers (Sage, data not shown). More experiments are needed to determine the exact mechanism of suppression. There are many ways Tregs are thought to suppress cells such as through direct cytolysis, IL-2 sequestering and

production of IL-10 or TGF-β. Each one of these mechanisms will need to be tested individually to determine how TFR cells suppress TFH cells and B cells.

Our studies demonstrate the dynamic control of antibody production by lymph node TFH and TFR cells. Initially, our attempts to activate B cells to produce antibody *in vitro* with total $CD4^+CXCR5^+$ cells resulted in little IgG secretion. However, when we separated TFH cells from TFR cells and used pure TFH cells in such experiments, we could detect robust IgG production. Of note, during an immune response to peptide/CFA, the *in vivo* dLN TFR:TFH ratio is ~1:5. When we cultured TFR and TFH cells at this ratio in our *in vitro* suppression assay, little antibody production was observed. This ratio should mirror the suppressed humoral immune response *in vivo*. These data may help to explain why *in vitro* antibody assays have not been widely used to quantitate B cell function previously.

TFR cells tend to be present predominantly at the borders of germinal centers, which may be explained by their relatively lower expression of CXCR5 compared to TFH cells and B cells, though other chemokines also may have roles. It is possible that close proximity of TFR cells to germinal center borders enables them to interact with TFH cells as they enter. This could make TFR cells the "gate-keepers" of the germinal center, inhibiting TFH cells as they enter and gain access to B cells undergoing somatic hypermutation and class switch recombination. The relative

lower expression of CXCR5 of TFR cells compared to TFH cells supports their positioning at the border of the germinal center. However, there are probably other unidentified chemokine receptors that may modulate positioning of these cells. The close positioning of TFR cells to the germinal cener border may provide a mechanism that inhibits autoimmunity, because without suppression of the TFH cell just as it enters the GC, the threshold for B cell activation may be lower. Lowering the threshold for a B cell response may lead to autoimmune antibody formation. In support of this, it has been hypothesized that TFR cells predominantly limit non-antigen specific antibody production[115], however our results provide evidence for antigen specificity of TFR cells since these cells expand in our recipients when we immunize the mice with NP-OVA. However, more experiments are needed to test the antigen specificity of the TFR cells in a more definitive manner.

Our studies suggest that the balance between TFR and TFH cells (and not individual numbers of each) within the germinal center itself may modulate the type and extent of humoral responses. The relative roles of TFR and TFH cells also may depend on the source or strength of antigenic stimulus, cytokine milieu, and tissue microenvironment, and further work is needed to investigate these issues. It will be interesting to compare different adjuvants to determine if some classes of adjuvants preferentially elicit expansion of TFH cells compard to TFR cells or vice versa. This information could be useful in rational design of vaccines. Two other adjuvants that

were tested in the course of these experiments were sheep red blood cells (SRBCs), which are classically used in mouse *in vivo* models, and Aluminum Hydroxide (Alum) which is a potent adjuvant used in vaccination of humans. In the case of SRBCs, which is an odd stimulus since it induces a xenograft response yet nevertheless elicits huge germinal center B cell numbers, both TFH and TFR cells are expanded greatly. In the case of Alum, there is a very small amount of TFH and TFR differentiation and both subsets seem to polarize equivalently. Clearly, more experiments need to be performed. There is an increasing literature on the role of toll-like receptors (TLRs) during vaccination[142] and sequential analysis of individual innate signals (individual TLRs, NLRs, etc) on B cells and DCs in the differentiation of TFH and TFR cells is a priority.

Surprisingly, we found substantial populations of TFR cells in the blood of mice. There are a number of reports describing TFH cells in the circulation of humans [88, 98] and one in mice [100]. To our knowledge, our work is the first description of TFR cells in the blood of any organism. In humans, blood TFH cells have been shown to provide B cell help for the production of antibody *in vitro.* Some studies show more efficient B cell antibody production by blood TFH cells compared to blood CXCR5$^-$ cells [88, 98] whereas other studies find no differences between blood TFH and CXCR5$^-$ cells [143]. Differences might relate to mixtures of blood TFH and TFR cells and their relative ratios in these experiments. Since most work describing blood TFH cells was

done in humans, little is known about the requirements for blood TFH differentiation and function. Here we show that murine blood TFH and TFR cell generation requires signals through ICOS and CD28, two costimulatory receptors essential for controlling TFH cells in the lymph node. Previous work showed that CD28 is essential for TFR cells in lymph nodes [115]. Here we demonstrate lymph node TFR cell generation also requires ICOS signaling. However, as previously mentioned, if TFR cell differentiation partially depends on TFH development, then it is still unknown whether CD28 and ICOS have Treg-intrinsic roles in TFR differentiation. Conditional knockouts could be used to investigate these questions.

Our transfer studies show that blood TFR cells are functional and can regulate antibody production *in vivo*. To study TFH and TFR function, we transferred blood TFH cells alone or with TFR cells into *Cd28*$^{-/-}$ or *Tcra*$^{-/-}$ mice, which lack both blood and lymph node TFH and TFR cells. Although technically challenging, this approach allowed us to analyze TFH and TFR cell function separately from differentiation. Our transfer studies demonstrate effective and specific control of humoral responses by blood TFH and TFR cells. Blood TFR cells are extremely potent at inhibiting TFH cell mediated antibody production, even when relatively few cells are transferred.

We hypothesize that blood TFR cells may represent a central memory pool that can be utilized to modulate humoral immunity, analogous to recently reported FoxP3^{+}

cells with regulatory memory to self-antigens [144] and similar to a proposed role for blood TFH cells [88]. High expression of CD62L and CD44 on blood TFR cells along with their ability to home back to lymph nodes strongly support this idea. Blood TFH cells may migrate to lymph nodes and interact with cognate B cells rapidly upon antigen exposure, whereas naïve T cells need at least two to four days to differentiate and upregulate CXCR5. This would make the blood TFH memory cells the "first responders" and may help direct the extent of a humoral response. Additionally, blood TFR cells homing to lymph nodes would be able to suppress early B cell responses, before dLN nTregs could fully differentiate into TFR cells.

The function of blood TFR cells may also be to ensure systemic control of humoral immune responses. For instance, if a self-reactive humoral immune response is initiated in a specific lymph node, the TFR cells primed there may be able to distribute through the circulation to other secondary lymphoid organs in order to prevent subsequent reactions to self antigen that may be present in multiple locations. Moreover, antibody secreting cells (ASCs) have been demonstrated to migrate and reside within tissues such as the skin and gut [145], and it is possible that TFR cells may also migrate to these locations in order to control antibody production from these ASCs. Thus, TFR cells may have expanded roles outside of lymphoid organs. Further work is needed to determine if TFR cells that migrate to tissues maintain their CXCR5 expression and develop methods to track these cells.

During the germinal center reaction, B cells can differentiate into memory B cells that persist for long periods of time or plasma cells that circulate and produce large amounts of antibody. Beyond their ability to directly suppress antibody responses, TFR cells may be instrumental in determining B cell fates and control whether an immune response generates plasma cells or memory B cells. For example, cytokines produced by TFR cells may direct GC B cell differentiation into memory B cells and away from plasma cells. We observed strong reductions in plasma cell numbers in our transfer experiments in which wild-type TFR cells were transferred along with wild-type TFH cells into CD28 deficient mice supporting this idea. PD-1 and PD-1 ligand deficiency result in decreased numbers of long-lived plasma cells [110], and further work is needed to determine if this is related to enhanced TFR cell numbers and suppressive capacity in PD-1 deficient mice. If TFR cells can direct B cell fates, this would have implications for rational design of vaccines. For instance, by transferring TFR cells or selectively boosting TFR cells during vaccination, it may be possible to divert the B cell lineage development into memory B cells, producing less antibody production in the short term while generating greater responses in the long term.

It also will be interesting to determine if inappropriate B cells responses may result from altered TFR function. For instance, elderly individuals tend to have reduced

antibody generation and do not develop long-lived plasma cells during vaccination leaving them more susceptible to infections[146]. This may be due to increased TFR function, decreased TFH function, or both. Moreover, it is also possible that TFR cells may be instrumental in preventing systemic autoimmunity, and underlie many systemic autoimmune diseases. For example, there may be deficiencies in TFR cell function leading to heightened TFH responses in these diseases. Therefore, measuring TFH and TFR cell ratios within the blood may be a worth-while diagnostic tool. This information may also be important for developing therapeutic strategies using TFR cells. By expanding either TFH or TFR cells from patient blood *in vitro*, it may be possible to enhance antibody responses by transferring TFH cells or to inhibit systemic autoimmunity by transferring TFR cells.

In summary, we define a new role for PD-1 in regulating immune responses, by inhibiting differentiation and function of T follicular regulatory cells in both lymph node and blood. A better understanding of TFR and TFH interactions has the potential to provide novel insights into mechanisms that regulate humoral immunity. Whether TFH and TFR cells regulate memory B cell responses is unknown and such knowledge may enable novel vaccination strategies to enhance humoral immunity. Further understanding of how PD-1 regulates humoral immunity may suggest strategies for manipulating this pathway to enhance protective immunity and long-term memory or to inhibit systemic autoimmunity.

Chapter 3. General Discussion

At a first glance the two studies presented here seem far removed. How can studying the intimate details of TCR signaling *in vitro* relate to the functions of a specific subset of Tregs in modulation of antibody responses *in vivo*? The two subjects are closer than they appear. At the heart of both studies is the requirement for T cells to be properly activated. In the case of sensing antigen *in vitro*, T cell ILPs are responsible for identifying and responding to cognate antigen. Without ILPs, memory T cells cannot efficiently respond and flux calcium, leading to inefficient activation.

The requirement for sensing antigen can also be applied to TFR cells. In order for TFR cells to develop, the nTreg cells need to find and respond to antigen, presumably via dendritic cells within the T cell zone. Before this process can occur, the nTreg must get into the lymph node by transmigrating through the high endothelial venules. Since CD4 T cells use ILPs to transmigrate through the endothelium, it seems likely that the nTreg will already have ILP machinery in use when it comes into contact with DCs. When the nTreg locates a DC, it must be efficiently activated in order to differentiate. We hypothesize that in this setting it is the ILPs on the nTreg cells that provide efficient antigen recognition so that the nTreg can initiate the TFR differentiation program.

TFR sensing of antigen with ILPs is most likely necessary during the initial priming of the natural T regulatory cells into TFR cells as well as during effector function later in the B cell zone. Here we show that ILPs are relevant both during CD4 T interaction with dendritic cells as well as B cells. Since TFR cells reside in the B cell follicle during immune responses, they almost certainly would be able to use ILP structures to probe B cells looking for antigen. In addition, it is possible that the close membrane-membrane contact that the ILPs elicit may be responsible for directed cytokine production to the B cells by the TFR cells. If TFR cells have ability to directly lyse B cells, the ILPs may also deliver cytotoxic granules. Without the close membrane contact, TFR suppression may suppress or injure bystander cells leading to adverse pathologies.

The studies of TFR cells also demonstrate nicely the need for regulated T cell activation, which can be controlled properly by ILPs. For instance, dysfunctional ILPs lead to inefficient antigen recognition, leading to reduced T cell activation. Our *in vivo* models nicely demonstrate how altered T cell activation can change an immune response. PD-1 signaling results in dephosphorylation of proximal TCR signaling which is functionally similar to disturbing ILP formation, because downstream TCR responses such as calcium flux are attenuated in both. In the case of TFR cells, we demonstrate here that decreased TCR signaling (via PD-1) limits

TFR differentiation, suppression and exit from the lymph node. Thus, we can speculate that weakened ILP function specifically on regulatory cells could limit TFR generation, and therefore lead to increased antibody production that may lead to autoimmune disease. My work illustrates how lessons from separate areas of immunology can be used together to understand immunity.

Chapter 4. Bibliography

1. **Sage, P.T. *et al.* Antigen Recognition Is Facilitated by Invadosome-like Protrusions Formed by Memory/Effector T Cells. *J Immunol* 188, 3686-3699 (2012).**

2. **Francisco, L.M., Sage, P.T. & Sharpe, A.H. The PD-1 pathway in tolerance and autoimmunity. *Immunol Rev* 236, 219-242 (2009).**

3. **von Andrian, U.H. & Mackay, C.R. T-cell function and migration. Two sides of the same coin. *N Engl J Med* 343, 1020-1034 (2000).**

4. **Sage, P.T. & Carman, C.V. Settings and mechanisms for trans-cellular diapedesis. *Front Biosci* 14, 5066-5083 (2009).**

5. **Rudolph, M.G., Stanfield, R.L. & Wilson, I.A. How TCRs bind MHCs, peptides, and coreceptors. *Annu Rev Immunol* 24, 419-466 (2006).**

6. **Weinbaum, S., Tarbell, J.M. & Damiano, E.R. The structure and function of the endothelial glycocalyx layer. *Annual review of biomedical engineering* 9, 121-167 (2007).**

7. **Bell, G.I., Dembo, M. & Bongrand, P. Cell adhesion. Competition between nonspecific repulsion and specific bonding. *Biophysical journal* 45, 1051-1064 (1984).**

8. **Springer, T.A. Adhesion receptors of the immune system. *Nature* 346, 425-434 (1990).**

9. **Gubbels, J.A. *et al.* MUC16 provides immune protection by inhibiting synapse formation between NK and ovarian tumor cells. *Molecular cancer* 9, 11 (2010).**

10. **Komatsu, M., Yee, L. & Carraway, K.L. Overexpression of sialomucin complex, a rat homologue of MUC4, inhibits tumor killing by lymphokine-activated killer cells. *Cancer Res* 59, 2229-2236 (1999).**

11. **Tsuboi, S. & Fukuda, M. Roles of O-linked oligosaccharides in immune responses. *Bioessays* 23, 46-53 (2001).**

12. **van de Wiel-van Kemenade, E. *et al.* Episialin (MUC1) inhibits cytotoxic lymphocyte-target cell interaction. *J Immunol* 151, 767-776 (1993).**

13. **Manjunath, N., Correa, M., Ardman, M. & Ardman, B. Negative regulation of T-cell adhesion and activation by CD43. *Nature* 377, 535-538 (1995).**

14. **Shaw, A.S. & Dustin, M.L. Making the T cell receptor go the distance: a topological view of T cell activation. *Immunity* 6, 361-369 (1997).**

15. **Monks, C.R., Freiberg, B.A., Kupfer, H., Sciaky, N. & Kupfer, A. Three-dimensional segregation of supramolecular activation clusters in T cells. *Nature* 395, 82-86 (1998).**

16. **Delon, J., Stoll, S. & Germain, R.N. Imaging of T-cell interactions with antigen presenting cells in culture and in intact lymphoid tissue. *Immunol Rev* 189, 51-63 (2002).**

17. **Brossard, C. *et al.* Multifocal structure of the T cell - dendritic cell synapse. *Eur J Immunol* 35, 1741-1753 (2005).**

18. **Dustin, M.L. The cellular context of T cell signaling. *Immunity* 30, 482-492 (2009).**

19. **Choudhuri, K., Wiseman, D., Brown, M.H., Gould, K. & van der Merwe, P.A. T-cell receptor triggering is critically dependent on the dimensions of its peptide-MHC ligand. *Nature* 436, 578-582 (2005).**

20. **Balagopalan, L., Sherman, E., Barr, V.A. & Samelson, L.E. Imaging techniques for assaying lymphocyte activation in action. *Nat Rev Immunol* 11, 21-33 (2011).**

21. **Cebecauer, M., Spitaler, M., Serge, A. & Magee, A.I. Signalling complexes and clusters: functional advantages and methodological hurdles. *Journal of cell science* 123, 309-320 (2010).**

22. **Huse, M. *et al.* Spatial and temporal dynamics of T cell receptor signaling with a photoactivatable agonist. *Immunity* 27, 76-88 (2007).**

23. **Oddos, S. *et al.* High-speed high-resolution imaging of intercellular immune synapses using optical tweezers. *Biophysical journal* 95, L66-68 (2008).**

24. **Grakoui, A. *et al.* The immunological synapse: a molecular machine controlling T cell activation. *Science* 285, 221-227 (1999).**

25. **Bunnell, S.C. *et al.* T cell receptor ligation induces the formation of dynamically regulated signaling assemblies. *The Journal of cell biology* 158, 1263-1275 (2002).**

26. **Yokosuka, T. *et al.* Newly generated T cell receptor microclusters initiate and sustain T cell activation by recruitment of Zap70 and SLP-76. *Nature immunology* 6, 1253-1262 (2005).**

27. **Seminario, M.C. & Bunnell, S.C. Signal initiation in T-cell receptor microclusters. *Immunol Rev* 221, 90-106 (2008).**

28. **Dustin, M.L. Supported bilayers at the vanguard of immune cell activation studies. *Journal of structural biology* 168, 152-160 (2009).**

29. **Springer, T.A. Traffic signals for lymphocyte recirculation and leukocyte emigration: the multistep paradigm. *Cell* 76, 301-314 (1994).**

30. **Butcher, E.C. Leukocyte-endothelial cell recognition: three (or more) steps to specificity and diversity. *Cell* 67, 1033-1036 (1991).**

31. **Choi, J., Enis, D.R., Koh, K.P., Shiao, S.L. & Pober, J.S. T lymphocyte-endothelial cell interactions. *Annu Rev Immunol* 22, 683-709 (2004).**

32. **Pober, J.S. & Sessa, W.C. Evolving functions of endothelial cells in inflammation. *Nat Rev Immunol* 7, 803-815 (2007).**

33. **Marelli-Berg, F.M., Okkenhaug, K. & Mirenda, V. A two-signal model for T cell trafficking. *Trends Immunol* 28, 267-273 (2007).**

34. **Marelli-Berg, F.M. *et al.* Major histocompatibility complex class II-expressing endothelial cells induce allospecific nonresponsiveness in naive T cells. *J Exp Med* 183, 1603-1612 (1996).**

35. **Ma, W. & Pober, J.S. Human endothelial cells effectively costimulate cytokine production by, but not differentiation of, naive CD4+ T cells. *J Immunol* 161, 2158-2167 (1998).**

36. **Perez, V.L., Henault, L. & Lichtman, A.H. Endothelial antigen presentation: stimulation of previously activated but not naive TCR-transgenic mouse T cells. *Cellular immunology* 189, 31-40 (1998).**

37. **Epperson, D.E. & Pober, J.S. Antigen-presenting function of human endothelial cells. Direct activation of resting CD8 T cells. *J Immunol* 153, 5402-5412 (1994).**

38. **Shiao, S.L. *et al.* Human Effector Memory CD4+ T Cells Directly Recognize Allogeneic Endothelial Cells In Vitro and In Vivo. *J Immunol* 179, 4397-4404 (2007).**

39. **Carman, C.V. *et al.* Transcellular diapedesis is initiated by invasive podosomes. *Immunity* 26, 784-797 (2007).**

40. **Bao, X. *et al.* Endothelial heparan sulfate controls chemokine presentation in recruitment of lymphocytes and dendritic cells to lymph nodes. *Immunity* 33, 817-829 (2010).**

41. **Linder, S. Invadosomes at a glance. *Journal of cell science* 122, 3009-3013 (2009).**

42. **Carman, C.V. Mechanisms for transcellular diapedesis: probing and pathfinding by 'invadosome-like protrusions'. *Journal of cell science* 122, 3025-3035 (2009).**

43. **Linder, S. & Aepfelbacher, M. Podosomes: adhesion hot-spots of invasive cells. *Trends in cell biology* 13, 376-385 (2003).**

44. **Carman, C.V. & Springer, T.A. A transmigratory cup in leukocyte diapedesis both through individual vascular endothelial cells and between them. *The Journal of cell biology* 167, 377-388 (2004).**

45. **Gomez, T.S. *et al.* HS1 functions as an essential actin-regulatory adaptor protein at the immune synapse. *Immunity* 24, 741-752 (2006).**

46. **Sarkar, D. *et al.* Chemical engineering of mesenchymal stem cells to induce a cell rolling response. *Bioconjugate chemistry* 19, 2105-2109 (2008).**

47. **Anton, I.M. *et al.* WIP deficiency reveals a differential role for WIP and the actin cytoskeleton in T and B cell activation. *Immunity* 16, 193-204 (2002).**

48. **Wulfing, C. *et al.* Costimulation and endogenous MHC ligands contribute to T cell recognition. *Nature immunology* 3, 42-47 (2002).**

49. **Okamura, H. *et al.* Concerted dephosphorylation of the transcription factor NFAT1 induces a conformational switch that regulates transcriptional activity. *Molecular cell* 6, 539-550 (2000).**

50. **Billadeau, D.D., Nolz, J.C. & Gomez, T.S. Regulation of T-cell activation by the cytoskeleton. *Nat Rev Immunol* 7, 131-143 (2007).**

51. **Butler, B., Kastendieck, D.H. & Cooper, J.A. Differently phosphorylated forms of the cortactin homolog HS1 mediate distinct functions in natural killer cells. *Nature immunology* 9, 887-897 (2008).**

52. **Dehring, D.A. *et al.* Hematopoietic lineage cell-specific protein 1 functions in concert with the Wiskott-Aldrich syndrome protein to promote podosome array organization and chemotaxis in dendritic cells. *J Immunol* 186, 4805-4818 (2011).**

53. **Fooksman, D.R. *et al.* Functional anatomy of T cell activation and synapse formation. *Annu Rev Immunol* 28, 79-105 (2010).**

54. **Trautmann, A. & Valitutti, S. The diversity of immunological synapses. *Curr Opin Immunol* 15, 249-254 (2003).**

55. **Bunnell, S.C. Multiple microclusters: diverse compartments within the immune synapse. *Curr Top Microbiol Immunol* 340, 123-154 (2010).**

56. **Dovas, A. & Cox, D. Signaling networks regulating leukocyte podosome dynamics and function. *Cellular signalling* 23, 1225-1234 (2011).**

57. **Arrieumerlou, C., Randriamampita, C., Bismuth, G. & Trautmann, A. Rac is involved in early TCR signaling. *J Immunol* 165, 3182-3189 (2000).**

58. **Hughes, K., Edin, S., Antonsson, A. & Grundstrom, T. Calmodulin-dependent kinase II mediates T cell receptor/CD3- and phorbol ester-induced activation of IkappaB kinase. *The Journal of biological chemistry* 276, 36008-36013 (2001).**

59. **Epperson, D.E. *et al.* Cytokines increase transporter in antigen processing-1 expression more rapidly than HLA class I expression in endothelial cells. *J Immunol* 149, 3297-3301 (1992).**

60. **Turesson, C. Endothelial expression of MHC class II molecules in autoimmune disease. *Current pharmaceutical design* 10, 129-143 (2004).**

61. **Manes, T.D., Shiao, S.L., Dengler, T.J. & Pober, J.S. TCR signaling antagonizes rapid IP-10-mediated transendothelial migration of effector memory CD4+ T cells. *J Immunol* 178, 3237-3243 (2007).**

62. **Manes, T.D. & Pober, J.S. Antigen presentation by human microvascular endothelial cells triggers ICAM-1-dependent transendothelial protrusion by, and fractalkine-dependent transendothelial migration of, effector memory CD4+ T cells. *J Immunol* 180, 8386-8392 (2008).**

63. **Rodig, N. *et al.* Endothelial expression of PD-L1 and PD-L2 down-regulates CD8+ T cell activation and cytolysis. *Eur J Immunol* 33, 3117-3126 (2003).**

64. **Koni, P.A. *et al.* Conditional vascular cell adhesion molecule 1 deletion in mice: impaired lymphocyte migration to bone marrow. *J Exp Med* 193, 741-754 (2001).**

65. **Laouar, Y., Welte, T., Fu, X.Y. & Flavell, R.A. STAT3 is required for Flt3L-dependent dendritic cell differentiation. *Immunity* 19, 903-912 (2003).**

66. **Fujimoto, T. *et al.* Step-wise divergence of primitive and definitive haematopoietic and endothelial cell lineages during embryonic stem cell differentiation. *Genes Cells* 6, 1113-1127 (2001).**

67. **Shulman, Z. *et al.* Lymphocyte crawling and transendothelial migration require chemokine triggering of high-affinity LFA-1 integrin. *Immunity* 30, 384-396 (2009).**

68. **Gerard, A., van der Kammen, R.A., Janssen, H., Ellenbroek, S.I. & Collard, J.G. The Rac activator Tiam1 controls efficient T-cell trafficking and route of transendothelial migration. *Blood* 113, 6138-6147 (2009).**

69. **Albiges-Rizo, C., Destaing, O., Fourcade, B., Planus, E. & Block, M.R. Actin machinery and mechanosensitivity in invadopodia, podosomes and focal adhesions. *Journal of cell science* 122, 3037-3049 (2009).**

70. **Bunnell, S.C. *et al.* Persistence of cooperatively stabilized signaling clusters drives T-cell activation. *Mol Cell Biol* 26, 7155-7166 (2006).**

71. **Wetzel, S.A., McKeithan, T.W. & Parker, D.C. Live-cell dynamics and the role of costimulation in immunological synapse formation. *J Immunol* 169, 6092-6101 (2002).**

72. **Barcia, C. *et al.* CD20, CD3, and CD40 ligand microclusters segregate three-dimensionally in vivo at B-cell-T-cell immunological synapses after viral immunity in primate brain. *J Virol* 82, 9978-9993 (2008).**

73. **Barcia, C. *et al.* T cells' immunological synapses induce polarization of brain astrocytes in vivo and in vitro: a novel astrocyte response mechanism to cellular injury. *PLoS One* 3, e2977 (2008).**

74. **Henrickson, S.E. *et al.* T cell sensing of antigen dose governs interactive behavior with APC - an integrative mechanism that sets a threshold for T cell activation. *Nature immunology* (in press).**

75. **Rudd, P.M., Elliott, T., Cresswell, P., Wilson, I.A. & Dwek, R.A. Glycosylation and the immune system. *Science* 291, 2370-2376 (2001).**

76. **Valitutti, S., Muller, S., Cella, M., Padovan, E. & Lanzavecchia, A. Serial triggering of many T-cell receptors by a few peptide-MHC complexes. *Nature* 375, 148-151 (1995).**

77. **Negulescu, P.A., Krasieva, T.B., Khan, A., Kerschbaum, H.H. & Cahalan, M.D. Polarity of T cell shape, motility, and sensitivity to antigen. *Immunity* 4, 421-430 (1996).**

78. **Wei, X., Tromberg, B.J. & Cahalan, M.D. Mapping the sensitivity of T cells with an optical trap: polarity and minimal number of receptors for Ca(2+) signaling. *Proc Natl Acad Sci U S A* 96, 8471-8476 (1999).**

79. **Ma, Z., Sharp, K.A., Janmey, P.A. & Finkel, T.H. Surface-anchored monomeric agonist pMHCs alone trigger TCR with high sensitivity. *PLoS biology* 6, e43 (2008).**

80. **Burbach, B.J., Medeiros, R.B., Mueller, K.L. & Shimizu, Y. T-cell receptor signaling to integrins. *Immunol Rev* 218, 65-81 (2007).**

81. **Perez-Moreno, M., Jamora, C. & Fuchs, E. Sticky business: orchestrating cellular signals at adherens junctions. *Cell* 112, 535-548 (2003).**

82. **Harwood, N.E. & Batista, F.D. New insights into the early molecular events underlying B cell activation. *Immunity* 28, 609-619 (2008).**

83. **Luxenburg, C. *et al.* The architecture of the adhesive apparatus of cultured osteoclasts: from podosome formation to sealing zone assembly. *PLoS One* 2, e179 (2007).**

84. **Destaing, O. *et al.* The tyrosine kinase activity of c-Src regulates actin dynamics and organization of podosomes in osteoclasts. *Molecular biology of the cell* 19, 394-404 (2008).**

85. **Saltel, F., Destaing, O., Bard, F., Eichert, D. & Jurdic, P. Apatite-mediated actin dynamics in resorbing osteoclasts. *Molecular biology of the cell* 15, 5231-5241 (2004).**

86. **Sage, P.T., Francisco, L.M., Carman, C.V. & Sharpe, A.H. The receptor PD-1 controls follicular regulatory T cells in the lymph nodes and blood. *Nature immunology* (2012).**

87. **Shlomchik, M.J. & Weisel, F. Germinal center selection and the development of memory B and plasma cells. *Immunol Rev* 247, 52-63 (2012).**

88. **Schaerli, P. *et al.* CXC chemokine receptor 5 expression defines follicular homing T cells with B cell helper function. *J Exp Med* 192, 1553-1562 (2000).**

89. **Breitfeld, D. *et al.* Follicular B helper T cells express CXC chemokine receptor 5, localize to B cell follicles, and support immunoglobulin production. *J Exp Med* 192, 1545-1552 (2000).**

90. **Crotty, S. Follicular helper CD4 T cells (TFH). *Annu Rev Immunol* 29, 621-663 (2011).**

91. **McHeyzer-Williams, M., Okitsu, S., Wang, N. & McHeyzer-Williams, L. Molecular programming of B cell memory. *Nat Rev Immunol* 12, 24-34 (2012).**

92. **Poholek, A.C. *et al.* In vivo regulation of Bcl6 and T follicular helper cell development. *J Immunol* 185, 313-326 (2010).**

93. **Cannons, J.L. *et al.* Optimal germinal center responses require a multistage T cell:B cell adhesion process involving integrins, SLAM-associated protein, and CD84. *Immunity* 32, 253-265 (2010).**

94. **Johnston, R.J. *et al.* Bcl6 and Blimp-1 are reciprocal and antagonistic regulators of T follicular helper cell differentiation. *Science* 325, 1006-1010 (2009).**

95. **Nurieva, R.I. *et al.* Bcl6 mediates the development of T follicular helper cells. *Science* 325, 1001-1005 (2009).**

96. **Choi, Y.S. *et al.* ICOS receptor instructs T follicular helper cell versus effector cell differentiation via induction of the transcriptional repressor Bcl6. *Immunity* 34, 932-946 (2011).**

97. **Nurieva, R.I. *et al.* Generation of T follicular helper cells is mediated by interleukin-21 but independent of T helper 1, 2, or 17 cell lineages. *Immunity* 29, 138-149 (2008).**

98. **Morita, R. *et al.* Human blood CXCR5(+)CD4(+) T cells are counterparts of T follicular cells and contain specific subsets that differentially support antibody secretion. *Immunity* 34, 108-121 (2011).**

99. **Saito, R. *et al.* Altered expression of chemokine receptor CXCR5 on T cells of myasthenia gravis patients. *Journal of neuroimmunology* 170, 172-178 (2005).**

100. **Simpson, N. *et al.* Expansion of circulating T cells resembling follicular helper T cells is a fixed phenotype that identifies a subset of severe systemic lupus erythematosus. *Arthritis and rheumatism* 62, 234-244 (2010).**

101. **Ishida, Y., Agata, Y., Shibahara, K. & Honjo, T. Induced expression of PD-1, a novel member of the immunoglobulin gene superfamily, upon programmed cell death. *Embo J* 11, 3887-3895 (1992).**

102. **Yokosuka, T. *et al.* Programmed cell death 1 forms negative costimulatory microclusters that directly inhibit T cell receptor signaling by recruiting phosphatase SHP2. *J Exp Med* 209, 1201-1217 (2012).**

103. **Polanczyk, M.J., Hopke, C., Vandenbark, A.A. & Offner, H. Treg suppressive activity involves estrogen-dependent expression of programmed death-1 (PD-1). *Int Immunol* 19, 337-343 (2007).**

104. **Wang, L. *et al.* Programmed death 1 ligand signaling regulates the generation of adaptive Foxp3+CD4+ regulatory T cells. *Proc Natl Acad Sci U S A* 105, 9331-9336 (2008).**

105. **Francisco, L.M. *et al.* PD-L1 regulates the development, maintenance, and function of induced regulatory T cells. *J Exp Med* 206, 3015-3029 (2009).**

106. **Wang, C., Li, Y., Proctor, T.M., Vandenbark, A.A. & Offner, H. Down-modulation of programmed death 1 alters regulatory T cells and promotes experimental autoimmune encephalomyelitis. *Journal of neuroscience research* 88, 7-15 (2010).**

107. **Amarnath, S. *et al.* The PDL1-PD1 axis converts human TH1 cells into regulatory T cells. *Science translational medicine* 3, 111ra120 (2011).**

108. **Freeman, G.J. *et al.* Engagement of the PD-1 immunoinhibitory receptor by a novel B7 family member leads to negative regulation of lymphocyte activation. *J Exp Med* 192, 1027-1034 (2000).**

109. **Latchman, Y. *et al.* PD-L2 is a second ligand for PD-1 and inhibits T cell activation. *Nature immunology* 2, 261-268 (2001).**

110. **Good-Jacobson, K.L. *et al.* PD-1 regulates germinal center B cell survival and the formation and affinity of long-lived plasma cells. *Nature immunology* 11, 535-542 (2010).**

111. **Hamel, K.M. *et al.* B7-H1 expression on non-B and non-T cells promotes distinct effects on T- and B-cell responses in autoimmune arthritis. *Eur J Immunol* 40, 3117-3127 (2010).**

112. **Kawamoto, S. *et al.* The inhibitory receptor PD-1 regulates IgA selection and bacterial composition in the gut. *Science* 336, 485-489 (2012).**

113. **Hams, E. *et al.* Blockade of B7-H1 (programmed death ligand 1) enhances humoral immunity by positively regulating the generation of T follicular helper cells. *J Immunol* 186, 5648-5655 (2011).**

114. **Velu, V. *et al.* Enhancing SIV-specific immunity in vivo by PD-1 blockade. *Nature* 458, 206-210 (2009).**

115. **Linterman, M.A. *et al.* Foxp3+ follicular regulatory T cells control the germinal center response. *Nat Med* 17, 975-982 (2011).**

116. Chung, Y. *et al.* Follicular regulatory T cells expressing Foxp3 and Bcl-6 suppress germinal center reactions. *Nat Med* 17, 983-988 (2011).

117. Wollenberg, I. *et al.* Regulation of the germinal center reaction by Foxp3+ follicular regulatory T cells. *J Immunol* 187, 4553-4560 (2011).

118. Josefowicz, S.Z., Lu, L.F. & Rudensky, A.Y. Regulatory T cells: mechanisms of differentiation and function. *Annu Rev Immunol* 30, 531-564 (2012).

119. Keir, M.E., Freeman, G.J. & Sharpe, A. PD-1 regulates self-reactive CD8+ T cell responses to antigen in lymph nodes and tissues. *Journal of Immunology* 179, 5064-5070 (2007).

120. Latchman, Y.E. *et al.* PD-L1-deficient mice show that PD-L1 on T cells, antigen-presenting cells, and host tissues negatively regulates T cells. *Proc Natl Acad Sci U S A* 101, 10691-10696 (2004).

121. Keir, M.E. *et al.* Tissue expression of PD-L1 mediates peripheral T cell tolerance. *J Exp Med* 203, 883-895 (2006).

122. McAdam, A.J. *et al.* ICOS is critical for CD40-mediated antibody class switching. *Nature* 409, 102-105 (2001).

123. Shahinian, A. *et al.* Differential T cell costimulatory requirements in CD28-deficient mice. *Science* 261, 609-612 (1993).

124. Bettelli, E. *et al.* Reciprocal developmental pathways for the generation of pathogenic effector TH17 and regulatory T cells. *Nature* 441, 235-238 (2006).

125. Bettelli, E. *et al.* Myelin oligodendrocyte glycoprotein-specific T cell receptor transgenic mice develop spontaneous autoimmune optic neuritis. *J Exp Med* 197, 1073-1081 (2003).

126. Bauquet, A.T. *et al.* The costimulatory molecule ICOS regulates the expression of c-Maf and IL-21 in the development of follicular T helper cells and TH-17 cells. *Nature immunology* 10, 167-175 (2009).

127. Scholzen, T. & Gerdes, J. The Ki-67 protein: from the known and the unknown. *Journal of cellular physiology* 182, 311-322 (2000).

128. Fife, B.T. *et al.* Interactions between PD-1 and PD-L1 promote tolerance by blocking the TCR-induced stop signal. *Nature immunology* 10, 1185-1192 (2009).

129. Cretney, E. *et al.* The transcription factors Blimp-1 and IRF4 jointly control the differentiation and function of effector regulatory T cells. *Nature immunology* 12, 304-311 (2011).

130. Martins, G.A. *et al.* Transcriptional repressor Blimp-1 regulates T cell homeostasis and function. *Nature immunology* 7, 457-465 (2006).

131. Zhou, L. *et al.* TGF-beta-induced Foxp3 inhibits T(H)17 cell differentiation by antagonizing RORgammat function. *Nature* 453, 236-240 (2008).

132. Kaech, S.M., Wherry, E.J. & Ahmed, R. Effector and memory T-cell differentiation: implications for vaccine development. *Nat Rev Immunol* 2, 251-262 (2002).

133. Baaten, B.J. *et al.* CD44 regulates survival and memory development in Th1 cells. *Immunity* 32, 104-115 (2010).

134. Bollyky, P.L. *et al.* CD44 costimulation promotes FoxP3+ regulatory T cell persistence and function via production of IL-2, IL-10, and TGF-beta. *J Immunol* 183, 2232-2241 (2009).

135. Beswick, E.J., Pinchuk, I.V., Das, S., Powell, D.W. & Reyes, V.E. Expression of the programmed death ligand 1, B7-H1, on gastric epithelial cells after Helicobacter pylori exposure promotes development of CD4+ CD25+ FoxP3+ regulatory T cells. *Infect Immun* 75, 4334-4341 (2007).

136. Lucas, J.A. *et al.* Programmed death ligand 1 regulates a critical checkpoint for autoimmune myocarditis and pneumonitis in MRL mice. *J Immunol* 181, 2513-2521 (2008).

137. Barber, D.L. *et al.* Restoring function in exhausted CD8 T cells during chronic viral infection. *Nature* 439, 682-687 (2006).

138. Fourcade, J. *et al.* Upregulation of Tim-3 and PD-1 expression is associated with tumor antigen-specific CD8+ T cell dysfunction in melanoma patients. *J Exp Med* 207, 2175-2186 (2010).

139. Porichis, F. *et al.* Responsiveness of HIV-specific CD4 T cells to PD-1 blockade. *Blood* 118, 965-974 (2011).

140. Wang, J. *et al.* Establishment of NOD-Pdcd1-/- mice as an efficient animal model of type I diabetes. *Proc Natl Acad Sci U S A* 102, 11823-11828 (2005).

141. Okazaki, T., Maeda, A., Nishimura, H., Kurosaki, T. & Honjo, T. PD-1 immunoreceptor inhibits B cell receptor-mediated signaling by recruiting src homology 2-domain-containing tyrosine phosphatase 2 to phosphotyrosine. *Proc Natl Acad Sci U S A* 98, 13866-13871 (2001).

142. Rawlings, D.J., Schwartz, M.A., Jackson, S.W. & Meyer-Bahlburg, A. Integration of B cell responses through Toll-like receptors and antigen receptors. *Nat Rev Immunol* 12, 282-294.

143. Kim, C.H. *et al.* Subspecialization of CXCR5+ T cells: B helper activity is focused in a germinal center-localized subset of CXCR5+ T cells. *J Exp Med* 193, 1373-1381 (2001).

144. Rosenblum, M.D. *et al.* Response to self antigen imprints regulatory memory in tissues. *Nature* 480, 538-542 (2011).

145. Mora, J.R. & von Andrian, U.H. Differentiation and homing of IgA-secreting cells. *Mucosal Immunol* 1, 96-109 (2008).

146. Weng, N.P. Aging of the immune system: how much can the adaptive immune system adapt? *Immunity* 24, 495-499 (2006).

Publications

The following are my publications during my graduate student career.

1. **Sage, P. T.**, and C. V. Carman. 2009. Settings and mechanisms for trans-cellular diapedesis. *Front Biosci* 14:5066-5083.

2. Francisco, L. M., **P. T. Sage**, and A. H. Sharpe. 2009. The PD-1 pathway in tolerance and autoimmunity. *Immunol Rev* 236:219-242.

3. Koduru, S., L. Kumar, M. J. Massaad, N. Ramesh, S. Le Bras, E. Ozcan, M. K. Oyoshi, M. Kaku, Y. Fujiwara, L. Kremer, S. King, R. Fuhlbrigge, S. Rodig, **P. Sage**, C. Carman, P. Alcaide, F. W. Luscinskas, and R. S. Geha. 2010. Cdc42 interacting protein 4 (CIP4) is essential for integrin-dependent T-cell trafficking. *Proc Natl Acad Sci U S A* 107:16252-16256.

4. Riella, L. V., T. Watanabe, **P. T. Sage**, J. Yang, M. Yeung, J. Azzi, V. Vanguri, A. Chandraker, A. H. Sharpe, M. H. Sayegh, and N. Najafian. 2011. Essential role of PDL1 expression on nonhematopoietic donor cells in acquired tolerance to vascularized cardiac allografts. *Am J Transplant* 11:832-840.

5. Jin, Y., S. K. Chauhan, J. El Annan, **P. T. Sage**, A. H. Sharpe, and R. Dana. 2011. A novel function for programmed death ligand-1 regulation of angiogenesis. *Am J Pathol* 178:1922-1929.

6. **Sage, P. T.**, L. M. Varghese, R. Martinelli, T. E. Sciuto, M. Kamei, A. M. Dvorak, T. A. Springer, A. H. Sharpe, and C. V. Carman. 2012. Antigen Recognition Is Facilitated by Invadosome-like Protrusions Formed by Memory/Effector T Cells. *J Immunol* 188:3686-3699.

7. **Sage, P. T**., L. M. Francisco, C. V. Carman, and A. H. Sharpe. 2012. The receptor PD-1 controls follicular regulatory T cells in the lymph nodes and blood. *Nature immunology*.

Appendix A

This is a reprint of:

> Sage, P.T. *et al.* Antigen Recognition Is Facilitated by Invadosome-like Protrusions Formed by Memory/Effector T Cells. *J Immunol* 188, 3686-3699 (2012). *Copyright 2012 American Association of Immunologists Inc.*

Antigen Recognition Is Facilitated by Invadosome-like Protrusions Formed by Memory/Effector T Cells

Peter T. Sage,*,† Laya M. Varghese,† Roberta Martinelli,† Tracey E. Sciuto,‡ Masataka Kamei,† Ann M. Dvorak,‡ Timothy A. Springer,§ Arlene H. Sharpe,* and Christopher V. Carman†

Adaptive immunity requires that T cells efficiently scan diverse cell surfaces to identify cognate Ag. However, the basic cellular mechanisms remain unclear. In this study, we investigated this process using vascular endothelial cells, APCs that possess a unique and extremely advantageous, planar morphology. High-resolution imaging revealed that CD4 memory/effector T cells dynamically probe the endothelium by extending submicron-scale, actin-rich "invadosome/podosome-like protrusions" (ILPs). The intimate intercellular contacts enforced by ILPs consistently preceded and supported T cell activation in response to endothelial MHC class II/Ag. The resulting calcium flux stabilized dense arrays of ILPs (each enriched in TCR, protein kinase C-θ, ZAP70, phosphotyrosine, and HS1), forming what we term a podo-synapse. Similar findings were made using CD8 CTLs on endothelium. Furthermore, careful re-examination of both traditional APC models and professional APCs suggests broad relevance for ILPs in facilitating Ag recognition. Together, our results indicate that ILPs function as sensory organelles that serve as actuators of immune surveillance. ***The Journal of Immunology*****, 2012, 188: 3686–3699.**

Adaptive immunity relies on the ability of TCRs expressed on lymphocytes to efficiently recognize peptide Ag bound to MHC molecules (1). During the priming phase, naive lymphocytes must constitutively scan professional APCs within lymph nodes. During the effector phase, memory/effector T cells need to effectively survey an extremely wide range of APCs and potential target cells within peripheral tissues. Fundamental cellular mechanisms for such immune surveillance activities remain incompletely understood.

At the heart of immune surveillance is the requirement for T cells to form extremely intimate (~14 nm, the total height of the TCR–MHC complex) (2) contacts with apposing cells to sample MHC/Ag. However, the surfaces of all cells are modified by a relatively thick (50–500 nm) gel-like polysaccharide coat termed the glycocalyx (3), which provides a formidable energy barrier (via steric and electrostatic repulsion) to close membrane–membrane encounter (4, 5). In this way, TCR and MHC are effectively shielded and immune recognition is opposed (5–10). Thus, a fundamental question is, how do T cells overcome this energy barrier to engage immune receptors?

It has long been appreciated that as a consequence of Ag recognition, specialized cell–cell interfaces form that involve membrane alignment, cytoskeletal remodeling, clustering/segregation of immune receptors/adhesion molecules, and glycocalyx components (5, 11–15). These "immunological synapses" (ISs) form within minutes of Ag recognition and are thought to amplify and sustain signaling, as well as facilitate exchange of cytokine and/or cytotoxic materials (5, 11–15). However, detailed mechanisms facilitating initial Ag sampling between T cells and APCs, and how these lead to early IS formation, are not completely understood (16, 17). This stems from technical challenges associated with irregular topologies of APC surfaces and poorly controlled orientation of the cell–cell interaction planes, issues that profoundly limit the requisite imaging approaches (16–18).

Investigators have partially circumvented these restrictions by developing planar substrate models (i.e., lipid bilayers and Ab-coated surfaces) that provide optimal spatiotemporal resolution for monitoring Ag response dynamics (19–23). These models have afforded invaluable insights, such as the discovery of TCR microclusters as critical mediators of effective signaling (15, 19–22). However, these systems lack key features of cellular APC surfaces, such as the glycocalyx, topological deformability, and molecular complexity. Therefore, it remains uncertain how to translate such findings to physiologic cell–cell immune surveillance.

In this study, we used vascular endothelial cells (ECs) as a planar APC model to interrogate the details of initial Ag recognition dynamics on a physiologic cellular substrate. ECs represent the interface between the blood circulation and tissue, and play critical roles in regulating immune cell trafficking (1, 24, 25). The dis-

*Department of Microbiology and Immunobiology, Harvard Medical School, Boston, MA 02115 †Department of Medicine, Center for Vascular Biology Research, Beth Israel Deaconess Medical Center, Harvard Medical School, Boston, MA 02215; ‡Department of Pathology, Center for Vascular Biology Research, Beth Israel Deaconess Medical Center, Harvard Medical School, Boston, MA 02215; and §Department of Pathology, Immune Disease Institute, Harvard Medical School, Boston, MA 02115

Received for publication September 14, 2011. Accepted for publication February 13, 2012.

This work was supported by the National Institutes of Health (Grants T32 AI070085 to P.T.S., AI078897 to A.H.S., and HL04006 to C.V.C.) and the American Heart Association, the Arthritis Foundation, and the Roche Organ Transplant Research Foundation (to C.V.C.).

Address correspondence and reprint requests to Christopher V. Carman, Harvard Medical School—Beth Israel Deaconess Medical Center, 330 Brookline Avenue, RN234, Boston, MA 02215. E-mail address: ccarman@bidmc.harvard.edu

The online version of this article contains supplemental material.

Abbreviations used in this article: BMDC, bone marrow-derived dendritic cell; CAMKII, calcium-calmodulin–dependent kinase II; CHO, Chinese hamster ovary; DC, dendritic cell; EC, endothelial cell; HDMVEC, human dermal microvascular EC; HLMVEC, human lung microvascular EC; HS1, hematopoietic lineage cell-specific protein 1; HUVEC, human umbilical vein EC; ILP, invadosome/podosome-like protrusion; IRM, interference reflection microscopy; IS, immunological synapse; iT_{mem}, induced/expanded human T memory cell; mem-DsRed, palmitoylated DsRed; mem-YFP, palmitoylated YFP; MHC-I, MHC class I; MHC-II, MHC class II; nT_{mem}, natural human T memory cell; PKC, protein kinase C; SA, streptavidin; SEB, staphylococcal enterotoxin B; TSST, toxic shock syndrome toxin 1.

www.jimmunol.org/cgi/doi/10.4049/jimmunol.1102594

covery that ECs express MHC class I (MHC-I), MHC class II (MHC-II), and a large number of costimulatory molecules (e.g., CD40, LFA-3, ICOSL, 4-1BB, OX40L, TL1A, PD-L1, but not CD80 and CD86) has led to the controversial hypothesis that endothelium can also function as a type of APC (26–28). Indeed, several studies have demonstrated that endothelium can effectively restimulate CD4 and CD8 memory/effector, but not naive, T cells (29–33). Critically, when grown in vitro, ECs form virtually planar cell surfaces that are ideal for high spatiotemporal resolution imaging of topological dynamics (34).

This study provides a detailed investigation of the initial events in CD4 and CD8 T cell scanning for Ag. We previously discovered that lymphocytes actively probe the surface of the endothelium by dynamic insertion and retraction of submicron-scale, actin-rich cylindrical protrusions related to invadosomes (35), termed invadosome/podosome–like protrusions (ILPs) (34). These were demonstrated to function in supporting migratory pathfinding (34, 36). In this study, we found that dynamic ILP probing by CD4 and CD8 memory/effector lymphocytes enforces close T cell–EC apposition, which seems to facilitate Ag recognition and TCR signaling. Moreover, T cell activation is sustained through a novel IS architecture dominated by dense arrays of calcium-stabilized ILPs (each enriched in signaling molecules) that we term a podosynapse. Complementary studies with model substrates and professional APCs (B cells and dendritic cells [DCs]) suggest that rather than being a unique feature of T cell–EC ISs, ILPs are uniquely revealed in this setting. Together, our results indicate that memory/effector T cells use ILPs to facilitate efficient search for Ag and to help sustain the resulting signaling responses.

Materials and Methods

Cells

Natural human T memory cells (nT_{mem}; $CD4^+CD45RO^+CD45RA^-$) were isolated via negative selection from peripheral blood using a CD4 T cell isolation kit, followed by $CD45RA^+$ cell depletion (Miltenyi Biotec) to >95% purity. Induced/expanded human T memory cells (iT_{mem}; $CD4^+CD45RO^+$) were made by culturing peripheral blood buffy coats for 72 h in 1 μg/ml bacterial superantigens staphylococcal enterotoxin B (SEB) and toxic shock syndrome toxin 1 (TSST; Toxin Technology). CD4 memory cells were enriched by using a CD4 T cell memory negative isolation kit (Miltenyi Biotec). Cells were cultured 3–10 d in 20 ng/ml IL-15 (R&D Systems) to maintain memory phenotype. Mouse CD4 or CD8 T cells were isolated by magnetic separation from either $OTII^+TCR\alpha^{-/-}CD45.1^{+/+}$ or $OTI^+Thy1.1^{+/+}$ mice and activated with irradiated splenocytes in the presence of 30 μg/ml OVA 323–339 (OTII) or 500 ng/ml OVA-SIINFEKL (OTI) supplemented with IL-2 for 3 d. T cells were reselected with MACS beads and rested in culture in the presence of IL-2 for a further 3 d. Human lung microvascular ECs (HLMVECs), human dermal microvascular ECs (HDMVECs), and human umbilical vein ECs (HUVECs) were from Lonza and cultured on fibronectin (10 μg/ml; Invitrogen) in EBM-2 MV media (Lonza). Mouse heart ECs were isolated from C57BL/6 mice by collagenization of heart tissue followed by positive selection with anti-CD31 (MEC13.3)–coated beads (Invitrogen). ECs were cultured for 7 d in media with EC growth supplement (Biomedical Technologies) followed by reselection with beads coupled to anti-CD102. ECs were >95% purity based on expression of $CD105^+CD102^+$. ECs were transfected by Amaxa electroporation according to manufacturer's instructions (Lonza). Palmitoylated YFP (mem-YFP) and soluble monomeric DsRed were from Clontech. Palmitoylated DsRed (mem-DsRed) and ICAM-1–GFP were generated as described previously (34). ECs were activated for 48 h with 100 ng/ml IFN-γ (R&D Systems) and 12 h with 50 ng/ml TNF-α (R&D Systems). Priess B cell line was a gift from Dr. Kai Wucherpfennig. Chinese hamster ovary (CHO)-K1 epithelial cells were from American Type Culture Collection. Murine bone marrow-derived DCs (BMDCs) were prepared from bone marrow cells cultured in 30 ng/ml GM-CSF (PeproTech) for 6 d.

Transendothelial migration

Lymphocyte transendothelial migration assays were conducted in both static and shear conditions as described previously (34). In some cases, T cells were added to 8-μm pore transwell inserts that were preceded with ECs and then collected from the bottom chamber 6 h later and analyzed by flow cytometry.

Live-cell imaging and analysis

Live-cell imaging was performed on an Axiovert S200 microscope with Axiovision software (Zeiss). For calcium imaging, T cells were preincubated with 1 μg/ml Fura-2–AM or Fluo-4–AM (Invitrogen) for 30 min. For Fura-2, standard Fura-2 filters were used according to manufacturer's instructions (Chroma) and ratiometric calcium flux was calculated (340_{nm}EX-510_{nm}EM-background/380_{nm}EX-510_{nm}EM-background) for each cell using Axiovision. For Fluo-4, green fluorescence filters were used and basal fluorescence signal was established by imaging cells on uncoated chambers. T cell polarity was calculated from bright-field images as the ratio of the greatest edge-to-edge dimension in the *x–y* plane (i.e., the long axis) divided by the perpendicular axis. Migration velocity was measured for cells using the Axiovision Cell Tracking Module. Podo-print/ILP lifetimes were assessed using podo-print appearance and disappearance on mem-dsRed– or mem-YFP–transfected ECs as a readout for the presence of ILPs (34). Podo-print/ILP lifetimes were calculated as follows: the last time point when an individual podo-print/ILP was visible − the time point when that podo-print/ILP first appeared. Podo-print/ILP lateral translocation was assessed by determining the distance between the T cell centroid and the first and last positions of an individual podo-print/ILP during its lifetime. Podo-print/ILP index, a measure of the total number of ILPs per cell, was calculated at 5 min after addition of T cells. "Offset time" was used to describe relative time between first podo-print/ILP formation and calcium flux rise above background. Temporal resolution was limited to 10 s, the maximal achievable acquisition frame rate of this analysis. Data was then sorted into 10-s interval bins.

For selected studies, lymphocytes were preincubated, or lymphocyte and APCs coincubated, with select pharmaceutical agents, including latrunculin A (1 μg/ml; Sigma), BAPTA-AM (40 μM, Sigma), BTP2 (20 μM; Calbiochem), thapsigargin (1 μM Sigma), and calcium-calmodulin–dependent kinase II (CAMKII) inhibitor CK59 (50 μM; EMD Biosciences) as indicated. For calcium blockade conditions, T cells were pretreated with BAPTA-AM and BTP2 in imaging buffer containing high (45 mM) potassium. T cells were added to ECs and imaged with additional BTP2 for the duration of imaging.

Fixed cell imaging

Fixed cell samples were imaged on an LSM 510 confocal microscope (Zeiss). Samples were fixed and stained for αL integrin (TS2/4), ICAM-1 (IC1/11), F-actin (phalloidin), MHC-II (WR18; Abcam), protein kinase C (PKC)-θ, talin (rabbit anti-talin, a gift from Dr. Keith Burridge), CD3 (OKT3; eBioscience), CD43 (L60; BD Biosciences), CD45 (HI30 or UCHL1; eBioscience), hematopoietic lineage cell-specific protein 1 (HS1; clone 9 [BD Biosciences] or rabbit anti-HS1 [Cell Signaling]), ZAP70 (Santa Cruz), phosphotyrosine (4G10 platinum; Millipore), or NFAT (BD Biosciences). Transmigration was analyzed by confocal microscopy as described previously (37).

CTL killing assay

For specific killing assay, murine ECs were labeled with either 0.6 or 0.02 μM CFSE ($CFSE^{hi}$ and $CFSE^{low}$, respectively). The $CFSE^{hi}$ population was pulsed with 1 μg/ml SIINFEKL for 20 min. Both $CFSE^{hi}$ and $CFSE^{low}$ populations were plated together in a 1:1 ratio. Activated OTI CD8 T cells were rested for 5 h and added to monolayers in a 3:1 T cell/target cell ratio. Cultures were stained for CD105 to differentiate the ECs from T cells and analyzed by flow cytometry. Specific lysis was calculated by the following equation: $1 - ([CFSE^{hi}/(CFSE^{hi} + CFSE^{low})]/[\text{control } CFSE^{hi}/CFSE^{low}])*100$.

Planar coated glass APC model

Coated glass IS models were prepared as described previously (20, 38). In brief, imaging chambers were coated with ICAM-1–Fc (10 μg/ml; R&D Systems) alone or together with anti-CD3, anti-CD43, anti-CD45, or control IgG Ab (10 μg/ml). Fluo-4–labeled lymphocytes were added and imaged by fluorescence and interference reflection microscopy (IRM).

Coated cell APC model

CHO-K1 cells were transfected with ICAM-1-GFP and soluble dsRed via electroporation. Cells were then coated with Abs via a biotin/streptavidin (SA)-based approach (39). Cells were subjected to primary amine-targeted

cell surface biotinylation for 15 min with biotin-NHS-ester (0.5 μg/ml; Thermo Electron). Cells were incubated with SA at 10 μg/ml for 15 min. Cells were then incubated with biotinylated anti-CD3, -CD43, or -CD45 (eBioscience) at 10 μg/ml for 15 min.

T cell activation by CD3 cross-linking

Fluo-4–labeled T cells were settled onto uncoated glass chambers, 10 μg/ml anti-CD3 and -CD28 were added to the imaging chambers, and calcium was monitored.

Transmission electron microscopy

Transmission electron microscopy of T cell–APC complexes was performed as described previously (34). Fifty randomly selected micrographs were analyzed by enumerating zones of membrane apposition (<20 nm) and correlating them with respect to ILP location.

Statistical analysis

Error bars represent SE or SD as indicated. The p values were calculated via unpaired Student t tests in GraphPad Prism. Statistical significance is indicated with p values as follows: $^{***}p < 0.0005$, $^{**}p < 0.005$, $^{*}p < 0.05$.

Results

Endothelial-presented Ag promotes activation of CD4 memory T cells

We wanted to elucidate the mechanisms by which memory/effector T cells probe for Ag using ECs as model APCs. Therefore, we isolated natural CD4 memory-like lymphocytes (nT_{mem}) and generated induced/expanded CD4 memory-like lymphocytes (iT_{mem}) from human peripheral blood. The isolated nT_{mem} were $CD4^+$, $CD45RO^+$, and contained both central memory and effector memory T cells (~78 and ~22%, respectively) based on CD62L staining (Supplemental Fig. 1A). The iT_{mem} were slightly more polarized toward the effector memory T cell subtype (~69 versus ~31%; Supplemental Fig. 1B). Monolayers of HLMVECs, HDMVECs, and HUVECs were used as models for the vasculature. In vivo endothelial MHC-II expression is dependent on IFN-γ (26). This was recapitulated in vitro by culturing ECs with exogenous IFN-γ (Supplemental Fig. 1C). Endothelium was additionally activated with TNF-α to promote an inflamed phenotype.

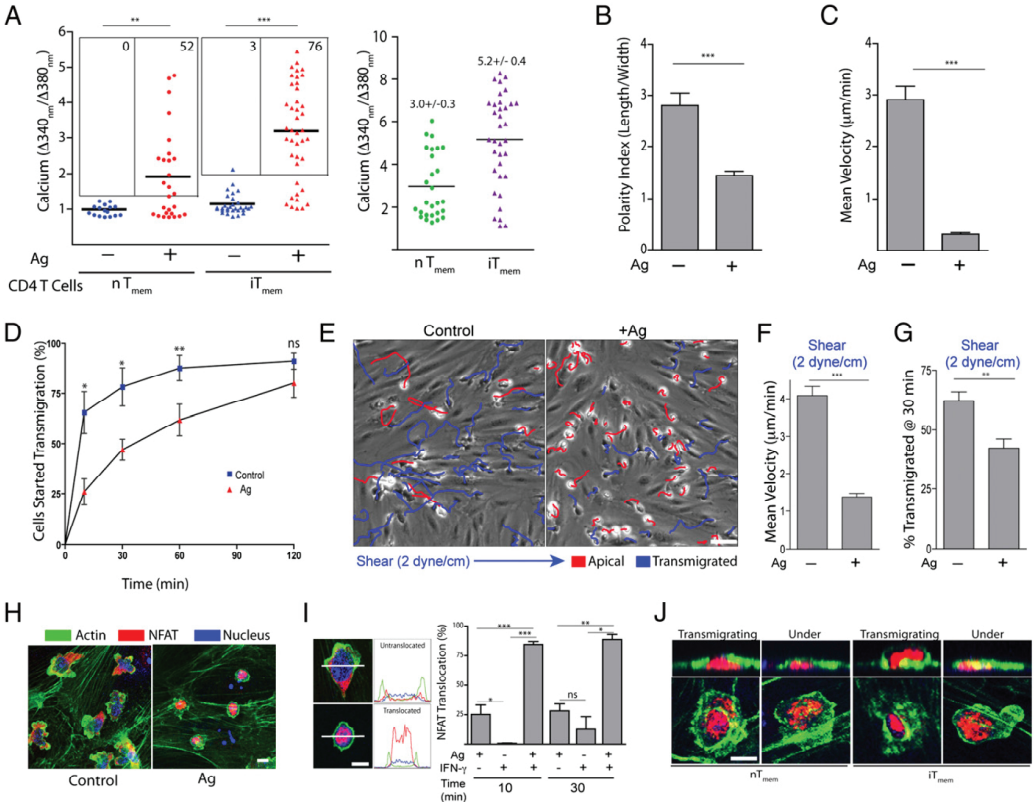

FIGURE 1. Human microvascular ECs are capable of Ag-specific stimulation of CD4 memory-like T cells. (**A**) Human CD4 nT_{mem} (circles) or iT_{mem} (triangles) were loaded with Fura-2 and incubated on Ag-pulsed HLMVECs. Calcium flux at 5 min (*left*) or at maximal value over a 30-min duration (*right*) were plotted. (**B** and **C**) iT_{mem} were incubated on HLMVEC pulsed with Ag and T cell polarity (length/width ratio) at 5 min, and velocity was calculated over a 30-min duration. (**D**) iT_{mem} transendothelial migration was scored on Ag pulsed ECs as described in *Materials and Methods*. (**E**) iT_{mem} were infused over Ag-pulsed HLMVEC at 2 dyne/cm^2 and imaged. Depicted is an end-point image with migration tracks of apical (blue) and transmigrated (red) lymphocytes. See also Supplemental Video 1. (**F** and **G**) Lateral migration velocities for T cells from (E) during both prediapedesis and postdiapedesis phases of migration over 30 min (F) and percentage of iTmem transmigrated were measured (G). (**H**) Representative images of nT_{mem} incubated on Ag-pulsed HLMVEC and staining for actin (green), NFAT (red), and nucleus (blue). (**I**) nT_{mem} were incubated on activated HLMVEC. Nuclear NFAT translocation was scored according to line scan profiles (*left*). (**J**) Samples were acquired as in (H), and representative transmigrating or transmigrated ('Under') lymphocytes are shown. Data represent mean ± SD (B, C) or SEM (D, F, G, I). Scale bars, 5 μm. $^{*}p < 0.05$, $^{**}p < 0.005$, $^{***}p < 0.0005$.

Next, we set up live-cell analysis to concomitantly monitor T cell activation (i.e., calcium flux) and migration on endothelium pulsed with Ag (i.e., bacterial superantigen, a widely used model Ag) (38, 40, 41). In the absence of Ag, nT_{mem} and iT_{mem} fluxed little calcium (Fig. 1A), remained polarized (Fig. 1B), and underwent continuous lateral (Fig. 1C) and transendothelial migration (i.e., "diapedesis"; Fig. 1D). On HLMVECs pulsed with Ag (1 μg/ml SEB and TSST), T cells rapidly fluxed calcium, lost polarity, and arrested migration (Fig. 1A–C). Similar results were found with alternate Ag (e.g., SEE and MAM) presented by HDMVECs or HUVECs (Supplemental Fig. 1D and data not shown). In addition, in the absence of Ag, the majority of iT_{mem} transmigrated within 30 min, whereas in the presence of Ag, diapedesis was delayed by ~30–60 min (Fig. 1D). Thus, the migratory stop signal was transient. IT_{mem} also exhibited Ag-dependent transient migration arrest under conditions of laminar fluid shear flow conditions similar to those found in microvasculature in vivo (2 dyne/cm^2; Fig. 1E–G, Supplemental Video 1).

During T cell activation, the transcription factor NFAT translocates from the cytoplasm to the nucleus. Incubation of nT_{mem} on

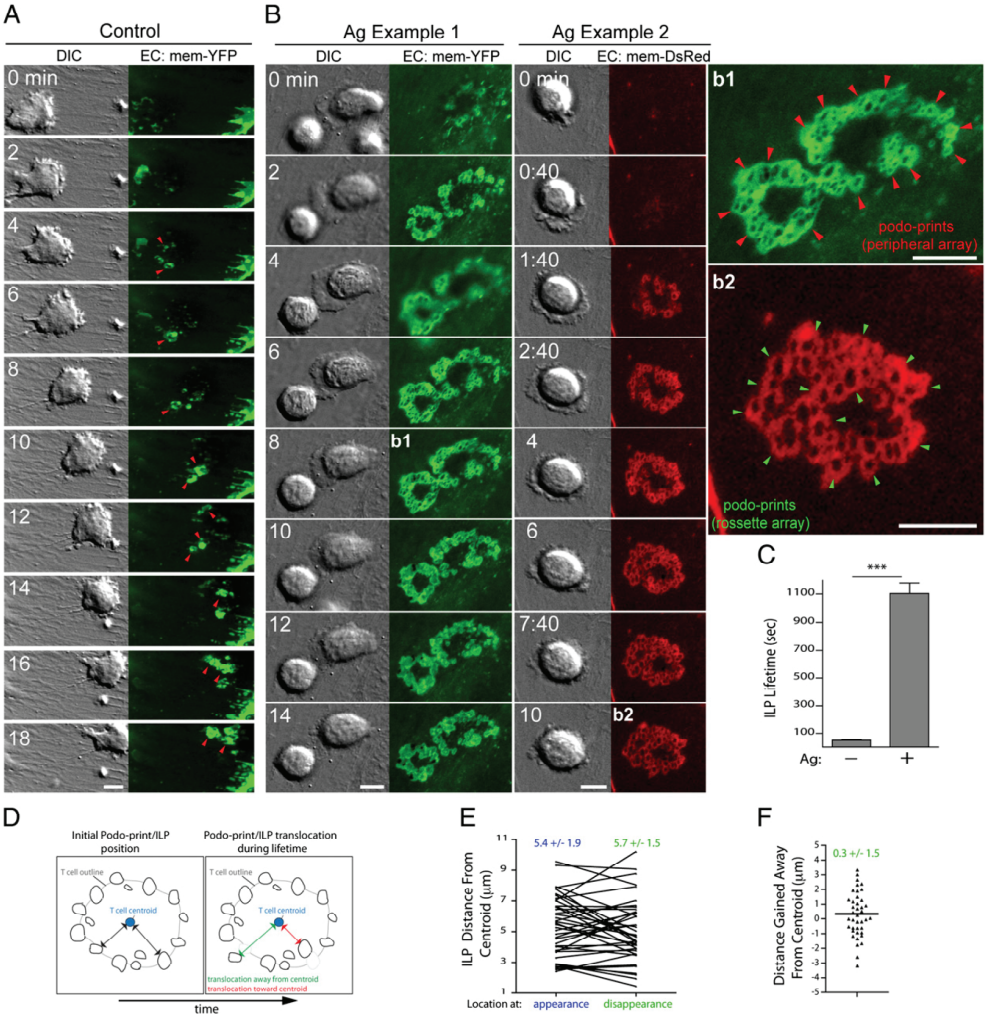

FIGURE 2. CD4 memory-like T cells form stabilized arrays of ILPs on Ag-presenting endothelium. (**A** and **B**) HLMVECs were transfected with mem-YFP or mem-DsRed, activated, and pulsed without (A) or with (B) Ag (TSST/SEB). iT_{mem} were imaged live on addition to ECs. Individual frames at selected time intervals are shown. Arrows indicate fluorescent rings formed on endothelium under adherent lymphocytes. The corresponding control (A) and Ag (**b1** and **b2**) videos are provided as Supplemental Videos 2–4, respectively. (**C**) Podo-print/ILP lifetimes from imaging studies as in (A) and (B). Data represent mean ± SEM of at least 80 ILPs formed by at least 25 cells from ≥3 separate experiments. (**D**) Schematic representation of podo-print/ILP lateral translocation analysis. Gray "T cell outline" represents a T cell–EC contact area with the "T cell centroid" indicated as a blue circle and individual podo-prints indicated as black rings. The linear distance between the centroid and podo-print was measured at both the first and last appearance of an individual podo-print/ILP during its lifetime. (**E** and **F**) Podo-print/ILP distances were measured as in (D). Distances from the cell centroid at time of formation and disappearance were plotted for individual podo-prints (E). Data from (E) was further processed to report change in distance (F). Scale bars, 5 μm. ***$p <$ 0.0005.

Ag-pulsed ECs promoted robust nuclear translocation of NFAT (Fig. 1H, 1I). Significantly, transmigrating nT_{mem} and iT_{mem} retained nuclear NFAT, demonstrating that these cells remained activated (Fig. 1J). NT_{mem} on endothelium that was pulsed with Ag but not pretreated with IFN-γ (and therefore lacked strong MHC-II expression) exhibited little NFAT translocation (Fig. 1I), confirming that the responses to Ag-pulsed endothelium were MHC-II dependent.

To show that T cells achieved complete activation, we conducted studies using a transwell system, in which T cells loaded into an upper chamber migrated across an EC monolayer to reach the lower chamber. Flow cytometry revealed that after migrating across Ag-pulsed ECs, iT_{mem} showed increased surface expression of CD69 and a reduction in CD62L (Supplemental Fig. 1E). In addition, in these nonpolarizing conditions, a subset of the iT_{mem} upregulated IFN-γ expression (Supplemental Fig. 1F, 1G) and increased proliferation (Supplemental Fig. 1H). Collectively, these results demonstrate that endothelium is able to present model Ag in an MHC-II–dependent manner to CD4 memory/effector lymphocytes, which induces a transient delay in diapedesis and T cell activation.

ILP arrays dominate the T cell–EC interface during activation

Next, we investigated the cellular and molecular basis for T cell activation in our endothelial APC model. Previously, we used fluorescent membrane markers (mem-YFP or mem-DsRed) expressed in the ECs to detect topological changes in the plasma membrane (34). In this way, we demonstrated that ~0.5-μm fluorescent rings that formed dynamically on the endothelium under migrating T cells corresponded to cylinder-shaped cell surface invaginations (i.e., "podo-prints") induced by lymphocyte ILPs. Thus, podo-prints formed on the EC surface served as an indirect but sensitive readout for T cell ILPs (34). In this study, we similarly observed in control settings that podo-prints formed and disappeared

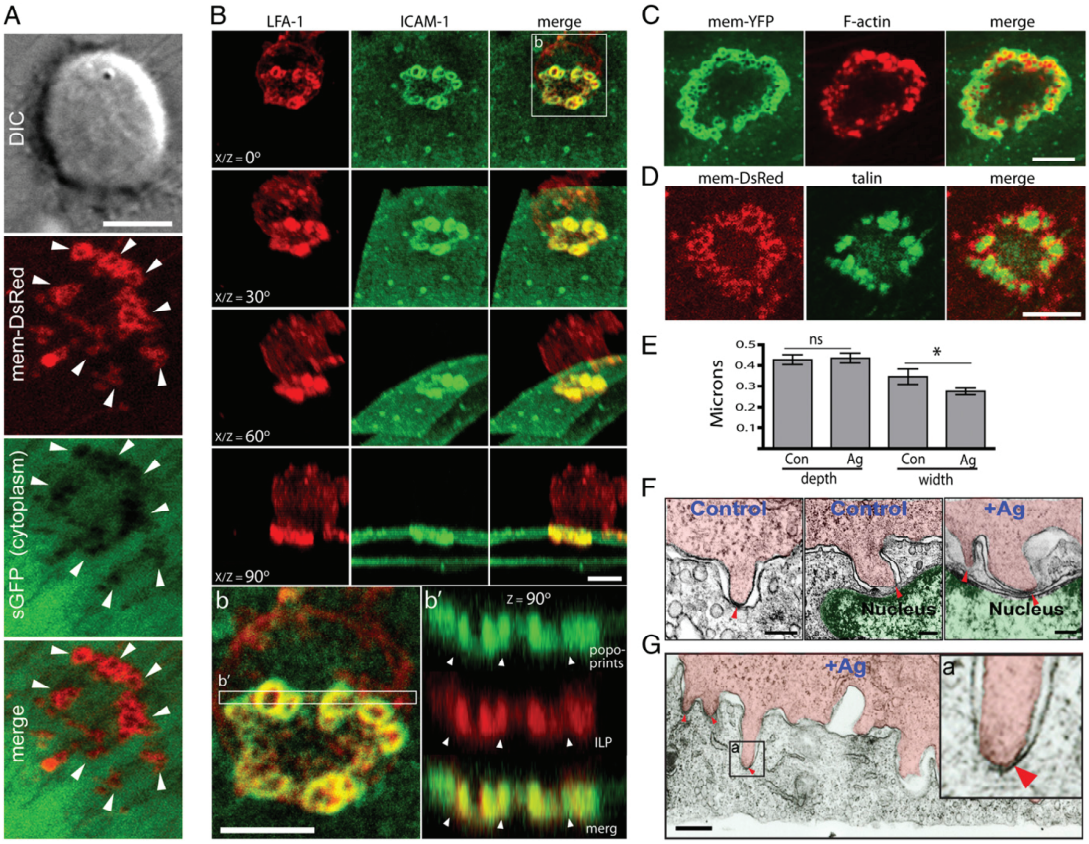

FIGURE 3. Ag-stabilized ILPs exhibit a discrete three-dimensional architecture. (**A**) Ag-stabilized T cell ILPs protrude into the EC surface. Imaging was conducted as in Fig. 2B on HLMVECs coexpressing soluble, cytoplasmic GFP (green) and mem-DsRed (red). (**B**) Three-dimensional reconstruction from confocal imaging of podo-prints and ILPs. iT_{mem} were incubated for 20 min on activated Ag-pulsed (SEE) HUVECs and then fixed, stained for ICAM-1 (green) and LFA-1(red), and imaged by confocal microscopy. Sections were digitally reconstructed and projected as three-dimensional renderings. (**b**) Magnified view of the ILP arrays. (**b′**) Orthogonal cross section. See also Supplemental Video 5. (**C** and **D**) Ag-stabilized ILPs are enriched in actin and talin. Mem-YFP–transfected (C; green) or mem-DsRed–transfected (D; red) HLMVECs were pulsed with Ag (TSST/SEB) and incubated with iT_{mem} for 5 min and stained for F-actin (C; red) or talin (D; green). (**E**) Quantitation of ultrastructural depth and width of T cell ILPs. Samples as in (C) were imaged by electron microscopy and ILPs were measured. Data represent mean ± SEM from at least 100 ILPs from at least 20 representative micrographs per condition. (**F** and **G**) ILPs enforce close T cell–EC membrane apposition in the absence and presence of Ag. T cell and endothelial nuclei are indicated with red and green overlays, respectively. Arrows and (**a**) highlight regions of extremely close lymphocyte–EC membrane apposition enforced at the ILP tips. Scale bars, 5 μm (A–D); 500 nm (F, G). *$p < 0.05$. ns, Not significant.

continuously (with lifetimes of tens of seconds) under the leading edge lamellipodia of migrating iT_{mem} (Fig. 2A, 2C, Supplemental Video 2). Strikingly, when ECs were pulsed with Ag, iT_{mem} rapidly formed dense arrays of podo-prints largely localized at the periphery of the T cell–EC interface under symmetrical lamellipodia (Fig. 2B, example 1, and Supplemental Video 3). A minority (~20–30%) of the iT_{mem} cells formed rosette-type podo-print arrays that lacked bias for the cell periphery (Fig. 2B, example 2, and Supplemental Video 4). In both cases, podo-prints/ILPs were significantly stabilized (lifetimes of ~18 min; Fig. 2C) and exhibited limited lateral translocation (0.31 ± 1.5 μm; Fig. 2D–F). After ~30 min of contact, ILPs began to disappear and T cells initiated transmigration (Supplemental Video 4 and data not shown).

As confirmation that the earlier observations reflected three-dimensional podo-prints in response to T cell ILPs, we cotransfected endothelium with mem-DsRed together with soluble GFP as a marker for cytoplasmic volume (34). This showed individual fluorescent membrane rings of each podo-print, in fact, represented cytosol-displacing invaginations into the EC surface (Fig. 3A). Furthermore, confocal imaging showed that podo-prints were ICAM-1–enriched cylindrical EC invaginations into which T cell ILPs extended (Fig. 3B, Supplemental Video 5). ILPs were enriched in LFA-1 (Fig. 3B), F-actin (Fig. 3C), and talin (Fig. 3D), similarly to invadosomes (35, 36). Analogous structures formed under physiologic shear flow (Supplemental Fig. 2A), with diverse ECs (including HLMVECs [Fig. 3A, 3C, 3D], HUVECs [Fig. 3B], HDMVECs [data not shown]), with nT_{mem} (Supplemental Fig. 2B), and with alternate Ag (Fig. 3B, Supplemental Fig. 2D). Similar structures also formed when previously activated murine OT-II $CD4^+$ T cells were incubated on heart microvascular ECs pulsed with OVA 323–339 peptide Ag (Supplemental Fig. 2E).

To assess the T cell–EC interaction in greater detail, we used transmission electron microscopy. In the absence of Ag, ILPs averaged 430 ± 34 nm in depth and 348 ± 33 nm in width (Fig. 3E, 3F). In the presence of Ag, ILPs were similar in morphology and size (depth = 437 nm, width = 277 nm), but tended to form in denser clusters (Fig. 3E–G). An important feature of the ILPs, whether in the absence or presence of Ag, was the existence of zones of extremely close T cell–EC apposition, typically at the tips of the ILPs as if driven by ILP extension (Fig. 3F, 3G, arrows). Although not exclusive to these locations, quantitative analysis revealed that intercellular contacts of <20 nm were 9-fold greater at ILP tips compared with other regions. The idea that ILPs can exert significant force is supported by their ability to both drive

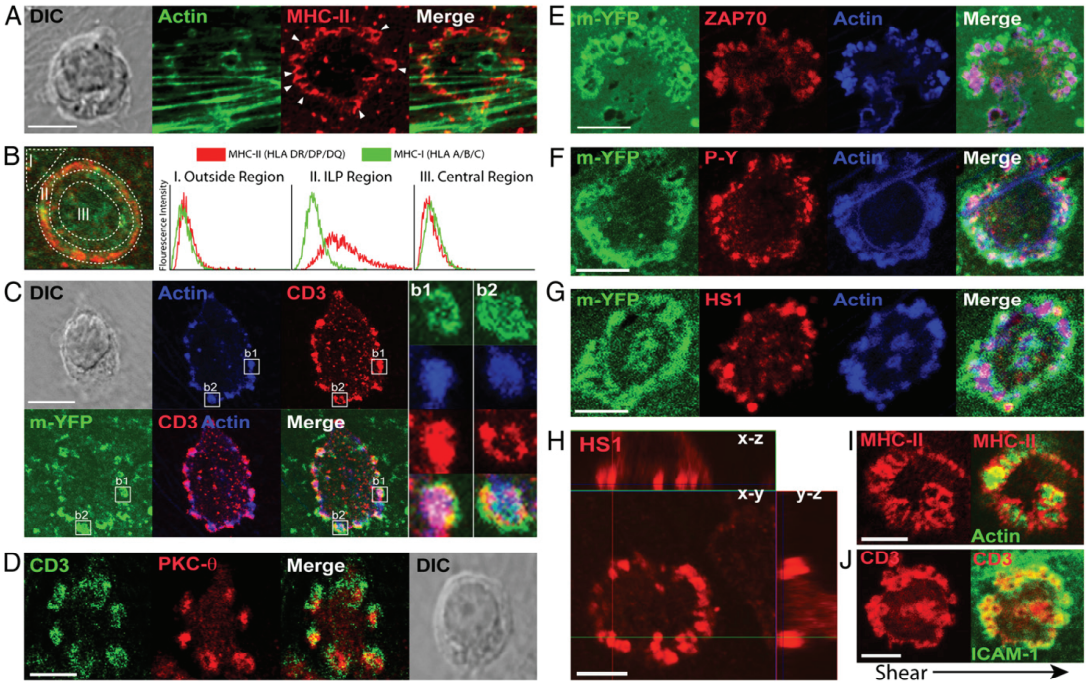

FIGURE 4. Ag stabilized ILPs are foci for immune signaling. IT_{mem} cells were incubated with activated, Ag pulsed (TSST/SEB) HLMVEC for 5 min, fixed, and stained as indicated and imaged by confocal microscopy. (**A**) Ag-stabilized ILPs (F-actin, green) protrude into MHC-II (red)–enriched podo-prints. Arrows indicate MHC-II–enriched podo-prints. (**B**) Samples as in (A) were stained for MHC-II (HLA-DR/DP/DQ; red) and MHC-I (HLA A/B/C; green). Schematic of gated regions of interest is shown on the *left* and included a region outside of the IS (I), the ILP-rich region of the IS (II), and the central region of the IS (III). *Right panels* show pixel fluorescence intensity histograms for regions I–III. (**C**) ILPs (F-actin, blue) protruding into podo-prints (mem-YFP, green) are enriched in CD3 (red). Within individual ILPs, CD3 is predominantly focused at the tip (**b1**) and, to a lesser extent, the edge (**b2**). (**D**) PKC-θ (red) is enriched with CD3 (green) in ILPs. (**E**–**G**) ILPs (F-actin, blue) colocalize with ZAP70 (E; red), phosphotyrosine (F; red), and HS1 (G; red). (**H**) HS1 (red) is highly enriched in ILPs. Cross-sectional views from serial-section confocal microscopy are shown of a lymphocyte adherent to the endothelium-presenting Ag. See three-dimensional rotation in Supplemental Video 6. (**I** and **J**) ILP arrays were allowed to form as above with the additional presence of physiologic laminar fluid shear flow (2.0 dyne/cm^2; arrow indicates direction). (I) MHC-II (red) and F-actin (green) are shown. (J) CD3 (red) and ICAM-1 (green) are shown. Scale bars, 5 μm.

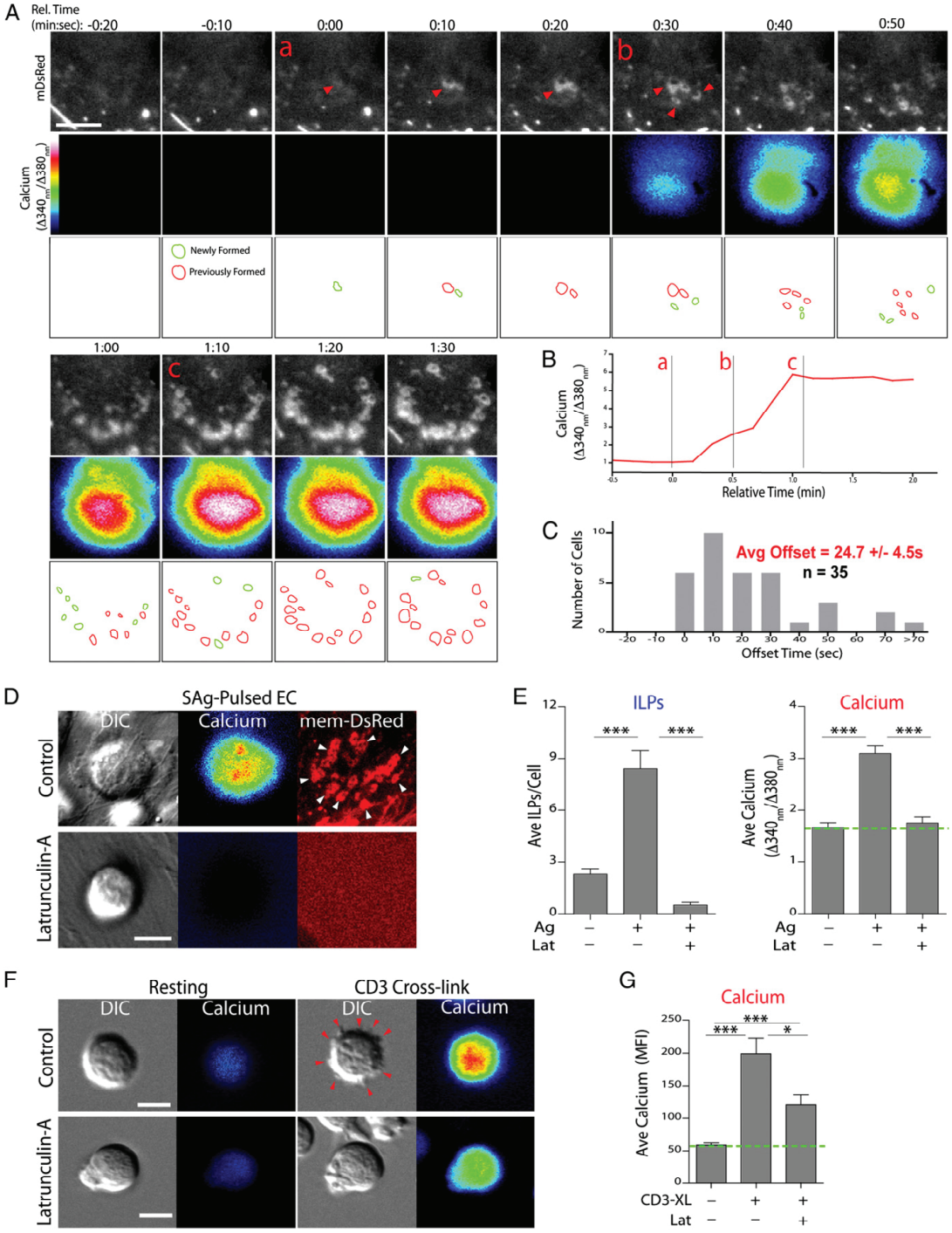

FIGURE 5. T cell ILP formation precedes and supports efficient Ag recognition. (**A**) IT_{mem} were labeled with Fura-2 and imaged live (at a maximal temporal resolution of 10 s) during migration on mem-DsRed–transfected, Ag-pulsed HLMVECs. *Upper panels* show mem-DsRed. Arrows indicate initial ILP formation. *Middle panels* indicate calcium flux values on a rainbow scale. *Lower panels* provide a schematic representation of newly formed (green) and previously formed (in relation to previous field; red) podo-prints. (**a**) Frame of initial ILP/podo-print. (**b**) Frame when calcium flux rises above background. (**c**) Frame when the peripheral ILP array is stabilized. Note this correlates with peak calcium flux. See also (*Figure legend continues*)

transcellular diapedesis (34) and to displace/deform organelles such as the nucleus (Fig. 3F).

Ag-stabilized ILPs share features of traditional TCR signaling microclusters

To address how these ILP-dominated cell–cell interfaces relate to TCR signaling, we stained for traditional IS markers (15, 20, 21). Confocal microscopy revealed that podo-prints on endothelium were modestly, but consistently, enriched in MHC-II compared with MHC-I or mem-YFP (Fig. 4A, 4B, Supplemental Fig. 3A), whereas T cell ILPs were enriched in CD3 (Fig. 4C, Supplemental Fig. 3B). Comparable enrichment formed under physiologic shear flow (Fig. 4I, 4J). In <5% of T cells, CD3 was distributed into a central supramolecular activation cluster–like cluster rather than in peripheral ILPs (Supplemental Fig. 3C).

Molecules implicated in TCR signaling, including PKC-θ (Fig. 4D, Supplemental Fig. 3D), ZAP70 (Fig. 4E), and phosphotyrosine (Fig. 4F) were also enriched in ILP cores, suggesting active signaling at these sites. The cortactin homolog HS1, a known regulator of both podosomes and ISs (38, 42–44), showed particularly strong enrichment (Fig. 4G, 4H, Supplemental Video 6). Alternatively, the inhibitory molecules CD43 and CD45 localized primarily to the region outside of the T cell–EC interface (Supplemental Fig. 3B). These observations suggest that ILPs may serve as discrete loci for TCR signaling with general features similar to TCR signaling microclusters and "multifocal" synapses (15, 21, 22, 45–47).

Collectively, these experiments show that CD4 iT_{mem} activation caused by EC MHC-II/Ag is coupled to cell–cell interfaces dominated by arrays of ILPs that are enriched in TCR signaling molecules. We term this previously undescribed architecture, which shares features of both podosome belts/rosettes and multifocal ISs, a "podo-synapse."

ILPs support efficient Ag recognition and sustained signaling

To determine the functional relationship between ILP formation and T cell activation, we concomitantly monitored calcium flux and ILP dynamics. In the presence of Ag, calcium flux was evident shortly after the first appearance of ILPs. It then peaked several minutes later and gradually decayed over the following 5–60 min (Fig. 5A, 5B, Supplemental Video 7). Calcium flux always occurred subsequent to (or in the same 10-s interval as) the appearance of at least one ILP, with an average offset time of ∼25 s (Fig. 5C). In turn, stabilized ILP arrays and symmetric lamellipodia became evident in the ∼30–60 s following the increase in calcium (Fig. 5A, 5B, Supplemental Video 7).

These observations suggested that the close intercellular contacts driven by ILPs may promote initial Ag recognition and TCR triggering. Testing this hypothesis is challenging because both ILPs and TCR signaling are fundamentally dependent on F-actin assembly and many of the same actin regulatory pathways (34, 35, 38, 42–44, 48). Thus, we simply compared effects of F-actin inhibition (via latrunculin A) on T cell activation through an Ag-pulsed APC versus direct TCR cross-linking. When stimulated by Ag-pulsed ECs, iT_{mem} pretreatment with latrunculin A caused 100% blockade of both ILP formation and calcium flux during the first 5 min of coincubation (Fig. 5D, 5E). By contrast, when TCRs were stimulated directly by anti-CD3/CD28 cross-linking, significant (although attenuated by ∼60%), immediate calcium flux was elicited in the presence of latrunculin A (Fig. 5F, 5G), as shown previously (49). From this we conclude that the total latrunculin A-induced blockade of early response to Ag-pulsed ECs reflects a defect in initial Ag recognition/TCR triggering (Fig. 5F, 5G). We speculate that ILP formation may represent the latrunculin A-sensitive process behind this defect.

Calcium flux is necessary and sufficient for Ag-mediated ILP stabilization

Next, we investigated the transition from dynamic ILP probing to formation of stable ILP arrays. Given the correlation between increase in calcium and appearance of ILP arrays, we hypothesized that calcium may be key for stabilizing ILPs. To test this, we pretreated T cells with the calcium chelator BAPTA and the CRAC channel inhibitor BTP2. On Ag-pulsed ECs, this greatly inhibited calcium flux in iT_{mem}, which correlated with strong reduction in the number of stabilized ILPs (Fig. 6A–C). To determine whether calcium flux was sufficient to stabilize ILPs, iT_{mem} were incubated on ECs in the absence of Ag, followed by application of thapsigargin to directly increase intracellular calcium. This caused iT_{mem} already engaged in dynamic ILP probing to arrest migration and stabilize ILP clusters (Fig. 6D–G). Thus, whereas dynamic ILP probing of ECs by iT_{mem} seems to facilitate initial Ag recognition, the resulting increase in calcium is both necessary and sufficient to drive accumulation/stabilization of ILPs into podo-synapses.

The earlier findings point to a positive feedback loop for sustaining TCR signaling. To break this loop, we sought to block proximal signaling downstream of calcium flux, specifically targeting CAMKII via the inhibitor CK59 (50). Treatment with CK59 attenuated Ag-mediated ILP stabilization by ∼50% (Fig. 6H), which was coupled to a proportional decrease in calcium flux (Fig. 6I). This result supports the interdependence between ILPs and calcium flux.

CD8 CTLs use ILPs to probe for Ag

The endothelium has been shown to initiate MHC-I/Ag-dependent activation of CD8 CTLs leading to direct killing of ECs (31, 32). To investigate these responses, we incubated previously activated murine OT-I CD8 T cells on murine heart microvascular ECs pulsed with SIINFEKL peptide Ag. Ag-pulsed ECs initiated a rapid calcium flux (Fig. 7A) that was coupled to progressive specific lysis of ECs over a 4-h duration (∼50% lysis ∼2 h; Fig. 7B). Live-cell imaging showed that in the absence of Ag, CTLs avidly probed the endothelium with dynamic ILPs while migrating without fluxing calcium (Fig. 7C, Supplemental Video 8). In the presence of Ag, initial ILPs were rapidly followed by calcium flux (offset time = 32.8 ± 6.6 s), which then led to migrational arrest and formation of peripheral ILP arrays similar to those formed by CD4 effector T cells (Fig. 7D, 7E). Thus, T cell ILPs seem to be a general feature of Ag sensing on ECs.

Supplemental Video 7. (**B**) Graphical representation of calcium flux with *frames a–c* noted. (**C**) Quantitation of ILP-calcium flux offset time. Live-cell imaging was as in (A) and offset time (time from when first ILP forms until calcium flux rises above background) was calculated. Data were binned into 10-s intervals, and average ± SEM is shown for 35 individual T cells from 3 separate experiments. (**D**) Imaging was performed as in (A) with additional pretreatment of T cells with latrunculin A before addition to Ag-pulsed EC monolayers. (**E**) Podo-print/ILP index (average number of podo-prints/ILPs per cell) and average calcium flux at 5 min was calculated. Both analyses are pooled mean ± SEM from three separate experiments. (**F**) IT_{mem} were labeled with Fluo-4 and imaged live with anti-CD3/CD28 cross-linking with or without latrunculin A pretreatment. *Left panels* show resting T cells. *Right panels* show activated T cells imaged 60 s after addition of cross-linking Abs. Arrows indicate de novo formation of micron-scale T cell protrusions. (**G**) Average calcium flux was calculated from three separate experiments as in (F). Scale bars, 5 μm. Data represent mean ± SEM. $*p < 0.05$, $***p < 0.0005$.

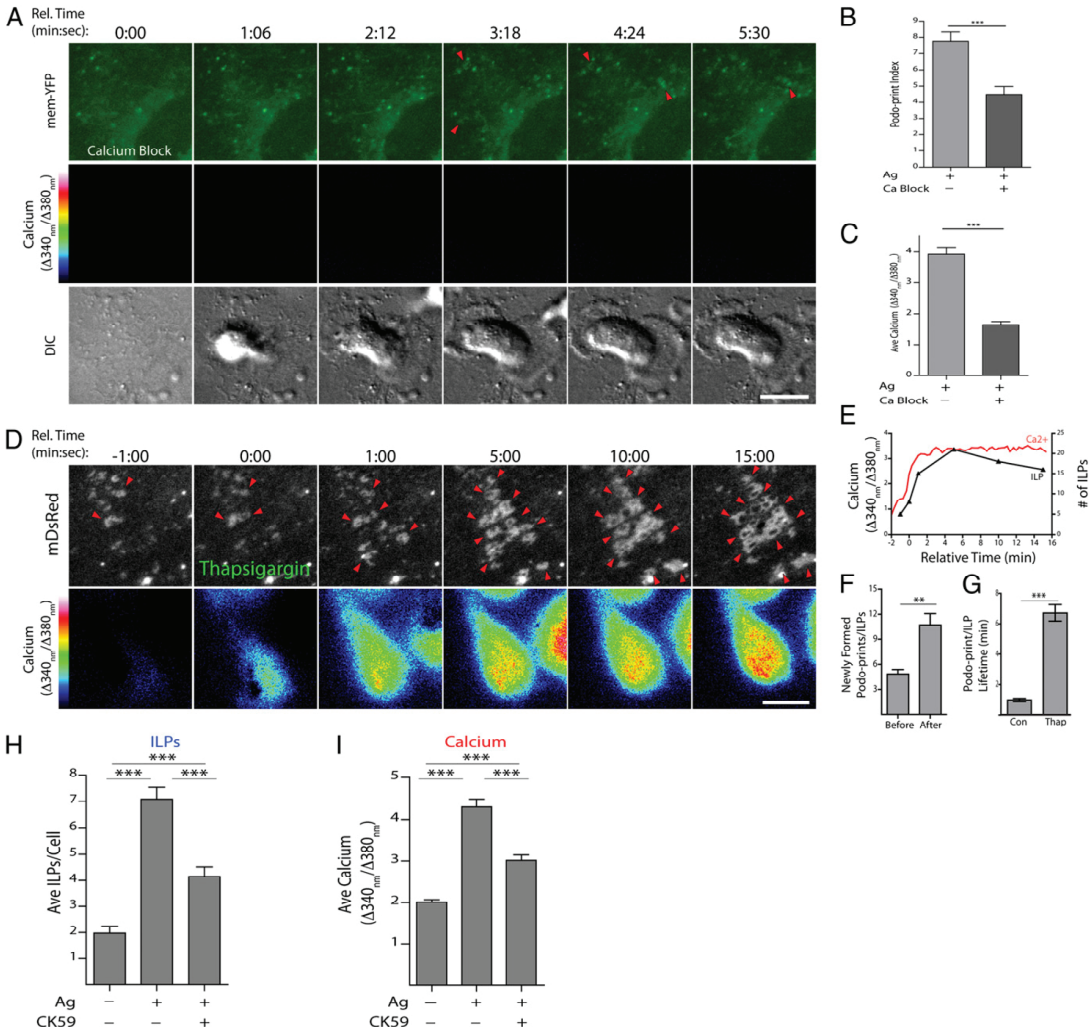

FIGURE 6. Calcium flux is necessary and sufficient for ILP stabilization. (**A**) IT_{mem} were Fura-2 labeled, pretreated with the calcium chelator BAPTA and the CRAC channel inhibitor BTP2, and imaged live on Ag-pulsed ECs. Arrows indicate a few sporadically formed podo-prints. (**B** and **C**) Podo-print/ILP index (B) and average calcium flux (C) were calculated at 5 min for experiments as in (A). (**D**) Live-cell imaging was conducted in the absence of Ag before and after addition of the calcium ionophore thapsigargin (at time = '0:00'). Arrows indicate ILPs/podo-prints. (**E**) Correlation of calcium flux with ILP number after addition of thapsigargin. (**F**) Quantitation of the number of newly formed ILPs in the 2 min before and after addition of thapsigargin. (**G**) Quantitation of the lifetime of ILPs with or without addition of thapsigargin. (**H** and **I**) Imaging and analysis was performed as in (A)–(C) except T cells were pretreated with the CAMKII inhibitor CK59. Data represent mean ± SEM. Scale bars, 5 μm. $^{**}p < 0.005$, $^{***}p < 0.0005$.

A planar-coated cell model for Ag recognition

We next considered whether ILPs either represent unique features of T cell–endothelial Ag recognition or may be more broadly relevant and uniquely revealed by endothelium. We speculated that the rigidity of coated substrate models may frustrate/mask ILP formation, whereas orientation/resolution issues might obscure detection of ILPs with traditional cellular APCs (16–18).

First, we simply asked whether evidence consistent with ILPs could be detected in a coated glass model (Fig. 8A). IT_{mem} plated on glass coated with ICAM-1 and anti-CD3 (but not anti-CD43/CD45) Ab rapidly fluxed calcium (Supplemental Fig. 4A–C). IRM revealed that initial "microcontacts" (~0.2- to 1-μm dots consistent with T cell ILPs and/or microvilli) always preceded calcium flux (Supplemental Fig. 4B, 4C; offset time = 21.4 s). New microcontacts also continued to form after T cell spreading (Fig. 8B, Supplemental Fig. 4D, 4E, Supplemental Video 9).

We hypothesized that these microcontacts at least partly reflected ILP activity that was mechanically frustrated by the rigid substrate. To test this, we designed a "coated-cell APC" model whereby the earlier Ab-coated glass substrate was recapitulated on the surface of a deformable CHO-K1 cell (Fig. 8C, Supplemental Fig. 4F). In this setting, clear three-dimensional ILP arrays were readily detected that were coupled to calcium flux (Fig. 8D, Supplemental Video 10). As with iT_{mem} on ECs, initial ILPs al-

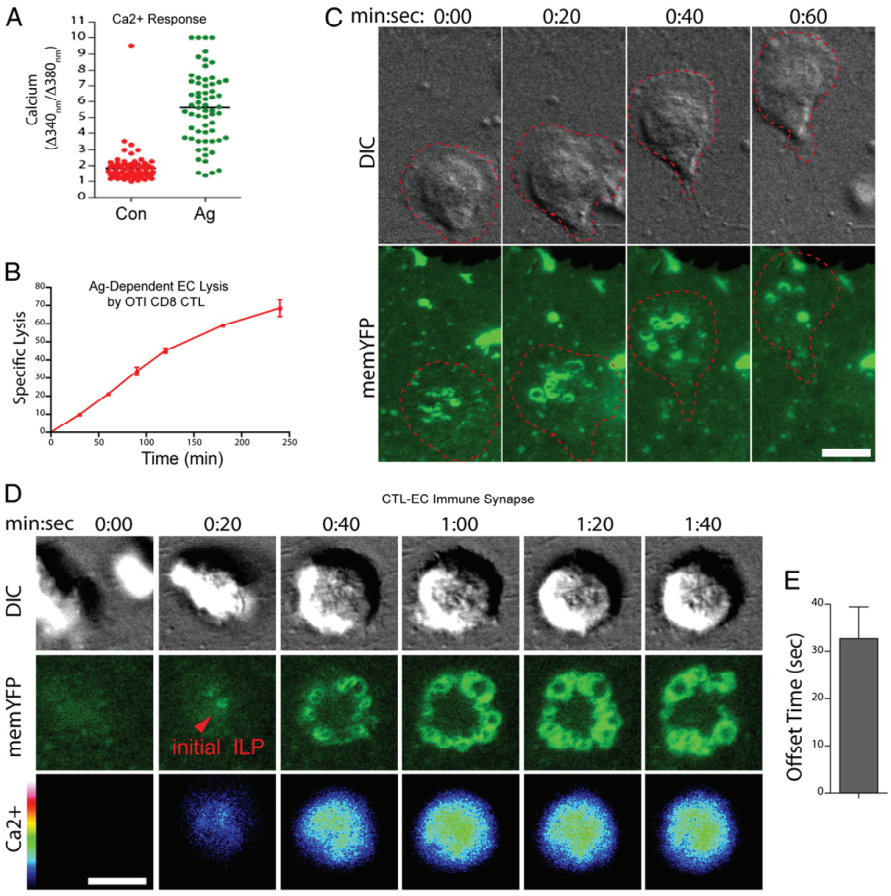

FIGURE 7. Murine CD8 CTLs use ILPs to sense Ag-bound MHC-I on endothelium. (**A**) Previously activated murine OTI CD8 T cells (CTLs) were imaged on mem-YFP–transfected, mouse heart microvascular ECs pulsed with SIINFEKL. Individual ratiometric calcium flux values at 5 min were plotted for ±Ag conditions. (**B**) CTLs were added to mixed cultures of Ag-pulsed/unpulsed ECs, and percentage of specific lysis is plotted at indicated time points. (**C**) CTLs were imaged during EC probing in the absence of Ag. Differential interference contrast and mem-YFP are shown in the *upper* and *lower panels*, respectively. Dashed line represents the outline of the migrating CTL under which transient ILPs are continuously formed. See also corresponding Supplemental Video 8. (**D**) Imaging was conducted as in (C) on ECs pulsed with SIINFEKL. Red arrow indicates initial ILP formation preceding calcium flux. (**E**) Average offset time for calcium flux relative to initial ILP formation. Data represent mean ± SEM. Scale bars, 5 μm.

ways preceded (Supplemental Fig. 4G; offset time ~56 s) and seemed to functionally support (Fig. 8E, 8F) initiation of calcium flux. These findings suggest a general tendency of memory/effector T cells to use ILPs to probe diverse substrates for recognition and response to Ag (as modeled in Fig. 9).

ILPs are involved in recognition of Ag presented by professional APCs

Next, we re-examined Ag recognition with professional APCs. Thus, iT_{mem} were incubated with Priess B cells pulsed with Ag and imaged by confocal microscopy. Equatorial cross sections recapitulate classic views (12) of the T cell–B cell IS whereby T cell LFA-1 shows enrichment in peripheral-supramolecular activation cluster–like peripheral membrane bulges (Supplemental Fig. 4H, *inset* 2, arrows). Cross sections taken at the edge of the IS additionally suggest presence of LFA-1–rich finger-like protrusions (Supplemental Fig. 4H, *insets* 1a–d) similar to ILPs formed on ECs (Fig. 3Bb). More compelling imaging of putative ILPs can be seen in occasional examples where the T cells settle on top of B cells such that the IS aligns with the optimal imaging plane (18) (Fig. 8G, Supplemental Video 11). Ultrastructural views, evident in a subset of micrographs, further support the presence of ILPs (Fig. 8H).

Finally, we investigated murine OTII CD4 T cells incubated with BMDCs coexpressing mem-YFP and soluble DsRed. T cells interacted with DCs both laterally (Fig. 8I, subset a) and to a lesser extent through en face contacts (Fig. 8I, subset b). In the former, side views of DC invaginations were readily evident that were similar to podo-prints/ILPs seen on endothelium (Fig. 8I, *panel* 3i). En face interactions also revealed discrete circular podo-prints/ILPs (Fig. 8I, *panels* 3ii, 3iii), although these were generally less obvious than those formed on endothelium because of the highly active and irregular surface topology of DCs. Dynamic imaging showed ILP probing preceded calcium flux, which, in turn, was coupled to peripheral ILP array formation (Fig. 8J). Ultrastructural confirmation of ILP formation could also be obtained

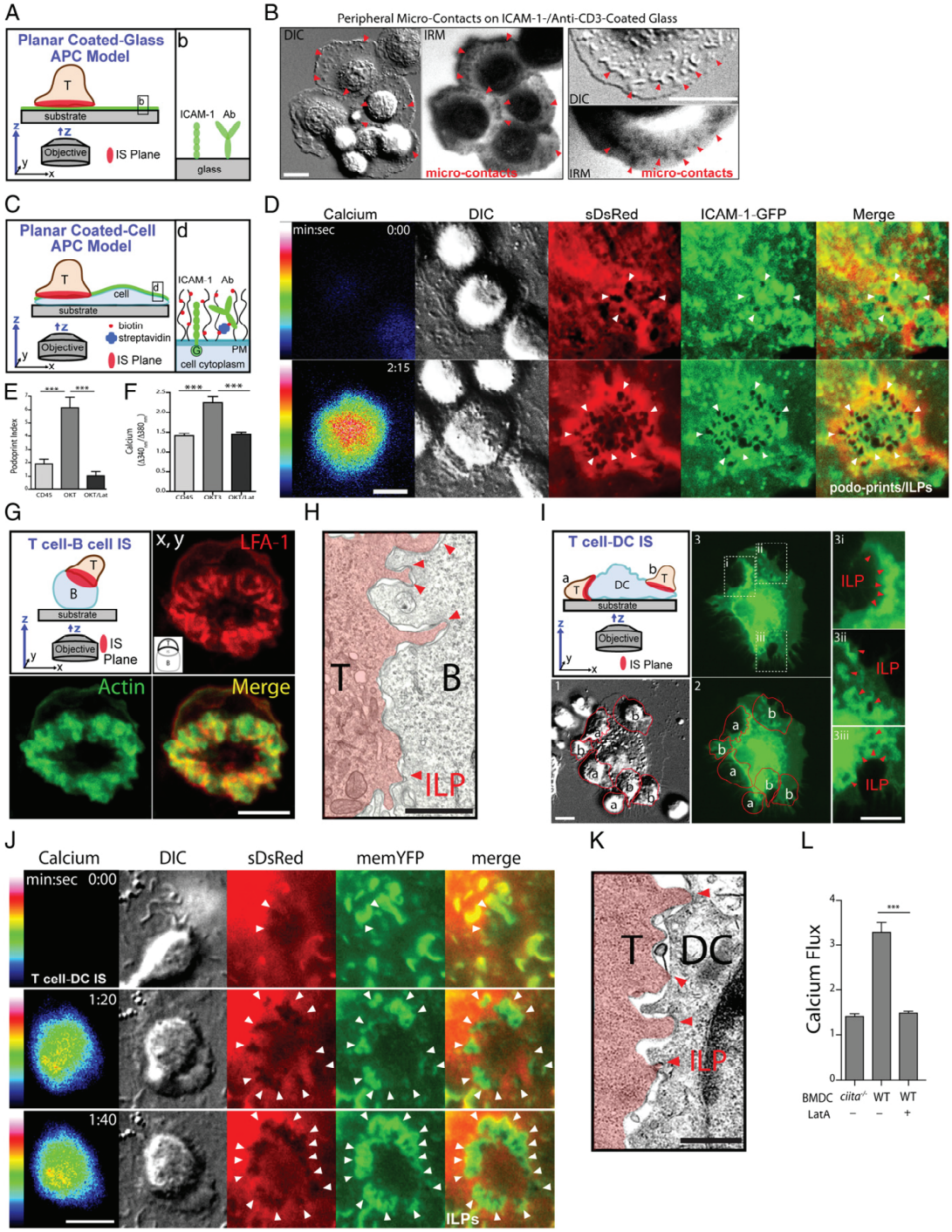

FIGURE 8. ILPs facilitate Ag recognition on professional APCs. (**A**) Schematic of the "coated-glass model" using ICAM-1– and Ab-coated glass. (**b**) Magnified view of the interaction surface. (**B**) iT_{mem} were added to an ICAM-1–Fc– and anti-CD3–coated glass chamber and imaged by differential interference contrast and IRM. Arrows indicate IRM-detected "microcontacts." (**C**) Schematic of the "planar coated-cell APC model." CHO-K1 cells expressing ICAM-1–GFP and soluble DsRed were surface "coated" with Abs against CD3, CD43, or CD45 using a biotin/SA capture approach (see also Supplemental Fig. 4F). (**d**) Magnified view of the interaction surface. (**D**) Cells prepared as in (C) coated with anti-CD3 Ab were (*Figure legend continues*)

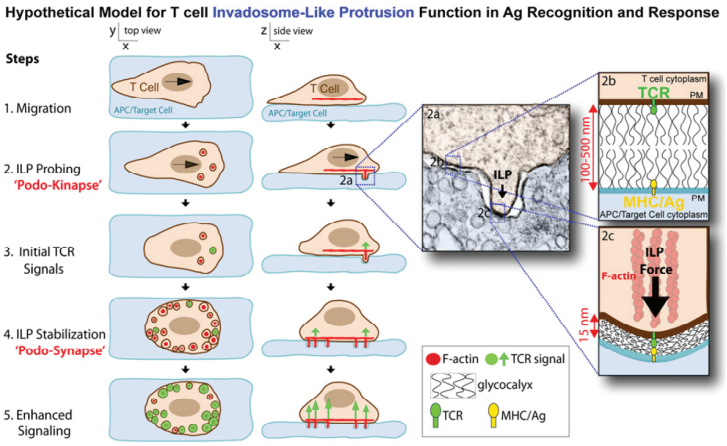

FIGURE 9. Hypothetical model for ILP function in Ag recognition and response. Schematic depicts top-down and side views of a memory/effector T cell interacting with an APC/target cell. Lymphocytes initiate lateral migration (Step 1) and begin to dynamically drive ILPs against the apposing cell (Step 2, **2a**). Close interactions between T and APC/target cells, which are partially opposed by the cell glycocalyces (**2b**), form preferentially (but not exclusively) at ILP tips (**2c**). We hypothesize that TCR/MHC interactions may be facilitated in these zones. Initial calcium released on Ag recognition (green overlay/arrows; Step 3) seems to be coupled to stabilization/accumulation of ILP arrays ("podo-synapses"; Step 4), which we hypothesize could, in turn, help sustain/enhance signaling (Step 5).

in a subset of electron micrographs (Fig. 8K). Finally, treatment of T cells with latrunculin A strongly inhibited both ILPs and initial calcium responses to Ag presented by DCs (Fig. 8L).

Discussion

Basic cellular mechanisms by which lymphocytes effectively scan for peptide Ag on apposing cells and how this leads to IS formation have remained mysterious. Our results investigating endothelium as a model APC indicate potential roles for ILPs in these processes. Our further studies with diverse Ag recognition settings suggest broad, previously unappreciated functions for ILPs as actuators of immune surveillance.

Vascular ECs represent intriguing and understudied APCs/target cells for adaptive immune responses. These MHC-I–, MHC-II–, and costimulator-expressing cells are strategically positioned at the blood–tissue interface to serve as unique sentinels for the immune system (26). Previous studies demonstrated that ECs can effectively restimulate memory/effector, but not naive, T cells (26–33). Thus, ECs have been hypothesized to serve as peripheral ancillary or "semiprofessional" APCs that contribute to the effector phase of adaptive immune responses. Although overall roles remain controversial, studies suggest that Ag presentation by ECs can influence T cell activation, differentiation, trafficking, and memory (26–28, 51). In this study, we demonstrate that CD4 and CD8 memory/effector T cells exhibited a transient arrest in migration coupled, respectively, to Th1 and cytotoxic responses on ECs presenting MHC/Ag, consistent with previous findings (31, 52, 53).

Importantly, ECs exhibit a virtually planar cell surface in vitro, which we previously established to be ideal for high spatiotemporal resolution imaging of topological dynamics (34). We reasoned that ECs might, therefore, serve as physiologic "planar APC/target cell" models uniquely suited to fill two key gaps in our understanding of immune surveillance mechanisms: 1) how initial MHC/Ag-sampling contacts form between T cells and APCs, and 2) how these lead to formation of productive ISs. Although planar APC substrates (i.e., lipid bilayers, Ab-coated glass) provide excellent imaging, which has led to critical insights to these dynamics (15, 19–22), such models are inherently limiting. Alternatively, details of physiologic cell–cell scanning dynamics are profoundly obscured by orientation-related imaging issues (16–18). The imaging afforded with our planar endothelial APC model in this study revealed unexpected involvement of ILPs in Ag recognition and response activities.

ILPs ("invadosome-like protrusions") are lymphocyte equivalents (36) to podosomes (formed largely by myeloid lineage cells) and invadopodia (formed by transformed cells), collectively termed "invadosomes" (35). Invadosomes and ILPs are actin-dependent cylindrical, protrusive organelles (~200–1000 nm in diameter and depth) that form on the ventral surface of migratory cells (35). Distinct from invadosomes, characterized to form on matrix, bone, glass/plastic substrates, T cell ILPs have only been seen on cellular substrates, as shown in a range of in vitro (34, 54, 55) and in vivo studies (reviewed in Ref. 56). In such settings, dynamic ILP probing seems to function in migratory pathfinding,

imaged live on addition of Fura-2–labeled iT_{mem}. *Panels* demonstrate relatively early and later phases of interaction as indicated. Arrows indicate podoprints/ILPs. See also Supplemental Video 10. (**E** and **F**) Imaging experiments were conducted as in (D), but T cells were pretreated with latrunculin A. Podoprint/ILP index (E) and calcium flux (F) were calculated. (**G**) IT_{mem} were incubated with Ag-pulsed Priess B cells for 5 min and stained for LFA-1 and actin. Image represents a three-dimensional projection of T cell settled on top of the B cells with the IS forming more nearly parallel to the *x*–*y* imaging plane. See also Supplemental Video 11. (**H**) Transmission electron micrograph of T cell–B cell IS as in (G). The T cell is identified by a red overlay. Arrows indicate close intercellular contacts formed by T cell ILPs. (**I**) Schematic (*upper left panel*) shows both lateral (a) and various en face (b) interfaces typically formed in vitro between T cells and the highly irregular surfaces of DCs. (**1**) and (**2**) show previously activated murine CD4 OT-II lymphocytes interacting with Ag-pulsed mem-YFP–transfected DCs (green, 2). Red outlines depict T cell perimeter based on DIC imaging (1). (**3**) is identical to (2) but shows three boxed regions (**i–iii**) expanded on the *left*. (3i) shows a lateral interaction in which the T cell has pushed small finger-like invagination into the side of the BMDC putatively formed by ILPs (arrows). (3ii) and (3iii) show en face interactions whereby ILPs seem to be extending normal to the imaging plane, giving rise to the typical ring-shaped podo-print appearance observed in endothelium (i.e., Fig. 2). (**J**) DCs were transfected with soluble monomeric DsRed and mem-YFP, pulsed with Ag, and CD4 OT-II T cells were added. *Panels* show cytoplasm displacing podo-prints/ILP (arrows), which precede calcium flux and are stabilized after calcium flux. (**K**) Transmission electron micrograph of T cell–DC IS as in (J) fixed after 5 min. The T cell is identified by a red overlay. Arrows indicate close intercellular contacts formed by T cell ILPs. (**L**) Calcium flux of previously activated CD4 OTII T cells 8 min after interaction with C57BL/6 (WT) or *Ciita*$^{-/-}$ Ag-pulsed DCs with or without latrunculin A pretreatment. Data represent mean ± SEM. Scale bars, 5 μm. ***$p < 0.0005$.

apparently serving as biomechanical sensors (34, 36, 54, 55, 57). These studies suggest that ILPs may also facilitate biochemical or "informational" scanning of diverse cell surfaces.

We speculated that the ILP scanning seen on ECs was uniquely revealed by this setting, rather than a unique feature of it. IRM imaging of a rudimentary APC model (anti-CD3–coated glass) showed that T cells form a series of microcontacts with the substrate that are consistent with either ILP or microvilli interactions. Similar microcontacts were previously shown to be enriched in F-actin, WASP, and TCR, and hypothesized to represent frustrated podosomes (20, 22). When we tested this hypothesis by recapitulating the same anti-CD3 activation stimuli on a pliable cell surface, we, indeed, found that the microcontacts transitioned into three-dimensional ILPs and podo-prints. Moreover, our studies using approaches optimized for imaging professional APCs (i.e., B cells and DCs) readily detected ILPs probing in these settings. Importantly, although dynamics, molecular composition, and three-dimensional architectures were not defined, extensive (largely EM-based) studies previously evidenced similar T cell protrusions extending against diverse APCs and target cell surfaces (21, 43, 58–63). Collectively, this suggests broad relevance for memory/effector T cells probing their cellular environment with ILPs. The important question of whether naive T cells similarly use ILPs remains to be addressed.

One possible role for ILP probing may be in enhancing the efficiency of Ag recognition. The act of Ag detection requires T cell and APC/target membranes to come within ~14 nm of each other (2, 64). Yet, all cell membranes are extensively shielded by ~50- to 500-nm-thick glycocalyces (3–5) that physically oppose close contact and negatively modulate immune recognition (5–10) (Fig. 9, *inset* 2b). In the periphery, patrolling effector/memory lymphocytes must effectively scan the surfaces of widely varying cell types (indeed, essentially any host cell could become a target), each with glycocalyces of different thicknesses and physicochemical properties. Forces provided by ILP (which form independently of Ag during lateral migration) (34) are sufficient to deform nuclear lamina, displace and distort cytoskeleton and intracellular organelles, and promote transcellular diapedesis (34). More than sufficient energy would, therefore, seem to be available at the tips of ILPs (Fig. 9, *inset* 2a) to overcome repulsion provided by the glycocalyx (Fig. 9, *inset* 2c).

Previous studies showed that lamellipodia of migrating lymphocytes are zones of heightened Ag recognition efficiency (65–67). In both our previous (34) and current work, we show that lamellipodia are also the predominant areas of ILP formation. Moreover, in our experimental system, ILPs, but not necessarily lamellipodia, consistently preceded calcium flux. Thus, although migration behaviors are necessary for immune surveillance, ILPs may function more directly in promoting intimate contacts, and thereby ensuring efficient Ag sampling. Our studies with latrunculin A are consistent with (although do not prove) such functional roles. It is also interesting to note that forces and membrane bending associated with ILPs are consistent with the hypothesized force-based mechanism for formal triggering of TCR signaling (22, 68–71). ILPs are probably not absolutely required for either TCR signaling or forming intimate T cell–APC/target contacts, but rather act to ensure efficiency and fidelity of immune surveillance.

Another possible function for ILPs may be to support signal amplification and sustenance. Our studies reveal dense arrays of calcium-stabilized ILPs that dominate the IS after Ag recognition. Individual ILPs showed enrichment in TCR and molecules suggestive of active signaling. This feature is generally not unlike TCR signaling microclusters defined using planar APC model substrates (14, 15, 20–22, 38, 72, 73), with the key distinction that ILPs have a discrete three-dimensional architecture. The well-developed concept that microclusters may function as "signalosomes" to amplify and sustain signaling by concentrating important molecules/activities might then be extended to include limited "reaction volumes" formed within ILPs (17, 74–78). In addition, the stable peripheral ILP arrays are strikingly similar to osteoclast "podosome-belts" (79, 80) that form sealing zones for directed secretion of bone-degrading enzymes (81). Thus, it may be hypothesized that peripheral podo-synapses may function analogously for directed secretion of cytokines or cytotoxic materials.

These studies collectively support the hypothesis that ILPs may serve as newly appreciated sensory organelles that facilitate Ag recognition and responses. By virtue of physical force exertion, ILPs literally allow T cells to get a deeper understanding of their local cellular environment. Such proactive "informational scanning" might ensure robust sampling of MHC/Ag on diverse cell types. It is tempting to speculate that stabilized TCR-enriched ILPs resulting from Ag recognition represent a clearer, more physiologic view of TCR microclusters and "multifocal" ISs characterized to date.

Disclosures

The authors have no financial conflicts of interest.

References

1. von Andrian, U. H., and C. R. Mackay. 2000. T-cell function and migration. Two sides of the same coin. *N. Engl. J. Med.* 343: 1020–1034.
2. Rudolph, M. G., R. L. Stanfield, and I. A. Wilson. 2006. How TCRs bind MHCs, peptides, and coreceptors. *Annu. Rev. Immunol.* 24: 419–466.
3. Weinbaum, S., J. M. Tarbell, and E. R. Damiano. 2007. The structure and function of the endothelial glycocalyx layer. *Annu. Rev. Biomed. Eng.* 9: 121–167.
4. Bell, G. I., M. Dembo, and P. Bongrand. 1984. Cell adhesion. Competition between nonspecific repulsion and specific bonding. *Biophys. J.* 45: 1051–1064.
5. Springer, T. A. 1990. Adhesion receptors of the immune system. *Nature* 346: 425–434.
6. Gubbels, J. A., M. Felder, S. Horibata, J. A. Belisle, A. Kapur, H. Holden, S. Petrie, M. Migneault, C. Rancourt, J. P. Connor, and M. S. Patankar. 2010. MUC16 provides immune protection by inhibiting synapse formation between NK and ovarian tumor cells. *Mol. Cancer* 9: 11.
7. Komatsu, M., L. Yee, and K. L. Carraway. 1999. Overexpression of sialomucin complex, a rat homologue of MUC4, inhibits tumor killing by lymphokine-activated killer cells. *Cancer Res.* 59: 2229–2236.
8. Tsuboi, S., and M. Fukuda. 2001. Roles of O-linked oligosaccharides in immune responses. *Bioessays* 23: 46–53.
9. van de Wiel-van Kemenade, E., M. J. Ligtenberg, A. J. de Boer, F. Buijs, H. L. Vos, C. J. Melief, J. Hilkens, and C. G. Figdor. 1993. Episialin (MUC1) inhibits cytotoxic lymphocyte-target cell interaction. *J. Immunol.* 151: 767–776.
10. Manjunath, N., M. Correa, M. Ardman, and B. Ardman. 1995. Negative regulation of T-cell adhesion and activation by CD43. *Nature* 377: 535–538.
11. Shaw, A. S., and M. L. Dustin. 1997. Making the T cell receptor go the distance: a topological view of T cell activation. *Immunity* 6: 361–369.
12. Monks, C. R., B. A. Freiberg, H. Kupfer, N. Sciaky, and A. Kupfer. 1998. Three-dimensional segregation of supramolecular activation clusters in T cells. *Nature* 395: 82–86.
13. Delon, J., S. Stoll, and R. N. Germain. 2002. Imaging of T-cell interactions with antigen presenting cells in culture and in intact lymphoid tissue. *Immunol. Rev.* 189: 51–63.
14. Brossard, C., V. Feuillet, A. Schmitt, C. Randriamampita, M. Romao, G. Raposo, and A. Trautmann. 2005. Multifocal structure of the T cell - dendritic cell synapse. *Eur. J. Immunol.* 35: 1741–1753.
15. Dustin, M. L. 2009. The cellular context of T cell signaling. *Immunity* 30: 482–492.
16. Balagopalan, L., E. Sherman, V. A. Barr, and L. E. Samelson. 2011. Imaging techniques for assaying lymphocyte activation in action. *Nat. Rev. Immunol.* 11: 21–33.
17. Cebecauer, M., M. Spitaler, A. Sergé, and A. I. Magee. 2010. Signalling complexes and clusters: functional advantages and methodological hurdles. *J. Cell Sci.* 123: 309–320.
18. Oddos, S., C. Dunsby, M. A. Purbhoo, A. Chauveau, D. M. Owen, M. A. Neil, D. M. Davis, and P. M. French. 2008. High-speed high-resolution imaging of intercellular immune synapses using optical tweezers. *Biophys. J.* 95: L66–L68.
19. Grakoui, A., S. K. Bromley, C. Sumen, M. M. Davis, A. S. Shaw, P. M. Allen, and M. L. Dustin. 1999. The immunological synapse: a molecular machine controlling T cell activation. Science 285: 221–227.
20. Bunnell, S. C., D. I. Hong, J. R. Kardon, T. Yamazaki, C. J. McGlade, V. A. Barr, and L. E. Samelson. 2002. T cell receptor ligation induces the formation of dynamically regulated signaling assemblies. *J. Cell Biol.* 158: 1263–1275.

21. Yokosuka, T., K. Sakata-Sogawa, W. Kobayashi, M. Hiroshima, A. Hashimoto-Tane, M. Tokunaga, M. L. Dustin, and T. Saito. 2005. Newly generated T cell receptor microclusters initiate and sustain T cell activation by recruitment of Zap70 and SLP-76. *Nat. Immunol.* 6: 1253–1262.
22. Seminario, M. C., and S. C. Bunnell. 2008. Signal initiation in T-cell receptor microclusters. *Immunol. Rev.* 221: 90–106.
23. Dustin, M. L. 2009. Supported bilayers at the vanguard of immune cell activation studies. *J. Struct. Biol.* 168: 152–160.
24. Springer, T. A. 1994. Traffic signals for lymphocyte recirculation and leukocyte emigration: the multistep paradigm. *Cell* 76: 301–314.
25. Butcher, E. C. 1991. Leukocyte-endothelial cell recognition: three (or more) steps to specificity and diversity. *Cell* 67: 1033–1036.
26. Choi, J., D. R. Enis, K. P. Koh, S. L. Shiao, and J. S. Pober. 2004. T lymphocyte-endothelial cell interactions. *Annu. Rev. Immunol.* 22: 683–709.
27. Pober, J. S., and W. C. Sessa. 2007. Evolving functions of endothelial cells in inflammation. *Nat. Rev. Immunol.* 7: 803–815.
28. Marelli-Berg, F. M., K. Okkenhaug, and V. Mirenda. 2007. A two-signal model for T cell trafficking. *Trends Immunol.* 28: 267–273.
29. Marelli-Berg, F. M., R. E. Hargreaves, P. Carmichael, A. Dorling, G. Lombardi, and R. I. Lechler. 1996. Major histocompatibility complex class II-expressing endothelial cells induce allospecific nonresponsiveness in naive T cells. *J. Exp. Med.* 183: 1603–1612.
30. Ma, W., and J. S. Pober. 1998. Human endothelial cells effectively costimulate cytokine production by, but not differentiation of, naive CD4+ T cells. *J. Immunol.* 161: 2158–2167.
31. Perez, V. L., L. Henault, and A. H. Lichtman. 1998. Endothelial antigen presentation: stimulation of previously activated but not naïve TCR-transgenic mouse T cells. *Cell. Immunol.* 189: 31–40.
32. Epperson, D. E., and J. S. Pober. 1994. Antigen-presenting function of human endothelial cells. Direct activation of resting CD8 T cells. *J. Immunol.* 153: 5402–5412.
33. Shiao, S. L., N. C. Kirkiles-Smith, B. R. Shepherd, J. M. McNiff, E. J. Carr, and J. S. Pober. 2007. Human effector memory CD4+ T cells directly recognize allogeneic endothelial cells in vitro and in vivo. *J. Immunol.* 179: 4397–4404.
34. Carman, C. V., P. T. Sage, T. E. Sciuto, M. A. de la Fuente, R. S. Geha, H. D. Ochs, H. F. Dvorak, A. M. Dvorak, and T. A. Springer. 2007. Transcellular diapedesis is initiated by invasive podosomes. *Immunity* 26: 784–797.
35. Linder, S. 2009. Invadosomes at a glance. *J. Cell Sci.* 122: 3009–3013.
36. Carman, C. V. 2009. Mechanisms for transcellular diapedesis: probing and pathfinding by 'invadosome-like protrusions'. *J. Cell Sci.* 122: 3025–3035.
37. Carman, C. V., and T. A. Springer. 2004. A transmigratory cup in leukocyte diapedesis both through individual vascular endothelial cells and between them. *J. Cell Biol.* 167: 377–388.
38. Gomez, T. S., S. D. McCarney, E. Carrizosa, C. M. Labno, E. O. Comiskey, J. C. Nolz, P. Zhu, B. D. Freedman, M. R. Clark, D. J. Rawlings, et al. 2006. HS1 functions as an essential actin-regulatory adaptor protein at the immune synapse. *Immunity* 24: 741–752.
39. Sarkar, D., P. K. Vemula, G. S. Teo, D. Spelke, R. Karnik, Y. Wee, and J. M. Karp. 2008. Chemical engineering of mesenchymal stem cells to induce a cell rolling response. *Bioconjug. Chem.* 19: 2105–2109.
40. Antón, I. M., M. A. de la Fuente, T. N. Sims, S. Freeman, N. Ramesh, J. H. Hartwig, M. L. Dustin, and R. S. Geha. 2002. WIP deficiency reveals a differential role for WIP and the actin cytoskeleton in T and B cell activation. *Immunity* 16: 193–204.
41. Wülfing, C., A. Bauch, G. R. Crabtree, and M. M. Davis. 2000. The vav exchange factor is an essential regulator in actin-dependent receptor translocation to the lymphocyte-antigen-presenting cell interface. *Proc. Natl. Acad. Sci. USA* 97: 10150–10155.
42. Billadeau, D. D., J. C. Nolz, and T. S. Gomez. 2007. Regulation of T-cell activation by the cytoskeleton. *Nat. Rev. Immunol.* 7: 131–143.
43. Butler, B., D. H. Kastendieck, and J. A. Cooper. 2008. Differently phosphorylated forms of the cortactin homolog HS1 mediate distinct functions in natural killer cells. *Nat. Immunol.* 9: 887–897.
44. Klos Dehring, D. A., F. Clarke, B. G. Ricart, Y. Huang, T. S. Gomez, E. K. Williamson, D. A. Hammer, D. D. Billadeau, Y. Argon, and J. K. Burkhardt. 2011. Hematopoietic lineage cell-specific protein 1 functions in concert with the Wiskott-Aldrich syndrome protein to promote podosome array organization and chemotaxis in dendritic cells. *J. Immunol.* 186: 4805–4818.
45. Fooksman, D. R., S. Vardhana, G. Vasiliver-Shamis, J. Liese, D. A. Blair, J. Waite, C. Sacristán, G. D. Victora, A. Zanin-Zhorov, and M. L. Dustin. 2010. Functional anatomy of T cell activation and synapse formation. *Annu. Rev. Immunol.* 28: 79–105.
46. Trautmann, A., and S. Valitutti. 2003. The diversity of immunological synapses. *Curr. Opin. Immunol.* 15: 249–254.
47. Bunnell, S. C. 2010. Multiple microclusters: diverse compartments within the immune synapse. *Curr. Top. Microbiol. Immunol.* 340: 123–154.
48. Dovas, A., and D. Cox. 2011. Signaling networks regulating leukocyte podosome dynamics and function. *Cell. Signal.* 23: 1225–1234.
49. Arrieumerlou, C., C. Randriamampita, G. Bismuth, and A. Trautmann. 2000. Rac is involved in early TCR signaling. *J. Immunol.* 165: 3182–3189.
50. Hughes, K., S. Edin, A. Antonsson, and T. Grundström. 2001. Calmodulin-dependent kinase II mediates T cell receptor/CD3- and phorbol ester-induced activation of IkappaB kinase. *J. Biol. Chem.* 276: 36008–36013.
51. Turesson, C. 2004. Endothelial expression of MHC class II molecules in autoimmune disease. *Curr. Pharm. Des.* 10: 129–143.
52. Manes, T. D., S. L. Shiao, T. J. Dengler, and J. S. Pober. 2007. TCR signaling antagonizes rapid IP-10-mediated transendothelial migration of effector memory CD4+ T cells. *J. Immunol.* 178: 3237–3243.
53. Manes, T. D., and J. S. Pober. 2008. Antigen presentation by human microvascular endothelial cells triggers ICAM-1-dependent transendothelial protrusion by, and fractalkine-dependent transendothelial migration of, effector memory CD4+ T cells. *J. Immunol.* 180: 8386–8392.
54. Shulman, Z., V. Shinder, E. Klein, V. Grabovsky, O. Yeger, E. Geron, A. Montresor, M. Bolomini-Vittori, S. W. Feigelson, T. Kirchhausen, et al. 2009. Lymphocyte crawling and transendothelial migration require chemokine triggering of high-affinity LFA-1 integrin. *Immunity* 30: 384–396.
55. Gérard, A., R. A. van der Kammen, H. Janssen, S. I. Ellenbroek, and J. G. Collard. 2009. The Rac activator Tiam1 controls efficient T-cell trafficking and route of transendothelial migration. *Blood* 113: 6138–6147.
56. Sage, P. T., and C. V. Carman. 2009. Settings and mechanisms for trans-cellular diapedesis. *Front. Biosci.* 14: 5066–5083.
57. Albiges-Rizo, C., O. Destaing, B. Fourcade, E. Planus, and M. R. Block. 2009. Actin machinery and mechanosensitivity in invadopodia, podosomes and focal adhesions. *J. Cell Sci.* 122: 3037–3049.
58. Bunnell, S. C., A. L. Singer, D. I. Hong, B. H. Jacque, M. S. Jordan, M. C. Seminario, V. A. Barr, G. A. Koretzky, and L. E. Samelson. 2006. Persistence of cooperatively stabilized signaling clusters drives T-cell activation. *Mol. Cell. Biol.* 26: 7155–7166.
59. Wetzel, S. A., T. W. McKeithan, and D. C. Parker. 2002. Live-cell dynamics and the role of costimulation in immunological synapse formation. *J. Immunol.* 169: 6092–6101.
60. Barcia, C., A. Gomez, V. de Pablos, E. Fernández-Villalba, C. Liu, K. M. Kroeger, J. Martín, A. F. Barreiro, M. G. Castro, P. R. Lowenstein, and M. T. Herrero. 2008. CD20, CD3, and CD40 ligand microclusters segregate three-dimensionally in vivo at B-cell-T-cell immunological synapses after viral immunity in primate brain. *J. Virol.* 82: 9978–9993.
61. Barcia, C., N. S. Sanderson, R. J. Barrett, K. Wawrowsky, K. M. Kroeger, M. Puntel, C. Liu, M. G. Castro, and P. R. Lowenstein. 2008. T cells' immunological synapses induce polarization of brain astrocytes in vivo and in vitro: a novel astrocyte response mechanism to cellular injury. *PLoS ONE* 3: e2977.
62. Barcia, C., Jr., A. Gómez, J. M. Gallego-Sanchez, A. Perez-Vallés, M. G. Castro, P. R. Lowenstein, C. Barcia, Sr., and M. T. Herrero. 2009. Infiltrating CTLs in human glioblastoma establish immunological synapses with tumorigenic cells. *Am. J. Pathol.* 175: 786–798.
63. Davis, D. M. 2009. Mechanisms and functions for the duration of intercellular contacts made by lymphocytes. *Nat. Rev. Immunol.* 9: 543–555.
64. Rudd, P. M., T. Elliott, P. Cresswell, I. A. Wilson, and R. A. Dwek. 2001. Glycosylation and the immune system. *Science* 291: 2370–2376.
65. Valitutti, S., M. Dessing, K. Aktories, H. Gallati, and A. Lanzavecchia. 1995. Sustained signaling leading to T cell activation results from prolonged T cell receptor occupancy. Role of T cell actin cytoskeleton. *J. Exp. Med.* 181: 577–584.
66. Negulescu, P. A., T. B. Krasieva, A. Khan, H. H. Kerschbaum, and M. D. Cahalan. 1996. Polarity of T cell shape, motility, and sensitivity to antigen. *Immunity* 4: 421–430.
67. Wei, X., B. J. Tromberg, and M. D. Cahalan. 1999. Mapping the sensitivity of T cells with an optical trap: polarity and minimal number of receptors for Ca(2+) signaling. *Proc. Natl. Acad. Sci. USA* 96: 8471–8476.
68. Ma, Z., K. A. Sharp, P. A. Janmey, and T. H. Finkel. 2008. Surface-anchored monomeric agonist pMHCs alone trigger TCR with high sensitivity. *PLoS Biol.* 6: e43.
69. Ma, Z., P. A. Janmey, and T. H. Finkel. 2008. The receptor deformation model of TCR triggering. *FASEB J.* 22: 1002–1008.
70. Groves, J. T. 2007. Bending mechanics and molecular organization in biological membranes. *Annu. Rev. Phys. Chem.* 58: 697–717.
71. Xu, C., E. Gagnon, M. E. Call, J. R. Schnell, C. D. Schwieters, C. V. Carman, J. J. Chou, and K. W. Wucherpfennig. 2008. Regulation of T cell receptor activation by dynamic membrane binding of the CD3epsilon cytoplasmic tyrosine-based motif. *Cell* 135: 702–713.
72. Dustin, M. L., S. Y. Tseng, R. Varma, and G. Campi. 2006. T cell-dendritic cell immunological synapses. *Curr. Opin. Immunol.* 18: 512–516.
73. Saito, T., and T. Yokosuka. 2006. Immunological synapse and microclusters: the site for recognition and activation of T cells. *Curr. Opin. Immunol.* 18: 305–313.
74. Burbach, B. J., R. B. Medeiros, K. L. Mueller, and Y. Shimizu. 2007. T-cell receptor signaling to integrins. *Immunol. Rev.* 218: 65–81.
75. Perez-Moreno, M., C. Jamora, and E. Fuchs. 2003. Sticky business: orchestrating cellular signals at adherens junctions. *Cell* 112: 535–548.
76. Harwood, N. E., and F. D. Batista. 2008. New insights into the early molecular events underlying B cell activation. *Immunity* 28: 609–619.
77. Vicente-Manzanares, M., and F. Sánchez-Madrid. 2004. Role of the cytoskeleton during leukocyte responses. *Nat. Rev. Immunol.* 4: 110–122.
78. Miranti, C. K., and J. S. Brugge. 2002. Sensing the environment: a historical perspective on integrin signal transduction. *Nat. Cell Biol.* 4: E83–E90.
79. Luxenburg, C., D. Geblinger, E. Klein, K. Anderson, D. Hanein, B. Geiger, and L. Addadi. 2007. The architecture of the adhesive apparatus of cultured osteoclasts: from podosome formation to sealing zone assembly. *PLoS ONE* 2: e179.
80. Destaing, O., A. Sanjay, C. Itzstein, W. C. Horne, D. Toomre, P. De Camilli, and R. Baron. 2008. The tyrosine kinase activity of c-Src regulates actin dynamics and organization of podosomes in osteoclasts. *Mol. Biol. Cell* 19: 394–404.
81. Saltel, F., O. Destaing, F. Bard, D. Eichert, and P. Jurdic. 2004. Apatite-mediated actin dynamics in resorbing osteoclasts. *Mol. Biol. Cell* 15: 5231–5241.

Appendix B

This is a reprint of:

> Sage, P.T., Francisco, L.M., Carman, C.V. & Sharpe, A.H. The receptor PD-1 controls follicular regulatory T cells in the lymph nodes and blood. *Nature immunology* (2012). doi:10.1038/ni.2496

nature immunology

The receptor PD-1 controls follicular regulatory T cells in the lymph nodes and blood

Peter T Sage[1,2], Loise M Francisco[1,3], Christopher V Carman[2] & Arlene H Sharpe[1,3]

CD4$^+$CXCR5$^+$Foxp3$^+$ follicular regulatory T cells (T_{FR} cells) inhibit humoral immunity mediated by CD4$^+$CXCR5$^+$Foxp3$^-$ follicular helper T cells (T_{FH} cells). Although the inhibitory receptor PD-1 is expressed by both cell types, its role in the differentiation of T_{FR} cells is unknown. Here we found that mice deficient in PD-1 and its ligand PD-L1 had a greater abundance of T_{FR} cells in the lymph nodes and that those T_{FR} cells had enhanced suppressive ability. We also found substantial populations of T_{FR} cells in mouse blood and demonstrated that T_{FR} cells in the blood homed to lymph nodes and potently inhibited T_{FH} cells *in vivo*. T_{FR} cells in the blood required signaling via the costimulatory receptors CD28 and ICOS but were inhibited by PD-1 and PD-L1. Our findings demonstrate mechanisms by which the PD-1 pathway regulates antibody production and help reconcile inconsistencies surrounding the role of this pathway in humoral immunity.

Follicular helper T cells (T_{FH} cells) are a subset of CD4$^+$ T cells that are essential for helping cognate B cells form and maintain the germinal center (GC) reaction and for the development of humoral immune responses. These cells are universally defined by expression of the chemokine receptor CXCR5, which directs them to B cell follicles via gradients of the chemokine CXCL13 (ref. 1). T_{FH} cells also express the transcription factor Bcl-6 and have high expression of the costimulatory receptor ICOS. Both Bcl-6 and ICOS are critical for the differentiation and maintenance of T_{FH} cells[1–4]. In addition, T_{FH} cells secrete large amounts of interleukin 21 (IL-21), which aids in the formation of GCs, isotype switching and the formation of plasma cells[5]. In humans and mice, functionally similar T_{FH} cells can be found in secondary lymphoid organs. CXCR5$^+$ T_{FH} cells are also present in peripheral blood and are found in greater abundance in people with autoantibodies, including patients with systemic lupus erythematosus, myasthenia gravis or juvenile dermatomyositis. However, the function of circulating T_{FH} cells has remained unclear[6–9].

T_{FH} cells also have high expression of the inhibitory receptor PD-1 (CD279). Signaling through PD-1 attenuates signaling from the T cell antigen receptor (TCR) and inhibits the population expansion, cytokine production and cytolytic function of T cells. In addition, PD-1 promotes the development of induced regulatory T cells (T_{reg} cells) from naive lymphocytes[10–14]. PD-1 has two ligands: PD-L1 (B7-H1) and PD-L2 (B7-DC). PD-L1 has wider expression than does PD-L2, but both PD-L1 and PD-L2 can be expressed on GC B cells and dendritic cells[15]. Perturbation studies have suggested critical roles for this pathway in regulating humoral immune responses. However, there are conflicting reports about the function of the PD-1 pathway in controlling humoral immunity. When interactions between PD-1 and its ligand(s) are prevented, some studies have found attenuated humoral responses[16–18], whereas others have observed heightened humoral responses[19,20].

PD-1 also is found on the CD4$^+$CXCR5$^+$ subset of cells called 'follicular regulatory T cells' (T_{FR} cells), which express the transcription factors Foxp3, Bcl-6 and Blimp-1 and function to inhibit the GC response[21–23]. These cells originate from natural T_{reg} cells but have expression of ICOS, CXCR5 and PD-1 similar in amount to that of T_{FH} cells. As ICOS, CXCR5 and PD-1 have been widely used to identify and purify 'T_{FH} cells', it seems likely that the inability to define clear functions for PD-1 in GC responses derives from experimental systems that contain mixtures of stimulatory T_{FH} cells and inhibitory T_{FR} cells. Separate analyses of the function of PD-1 on T_{FH} cells and T_{FR} cells are needed to elucidate how PD-1 controls humoral immunity and to gain insight into the individual roles of T_{FR} cells and T_{FH} cells in the regulation of antibody production.

Here we found that PD-1–PD-L1 interactions inhibited the number of T_{FR} cells, but not of T_{FH} cells, in the lymph nodes. PD-1-deficient mice had more T_{FR} cells in the lymph nodes than did wild-type mice. PD-1-deficient T_{FR} cells in the lymph nodes had an enhanced ability to suppress both the activation of naive T cells and antibody production *in vitro*. In addition, we found that T_{FR} cells were present in the peripheral blood of mice and that these circulating cells potently regulated humoral immune responses *in vivo*. Through the use of transfer approaches, we found that T_{FH} cells in the blood promoted antibody production, whereas T_{FR} cells in the blood strongly inhibited antibody production *in vivo*. We further found that the PD-1 pathway inhibited the function of T_{FR} cells in the blood and that PD-1-deficient T_{FR} cells in the blood had enhanced suppressive ability *in vivo*. Together our studies identify a previously unknown immunoregulatory role for the PD-1–PD-L1 pathway in limiting the

[1]Department of Microbiology and Immunobiology, Harvard Medical School, Boston, Massachusetts, USA. [2]Department of Medicine, Beth Israel Deaconess Medical Center, Boston, Massachusetts, USA. [3]Department of Pathology, Brigham and Women's Hospital, Boston, Massachusetts, USA. Correspondence should be addressed to A.H.S. (arlene_sharpe@hms.harvard.edu).

Received 1 October; accepted 15 November; published online 16 December 2012; doi:10.1038/ni.2496

differentiation and function of T_{FR} cells and further demonstrate the dynamic control of humoral immune responses through the migration of T_{FR} cells from the circulation into the lymph nodes to control antibody production *in vivo*.

RESULTS

PD-1 controls T_{FR} cells

To analyze the role of PD-1 in controlling T_{FR} cells, we first assessed PD-1 expression on $CD4^+$ T cell subsets in the draining lymph nodes of wild-type C57BL/6 mice immunized subcutaneously with myelin oligodendrocyte glycoprotein peptide (amino acids 35–55) emulsified in complete Freund's adjuvant (collectively called 'MOG' here), an immunization that breaks tolerance and also results in the effective generation of T_{FH} cells[24]. We defined T_{FR} cells as $CD4^+ICOS^+CXCR5^+Foxp3^+CD19^-$, a gating strategy that separated T_{FR} cells from $CD4^+ICOS^+CXCR5^+Foxp3^-CD19^-$ T_{FH} cells, the cell type previously thought to solely constitute the $CD4^+CXCR5^+$ gate (**Fig. 1a**). T_{FH} cells had higher expression of PD-1 protein than did $ICOS^+CXCR5^-$ effector-like cells or $ICOS^-CXCR5^-$ naive cells (called 'naive cells' here) in the draining lymph nodes on day 7 after immunization (**Fig. 1b**). Notably, T_{FR} cells had even higher expression of PD-1 protein than did any other $CD4^+$ T cell subset examined, including T_{FH} cells (**Fig. 1b**).

To determine the functional importance of PD-1 expression on T_{FR} cells, we immunized wild-type and PD-1-deficient (*Pdcd1*$^{-/-}$) mice and analyzed T_{FR} cells 7 d later. The frequency of T_{FR} cells in the $CD4^+Foxp3^+$ gate was about 4% in wild-type lymph nodes and <1% of all $CD4^+$ T cells. In contrast, the frequency of T_{FR} cells in *Pdcd1*$^{-/-}$ mice was about 10% of the $CD4^+Foxp3^+$ gate and >2% of all $CD4^+$ T cells (**Fig. 1c,d**). Because the total number of $CD4^+$ T cells was typically about twofold higher in the PD-1-deficient lymph nodes than in wild-type lymph nodes, a twofold-greater frequency of T_{FR} cells indicated an approximately fourfold-greater absolute number of T_{FR} cells (data not shown). When determined as a percentage of all $CD4^+ICOS^+CXCR5^+$ cells (and therefore as the percentage of $CD4^+$ T cells that could respond to CXCL13 and migrate to the B cell zone), *Pdcd1*$^{-/-}$ T_{FR} cells constituted 50% of that population, whereas wild-type T_{FR} cells constituted only about 20% (**Fig. 1d**). We also observed a much greater frequency of T_{FR} cells in *Pdcd1*$^{-/-}$ mice when we immunized the mice with other classic B cell antigens, such as the hapten NP (4-hydroxy-3-nitrophenylacetyl) conjugated to ovalbumin (NP-OVA; **Supplementary Fig. 1**). We did not find a significant difference in the frequency of $Foxp3^-$ T_{FH} cells (called 'T_{FH} cells' here) when determined as a percentage of all $CD4^+$ T cells in wild-type and *Pdcd1*$^{-/-}$ mice on day 7 after immunization with MOG (**Fig. 1e**) or NP-OVA (**Supplementary Fig. 1**).

As PD-1 can be expressed by many types of hematopoietic cells, including T cells, B cells, macrophages and some dendritic cells[15], we next investigated whether PD-1 regulates T_{FR} cells directly by controlling their generation from $Foxp3^+$ T_{reg} cells. To track the fate of $Foxp3^+$ cells after transfer into wild-type mouse recipients, we used antigen-specific $Foxp3^+$ T cells from 2D2 mice, which have transgenic expression of a MOG-specific TCR, for these studies. We sorted $Foxp3^+$ T_{reg} cells from wild-type 2D2 or *Pdcd1*$^{-/-}$ 2D2 mice that expressed a Foxp3–green fluorescent protein (GFP) reporter (Foxp3-GFP reporter mice), then transferred 2×10^5 wild-type or *Pdcd1*$^{-/-}$ 2D2 $CD4^+CXCR5^-Foxp3^+$ cells into wild-type recipient mice. We immunized the recipients with MOG and analyzed cells in the draining lymph nodes 7 d later. A greater frequency (**Fig. 1f,g**) and absolute number (**Fig. 1h**) of *Pdcd1*$^{-/-}$ 2D2 T_{reg} cells than wild-type 2D2 T_{reg} cells upregulated CXCR5 and thus differentiated into T_{FR} cells. The greater frequency of *Pdcd1*$^{-/-}$ T_{FR} cells in the immunized recipients of cell transfer was similar to but slightly less than the greater frequency of T_{FR} cells in immunized mice lacking PD-1 on all cells (**Fig. 1d,g**). These results demonstrated that PD-1 controlled the differentiation of $Foxp3^+$ T_{reg} cells into T_{FR} cells.

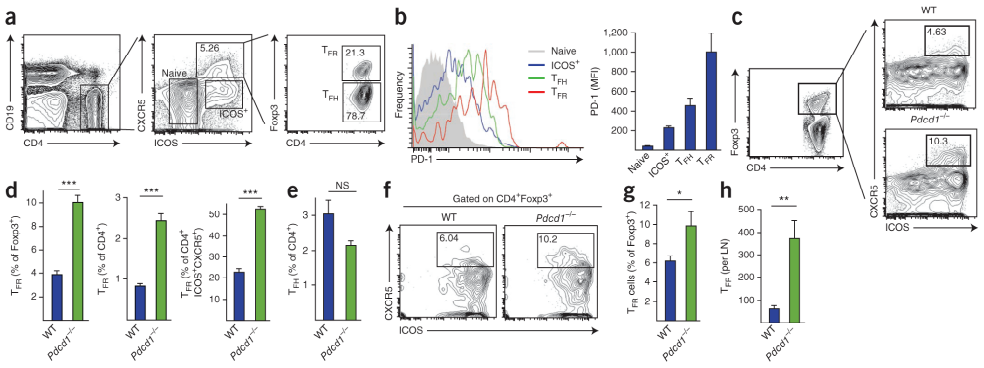

Figure 1 PD-1 signaling in Foxp3 T_{reg} cells limits generation of T_{FR} cells. (**a**) Quantification of naive ($CD4^+ICOS^-CXCR5^-CD19^-$) cells and $ICOS^+$ ($CD4^+ICOS^+CXCR5^-CD19^-$) cells (middle) and T_{FR} ($CD4^+Foxp3^+ICOS^+CXCR5^+CD19^-$) cells and T_{FH} ($CD4^+Foxp3^-ICOS^+CXCR5^+CD19^-$) cells (right) in draining lymph nodes of wild-type mice 7 d after immunization with MOG. Numbers in outlined areas indicate percent cells in each throughout. (**b**) PD-1 expression on wild-type naive, $ICOS^+$, T_{FR} and T_{FH} cells gated as in **a**, assessed by flow cytometry. (**c**) Gating of T_{FR} cells among total $Foxp3^+$ cells in wild-type and *Pdcd1*$^{-/-}$ mice 7 d after immunization with MOG. (**d**) Quantification of wild-type and *Pdcd1*$^{-/-}$ T_{FR} cells from the inguinal lymph nodes, gated in **c**, presented as frequency among $CD4^+Foxp3^+$ cells (left), total $CD4^+$ T cells (middle) or in the $CD4^+ICOS^+CXCR5^+CD19^-$ gate (right). (**e**) Quantification of wild-type and *Pdcd1*$^{-/-}$ T_{FH} cells from the inguinal lymph nodes, as a percentage of $CD4^+$ T cells. (**f**) Gating of T_{FR} cells from the lymph nodes of wild-type recipients given wild-type 2D2 and *Pdcd1*$^{-/-}$ 2D2 $CD4^+Foxp3^+CXCR5^-$ T_{reg} cells (2×10^5), followed by immunization with MOG and analysis 7 d later. (**g**,**h**) Quantification of T_{FR} cells from transfer experiments as in **f**, presented as the frequency of $Foxp3^+$ cells on day 7 after immunization (**g**) or total cells per lymph node (**h**). NS, not significant; $^*P < 0.05$, $^{**}P < 0.005$ and $^{***}P < 0.0005$ (unpaired Student's *t*-test). Data are representative of at least two experiments with at least five mice per group (error bars, s.e.m.).

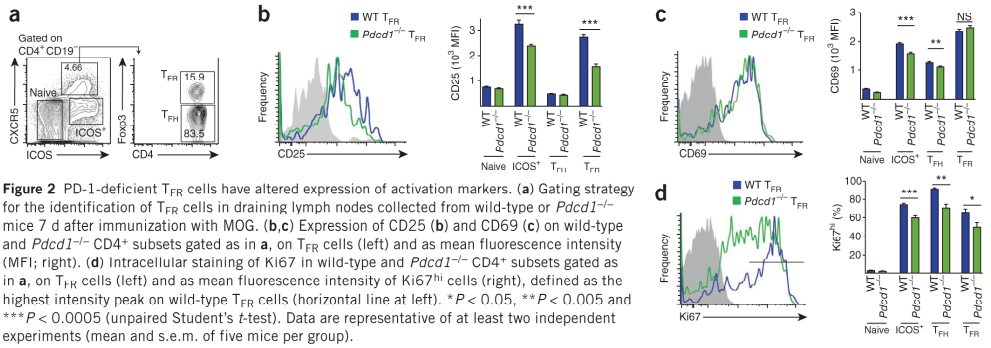

Figure 2 PD-1-deficient T_{FR} cells have altered expression of activation markers. (**a**) Gating strategy for the identification of T_{FR} cells in draining lymph nodes collected from wild-type or *Pdcd1*$^{-/-}$ mice 7 d after immunization with MOG. (**b**,**c**) Expression of CD25 (**b**) and CD69 (**c**) on wild-type and *Pdcd1*$^{-/-}$ CD4$^+$ subsets gated as in **a**, on T_{FR} cells (left) and as mean fluorescence intensity (MFI; right). (**d**) Intracellular staining of Ki67 in wild-type and *Pdcd1*$^{-/-}$ CD4$^+$ subsets gated as in **a**, on T_{FR} cells (left) and as mean fluorescence intensity of Ki67^{hi} cells (right), defined as the highest intensity peak on wild-type T_{FR} cells (horizontal line at left). $^*P < 0.05$, $^{**}P < 0.005$ and $^{***}P < 0.0005$ (unpaired Student's *t*-test). Data are representative of at least two independent experiments (mean and s.e.m. of five mice per group).

As CD25 (the α-chain of the receptor for IL-2) is often used as a marker for T_{reg} cells, we next compared CD25 expression on wild-type and *Pdcd1*$^{-/-}$ T_{FR} cells immediately after isolation (**Fig. 2a**). *Pdcd1*$^{-/-}$ T_{FR} cells had lower expression of CD25 than did wild-type T_{FR} cells (**Fig. 2b**). The attenuated CD25 expression in PD-1-deficient T_{FR} cells was probably not due to less activation because expression of the early activation marker CD69 was almost completely identical on wild-type and *Pdcd1*$^{-/-}$ T_{FR} cells (**Fig. 2c**). To compare the proportion of wild-type and *Pdcd1*$^{-/-}$ T_{FR} cells that were proliferating on day 7 after immunization with MOG, we examined expression of Ki67, a marker widely used to identify cells that are actively dividing. Wild-type CXCR5$^-$ICOS$^+$ effector cells, T_{FH} cells and T_{FR} cells had high expression of Ki67. In contrast, wild-type CXCR5$^-$ICOS$^-$ 'naive' cells, which lacked expression of CD69 and CD25, had no Ki67 staining, consistent with their designation as naive (**Fig. 2d**). Wild-type T_{FR} cells had much higher expression of Ki67 than did *Pdcd1*$^{-/-}$ T_{FR} cells (**Fig. 2d**), which suggested that the greater abundance of T_{FR} cells in PD-1-deficient mice reflected more differentiation, not maintenance, of T_{FR} cells. Ki67 expression was similarly higher in wild-type ICOS$^+$ effector cells and T_{FH} cells than in *Pdcd1*$^{-/-}$ ICOS$^+$CXCR5$^-$ effector cells and T_{FH} cells. This indicated a lower amount of cycling of *Pdcd1*$^{-/-}$ effector cells at 7 d after immunization. The expression of other T_{reg} cell markers, such as CD103 and GITR, was not altered on T_{FR} cells in PD-1 deficient mice (**Supplementary Fig. 2**). Additionally, there was low but substantial expression of PD-L1 on wild-type and *Pdcd1*$^{-/-}$ T_{FR} cells (**Supplementary Fig. 2**). Together these data indicated that PD-1 was important in regulating the number of T_{FR} cells *in vivo*.

PD-1-deficient T_{FR} cells can home to GCs

We next compared the ability of wild-type and PD-1-deficient T_{FR} cells to enter the GC to inhibit the GC response. First we evaluated GC formation in lymph node sections collected 7 d after immunization with MOG. We identified GCs by the binding of peanut agglutinin and positive staining for the GC marker GL7 and lack of staining for immunoglobulin D (IgD; **Fig. 3a**). We determined that these GCs were active on the basis of their robust expression of Ki67 (**Fig. 3b**). Similar to published reports[21,22], we found CD4$^+$Foxp3$^+$ T_{FR} cells in the GCs of immunized mice (**Fig. 3c**). The Foxp3 protein in the T_{FR} cells was mostly nuclear, given its localization together with the DNA-intercalating dye DAPI (**Fig. 3d**).

We then investigated whether the phenotypically distinct PD-1-deficient T_{FR} cells were able to migrate to GCs similarly to wild-type T_{FR} cells because blockade of PD-1 can prolong the TCR 'stop signal' and diminish T cell migration[25]. We immunized wild-type and PD-1-deficient mice with MOG and analyzed lymph node sections 7 d later for expression of IgD, GL7 and Foxp3 (**Fig. 3e**). Although the GC area (**Fig. 3f**) and number of GCs per lymph node (data not shown) were equivalent in wild-type and *Pdcd1*$^{-/-}$ mice, there were slightly more Foxp3$^+$ cells (and therefore T_{FR} cells) located within the GC borders in *Pdcd1*$^{-/-}$ mice than in wild-type mice (**Fig. 3g**). However, as this was proportional to the greater number of T_{FR} cells in PD-1-deficient mice determined by flow cytometry, these data demonstrated that PD-1-deficient T_{FR} cells were not defective in homing to GCs and were able to enter the GC like wild-type T_{FR} cells.

The location of Foxp3$^+$ T_{FR} cells in the GC did not differ significantly for wild-type and *Pdcd1*$^{-/-}$ mice (**Fig. 3h**). In both wild-type and *Pdcd1*$^{-/-}$ mice, the Foxp3$^+$ cells tended to reside near the GC border, with more than half of the nuclei of Foxp3$^+$ cells being positioned within 10 μm of the border. Furthermore, when we quantified CXCR5 fluorescence by flow cytometry, we found similar CXCR5 expression on wild-type and *Pdcd1*$^{-/-}$ T_{FR} cells (**Fig. 3i**), which indicated a similar potential for these cells to respond to chemokine cues to migrate to GCs. Together these data indicated that the lymph nodes of immunized *Pdcd1*$^{-/-}$ mice had more T_{FR} cells and that these *Pdcd1*$^{-/-}$ T_{FR} cells were able to migrate into GCs to regulate B cell responses.

PD-1-deficient T_{FR} cells more potently inhibit antibody

We next assessed the function of T_{FR} cells from wild-type and *Pdcd1*$^{-/-}$ mice. T_{FR} cells have higher expression of the T_{reg} cell–associated receptor GITR on the surface than do T_{FH} cells, which allowed us to separate T_{FH} cells and T_{FR} cells in a similar manner to that of intracellular staining for Foxp3 (**Fig. 4a**). For functional studies, we sorted T_{FR} cells from immunized mice by defining the lymph node CD4$^+$ICOS$^+$CXCR5$^+$CD19$^-$GITR$^+$ population as T_{FR} cells and the CD4$^+$ICOS$^+$CXCR5$^+$CD19$^-$GITR$^-$ population as T_{FH} cells (**Fig. 4b**). Sorting in this way resulted in a considerable abundance of *Foxp3* mRNA in the GITR$^+$ (T_{FR}) population but essentially no *Foxp3* mRNA in the GITR$^-$ (T_{FH}) population (**Fig. 4b**), which confirmed the utility of this gating strategy for the isolation of T_{FR} cells and T_{FH} cells for functional assays. Furthermore, we were able to use this sorting strategy to compare wild-type and PD-1-deficient T_{FR} cells, as GITR expression was identical on wild-type and PD-1-deficient T_{FR} cells (**Supplementary Fig. 3**).

T_{FR} cells have high expression of Blimp-1 and moderate expression of Bcl-6 (ref. 21). Bcl-6 and Blimp-1 reciprocally modulate each other[2]; inhibition of Blimp-1 by Bcl-6 is essential for maintenance of

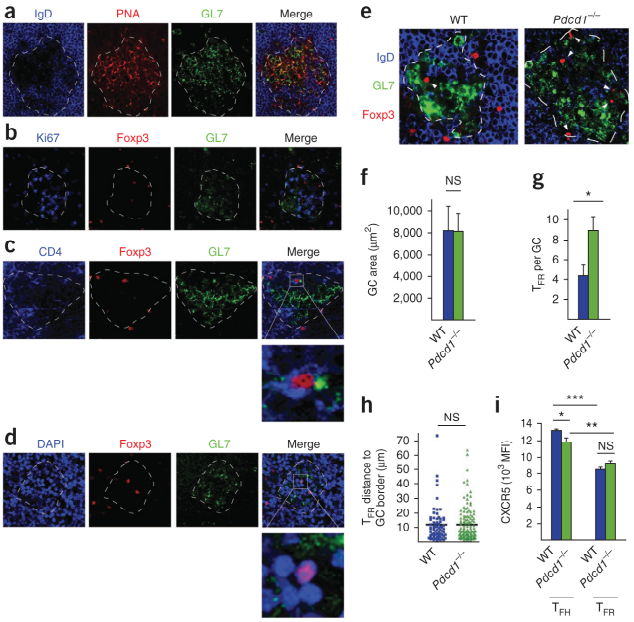

Figure 3 PD-1-deficient T_{FR} cells are able to home to GCs. (**a**) Microscopy of draining lymph nodes from wild-type mice 7 d after immunization with MOG, stained for GL7 (green), binding of peanut agglutinin (PNA; red) and IgD (blue). GCs (white dashed lines) are $PNA^+GL7^+IgD^-$. (**b**) Microscopy of GC sections as in **a**, stained for Ki67 (blue), Foxp3 (red) and GL7 (green). (**c**) Microscopy of the colocalization of CD4 (blue) and Foxp3 (red) and GL7 (green) in sections as in **a**; outlined area (far right) indicates area enlarged below, with $CD4^+$ staining on $Foxp3^+$ cells. (**d**) Microscopy of the localization of Foxp3 in the nucleus in sections stained with DAPI (blue) and for Foxp3 (red) and GL7 (green) in sections as in **a**; outlined area (far right) indicates area enlarged below, showing Foxp3 in $DAPI^+$ nuclei. (**e**) Microscopy of $Foxp3^+$ T_{FR} cells in GCs of draining lymph nodes obtained from wild-type and *Pdcd1*$^{-/-}$ mice 7 d after immunization with MOG. (**f**) Area of GCs as in **e**, calculated as the area in the dashed lines in **e** (mean area per lymph node). (**g**) $Foxp3^+$ cells in GCs as in **e** (mean per GC). (**h**) Distance from $Foxp3^+$ cells to the border of GCs as in **e** (dashed line in **e**). Each symbol represents an individual FoxP3$^+$ cell; small horizontal lines indicate the mean. (**i**) CXCR5 expression on wild-type and *Pdcd1*$^{-/-}$ T_{FH} and T_{FR} cells 7 d after MOG immunization, assessed by flow cytometry. Original magnification, ×400 (**a**,**b**,**e** and main image in **c**,**d**), ×2,480 (**c**, enlargement) or ×2320 (**d**, enlargement). NS, not significant; $*P < 0.05$, $**P < 0.005$, $***P < 0.0005$ (unpaired Student's *t*-test). Data are representative of three experiments (**a**–**d**,**i**; mean and s.e.m. of five mice per group in **i**) or two experiments (**e**–**h**; mean and s.e.m. of ten lymph nodes in **f**–**h**).

the T_{FH} phenotype, whereas Blimp-1 is important in the homeostasis of T_{reg} cells in general[26,27]. As relative expression of Bcl-6 and Blimp-1 determines the function of T_{FH} subsets, we compared intracellular Bcl-6 expression in wild-type T_{FR} cells with that in *Pdcd1*$^{-/-}$ T_{FR} cells by flow cytometry. Although T_{FR} cells had lower expression of Bcl-6 than did T_{FH} cells, wild-type and *Pdcd1*$^{-/-}$ T_{FR} cells had similar amounts of Bcl-6 (**Fig. 4c**). We next compared expression of the gene encoding Blimp-1 (*Prdm1*) in wild-type T_{FR} cells with that in *Pdcd1*$^{-/-}$ T_{FR} cells. We did not find any consistent difference between wild type and *Pdcd1*$^{-/-}$ T_{FR} cells in *Prdm1* mRNA expression (**Fig. 4d**). As Foxp3 can directly interact with and negatively regulate the function of the transcription factor RORγt[28], we also examined the expression of *Rorc* (which encodes RORγt) in wild-type and *Pdcd1*$^{-/-}$ T_{FR} cells. T_{FR} cells had lower expression of *Rorc* mRNA than did T_{FH} cells, but *Rorc* expression was higher in *Pdcd1*$^{-/-}$ T_{FR} cells than in wild-type T_{FR} cells (**Fig. 4e**). In addition, we compared expression of the transcription factor IRF4 in wild-type T_{FR} cells with that in *Pdcd1*$^{-/-}$ T_{FR} cells, as Blimp-1 and IRF4 synergistically control the differentiation and effector functions of T_{reg} cells[26]. We found higher expression of *Irf4* mRNA in *Pdcd1*$^{-/-}$ T_{FR} cells than in wild-type T_{FR} cells (**Fig. 4f**).

IRF4 is essential for the suppressive ability of T_{reg} cells[26]. To determine if higher expression of *Irf4* mRNA in *Pdcd1*$^{-/-}$ T_{FR} cells resulted in more suppression of the proliferation of T cells, we set up an *in vitro* suppression assay in which we cultured sorted wild-type $CD4^+CD62L^+Foxp3^-$ responder T cells (from unimmunized mice) labeled with the cytosolic dye CFSE, wild-type $GL7^-$ B cells from MOG-immunized wild-type mice and T_{FR} cells sorted from MOG-immunized wild-type or *Pdcd1*$^{-/-}$ mice, together with antibody to CD3 (anti-CD3) and anti-IgM. The responder T cells had substantial upregulation of the expression of CD69 after 3 d of culture with wild-type B cells. However, when we added wild-type T_{FR} cells (at a ratio of 1:1:1 with responder T cells and B cells as described above), the CD69 expression on the responder T cells was much lower (**Fig. 4g**), consistent with the function of T_{FR} cells in suppressing T cell activation. CD69 upregulation was inhibited to an even greater extent in responder T cells cultured with *Pdcd1*$^{-/-}$ T_{FR} cells. Moreover, *Pdcd1*$^{-/-}$ T_{FR} cells attenuated the proliferation of responder T cells, in contrast to wild-type T_{FR} cells, which did not inhibit the proliferation of responder T cells during the 3-day culture period (**Fig. 4h**).

Although T_{FR} cells are thought to inhibit the GC response *in vivo*, it is unclear whether T_{FR} cells directly inhibit the differentiation of T cells, the function of T_{FH} cells, the activation of B cells or all three. To assess the ability of T_{FR} cells to suppress antibody production by B cells *in vitro*, we cultured wild-type $GL7^-$ B cells with wild-type T_{FH} cells for 6 d in the presence or absence of T_{FR} cells (all from MOG-immunized mice), anti-IgM and anti-CD3. Wild-type B cells produced large amounts of IgG when cultured with wild-type T_{FH} cells plus anti-IgM and anti-CD3 (**Fig. 4i**). No significant IgG was produced when we used naive $CD4^+$ T cells in these experiments (**Fig. 4j**). When we added T_{FR} cells to the wells along with T_{FH} cells, almost no IgG was produced. The T_{FR} cell–mediated suppression was not due to the sequestering of anti-CD3 because there was equally good suppression at the two doses of anti-CD3 tested (**Fig. 4i**) and anti-CD3 was still present on the surface of the T_{FH} cells at the end of the suppression assay (**Supplementary Fig. 4**). *Pdcd1*$^{-/-}$ T_{FR} cells suppressed IgG production more than wild-type T_{FR} cells did at ratios

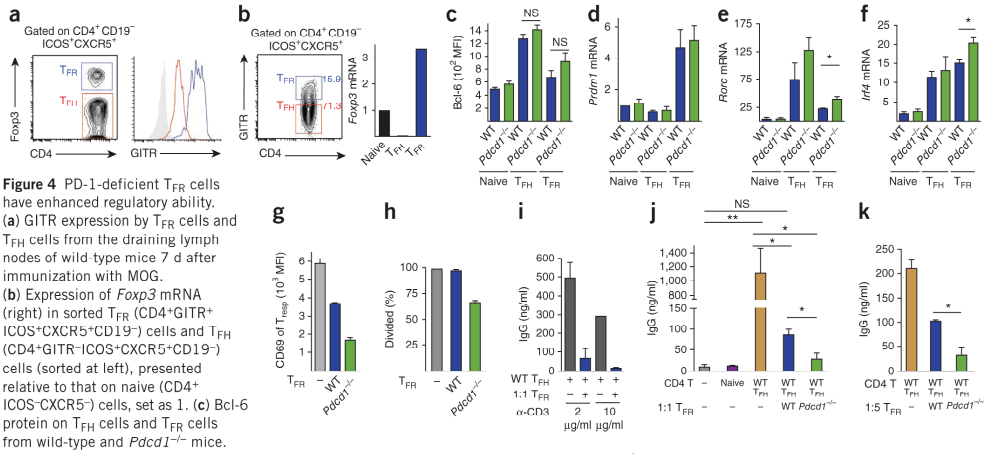

Figure 4 PD-1-deficient T_{FR} cells have enhanced regulatory ability. (**a**) GITR expression by T_{FR} cells and T_{FH} cells from the draining lymph nodes of wild-type mice 7 d after immunization with MOG. (**b**) Expression of *Foxp3* mRNA (right) in sorted T_{FR} ($CD4^+GITR^+ICOS^+CXCR5^+CD19^-$) cells and T_{FH} ($CD4^+GITR^-ICOS^+CXCR5^+CD19^-$) cells (sorted at left), presented relative to that on naive ($CD4^+ICOS^-CXCR5^-$) cells, set as 1. (**c**) Bcl-6 protein on T_{FH} cells and T_{FR} cells from wild-type and *Pdcd1*$^{-/-}$ mice. (**d**–**f**) Expression of *Prdm1* mRNA (**d**), *Rorc* mRNA (**e**) and *Irf4* mRNA (**f**) in wild-type and *Pdcd1*$^{-/-}$ T_{FR} and T_{FH} cells, presented relative to that in naive wild-type cells. (**g**) CD69 expression and (**h**) proliferation (assessed by CFSE dilution) of responder T cells in cultures of T_{FR} cells obtained from the draining lymph nodes of MOG-immunized wild-type and *Pdcd1*$^{-/-}$ mice and plated for 4 d (at a ratio of 1:1:1) with CFSE-labeled wild-type ($CD4^+CD62L^+Foxp3^-$) responder cells and $GL7^-$ B cells, plus anti-CD3 and anti-IgM. (**i**) IgG in supernatants of cultures of $GL7^-$ B cells obtained from the draining lymph nodes of MOG-immunized wild-type mice, incubated with wild-type T_{FH} cells in the presence (+) or absence (–) of T_{FR} cells, plus anti-IgM and various doses (bottom) of anti-CD3 (α-CD3). (**j**) IgG in supernatants of cultures as in **i**, with or without naive ($CD4^+ICOS^-CXCR5^-CD19^-$) T cells from MOG immunized wild type mice (left two bars) or with wild type T_{FH} cells in the presence or absence of wild type or *Pdcd1*$^{-/-}$ T_{FR} cells (at a ratio of 1:1; right three bars), plus anti-CD3 and anti-IgM. (**k**) IgG in culture supernatants of $GL7^-$ B cells obtained as in **i** and plated for 6 d with wild-type T_{FH} cells in the presence or absence of wild-type or *Pdcd1*$^{-/-}$ T_{FR} cells (at a ratio of 1:5), plus anti-CD3 and anti-IgM. $^*P < 0.05$ and $^{**}P < 0.005$ (unpaired Student's *t*-test). Data are representative of three experiments (**a**,**c**; error bars (**c**), s.e.m.), two experiments (**b**), (**d**–**f**; mean and s.e.m. of at least three independent experiments) or at least two experiments (**g**–**k**; mean and s.e.m. of at least three wells).

of T_{FR} cells to T_{FH} cells of 1:1 (**Fig. 4j**) and 1:5 (**Fig. 4k**), with PD-1-deficient T_{FR} cells resulting in 50% lower IgG production than that of wild-type T_{FR} cells. Together these data demonstrated not only that *Pdcd1*$^{-/-}$ mice had more T_{FR} cells but also that those *Pdcd1*$^{-/-}$ T_{FR} cells had greater suppressive capacity.

PD-1 controls T_{FR} cells in the blood

One possible explanation for the greater abundance of T_{FR} cells in lymph nodes of immunized PD-1-deficient mice might be that *Pdcd1*$^{-/-}$ T_{FR} cells were unable to exit the lymph node. Functional T_{FH} cells can be found in the blood of humans as well as mice[6,7,9], but whether T_{FR} cells circulate in the blood of humans or mice is not yet known. We found a distinct population of T_{FH} cells, as well as a smaller population of T_{FR} cells, in the blood of wild-type mice immunized with MOG (**Fig. 5a**,**b**). When we assessed the kinetics of the population expansion of T_{FH} cells and T_{FR} cells in the lymph node and blood of mice after MOG immunization, we found that the frequency of T_{FR} and T_{FH} cells increased in the draining lymph nodes of immunized wild-type mice over a 10-day period, and that T_{FH} cells, but not T_{FR} cells, increased substantially (by percentage) in the blood over this time (**Fig. 5b**). Thus, without antigenic stimulus, the ratio of T_{FR} cells to T_{FH} cells in the blood was fairly high (sometimes >1:1), but after the addition of a stimulus, the population expansion of T_{FH} cells in the blood was greater than that of T_{FR} cells in the blood, so that the ratio of T_{FR} cells to T_{FH} cells was about 1:5. To investigate whether wild-type T_{FH} cells and T_{FR} cells in the blood were quiescent or actively in the cell cycle, we assessed Ki67 expression in T_{FH} cells and T_{FR} cells from the draining lymph nodes and blood at 7 d after immunization. T_{FH} cells from the draining lymph nodes had higher Ki67 expression than did those in the blood (**Fig. 5c**). T_{FH} cells and T_{FR} cells in the blood and T_{FR} cells from the draining lymph nodes had similar expression of Ki67.

Next we investigated whether T_{FR} cells in the blood were inhibited to the same degree by PD-1 signaling as were T_{FR} cells from the lymph nodes. We immunized wild-type and *Pdcd1*$^{-/-}$ mice with MOG and 7 d later analyzed T_{FH} cells and T_{FR} cells from the blood. In wild-type mice, ~2–3% of $CD4^+Foxp3^-CD19^-$ cells in the blood were T_{FH} cells, but in the *Pdcd1*$^{-/-}$ mice, ~4–5% were T_{FH} cells (**Fig. 5d**). This greater frequency of *Pdcd1*$^{-/-}$ T_{FH} cells in blood was in contrast to results obtained for the lymph nodes, where *Pdcd1*$^{-/-}$ mice had a frequency of T_{FH} cells similar to, if not less than, that of wild-type mice (**Fig. 1e**). Notably, T_{FR} cells constituted ~3% of all $Foxp3^+$ cells in the blood of wild-type mice but >7% of $Foxp3^+$ cells in the blood of *Pdcd1*$^{-/-}$ mice (**Fig. 5d**,**e**). The greater frequency of $Foxp3^+$ cells seemed to be specific to the subset of T_{FR} cells in the blood, as the frequency of $Foxp3^+$ cells in the $ICOS^+CXCR5^-$ ($ICOS^+$) and $ICOS^-CXCR5^-$ naive cell gates was not greater in *Pdcd1*$^{-/-}$ mice (**Fig. 5f**). Together these data indicated that both T_{FR} cells and T_{FH} cells were present in the blood of mice and that both subsets were repressed by PD-1 signaling.

To investigate whether T_{FH} and T_{FR} cells in the blood had a central memory phenotype, we analyzed surface expression of CD62L and CD44. About 60% of wild-type and *Pdcd1*$^{-/-}$ T_{FR} cells in the blood had high expression of CD62L (**Supplementary Fig. 5**). This was in contrast to the finding that >90% of $ICOS^-CXCR5^-$ naive cells had high expression of CD62L. *Pdcd1*$^{-/-}$ T_{FH} cells had lower expression of CD62L than did wild-type T_{FH} cells. All wild-type and *Pdcd1*$^{-/-}$ T_{FR} cells in the blood had high expression of CD44, but *Pdcd1*$^{-/-}$ T_{FR} cells in the blood had slightly lower surface expression than did

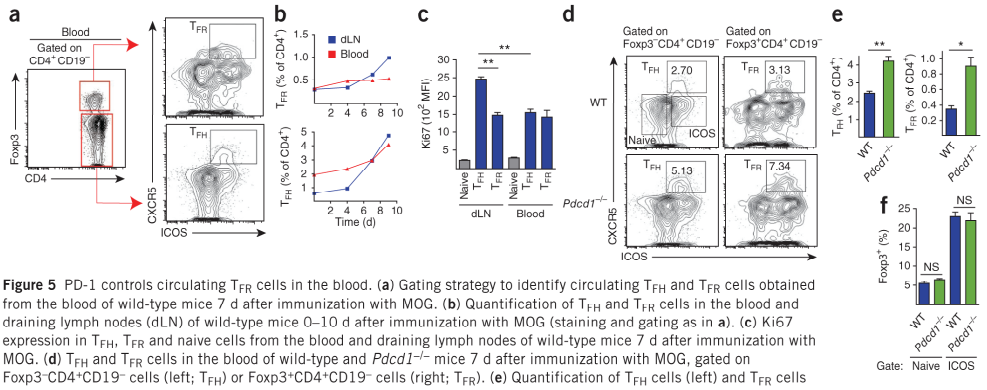

Figure 5 PD-1 controls circulating T_{FR} cells in the blood. (**a**) Gating strategy to identify circulating T_{FH} and T_{FR} cells obtained from the blood of wild-type mice 7 d after immunization with MOG. (**b**) Quantification of T_{FH} and T_{FR} cells in the blood and draining lymph nodes (dLN) of wild-type mice 0–10 d after immunization with MOG (staining and gating as in **a**). (**c**) Ki67 expression in T_{FH}, T_{FR} and naive cells from the blood and draining lymph nodes of wild-type mice 7 d after immunization with MOG. (**d**) T_{FH} and T_{FR} cells in the blood of wild-type and *Pdcd1*$^{-/-}$ mice 7 d after immunization with MOG, gated on Foxp3$^-$CD4$^+$CD19$^-$ cells (left; T_{FH}) or Foxp3$^+$CD4$^+$CD19$^-$ cells (right; T_{FR}). (**e**) Quantification of T_{FH} cells (left) and T_{FR} cells (right) in blood from mice as in **d**, presented as the percentage of CD4$^+$CD19$^-$ cells. (**f**) Quantification of CXCR5$^-$Foxp3$^+$ cells from mice as in **d**, presented as the percentage of CXCR5$^-$CD4$^+$ cells. NS, not significant; $^*P < 0.005$ and $^{**}P < 0.0005$ (unpaired Student's *t* test). Data are representative of at least two independent experiments (mean and s.e.m. of five mice in **c**,**e**,**f**).

their wild-type counterparts (**Supplementary Fig. 5**). Furthermore, T_{FR} cells in the blood had lower expression of PD-1 than did T_{FR} cells from the lymph nodes (**Supplementary Fig. 5**). Together these data indicated that T_{FR} cells in the blood were able to have a central memory homing phenotype.

The greater frequency of T_{FR} cells in *Pdcd1*$^{-/-}$ mice led us to investigate which PD-1 ligand was critical for controlling the generation of T_{FR} cells in the lymph nodes and blood. We first assessed the expression of PD-L1 and PD-L2 on B cells and DCs present in draining lymph nodes of immunized wild-type mice, because both B cells and DCs contribute to the proper differentiation and maintenance of T_{FH} cells in the lymph nodes[1]. It is not yet clear whether B cells or DCs or both are needed for the differentiation and/or maintenance of T_{FR} cells. To study GC B cells, we immunized mice with NP-OVA subcutaneously and, 12 d later, assessed the expression of PD-L1 and PD-L2 on Fas$^+$GL7$^+$CD19$^+$ GC B cells, as well as on CD138$^+$ plasma cells from the draining lymph nodes. We found that all B cell subsets had high expression of PD-L1, but only GC B cells had high expression of PD-L2 (**Fig. 6a**). To quantify the expression of PD-L1 and PD-L2 on DCs, we immunized mice with NP-OVA and analyzed DC populations from the draining lymph node 3 d later. Both CD8α$^+$ and CD8α$^-$ DC populations had high expression of PD-L1 and moderate expression of PD-L2 (**Fig. 6b**). A subpopulation of CD8α$^-$ DCs had high expression of PD-L2.

To determine which ligand was important for the generation of T_{FH} cells and T_{FR} cells, we immunized wild-type mice, PD-L1-deficient (*Cd274*$^{-/-}$) mice and PD-L2-deficient (*Pdcd1lg2*$^{-/-}$) mice with MOG and analyzed T_{FH} cells and T_{FR} cells in the draining lymph nodes and blood 7 d later. The frequency of T_{FH} cells in the lymph nodes of *Cd274*$^{-/-}$ and *Pdcd1lg2*$^{-/-}$ mice was similar to that of wild-type mice (**Fig. 6c**) and *Pdcd1*$^{-/-}$ mice (**Fig. 1e**). *Cd274*$^{-/-}$ mice, but not *Pdcd1lg2*$^{-/-}$ mice, had more T_{FH} cells in the blood, similar to that of *Pdcd1*$^{-/-}$ mice (**Fig. 5e**). *Cd274*$^{-/-}$ mice, but not *Pdcd1lg2*$^{-/-}$ mice, had more T_{FR} cells in the lymph nodes as well as the blood (**Fig. 6d**). Like *Pdcd1*$^{-/-}$ mice, *Cd274*$^{-/-}$ mice did not

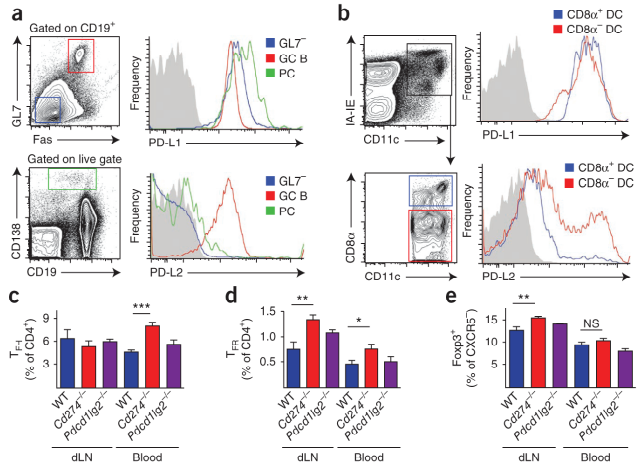

Figure 6 PD-L1 controls T_{FR} cells in the blood but PD-L2 does not. (**a**) Expression of PD-L1 and PD-L2 (right) on GL7$^-$ cells, GC B cells (GC B) and plasma cells (PC) obtained from the draining lymph nodes of wild-type mice 12 d after subcutaneous immunization with NP-OVA (gating at left). (**b**) Expression of PD-L1 and PD-L2 (right) on CD8α$^+$ and CD8α$^-$ DC subsets (gating at left) obtained from the draining lymph nodes of wild-type mice 3 d after immunization with NP-OVA. (**c**–**e**) T_{FH} cells (**c**), T_{FR} cells (**d**) and CXCR5$^-$Foxp3$^+$ CD4$^+$ T cells (**e**) in the draining lymph nodes and blood of wild-type mice, PD-L1-deficient (*Cd274*$^{-/-}$) mice and PD-L2-deficient (*Pdcd1lg2*$^{-/-}$) mice 7 d after immunization with MOG. NS, not significant; $^*P < 0.05$, $^{**}P < 0.005$ and $^{***}P < 0.0005$ (unpaired Student's *t*-test). Data are representative of at least two independent experiments (mean and s.e.m. of five mice per group in **c**–**e**).

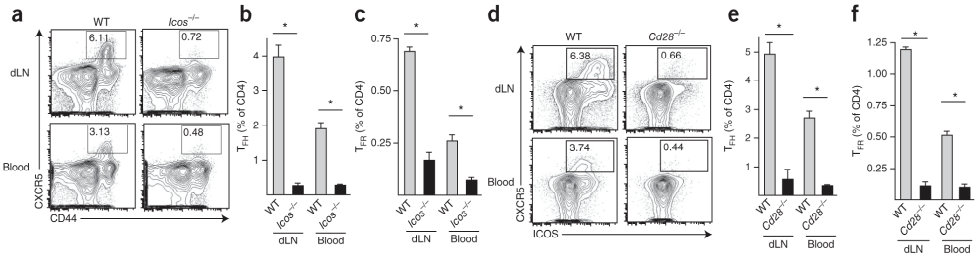

Figure 7 T_{FR} cells in the blood require costimulation via ICOS and CD28. (**a**) Gating of T_{FH} ($CD4^+CD44^+CXCR5^+Foxp3^-CD19^-$) cells and T_{FR} ($CD4^+CD44^+CXCR5^+Foxp3^+CD19^-$) cells in draining lymph nodes and blood obtained from wild-type and *Icos*$^{-/-}$ mice 7 d after immunization with MOG. (**b**,**c**) Quantification of T_{FH} cells (**b**) and T_{FR} cells (**c**) in the draining lymph nodes and blood of wild-type and *Icos*$^{-/-}$ mice as in **a**. (**d**) Gating strategy for T_{FH} ($CD4^+ICOS^+CXCR5^+Foxp3^-CD19^-$) cells and T_{FR} ($CD4^+ICOS^+CXCR5^+Foxp3^+CD19^-$) cells in wild-type and *Cd28*$^{-/-}$ mice immunized as in **a**. (**e**,**f**) Quantification of T_{FH} cells (**e**) and T_{FR} cells (**f**) in the lymph nodes and blood of wild-type *Cd28*$^{-/-}$ mice immunized as in **a** (gated as in **d**). *$P < 0.0005$ (unpaired Student's *t*-test). Data are representative of at least two independent experiments (mean and s.e.m. of five mice per group in **b**,**c**,**e**,**f**).

have a greater frequency of any non-T_{FR} $Foxp3^+$ effector cell in the blood (**Fig. 6e**). These studies demonstrated that PD-L1, but not PD-L2, was responsible for controlling T_{FR} cells in the lymph nodes and blood.

Blood T_{FH} and T_{FR} cells require CD28 and ICOS signals

We further investigated the costimulatory requirements for T_{FR} cells in the blood, focusing on the effects of costimulation by CD28 and ICOS on T_{FR} populations in the blood because of the important roles of these costimulatory receptors in controlling T_{FH} cells and T_{FR} cells from the lymph nodes. *Cd28*$^{-/-}$ mice are deficient in T_{FH} cells and T_{FR} cells in the lymph nodes[21], and *Icos*$^{-/-}$ mice are deficient in T_{FH} cells in the lymph nodes[24]. We analyzed *Cd28*$^{-/-}$ mice and *Icos*$^{-/-}$ mice for the presence of T_{FR} cells in the lymph nodes and blood 7 d after immunization with MOG. In wild-type mice, there were fewer T_{FH} cells and T_{FR} cells in the blood than in the draining lymph nodes (**Fig. 7a**,**b**). *Icos*$^{-/-}$ mice had considerably fewer T_{FR} cells (and T_{FH} cells) in the blood, as well as the lymph nodes (**Fig. 7a–c**). *Cd28*$^{-/-}$ mice had similar considerable deficiencies in the frequency of T_{FR} cells and T_{FH} cells in both lymph nodes and blood (**Fig. 7d–f**). Thus, ICOS and CD28 supplied essential costimulatory signals for T_{FR} cells and T_{FH} cells in the blood as well as the lymph nodes.

Enhanced suppression by *Pdcd1*$^{-/-}$ T_{FR} cells in the blood *in vivo*

We next investigated the function of T_{FR} cells in the blood in humoral immune responses. Because T_{FH} cells in human blood can function in the activation and antibody production of B cells *in vitro*[6,7], we investigated whether T_{FR} cells in the circulating blood contributed to the suppression of antibody production *in vivo*. To assess this, we designed transfer experiments in which we immunized wild-type donor mice with NP-OVA subcutaneously and 8 d later sorted T_{FR} ($CD4^+ICOS^+CXCR5^+GITR^+CD19^-$) cells and T_{FH} ($CD4^+ICOS^+CXCR5^+GITR^-CD19^-$) cells from the blood (**Fig. 8a**). We transferred those cells into *Cd28*$^{-/-}$ mice or mice deficient in the TCR α-chain (*Tcra*$^{-/-}$ mice) because they lack T_{FH} cells and T_{FR} cells in both blood and lymph nodes. This approach allowed us to determine if blood T_{FR} cells and T_{FH} cells could functionally regulate humoral responses separately from differentiation. As the transferred T_{FH} cells and T_{FR} cells in the blood were the only follicular T cells in *Cd28*$^{-/-}$ and *Tcra*$^{-/-}$ recipients, any responses in the draining lymph nodes would be due to trafficking of the T_{FR} cells and T_{FH} cells from the blood.

Initially, we adoptively transferred 4×10^4 T_{FH} cells alone or together with 2×10^4 T_{FR} cells into *Cd28*$^{-/-}$ mice (a ratio of T_{FR} cells to T_{FH} cells approximately twofold higher than is found in blood after immunization). We immunized recipients 1 d later with NP-OVA and analyzed titers of NP-specific IgG at 12 d after immunization (**Fig. 8a**). Without transfer of T_{FH} cells or T_{FR} cells from the blood, *Cd28*$^{-/-}$ mice were unable to produce large amounts of NP-specific IgG (**Fig. 8b**). The transfer of T_{FH} cells from the blood alone resulted in much higher titers of NP-specific IgG. Transfer of T_{FH} cells from the blood led to substantial production of IgG1, but also smaller increases in the production of immunoglobulins of other isotypes (data not shown). Transfer of T_{FR} cells from the blood along with T_{FH} cells from the blood resulted in robust inhibition of the production of NP-specific antibody (**Fig. 8b**), which demonstrated the potent regulatory ability of T_{FR} cells from the blood in suppressing antibody production. To evaluate the effect of T_{FR} cells on the generation of plasma cells, we collected draining lymph nodes, spleens and bone marrow from recipient mice 24 d after immunization and quantified plasma cells. $CD138^+$ plasma cells were absent from the lymph nodes of immunized *Cd28*$^{-/-}$ mice (**Fig. 8c**,**d**). The transfer of T_{FH} cells from the blood resulted in sizable populations of plasma cells in the draining lymph nodes, spleen and bone marrow (**Fig. 8c**,**d**). T_{FR} cells from the blood almost completely prevented formation and/or survival of plasma cells in all organs tested.

Next we transferred T_{FH} cells and/or T_{FR} cells from the blood into *Tcra*$^{-/-}$ recipients. The transfer of 4×10^4 T_{FH} cells resulted in a higher titer of NP-specific IgG than that of an NP-OVA–immunized wild-type mouse in most experiments (**Fig. 8e**). The robust antibody production elicited by T_{FH} cells from the blood depended on the 'follicular program' because transfer of total $CD4^+$ T cells from *Cxcr5*$^{-/-}$ mice or $CD4^+CD62L^+CXCR5^-Foxp3^-$ naive cells from wild-type mice resulted in background concentrations of antibody in these experiments (**Fig. 8e**). When we transferred T_{FR} cells from the blood together with T_{FH} cells from the blood, the titers of NP-specific antibody were much lower (**Fig. 8e**), which demonstrated the suppressive ability of the T_{FR} cells. The T_{FR} cells from the blood resulted in lower frequencies of both plasma cells in the spleen (**Fig. 8f**) and T_{FH} cells in the lymph nodes (**Fig. 8g**). When we compared the function of T_{FH} cells from the blood and T_{FH} cells from the draining lymph nodes after transfer into *Tcra*$^{-/-}$ recipients, we found that T_{FH} cells from the blood had a greater ability to promote the

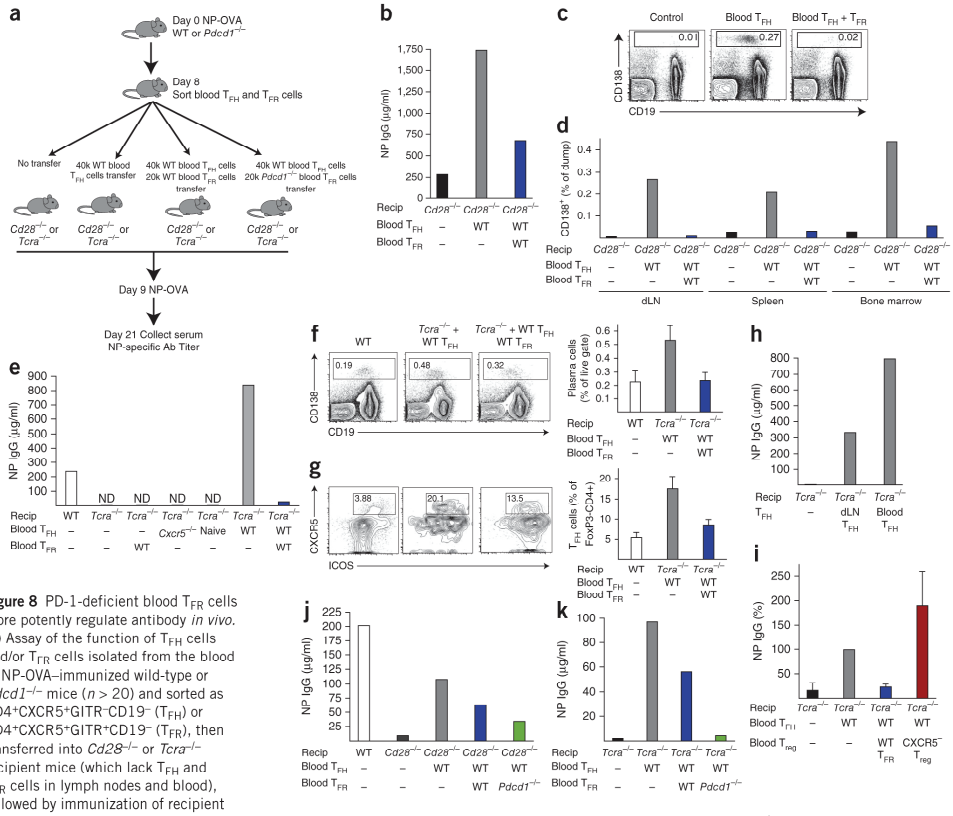

Figure 8 PD-1-deficient blood T_{FR} cells more potently regulate antibody *in vivo*. (**a**) Assay of the function of T_{FH} cells and/or T_{FR} cells isolated from the blood of NP-OVA–immunized wild-type or *Pdcd1*$^{-/-}$ mice ($n > 20$) and sorted as CD4$^+$CXCR5$^+$GITR$^-$CD19$^-$ (T_{FH}) or CD4$^+$CXCR5$^+$GITR$^+$CD19$^-$ (T_{FR}), then transferred into *Cd28*$^{-/-}$ or *Tcra*$^{-/-}$ recipient mice (which lack T_{FH} and T_{FR} cells in lymph nodes and blood), followed by immunization of recipient mice with NP-OVA and analysis of the serum 12 d later. 40k, 40,000; 20k, 20,000. (**b**) Titers of NP-specific IgG in *Cd28*$^{-/-}$ recipients of wild-type cells as in **a** (below graph). (**c**,**d**) Gating of CD138$^+$ plasma cells in draining lymph nodes (**c**) and quantification of CD138$^+$ plasma cells in draining lymph nodes, spleen and bone marrow of *Cd28*$^{-/-}$ recipients of no transfer (far left) or transfer of wild-type cells as in **a** (below graph in **d**), assessed 24 d after immunization. Dump, dump channel. (**e**) Titers of NP-specific IgG in wild-type mice or *Tcra*$^{-/-}$ recipients without cell transfer (left) or *Tcra*$^{-/-}$ recipients of CD4$^+$ T cells from blood of immunized *Cxcr5*$^{-/-}$ mice (*Cxcr5*$^{-/-}$), CD4$^+$CD62L$^+$Foxp3$^-$ cells from blood of unimmunized WT FoxP3 reporter mice (Naive) or T_{FH} cells and/or T_{FR} cells from the blood of immunized wild-type mice as in **a** (below graph). (**f**,**g**) CD138$^+$ plasma cells in the spleen (**f**) and T_{FH} cells from draining lymph nodes (**g**) of wild-type mice without cell transfer (left) and *Tcra*$^{-/-}$ recipients of wild-type T_{FH} cells and/or T_{FR} cells as in **a** (above plots or below graphs), assessed 12 d after immunization. (**h**) Titers of NP-specific IgG in immunized *Tcra*$^{-/-}$ mice given no cells (left) or T_{FH} cells (4×10^6) isolated from the draining lymph nodes (middle) or blood (right) of NP-OVA–immunized wild-type mice. (**i**) NP-specific IgG in immunized *Tcra*$^{-/-}$ mice given no cells (left) or wild-type T_{FH} cells with or without CXCR5$^-$Foxp3$^+$ T_{reg} cells (from blood of immunized Foxp3-GFP reporter mice) or T_{FR} cells (from the blood of immunized wild-type mice) as in **a** (below graph). All mice were immunized with NP-OVA. (**j**,**k**) Titers of NP-specific IgG in immunized *Cd28*$^{-/-}$ (**j**) or *Tcra*$^{-/-}$ (**k**) recipients of wild-type T_{FH} cells (4×10^4) and/or wild-type or *Pdcd1*$^{-/-}$ T_{FR} cells (1.5×10^4) from the blood of mice immunized 8 d before. Data are representative of two independent experiments (mean and s.e.m. of at least three mice per group in **f**,**g**,**i**). ND, none detected.

production of NP-specific IgG (**Fig. 8h**). The suppression of T_{FH} cells by T_{FR} cells also depended on the 'follicular program' in these cells because neither CD25$^+$CD62L$^+$ T_{reg} cells from the blood of *Cxcr5*$^{-/-}$ mice (data not shown) nor CXCR5$^-$Foxp3$^+$ T_{reg} cells from the blood of Foxp3-GFP reporter mice had the same suppressive ability as that of T_{FR} cells from the blood of wild-type mice (**Fig. 8i**).

Finally, we investigated the suppressive ability of PD-1-deficient blood T_{FR} cells *in vivo*, as PD-1-deficient T_{FR} cells from the lymph node suppressed antibody production more potently than did wild-type T_{FR} cells from the lymph node *in vitro*. We adoptively transferred 4×10^4 wild-type T_{FH} cells from the blood alone or together with 1.5×10^4 T_{FR} cells from the blood of wild-type or *Pdcd1*$^{-/-}$ mice into *Cd28*$^{-/-}$ or *Tcra*$^{-/-}$ recipients and immunized the recipients as described above (**Fig. 8a**). PD-1-deficient T_{FR} cells inhibited antibody production to a greater extent than did wild-type T_{FR} cells in *Cd28*$^{-/-}$ recipients (**Fig. 8j**) and *Tcra*$^{-/-}$ recipients (**Fig. 8k**), which demonstrated their greater suppressive ability. Together these data showed that T_{FR} cells from the blood potently inhibited antibody production *in vivo* and that PD-1 deficiency resulted in enhanced suppressive ability of T_{FR} cells.

DISCUSSION

The immunoregulatory functions of T_{FR} cells are only beginning to be elucidated, and little is known about how these cells differentiate and function. Although T_{FR} cells originate from different precursors than do T_{FH} cells, T_{FR} cells and T_{FH} cells have nearly identical receptors. Therefore, functional studies of T_{FH} cells have in fact examined mixtures of stimulatory T_{FH} cells and inhibitory T_{FR} cells. The PD-1 pathway regulates many arms of the immune response; however, biological complexity has led to inconsistencies about the role of this pathway in humoral immunity[16–20]. In this study we have identified a previously unknown mechanism by which PD-1 can regulate humoral immunity. PD-1 limits the generation and function of T_{FR} cells.

We found that PD-1 signaling inhibited the abundance of T_{FR} cells, not T_{FH} cells, in the lymph nodes, which skewed the ratio of T_{FR} cells to T_{FH} cells. It is possible that the greater suppressive ability of *Pdcd1*$^{-/-}$ T_{FR} cells, together with the higher ratio of T_{FR} cells to T_{FH} cells in *Pdcd1*$^{-/-}$ mice, resulted in the inhibition of T_{FH} cells. Alternatively, there may have been alterations in *Pdcd1*$^{-/-}$ T_{FH} cells that promoted their departure from the lymph nodes. Some studies have described a greater abundance of T_{FH} cells in PD-1–deficient mice; however, T_{FR} cells were not assessed in those studies[16,18,19]. It is likely that a greater abundance of T_{FR} cells in PD-1-deficient mice may have contributed to the greater abundance of T_{FH} cells and may explain conflicting data. For example, published studies have described a greater abundance of CD4$^+$CXCR5$^+$ cells in Peyer's patches of PD-1-deficient mice[18]. However, after transfer, those cells were nonfunctional in supporting IgA production. A greater abundance of T_{FR} cells in the T_{FH} gate in PD-1-deficient Peyer's patches may explain those data.

T_{FR} cells depend on the adaptor SAP, CD28 and Bcl-6 for differentiation[21,22]. However, the pathways that limit the differentiation of T_{FR} cells are less clear. Only the transcription factor Blimp-1 has been shown to inhibit the differentiation of T_{FR} cells[21]. Here we have identified PD-1 as a surface receptor that inhibited the development of T_{FR} cells. Our adoptive-transfer studies demonstrated a cell-intrinsic role for PD-1 in the differentiation of T_{FR} cells from Foxp3$^+$ T_{reg} cells. We hypothesize that rather than simply inhibiting responses, the PD-1 pathway may act as a molecular switch that controls cell-fate 'decisions'. The integration of signals through PD-1, TCRs and cytokine receptors may direct differentiation into various T cell subsets. For example, PD-L1 can promote the differentiation of induced T_{reg} cells from naive T cells[10–14,29]. However, we found that PD-1 inhibited the differentiation of T_{FR} cells. T_{FR} cells arise from natural T_{reg} cells[21]. Therefore, our studies suggest that PD-1 may have distinct roles in the differentiation of induced and natural T_{reg} cells.

Because of the recent discovery of T_{FR} cells, there is a lack of knowledge about T_{FR} cell biology, so we developed assays to analyze the function of T_{FR} cells. T_{FR} cells have the potential to inhibit the activation of naive T cells, T_{FH} cell function and/or the activation of B cells. Here we used specific assays for T_{FR} cell function *in vitro* and found that T_{FR} cells from the lymph nodes were potent at inhibiting antibody production but not effective at suppressing T cell activation. PD-1-deficient T_{FR} cells inhibited the activation of naive T cells and attenuated antibody production *in vitro* to a greater extent than did wild-type T_{FR} cells. Furthermore, our studies demonstrated the dynamic control of antibody production by T_{FH} cells and T_{FR} cells. Initially, our attempts to activate B cells *in vitro* with total CD4$^+$CXCR5$^+$ cells resulted in little IgG. However, when we separated T_{FH} cells from T_{FR} cells, we detected abundant IgG. Moreover, we found that *in vitro* and *in vivo*, the ratio of T_{FR} cells to T_{FH} cells, not the individual numbers of each, seemed to be critical in determining the extent of humoral immunity. Therefore, analyzing this ratio may be useful in predicting the extent of a humoral immune response.

We found substantial populations of T_{FR} cells in the blood of mice. Many reports have described T_{FH} cells in the circulation of humans[6,7], and one has described them in the blood of mice[9]. To our knowledge, our work is the first description of functional T_{FR} cells in the blood of any organism. T_{FH} cells in human blood have been shown to stimulate antibodies *in vitro*. Some studies have shown more efficient B cell antibody production by T_{FH} cells in the blood than by CXCR5$^-$ cells[6,7], whereas others have found no difference between T_{FH} cells from the blood and CXCR5$^-$ cells[30]. Such differences may relate to the ratio of T_{FH} cells to T_{FR} cells in those experiments. Here we found that the generation of T_{FH} cells and T_{FR} cells in the blood required signaling through ICOS and CD28, two costimulatory receptors essential for controlling T_{FH} cells in the lymph nodes.

Our transfer studies showed that T_{FR} cells from the blood were functional and were able to regulate antibody production *in vivo*. To study the function of T_{FR} cells, we transferred T_{FH} cells from the blood alone or with T_{FR} cells into *Cd28*$^{-/-}$ or *Tcra*$^{-/-}$ mice, which lack T_{FH} cells and T_{FR} cells in both blood and lymph nodes. Although it was technically challenging, this approach allowed us to analyze the function of T_{FH} cells and T_{FR} cells separately from differentiation. T_{FR} cells from the blood were extremely potent at inhibiting T_{FH} cell–mediated production of antibody, even when relatively few cells were transferred. We hypothesize that T_{FR} cells from the blood are a central memory pool that can be used to modulate humoral immunity, analogous to Foxp3$^+$ cells with regulatory memory[31]. The high expression of CD62L and CD44 on T_{FR} cells from the blood, along with their ability to home to lymph nodes, supports this idea. T_{FR} cells from the blood would be able to home to lymph nodes and suppress early B cell responses before natural T_{reg} cells differentiated into T_{FR} cells.

Beyond their ability to directly suppress antibody responses, T_{FR} cells may be instrumental in determining B cell fate. For example, T_{FR} cells may direct the differentiation of GC B cells away from plasma cells into memory B cells. If T_{FR} cells direct B cell fate, this would have implications for vaccines. Additionally, analyzing the ratio of T_{FR} cells to T_{FH} cells may be used to predict the quality and quantity of humoral immune responses *in vivo*. Furthermore, therapy with T_{FR} cells has potential for patients suffering from autoimmunity. By transferring T_{FR} cells, it may be possible to suppress autoantibody production while leaving other arms of the immune system intact. In summary, T_{FR} cells are potent suppressors of humoral immunity and are controlled by PD-1. Further work is needed to determine how modulation of these cells may be used therapeutically to enhance protective immunity and long-term memory or to inhibit autoimmune diseases.

METHODS

Methods and any associated references are available in the online version of the paper.

Note: Supplementary information is available in the online version of the paper.

ACKNOWLEDGMENTS

We thank R. Ortega, C. Armet, F. Gonzalez, N. Chouaki, D. Brown and S. Lee for technical assistance; G. Freeman for comments on the manuscript; and M. Carroll (Harvard Medical School) for the mouse anti-NP standard. Supported by the US National Institutes of Health (T32 AI070085 to P.T.S.; and R01 AI40614, P01 78897 and R37 AI38310 to A.H.S.).

AUTHOR CONTRIBUTIONS

P.T.S. did all experiments; P.T.S. and A.H.S. designed the studies, analyzed and interpreted the results and wrote the manuscript; and L.M.F. and C.V.C. provided technical help and edited the manuscript.

COMPETING FINANCIAL INTERESTS
The authors declare no competing financial interests.

Published online at http://www.nature.com/doifinder/10.1038/ni.2496.
Reprints and permissions information is available online at http://www.nature.com/reprints/index.html.

1. Crotty, S. Follicular helper CD4 T cells (T_{FH}). *Annu. Rev. Immunol.* **29**, 621–663 (2011).
2. Johnston, R.J. *et al.* Bcl6 and Blimp-1 are reciprocal and antagonistic regulators of T follicular helper cell differentiation. *Science* **325**, 1006–1010 (2009).
3. Nurieva, R.I. *et al.* Bcl6 mediates the development of T follicular helper cells. *Science* **325**, 1001–1005 (2009).
4. Choi, Y.S. *et al.* ICOS receptor instructs T follicular helper cell versus effector cell differentiation via induction of the transcriptional repressor Bcl6. *Immunity* **34**, 932–946 (2011).
5. Nurieva, R.I. *et al.* Generation of T follicular helper cells is mediated by interleukin-21 but independent of T helper 1, 2, or 17 cell lineages. *Immunity* **29**, 138–149 (2008).
6. Morita, R. *et al.* Human blood $CXCR5^+CD4^+$ T cells are counterparts of T follicular cells and contain specific subsets that differentially support antibody secretion. *Immunity* **34**, 108–121 (2011).
7. Schaerli, P. *et al.* CXC chemokine receptor 5 expression defines follicular homing T cells with B cell helper function. *J. Exp. Med.* **192**, 1553–1562 (2000).
8. Saito, R. *et al.* Altered expression of chemokine receptor CXCR5 on T cells of myasthenia gravis patients. *J. Neuroimmunol.* **170**, 172–178 (2005).
9. Simpson, N. *et al.* Expansion of circulating T cells resembling follicular helper T cells is a fixed phenotype that identifies a subset of severe systemic lupus erythematosus. *Arthritis Rheum.* **62**, 234–244 (2010).
10. Polanczyk, M.J., Hopke, C., Vandenbark, A.A. & Offner, H. T_{reg} suppressive activity involves estrogen-dependent expression of programmed death-1 (PD-1). *Int. Immunol.* **19**, 337–343 (2007).
11. Wang, L. *et al.* Programmed death 1 ligand signaling regulates the generation of adaptive $Foxp3^+CD4^+$ regulatory T cells. *Proc. Natl. Acad. Sci. USA* **105**, 9331–9336 (2008).
12. Francisco, L.M. *et al.* PD-L1 regulates the development, maintenance, and function of induced regulatory T cells. *J. Exp. Med.* **206**, 3015–3029 (2009).
13. Wang, C., Li, Y., Proctor, T.M., Vandenbark, A.A. & Offner, H. Down-modulation of programmed death 1 alters regulatory T cells and promotes experimental autoimmune encephalomyelitis. *J. Neurosci. Res.* **88**, 7–15 (2010).
14. Amarnath, S. *et al.* The PDL1–PD1 axis converts human TH1 cells into regulatory T cells. *Sci. Transl. Med.* **3**, 111ra120 (2011).
15. Francisco, L.M., Sage, P.T. & Sharpe, A.H. The PD-1 pathway in tolerance and autoimmunity. *Immunol. Rev.* **236**, 219–242 (2009).
16. Good-Jacobson, K.L. *et al.* PD-1 regulates germinal center B cell survival and the formation and affinity of long-lived plasma cells. *Nat. Immunol.* **11**, 535–542 (2010).
17. Hamel, K.M. *et al.* B7–H1 expression on non-B and non-T cells promotes distinct effects on T- and B-cell responses in autoimmune arthritis. *Eur. J. Immunol.* **40**, 3117–3127 (2010).
18. Kawamoto, S. *et al.* The inhibitory receptor PD-1 regulates IgA selection and bacterial composition in the gut. *Science* **336**, 485–489 (2012).
19. Hams, E. *et al.* Blockade of B7–H1 (programmed death ligand 1) enhances humoral immunity by positively regulating the generation of T follicular helper cells. *J. Immunol.* **186**, 5648–5655 (2011).
20. Velu, V. *et al.* Enhancing SIV-specific immunity *in vivo* by PD-1 blockade. *Nature* **458**, 206–210 (2009).
21. Linterman, M.A. *et al.* Foxp3+ follicular regulatory T cells control the germinal center response. *Nat. Med.* **17**, 975–982 (2011).
22. Chung, Y. *et al.* Follicular regulatory T cells expressing Foxp3 and Bcl-6 suppress germinal center reactions. *Nat. Med.* **17**, 983–988 (2011).
23. Wollenberg, I. *et al.* Regulation of the germinal center reaction by $Foxp3^+$ follicular regulatory T cells. *J. Immunol.* **187**, 4553–4560 (2011).
24. Bauquet, A.T. *et al.* The costimulatory molecule ICOS regulates the expression of c-Maf and IL-21 in the development of follicular T helper cells and T_H-17 cells. *Nat. Immunol.* **10**, 167–175 (2009).
25. Fife, B.T. *et al.* Interactions between PD-1 and PD-L1 promote tolerance by blocking the TCR-induced stop signal. *Nat. Immunol.* **10**, 1185–1192 (2009).
26. Cretney, E. *et al.* The transcription factors Blimp-1 and IRF4 jointly control the differentiation and function of effector regulatory T cells. *Nat. Immunol.* **12**, 304–311 (2011).
27. Martins, G.A. *et al.* Transcriptional repressor Blimp-1 regulates T cell homeostasis and function. *Nat. Immunol.* **7**, 457–465 (2006).
28. Zhou, L. *et al.* TGF-β-induced Foxp3 inhibits T_H17 cell differentiation by antagonizing RORγt function. *Nature* **453**, 236–240 (2008).
29. Beswick, E.J., Pinchuk, I.V., Das, S., Powell, D.W. & Reyes, V.E. Expression of the programmed death ligand 1, B7–H1, on gastric epithelial cells after *Helicobacter pylori* exposure promotes development of $CD4^+CD25^+FoxP3^+$ regulatory T cells. *Infect. Immun.* **75**, 4334–4341 (2007).
30. Kim, C.H. *et al.* Subspecialization of $CXCR5^+$ T cells: B helper activity is focused in a germinal center-localized subset of $CXCR5^+$ T cells. *J. Exp. Med.* **193**, 1373–1381 (2001).
31. Rosenblum, M.D. *et al.* Response to self antigen imprints regulatory memory in tissues. *Nature* **480**, 538–542 (2011).

ONLINE METHODS

Mice. Mice 6-10 weeks of age were used for all experiments. Wild-type C57BL/6 mice and *Tcra*$^{-/-}$ mice were from The Jackson Laboratory. *Pdcd1*$^{-/-}$, *Cd274*$^{-/-}$ and *Pdcd1lg2*$^{-/-}$ mice on the C57BL/6 background were generated in the Sharpe laboratory[32–34]. *Icos*$^{-/-}$ mice[35] and *Cd28*$^{-/-}$ mice[36] were generated as described. The 2D2–Foxp3-GFP mice were generated in the Sharpe laboratory by the crossing of Foxp3-GFP reporter mice[37] with 2D2 mice[38]. All mice were used according to the Harvard Medical School Standing Committee on Animals and National Institutes of Animal Healthcare Guidelines. Animal protocols were approved by the Harvard Medical School Standing Committee on Animals.

Immunization. For immunization with MOG, mice were given subcutaneous injection of 100 μg MOG (amino acids 35–55; University of California Los Angeles Biopolymers Facility) emulsified (at a ratio of 1:1) in an emulsion of *Mycobacterium tuberculosis* strain H37RA complete Freund's adjuvant (Difco) in their flanks. Then, 7 d later, mice were killed and inguinal lymph nodes (draining lymph nodes) and/or spleens were collected for flow cytometry. Blood was collected by cardiac puncture with a 1-cc syringe, and cells of the immune system were isolated by sucrose density centrifugation with Lymphocyte Separation Media (MP Biomedicals). For NP-OVA immunizations, 100 μg NP_{18} OVA (Biosearch Technologies) was used in an emulsion (at a ratio of 1:1) in *M. tuberculosis* H37RA complete Freund's adjuvant and was injected as described for MOG.

Enzyme-linked immunosorbent assay. For quantification of antibody production *in vitro*, total IgG was quantified in culture supernatants with a total IgG capture antibody (1010-01; Southern Biotech) and alkaline phosphatase–conjugated total IgG detection antibody (1030-04; Southern Biotech). For analysis of antibody production *in vivo*, serum was collected from mice at various time points. NP-specific antibody titers were measured by incubation of serum for 1 h in enzyme-linked immunosorbent assay plates coated with NP_{16}-BSA (Biosearch Technologies), followed by incubation with alkaline phosphatase–conjugated IgG-detection antibodies (1030-04; Southern Biotech). A standard curve was generated with antibody from an NP-specific IgG1 hybridoma (a gift from M. Carroll). That standard curve was used for the approximation of all IgG-subtype antibodies in the linear range of detection with a Spectramax Elisa plate reader (Molecular Devices).

Flow cytometry. Cells from lymphoid organs were isolated and resuspended in staining buffer (PBS containing 1% FCS and 2 mM EDTA) and were stained with the following directly labeled antibodies: anti-CD4 (RM4-5), anti-ICOS (15F9), anti-CD19 (6D5), anti-PD-1 (RMP1-30), anti-PD-L1 (10F.9G2), CD69 (H1.2F3; all from Biolegend); anti-Foxp3 (FJK-16S) and anti-Bcl-6 (mGI191E; both from eBioscience); and anti-Fas (Jo2), anti-GL7 (GL7) and anti-Ki67 (B56; all from BD Biosciences). For staining of CXCR5, biotinylated anti-CXCR5 (2G8; BD Biosciences) was used, followed by streptavidin-Brilliant Violet 421 (Biolegend). For intracellular staining, a Foxp3 Fix/Perm kit was used (eBioscience) after surface staining. All flow cytometry data were analyzed with an LSR II (BD Biosciences) with standard filter sets and were further analyzed with FlowJo software (TreeStar).

Confocal microscopy. Draining lymph nodes were embedded in optimum cutting temperature compound, and sections 8 μm in thickness were cut, fixed with 4% paraformaldehyde and stained, followed by imaging on a Zeiss LSM 510 confocal microscope by acquisition of *z*-stacks 0.5 μm in thickness with a 40× oil objective. GCs were quantified by drawing of outlines around GL7$^+$IgD$^-$ areas in the B cell zone. For quantification of Foxp3, GC zones were determined and *z*-stack images were scrolled through for identification of large Foxp3$^+$ spots. Axiovision (Zeiss) software was used for measurement of the distance from GC borders. For micrographs, single *z* slices were contrasted in a linear way and merged images were made in Adobe photoshop. Enlargements indicate digital enlargements made with Adobe photoshop.

Quantitative PCR. Standard TaqMAN probes (Applied Biosystems) and an ABI FasT9500 QPCR system were used according to the manufacturers' instructions for quantitative PCR. The abundance of mRNA was normalized to that of HPRT (hypoxanthine guanine phosphoribosyl transferase) or β_2-microglobulin, and the change-in-threshold (ΔC_T) method was used for quantification of mRNA ($2^{-\Delta\Delta CT}$). The abundance of RNA was normalized to that in naive T cells.

***In vitro* suppression assay.** Cell populations were sorted to a purity of 99% on a FACSAria II (BD Biosciences). For assays of suppression by T_{FR} cells, sorted cells were counted on an Accuri cytometer (BD Biosciences) by gating of live cells only, and 1×10^5 GL7$^-$ B cells from draining lymph nodes of wild-type mice immunized with MOG 7 d before, 1×10^5 CD4$^+$CD62L$^+$Foxp3$^-$ T responder cells from unimmunized wild-type Foxp3-GFP reporter mice (labeled with CFSE (carboxyfluorescein diacetate succinimidyl ester; Invitrogen)), and 1×10^5 T_{FR} cells from the draining lymph nodes of mice immunized with MOG 7 d before were plated with 2 μg/ml soluble anti-CD3 (2C11; BioXcell) and 5 μg/ml anti-IgM (115-006-020; Jackson Immunoresearch). After 3 d, cells were collected and stained with anti CD4 (RM4-5; Biolegend) and anti CD19 (6D5; Biolegend). The responder T cells were identified as CFSE$^+$ cells, and the percent divided cells was determined by flow cytometry by drawing of a gate outside a reference CFSE peak from unstimulated CFSE$^+$ cells. For *in vitro* antibody suppression, GL7$^-$ B cells from wild-type MOG-immunized mice were plated with T_{FH} cells and/or T_{FR} cells pooled from MOG-immunized wild-type or *Pdcd1*$^{-/-}$ mice and 2 μg/ml soluble anti-CD3 and anti-IgM (as described above). After 6 d, supernatants were collected for antibody analysis by enzyme-linked immunosorbent assay.

Adoptive transfer. For the transfer of 2D2 T_{reg} cells, 2×10^5 CD4$^+$CXCR5$^-$ Foxp3$^+$ cells were sorted from the spleens of unimmunized wild-type or *Pdcd1*$^{-/-}$ 2D2 Foxp3-GFP reporter mice and adoptively transferred intravenously into wild-type recipients, which were then immunized with MOG. For adoptive transfer of T_{FH} cells and T_{FR} cells from the blood, wild-type mice were immunized subcutaneously with NP-OVA as described above, and 8 d later blood was collected by cardiac puncture. T_{FH} cells and T_{FR} cells were sorted as described above. T_{FH} cells (4×10^4) from the blood, alone or together with T_{FR} cells (2×10^4) from the blood, were transferred into *Cd28*$^{-/-}$ or *Tcra*$^{-/-}$ mice, unless specified otherwise. The recipient mice were immunized with NP-OVA as described above. Serum and organs were collected and analyzed by enzyme-linked immunosorbent assay or flow cytometry.

Statistical analysis. Unpaired Student's *t*-test was used for all comparisons. *P* values of less than 0.05 were considered statistically significant.

32. Keir, M.E., Freeman, G.J. & Sharpe, A. PD-1 regulates self-reactive CD8$^+$ T cell responses to antigen in lymph nodes and tissues. *J. Immunol.* **179**, 5064–5070 (2007).
33. Latchman, Y.E. *et al.* PD-L1-deficient mice show that PD-L1 on T cells, antigen-presenting cells, and host tissues negatively regulates T cells. *Proc. Natl. Acad. Sci. USA* **101**, 10691–10696 (2004).
34. Keir, M.E. *et al.* Tissue expression of PD-L1 mediates peripheral T cell tolerance. *J. Exp. Med.* **203**, 883–895 (2006).
35. McAdam, A.J. *et al.* ICOS is critical for CD40-mediated antibody class switching. *Nature* **409**, 102–105 (2001).
36. Shahinian, A. *et al.* Differential T cell costimulatory requirements in CD28-deficient mice. *Science* **261**, 609–612 (1993).
37. Bettelli, E. *et al.* Reciprocal developmental pathways for the generation of pathogenic effector T_H17 and regulatory T cells. *Nature* **441**, 235–238 (2006).
38. Bettelli, E. *et al.* Myelin oligodendrocyte glycoprotein-specific T cell receptor transgenic mice develop spontaneous autoimmune optic neuritis. *J. Exp. Med.* **197**, 1073–1081 (2003).